



Ali Shiehnejadhesar MSc

Improved gas phase CFD simulation of biomass packed bed combustion

DOCTORAL THESIS

to achieve the university degree of
Doktor der technischen Wissenschaften
submitted to

Graz University of Technology

Supervisor

Dipl.-Ing. Dr.techn. Univ.-Doz. Prof., Ingwald Obernberger

Institute of Process and Particle Engineering

Graz, October 2015

AFFIDAVIT

I declare that I have authored this thesis independently, that I have not used other than the declared sources/resources, and that I have explicitly marked all material which has been quoted either literally or by content from the sources used. The text document uploaded to TUGRAZonline is identical to the present doctoral thesis.

October 2015

Date

Ali shiehne'adhesar

Signature



Acknowledgement

Without a doubt, this thesis would never have been finished without professional and emotional support of a number of people. I would like to express my sincere gratitude to all of them.

Foremost, I would like to acknowledge the head of Thermal Biomass Utilisation Group at the Institute of Process and Particle Engineering, Prof. Dr. Ingwald Obernberger for the continuous support of my Ph.D. study and research, for his invaluable guidance, enthusiasm, and immense knowledge. His guidance helped me in all the time of research and writing of this thesis. I am very grateful to the reviewer of this work Prof. Dr. Brink from Åbo Akademi University for carefully reviewing my thesis. My sincere thanks go to my scientific advisor Dr. Robert Scharler for his valuable assistance, unconditional support and encouraging discussions on combustion modelling throughout my study.

I would like to thank all my colleagues at BIOENERGY 2020+ GmbH for the enjoyable working atmosphere. I thank Dr. Mehrabian for his close friendship and his constructive discussions during the most tedious parts of this work.

Last but not least, I am very much indebted to my wife SAMANEH for her kind support in every possible way to see the completion of this work.

Abstract

CFD modelling is becoming increasingly important for the development and optimisation of biomass combustion plants. Here, gas phase combustion models play a key role concerning predictions of flow, temperature, and gaseous emissions (e.g. CO). The eddy break-up models (EBU) are the most prevalent Reynolds Averaged Navier–Stokes (RANS) based combustion models which have been successfully applied for a variety of combustion plants. However, in the region above the fuel bed and in small-scale biomass combustion applications (size-range $< 500 \text{ kW}_{\text{th}}$), the gas phase mixing and reaction progress is highly influenced by laminar and low turbulence zones. Here, the EBU gas phase combustion models, which are originally developed for highly turbulent flows, are not valid, leading to wrong predictions of the reaction progress and wrong concentrations of gas species (CO, NO_x species, etc.).

Therefore, an advanced hybrid gas phase reaction model was developed which is sensitive regarding local flow conditions. The hybrid model benefits from the combined finite rate kinetics (FRK) (i.e. the effects of turbulent fluctuations are neglected in the reaction rate prediction) as well as Eddy Dissipation Concept (EDC) (i.e. the effects of turbulent fluctuations are considered in the reaction rate prediction) models by means of the weighting functions in dependence of turbulent Reynolds number of the flow. The weighting functions determine the influence of turbulence on the overall reaction rate prediction. Therefore, the reaction rate prediction in low turbulence zones is mainly controlled by the FRK model while, in highly turbulence areas the performance of the model is identical to EDC. The hybrid model has been extensively validated for a series of diffusion methane jet flames covering laminar (Flame A), moderately turbulent (Flame B), and highly turbulent flow (Sandia Flame D) conditions. The simulation results showed that the prediction of a flame can be improved with the proposed hybrid combustion model. The weighting factors in the hybrid model are a function of the turbulent Reynolds number of the flow. This imposes problems in the near wall region, where the flow cannot be sufficiently resolved. It is the case in most of the real-scale combustion applications with wall-bounded flows. The reaction rate in the near wall cells is mainly controlled by the contribution of viscous and Reynolds stresses. Therefore, the hybrid model was further extended to account the near wall combustion condition.

Generally, the gas phase combustion models are very sensitive to the boundary conditions. In terms of biomass combustion, they are more sensitive to the boundary conditions at the surface of the fuel bed (turbulence and mixing degree) which are commonly provided by state-of-the-art CFD-based packed bed models. State-of-the-art packed bed models supply continuous concentration profiles as boundary conditions for subsequent CFD simulations of gas phase, leading to pre-mixed combustion conditions. However, in reality the “porous” nature of the packed bed leads to streak formation influencing gas mixing and combustion. Therefore, in order to account for the influence of the streaks on gas phase combustion, a gas streak model which is a correlation between the local gas residence time and a mixing time was developed based on numerical simulations. Moreover, the hybrid model was linked with the streak formation model and applied for the simulations of a pilot-scale grate furnace (nominal boiler load: $155 \text{ kW}_{\text{th}}$) and a small-scale under-feed stoker furnace (nominal boiler load: $20 \text{ kW}_{\text{th}}$). The predicted results are in good agreement with the measured values concerning CO and NO_x emissions. The streak formation model in combination with the hybrid gas phase combustion model showed a clear potential for an

improved NO_x prediction since it considers species mixing and reaction processes above the fuel bed with a higher accuracy.

Additionally, as a part of this thesis, a basic design tool for the automatic performance of parameter studies for the optimisation of biomass combustion plants was developed. The model consists of parameterisation and optimisation routines linked with an empirical packed bed combustion model as well as gas phase CFD models especially adapted for biomass grate furnaces. The CFD models applied for the simulation of turbulent reactive flow include: the Realizable k- ϵ Model for turbulence, the Discrete Ordinates Model for radiation and the Eddy Dissipation Model in combination with a global methane 3-step mechanism. This approach is numerically robust and reasonably accurate for most industrial applications, especially, it is very fast in terms of calculation time which is very important at the initial stage of design process for furnace manufactures. Finally, the routine developed was applied for the optimisation of a pilot-scale biomass grate furnace (nominal boiler load: 180 kW_{th}). The main focus was on the minimisation of CO emissions and the pressure loss by changing the diameter and angle of the secondary air nozzles. In order to combine the two optimisation variables (CO emissions and pressure loss over the secondary air nozzles) a weight function was defined according to their respective limits in a common function. The simulation results showed that the time of the optimisation process can be reduced considerably by the automatic routine developed and the evaluation of several independent design parameters is possible. This new procedure forms an important milestone towards automatic CFD-based furnace and boiler optimisations in the future.

Improved gas phase CFD simulation of biomass packed bed combustion

Ali Shiehnejadhesar

Institute of Process and Particle Engineering
Graz University of Technology
Inffeldgasse 21b, A 8010 Graz

This thesis is based on the following appended papers, in the text referred to by their Roman numerals I-V:

I Development of a gas phase combustion model suitable for low and high turbulence conditions

A. Shiehnejadhesar, R. Mehrabian, R. Scharler, G.M. Goldin, I. Obernberger
Fuel 2014;126:177-187

II Development of a streak formation model for an improved prediction of gas phase combustion in biomass grate furnaces

A. Shiehnejadhesar, R. Mehrabian, R. Scharler, I. Obernberger
10th European Conference on Industrial Furnaces and Boilers – Porto, Portugal, April 2015

III Development and validation of CFD models for gas phase reactions in biomass grate furnaces considering gas streak formation above the packed bed

A. Shiehnejadhesar, R. Scharler, R. Mehrabian, I. Obernberger
Fuel Processing Technology 2015;139:142-158

IV A new innovative CFD-based optimisation method for biomass combustion plants

A. Shiehnejadhesar, K. Schulze, R. Scharler, I. Obernberger
Biomass and Bioenergy 2013;53:48-53

V Automatic CFD optimisation of biomass combustion plants

A. Shiehnejadhesar, K. Schulze, R. Scharler, I. Obernberger
Proceedings of the 20th European Biomass Conference & Exhibition, June 2012, Milano, Italy, ISBN 978-88-89407-54-7, pp 756-760, ETA Renewable Energies (Ed.), Italy

Author's contribution

Paper I

The author performed the literature survey and model development. The code development and the flame simulations were accomplished by the author. The author performed the data post-processing and was responsible for preparation of the manuscript.

Paper II

The author performed the model development. All simulations were performed by the author. The author made the simulations post-processing and was responsible for preparation of the manuscript.

Paper III

The author performed the literature survey and model development. All simulations were accomplished by the author. The author performed the simulations post-processing and was responsible for preparation of the manuscript.

Paper IV and V

The author performed the model development. The simulations and post-processing of the data were accomplished by the author. The author was responsible for preparation of the manuscript.

Additional publication of relevance although not included in the thesis:

Papers in refereed journals

R. Mehrabian, A. Shiehnejadhesar, R. Scharler, I. Obernberger. Multi-physics modelling of packed bed biomass combustion. *Fuel* 2014;122:164-178

Workshops

A. Shiehnejadhesar. CFD optimisation of biomass combustion plants, lecture at the IEA Bioenergy Task 32 workshop: CFD aided design and other design tools for industrial biomass combustion plants organised in the framework of the 21st European Biomass Conference and Exhibition, June 2013, Copenhagen, Denmark

Conference proceedings

R. Mehrabian, A. Shiehnejadhesar, R. Scharler, I. Obernberger. Numerical modelling of biomass grate furnaces with a particle based model. *10th European Conference on Industrial Furnaces and Boilers – Porto, Portugal, April 2015*

Contents

Nomenclature	II
1 Introduction and objectives	1
2 Methodology	4
2.1 State-of-the-art CFD modelling of biomass combustion plants	5
2.1.1 Packed bed combustion modelling	5
2.1.2 Gas phase combustion modelling	6
2.1.2.1 The Eddy Dissipation Model (EDM)	7
2.1.2.2 The Eddy Dissipation Concept (EDC)	9
2.2 Hybrid gas phase combustion model	11
2.2.1 EDC model sensitivity analysis	11
2.2.2 Bulk flow	13
2.2.3 Near wall combustion approach	14
2.3 Streak formation model	17
2.3.1 Derivation of streak formation model constants	20
2.4 Routine for automatic CFD optimisation of biomass combustion plants	26
2.4.1 CFD model for biomass grate furnaces	26
2.4.2 Optimisation function	26
3 Modelling results – executive summary	29
3.1 Hybrid gas phase combustion model (Paper I)	29
3.1.1 Grid independency and effect of kinetic mechanisms	29
3.1.2 Molecular diffusion effect	30
3.1.3 Evaluation of the standard EDC at low Reynolds conditions	30
3.1.4 Test of the hybrid combustion model	32
3.2 Development of a streak formation model for an improved prediction of gas phase combustion in biomass grate furnaces (Papers II and III)	34
3.2.1 Model validation and application for a 150 kW _{th} grate furnace (paper II)	35
3.2.2 Model validation and application for a 20 kW _{th} under-feed stoker furnace (paper III)	38
3.3 Automatic CFD optimisation of biomass combustion plants (Papers IV and V)	45
4 Summary and conclusions	51
Bibliography	55
Annex	62

Nomenclature

Symbol	Unit	Description
A	$[(\mu\text{LL}^{-1})^{-2}]$	model constant of the weight function
B	$[\text{Pa}^{-1}]$	model constant of the weight function
$C_{j,r}$	$[\text{kgmol}\cdot\text{m}^{-3}]$	molar concentration of each reactant and product species j in reaction r
C_γ	[-]	EDC model constant
C_{D1}	[-]	EDC model constant
C_{D2}	[-]	EDC model constant
C_τ	[-]	EDC model constant
C_{fm}	[-]	tracer gas concentration in the fully mixed gas
$C_{(t)}$	[-]	local tracer gas
$D_{i,m}$	$[\text{m}^2\cdot\text{s}^{-1}]$	diffusion coefficient for species i in the mixture
D_b	$[\text{m}^2\cdot\text{s}^{-1}]$	molecular diffusivity
D_t	$[\text{m}^2\cdot\text{s}^{-1}]$	turbulent diffusivity
d_v	[m]	volume diameter
\bar{J}_i	$[\text{kg}\cdot\text{m}^{-1}\cdot\text{s}^{-1}]$	diffusion flux of species i
$K_{f,r}$	$[\text{s}^{-1}]$	forward rate constant for reaction r
$K_{b,r}$	$[\text{s}^{-1}]$	backward rate constant for reaction r
K	$[\text{m}^2\cdot\text{s}^{-2}]$	turbulent kinetic energy
\dot{m}	$[\text{kg}\cdot\text{s}^{-1}]$	mass flow rate
$M_{w,i}$	$[\text{kg}\cdot\text{kmol}^{-1}]$	molecular weight
MS	[-]	mixing state
MF	[-]	mixing function
N	[-]	number of species
N_R	[-]	number of reactions
Re	[-]	Reynolds number
Re_t	[-]	turbulent Reynolds number
Re_p	[-]	particle Reynolds number

R_i	$[\text{kg}\cdot\text{m}^{-3}\cdot\text{s}^{-1}]$	net rate of production of species i by chemical reaction
$\bar{R}_{i,r}$	$[\text{kgmol}\cdot\text{m}^{-3}\cdot\text{s}^{-1}]$	molar rate of creation/destruction of species i in reaction r
S_{ϕ_k}	$[\text{kg}\cdot\text{m}^{-3}]$	source term
S_{ct}	[-]	Schmidt number
t	[s]	residence time
Δt	[s]	time step
T	[K]	temperature
T_r	[-]	time scale ratio
u	$[\text{m}\cdot\text{s}^{-1}]$	fluid velocity
UDF	[-]	user-defined function
UDS	[-]	user-defined scalar
V	$[\text{m}^3]$	volume
V^\bullet	$[\text{m}^3\cdot\text{s}^{-1}]$	volumetric flow rate
Y_i	[-]	mass fraction of species i
Y_{CO}	$[\mu\text{LL}^{-1}]$	mole fraction of CO ($[\mu\text{LL}^{-1}]$ corresponds to [ppmv] in non-SI unit)

Greek symbols:

ε	$[\text{m}^2\cdot\text{s}^{-3}]$	turbulent dissipation rate
γ	[-]	length fraction of EDC fine scale
ν	$[\text{m}^2\cdot\text{s}^{-1}]$	kinematic viscosity
$\nu'_{i,r}$	[-]	stoichiometric coefficient for reactant i in reaction r
$\nu''_{i,r}$	[-]	stoichiometric coefficient for product i in reaction r
ρ	$[\text{kg}\cdot\text{m}^{-3}]$	density
τ_{EDC}	[s]	EDC time scale
\vec{v}	$[\text{m}\cdot\text{s}^{-1}]$	velocity vector
ϕ_k	[s]	scalar quantity (residence time)
Γ_k	$[\text{m}^2\cdot\text{s}^{-1}]$	diffusion coefficient
μ_t	$[\text{kg}\cdot\text{m}^{-1}\cdot\text{s}^{-1}]$	turbulent viscosity
μ_l	$[\text{kg}\cdot\text{m}^{-1}\cdot\text{s}^{-1}]$	laminar viscosity

Subscripts:

b,r	backward reaction
EDC	Eddy dissipation concept
EDM	Eddy dissipation model
FRK	Finite rate kinetics
f,r	forward reaction
i	species index
r	reaction
t	turbulent

1 Introduction and objectives

The production and supply of energy is one of the greatest concerns of human society. With regard to the facts that the fossil fuel resources are depleting rapidly, the necessity to find new energy resources is indispensable. During recent decades, the share of energy production by biomass combustion plants has been growing, because biomass is a CO₂ neutral source of energy in a sustainable agriculture/forestry system. A better understanding of the conversion processes involved in biomass combustion is necessary due to the increasing interest in improving the efficiency of combustion systems and reducing pollutant emissions. However, the combustion of biomass fuels in comparison with fossil fuels leads to higher emissions of particulate matter and higher NO_x emissions, the latter originating mainly from the fuel-bound nitrogen. Moreover, the general tendency towards the utilisation of agricultural biomass fuels with higher fuel-nitrogen content worsens the situation. Therefore, the further development and optimisation of biomass combustion technology is important and is not an easy task. This is due to the complex biomass conversion in the fuel bed on the grate, the reactive flow in the freeboard, and the intensive interaction between them. The increasing efficiency of computers and numerical methods is making the application of computational fluid dynamics (CFD) more attractive as a predictive tool among engineers for design and optimisation of biomass combustion plants.

The present work aims at the development and validations of advanced CFD based engineering tools suitable for simulation and optimisation of biomass packed-bed furnaces, whereas the following objectives were desired:

1. Development and validation of advanced gas phase combustion models for an improved gas phase prediction in biomass combustion plants including:
 - a) Hybrid gas phase combustion model suitable for low as well as high turbulence conditions
 - b) Streak formation model to account for the effect of flue gas streaks arising from the packed bed
2. Development of a basic design tool for the automatic performance of parameter studies for the optimisation of biomass combustion plants

At first, it should be noted that in packed-bed combustion the term “combustion” denotes both the thermal conversion of solid fuel in the packed bed and the combustion of the product gas released from the packed bed in the combustion chamber. In reality these processes interact. However, the interaction is usually not accounted for in the CFD modelling of the combustion process in the biomass packed bed furnaces [1], [2], [3] and [4]. The thermal conversion of solid fuel in the packed bed and the combustion processes in the gas phase are treated separately. Hence, the surface of the packed bed represents only the boundary of the problem for the subsequent numerical simulation of gas phase combustion. The work performed in this thesis concerned the modelling of the processes related to the gas phase only, while an empirical packed-bed model was used for the description of the thermal conversion of solid biomass [5]. In the gas phase, the combustion models play an important role as models concerning flow, temperature and

gaseous emissions prediction. The eddy break-up models (EBU) are the most prevalent Reynolds Averaged Navier–Stokes (RANS) based combustion models which have been successfully applied for a variety of combustion plants [6], [7], [8]. The popularity of the EBU combustion models come from their low computational costs especially for industrial applications in the context of RANS simulations. However, the empirical constants in the EBU models are not universally valid and need to be adapted depending on the application [4] and [9]. The EBU model first was proposed by Spalding [10] and later modified by Magnussen and Hjertager [11]. The main assumption of the EBU model is based on infinitely fast chemistry and assumes that the reaction rate is controlled by turbulent mixing [11]. The Eddy Dissipation Concept (EDC) is an extended version of the EBU model by Magnussen [12] which can incorporate detailed chemistry in the turbulent combustion calculation. However, in the region above the fuel bed and in small-scale biomass combustion applications (size-range $< 500 \text{ kW}_{\text{th}}$), the gas phase mixing and reaction progress is highly influenced by laminar and low turbulence zones. Here, the EBU gas phase combustion models, which are originally developed for highly turbulent flows, are not valid, leading to wrong predictions of the reaction progress and wrong concentrations of gas species (CO , NO_x species, etc.). Moreover, in biomass combustion plants, combustion normally takes place above the fuel bed in the primary combustion zone and in the front of incoming secondary air jets in the secondary combustion zone as well as in interaction with the surrounding walls. This flame-wall interaction is of great importance in turbulent combustion. The presence of the wall can cause several problems that are relevant to combustion. For example, a wall may quench the flame which may lead to undesired effects such as unburned hydrocarbons.

Therefore, the **first goal** of this thesis was mainly focused on the development of a hybrid gas phase combustion model to be applicable for low as well as high turbulent combustion since it was shown that the EDC is not valid below turbulent Reynolds number of 64 [13]. The model calculates the reaction rate with the finite rate kinetics and the EDC and finally an effective reaction rate is calculated with weighting factors in dependence of the turbulent Reynolds number of the flow. The model validation was performed based on the simulation of measured methane jet flames [14] covering laminar (Flame A), moderately turbulent (Flame B), and highly turbulent flow (Sandia Flame D) conditions. The weighting factors in the hybrid model are a function of the turbulent Reynolds number of the flow. This imposes problems in the near wall region, when the flow cannot be sufficiently resolved, which is true in most of the real-scale combustion applications with wall-bounded flows involved. The reaction rate in the near wall cells is mainly controlled by the contribution of viscous and Reynolds stresses. Therefore, the hybrid model was further extended to also account for the near wall combustion condition.

Generally, the gas phase combustion models are very sensitive to the boundary condition. In terms of biomass combustion, they are more sensitive to the boundary conditions at the surface of the fuel bed (turbulence and mixing degree) which is commonly provided by state-of-the-art CFD-based packed bed models. An empirical packed-bed model is usually being used for the calculation of composition, temperature and flue gas leaving the surface of the solid biomass fuel bed [5]. The empirical packed bed model, as most of

the common packed bed models, calculates profiles of partially premixed flue gas compositions not considering spatial concentration gradients of oxygen and volatiles since the fuel particles and the surrounding space cannot be resolved. However, in reality, the amount and distribution of combustibles and oxidiser in the gas released from the biomass particles in the fuel bed are locally strongly differing. Therefore, the “porous” nature of the packed bed leads to streak formation influencing gas mixing and combustion, which is not described by state-of-the-art CFD-based packed bed models.

Consequently, the **second goal** of the thesis was concentrated on the model development to account for the influence of the streaks on gas phase mixing and reactions (combustion, NO_x formation). The streak formation model is based on a correlation between the local gas residence time and mixing time, whereas the mixing time is defined as the necessary residence time to reach the fully mixed condition above the packed bed. A CFD case study with an ideally packed bed with spheres as fuel particles and non-reacting flow was performed to numerically derive the mixing time. The particle diameter was derived from the volume to surface area ratio of pellets according to EU standard. The volatiles were represented by CO₂ released from the surface of the particles. The volatiles release rate from a single particle was approximated by the value of an in-house developed model [15] for single particle conversion. The influence of relevant parameters, like bed height, volatiles mass flow rate and particle Reynolds number (calculated with the bulk flow velocity of primary air below the bed and the particle diameter), on mixing time was investigated. The results of this case study served as look-up table for the calculation of the mixing time in dependence of different influencing parameters.

Finally, the streak formation model was linked with the hybrid gas phase combustion model and tested for a pilot-scale biomass grate furnace (nominal boiler load: 150 kW_{th}) as well as an under-feed pellet stoker furnace (nominal boiler load: 20 kW_{th}) concerning the simulation of gas phase combustion and NO_x formation.

Moreover, CFD models are being successfully applied for the optimisation of existing biomass combustion plants in order to design and improve the plants with respect to lower CO emissions, the reduction of flue gas temperature peaks, as well as increased plant efficiencies. CFD can be applied for geometry optimisation or optimisation of plant operation (e.g. variation of air staging and simulation of CO-lambda-characteristics as a basis for an optimised plant control). However, even experienced scientific personnel need a large number of time-consuming simulations during a CFD-based design cycle. A “real” optimum typically cannot be found due to the complex interactions of the influencing parameters in the plant. While automatic CFD optimisation methods have been applied for the design of cyclones [16], [17], [18] and [19], the combustion chamber of engines [20], [21] and in the field of turbo machinery [22], [23] and [24] only manual optimisation methods have been applied in the field of biomass combustion plants [25], [26] and [27] due to the high degree of complexity of the processes in the plant and thus the higher number of influencing parameters.

Hence, the **third goal** of this thesis was the development of a design tool for the automatic performance of CFD-based parameter studies for the optimisation of biomass combustion plants. The model development consists of the parametrisation routines and optimisation functions that have been linked with a developed empirical packed bed combustion model as well as gas phase CFD models especially adapted for biomass grate furnaces. The CFD models applied for the simulation of turbulent reactive flow include: the Realizable k - ϵ Model for turbulence, the Discrete Ordinates Model for radiation and the Eddy Dissipation Model in combination with a global methane 3-step mechanism. This approach is numerically robust and reasonably accurate for most industrial applications, especially, it is very fast in terms of calculation time which is very important at the initial stage of design process for furnace manufactures. A pilot-scale grate furnace (nominal boiler load: 180 kW_{th}) was used to test and verify the efficiency of the optimisation routine developed. The main focus was on the minimisation of carbon monoxide emissions and the energy demand of the secondary air fan by changing the diameter and angle of secondary air nozzles. Additionally, a weight function was introduced to combine the two optimisation variables (CO emissions and pressure loss over the secondary air nozzles) according to their relevance in a common function.

2 Methodology

An overview about state-of-the-art CFD models usually applied for the simulation of biomass combustion plants is given in section 2.1. The models include the packed bed combustion model for the thermal conversion of solid biomass described in section 2.1.1 and the CFD models for modelling of turbulent reactive flows in the freeboard presented in section 2.1.2. In the context of gas phase combustion models, the well-known Eddy Dissipation Model (EDM) and the Eddy Dissipation Concept (EDC) that are generally used for the simulation of the gas phase combustion in biomass combustion plants are explained in sections 2.1.2.1 and 2.1.2.2. However, both the EDM and the EDC models were developed for high turbulent flows and the constants of the models need to be tuned dependent on the application, therefore, the idea of having a general hybrid gas phase combustion model that is valid for a broad range of applications is proposed in section 2.2. In this context, the limitation of the EDC model at low turbulent Reynolds conditions is discussed in section 2.2.1. Then, the hybrid gas phase combustion model is introduced in section 2.2.2 which combines the finite rate kinetics (FRK) and the EDC model with weighting factors in dependence of the local turbulent Reynolds number of the flow. The hybrid model gives results which are close to the FRK model when approaching the laminar regime, while the results are close to the EDC in the high turbulence region. The weighting factors in the hybrid model are a function of the turbulent Reynolds number of the flow. This imposes problems in the near wall region, when the flow cannot be sufficiently resolved, which is true in most of the real-scale combustion applications with wall-bounded flows involved. In the near wall zones, the reaction rate is mainly depending on the contribution of the viscous and Reynolds stresses. Therefore, a further extension of the hybrid model to account for the near wall combustion conditions is presented in section 2.2.3.

Generally, the gas phase combustion models are very sensitive to boundary conditions. In terms of biomass combustion, they are more sensitive to the boundary conditions at the surface of the fuel bed (turbulence and mixing degree) which is commonly provided by state-of-the-art CFD-based packed bed models. However, the “porous” nature of the packed bed leads to streak formation influencing gas mixing and combustion, which is not described by state-of-the-art CFD-based packed bed models. Hence, a streak formation model which explicitly considers the effects of streaks on the mixing is presented in section 2.3.

Finally, a CFD-based design tool for automatic optimisation of biomass combustion plants is introduced in section 2.4. The state-of-the-art CFD models applied for the simulation of biomass grate furnaces are explained in section 2.4.1. Then, an optimisation function is presented in section 2.4.2 to combine the optimisation target variables in a common function according to their relevance.

2.1 State-of-the-art CFD modelling of biomass combustion plants

In the following, state-of-the-art CFD models applied for the simulation of biomass combustion plants are described. The simulation of biomass combustion plants can be described by the biomass conversion in the fuel bed on the grate and the reactive flow in the freeboard whereas, the thermo-chemical conversion processes taking place in the fuel bed were treated separately by means of an empirical packed-bed model [5]. In this context, firstly the empirical packed bed model used for the calculation of composition, temperature and velocity of the flue gas released from the surface of the solid biomass fuel is described. Secondly, two model combinations usually applied for the simulations of turbulent reacting flows inside the combustion chamber are explained.

2.1.1 Packed bed combustion modelling

An empirical packed bed model [5] serves for the calculation of composition, temperature and velocity of the flue gas leaving the surface of the solid biomass fuel bed. The model consists mainly of three parts. The definition of one-dimensional profiles along the grate concerning the degradation of the fuel components as well as fuel drying (part 1: based on assumptions and experimental data from test runs). In combination with the definition of the conversion parameters (based on assumptions as well as experimental and literature data), which describe the formation of the most important flue gas components CH_4 , CO , CO_2 , H_2 , H_2O , O_2 as well as the NO_x precursors NH_3 , HCN and NO (part 2), the stepwise balancing of mass and energy fluxes released from the fuel bed is possible (part 3) [5], [28] and [29]. The calculation results are used as boundary profiles for subsequent CFD simulations of the turbulent reactive flow in the furnace.

Experimental data of the combustion and release behaviour for a variety of solid biomass fuels have been gained through several measurement campaigns in a lab-scale packed bed pot furnace reactor [30] and [31]. These experimental data include the concentration profiles of the N containing species NO , NH_3 , HCN , NO_2 and N_2O released from the fuel bed over time. The measured profiles are utilised for the derivation of release functions

for the most relevant NO_x precursors measured. The release functions of fuel nitrogen depend on the local air ratio (λ), the nitrogen content of the fuel as well as the N binding in the fuel (the kind of biomass fuel). The release functions were implemented in an in-house developed empirical packed bed combustion model [30] and [31], which serves as a basis for the subsequent CFD gas phase simulation of N species conversion.

When compared to more detailed fuel bed models based either on Euler-Euler approach, e.g. [32] and [33] or Euler-Lagrange approach, [34], the applied packed-bed model describes the complex in-bed thermal conversion processes in a very simple way. However, the results of the simulation applications [5], [35], [4], [36] and [37] showed that the empirical packed bed combustion model is sufficiently accurate for the calculation of the boundary conditions for the CFD simulation of flow and gas phase combustion in the furnace when only looking for qualitative results concerning combustion chamber and air nozzle design as well as the influence of air staging and biomass fuel on NO_x formation. However, it is noted, that the processes of solid biomass combustion on the grate itself cannot be described by the empirical packed bed combustion model.

2.1.2 Gas phase combustion modelling

Two model combinations are usually used for the simulation of turbulent reacting flow in the combustion chamber. The first model combination consists of the Realisable k- ϵ model for turbulence and the EDM turbulence chemistry interaction model which is adapted for biomass combustion with a global 3-step methane mechanism [5] and [38]. This model combination is commonly used for engineering applications in terms of its simplicity and time saving calculations. The second model combination consists of the Realisable k- ϵ Model for turbulence and the EDC turbulence chemistry interaction model with C-H-O subset of the Skeletal Kilpinen97 mechanism (12 species and 25 reactions) [39], which has extensively been validated for grate furnaces [40].

For both model combinations, the Discrete Ordinates model (DO) together with the Weighted-Sum-of-Gray-Gases (WSGG) method [41] was used to consider the effect of radiation in the simulations.

To sum up, the simulations of turbulent reactive flows in biomass packed-bed furnaces were performed in the following sequence:

- Simulation of the turbulent reactive flow using EDM, which is specially adapted for biomass grate furnaces with a global 3-step reaction mechanism [5] and [38]. This simulation provided a starting solution for the next step.
- Simulation of the turbulent reactive flow using EDC and the C-H-O subset of the Skeletal Kilpinen97 mechanism (12 species and 25 reactions) [39].
- Simulation of NO_x formation in a post-processing step applying the EDC with a detailed reaction mechanism (28 species and 102 reactions in total) [40].

Here, it is worth to mention that the EDM in combination with global reaction mechanisms is not able to describe complex interactions of turbulence and multi-step reaction kinetics as given in the case of NO_x formation in biomass combustion plants.

The In-Situ Adaptive Tabulation (ISAT) algorithm by Pope [42] has been used to speed-up the CPU-intensive treatment of the detailed reaction kinetics for the EDC simulations.

A detailed description of the EDM and the EDC models is provided in sections 2.1.2.1 and 2.1.2.2.

2.1.2.1 The Eddy Dissipation Model (EDM)

The EDM model by Magnussen and Hjertager [11] is a turbulence chemistry interaction model based on the Eddy Break-Up model of Spalding [10]. The EDM provides a closure for the chemical source term under the assumption of mixing limited combustion. The latter means that the chemical reactions are fast and the overall rate of reaction is controlled by the turbulent mixing rate. Hence, the eddy dissipation rate ε/k is proportional to the mixing and reaction rate, respectively. At first, the EDM was formulated for a single-step, infinitely fast irreversible reaction. The model was extended later on to take into account global reaction kinetics.

For a multi-component system, the species mass conservation equation is defined as follows:

$$\frac{\partial}{\partial t}(\rho Y_i) + \nabla \cdot (\rho \vec{v} Y_i) = -\nabla \cdot \vec{J}_i + R_i \quad \text{Eq. 2-1}$$

where ρ is the mixture density, Y_i is the mass fraction of species i , \vec{v} is the velocity vector, R_i is the net rate of production of species i by the chemical reactions, and \vec{J}_i is the diffusion flux of species i due to concentration gradients defined as:

$$J_i = -\left(\rho D_{i,m} + \frac{\mu_t}{Sc_t} \right) \nabla Y_i \quad \text{Eq. 2-2}$$

where the first term on the right-hand side of Eq. 2-2 is the molecular diffusion and the second term expresses the turbulent diffusion. The term, $D_{i,m}$ is the mass diffusion coefficient for species i in the mixture, and $Sc_t = \mu_t / \rho D_t$ is the turbulent Schmidt number (where μ_t is the turbulent viscosity and D_t is the turbulent diffusivity).

In ANSYS FLUENT, the net rate of production of species i due to reaction r , R_i , is given by the minimum of two rates:

$$R_i = \min((R_i)_{EDM}, (R_i)_{FRK}) \quad \text{Eq. 2-3}$$

where $(R_i)_{EDM}$ stands for the eddy dissipation rate and $(R_i)_{FRK}$ denotes the Arrhenius rate. The net reaction source of chemical species i is computed as the sum of the Arrhenius reaction sources over the N_R reactions that the species participates in:

$$(R_i)_{FRK} = M_{w,i} \sum_{r=1}^{N_R} \bar{R}_{i,r} \quad \text{Eq. 2-4}$$

Where $M_{w,i}$ is the molecular weight of species i and $\bar{R}_{i,r}$ is the Arrhenius molar rate of creation/destruction of species i in reaction r. The molar rate of creation/destruction of species i in reaction r ($\bar{R}_{i,r}$ in Eq. 2-4) is determined:

$$\bar{R}_{i,r} = (v''_{i,r} - v'_{i,r}) \left[k_{f,r} \prod_{j=1}^N [C_{j,r}]^{\eta'_{j,r}} - k_{b,r} \prod_{j=1}^N [C_{j,r}]^{v''_{j,r}} \right] \quad \text{Eq. 2-5}$$

where N is the number of chemical species in the system, $v'_{i,r}$ is the stoichiometric coefficient for reactant i in reaction r, $v''_{i,r}$ is the stoichiometric coefficient for product i in reaction r, $k_{f,r}$ is the forward rate constant for reaction r and $k_{b,r}$ is the backward rate constant for reaction r, $C_{j,r}$ is the molar concentration of species j in reaction r, and $\eta'_{i,r}$ is the rate exponent for reactant species j in reaction r.

The eddy dissipation rate is determined as the lowest (i.e., limiting) value of the mixing rates:

$$(R_i)_{EDM} = v'_{ir} M_{w,i} A_{mag} \rho \frac{\varepsilon}{k} \min \left(\min_{re} \left(\frac{Y_{re}}{v'_{re,r} M_{w,re}} \right), B_{mag} \frac{\sum_{pr} Y_{pr}}{\sum_i v''_{i,r} M_{w,i}} \right) \quad \text{Eq. 2-6}$$

where 're' denotes a particular reactant species and 'pr' stands for any product species in reaction r, Y_p is the mass fraction of any product species P and Y_R is the mass fraction of a particular reactant R. The expression above is a more general formulation of a simple 'fuel and oxidiser to product' system. In case of a single step global reaction, the eddy dissipation rate is related either to the break-up of the 'fuel' eddies or to the break-up of the 'oxidiser' eddies or to the decay of the 'product' eddies. Hence, the availability of the fuel, oxidiser or hot reaction products limits the reaction rate. The Arrhenius rate $(R_i)_{FRK}$ is determined without taking turbulent fluctuations into account. The Arrhenius rate was included (Eq. 2-3) as the rate-limiting step solely to prevent the rapid reaction progress at the inlet boundary of a premixed combustion problem.

The EDM is numerically robust and reasonably accurate for most industrial applications but cannot account for the strong coupling between turbulence and reaction kinetics. Furthermore, only global reaction mechanisms restricted to a few reaction steps can be meaningfully treated by EDM. Therefore, the EDM in combination with global reaction mechanisms is not able to describe complex interactions of turbulence and multi-step

reaction kinetics as given in case of NO_x formation in biomass combustion plants. Another important disadvantage of EDM is that the model constants, A_{mag} = 4 and B_{mag} = 0.5 are not universally valid. Usually, the model constant A_{mag} needs to be tuned in order to obtain reasonable results for a problem of interest.

2.1.2.2 The Eddy Dissipation Concept (EDC)

The EDC by Magnussen [12] represents an advancement of the EDM. The EDC is a more general model that allows detailed reaction kinetics to be considered. The EDC is based on the turbulent energy cascade, which means that larger eddies break up into smaller eddies and the reactions take place in the so-called fine structures, where the fluid is mixed on a micro-scale. In the EDC, the fluid is divided into the volume fraction of the fine structures $\gamma^* = \gamma^3$, where the reactions take place and the volume fraction $\gamma_0 = (1 - \gamma^3)$ of the surroundings, which are considered as inert. Hence, all reactions in the surrounding fluid are neglected. This assumption is the main simplification of the model [43].

The length fraction γ of fine scales is modelled as:

$$\gamma = C_\gamma \left(\frac{\nu \varepsilon}{k^2} \right)^{0.25} \quad \text{Eq. 2-7}$$

where C_γ is

$$C_\gamma = \left(\frac{3C_{D2}}{4C_{D1}^2} \right)^{0.25} = 2.1377, \quad \text{with } C_{D1} = 0.134, C_{D2} = 0.5 \quad \text{Eq. 2-8}$$

The time scale for the mass transfer from the fine structures to the surrounding fluid (i.e. the reactor residence time) is:

$$\tau_{EDC} = C_\tau \left(\frac{\nu}{\varepsilon} \right)^{0.25} \quad \text{with } C_\tau = \left(\frac{C_{D2}}{3} \right)^{1/2} = 0.4082 \quad \text{Eq. 2-9}$$

Here, ν is the kinematic viscosity; ε is the turbulent dissipation rate and k the turbulent kinetic energy.

The length fraction and the time scale sizes in terms of turbulent Reynolds number ($Re_t = k^2/\nu\varepsilon$) can be written as follows:

$$\gamma = C_\gamma (Re_t)^{-1/4} \quad \text{Eq. 2-10}$$

and

$$\tau_{EDC} = C_\tau Re_t^{-1/2} \frac{k}{\varepsilon} \quad \text{Eq. 2-11}$$

There are two different approaches for the calculation of the mass exchange between the fine structures and the surroundings. The first one is γ^3/τ_{EDC} [12], while the expression γ^2/τ_{EDC} has been used in recent papers [43] and [44]. The latter expression is derived assuming that the fine structures exchange mass mainly with fine structure regions and not with the whole surrounding flow [44]. The latter expression is used because it has shown better agreement with experimental data [43] and [44]. The fraction of fine structure is larger using latter expression rather than the first one. This is more realistic in situations with low turbulence level and slow chemistry [43]. Therefore, the source term in the species mass conservation equation (Eq. 2-1) for the mean species i based on the recent formulation is modelled as [44];

$$(R_i)_{EDC} = \rho \frac{\gamma^2 \chi}{\tau_{EDC}} (Y_i^* - Y_i^0) \quad \text{Eq. 2-12}$$

where Y^0 is the surrounding mass fraction of species i and Y^* is the fine structure mass fraction of species i . The term χ designates the fraction of the fine structure that is heated sufficiently and may react. The parameter χ accounts for finite-rate chemistry effects when the fast chemistry assumption is used. Since chemical kinetics (detailed and reduced) are used in this thesis the value of $\chi = 1$ is used. Gran [44] and [45] proposed that by setting the value of $\chi = 1$, the amount of reaction is controlled by chemistry.

The relation between the mass-averaged state and the surrounding species mass fraction is computed as [45]:

$$\bar{Y}_i = \gamma^3 Y_i^* + (1 - \gamma^3) Y_i^0 \quad \text{Eq. 2-13}$$

The surrounding species mass fraction can be obtained from Eq. 2-13 as following:

$$Y_i^0 = \frac{\bar{Y}_i - \gamma^3 \chi Y_i^*}{(1 - \gamma^3 \chi)} \quad \text{Eq. 2-14}$$

Now by substituting the surrounding species mass fraction (Eq. 2-14) into Eq. 2-12, the final expression for the mean chemical reaction rate can be re-written as following:

$$(R_i)_{EDC} = \frac{\rho \gamma^2}{\tau_{EDC} (1 - \gamma^3)} (Y_i^* - \bar{Y}_i) \quad \text{Eq. 2-15}$$

In the original formulation of the EDC [11] and [12] the fine structures are treated as perfectly stirred reactors (PSR). This circumstance may lead to convergence problems during the iterative solution of the highly non-linear algebraic equation system and causes a considerable numerical effort. It was shown [46] that a plug flow reactor (PFR) model can be implemented in the EDC instead of a PSR, which leads to a considerable simplification of the numerical solution process. An integration of the reaction rates over the residence time (or reaction time) in the fine structures via a time-stepping method can then be used for the calculation of the fine structure values. This is the formulation of

the EDC implemented in the CFD code ANSYS FLUENT. The EDC in this form is robust and can be used with detailed reaction mechanisms. However, the model has been developed for highly turbulent flows. Besides, the EDC model constants, indeed, have a strong effect on the local combustion-rate predictions. Therefore, the applicability of the EDC in low turbulent flow is, strictly seen, not valid. The direct integration (DI) of the stiff ODE system of Eq. 2-15 is very time-consuming due to the disparity of time-scales involved in the reaction mechanism. Therefore, in combination with the EDC, ANSYS FLUENT employs the In-Situ Adaptive Tabulation (ISAT) algorithm by Pope [42] to speed-up the CPU-intensive treatment of the detailed reaction kinetics.

2.2 Hybrid gas phase combustion model

In this section, the limitation of the EDC especially at low turbulent Reynolds conditions is investigated. Then, in the bulk flow the hybrid model is introduced which combines the finite rate kinetics and the EDC model with weighting factors in dependence of the local turbulent Reynolds number of the flow. Finally, the hybrid model is further extended to account for the near wall combustion conditions in turbulent reacting wall bounded flows.

2.2.1 EDC model sensitivity analysis

The EDC was originally developed for high Reynolds combustion flows. The main assumption of the model is that the reaction takes place in the so-called fine structures, which are in the order of the Kolmogorov eddy scale, where the dissipation occurs. The EDC model was derived based on the turbulent energy cascade model for highly turbulent flows. Magnussen [11] and [12] presented the EDC cascade model with a characteristic frequency or strain rate, whereas the mechanical energy transfers from the mean flow to heat. In the EDC cascade model for the transport of mechanical energy and thermal energy from the preceding level to the following one, a constant [47] has been introduced. In [47] it is argued that since the turbulent energy cascade is an approximation, the model constants are a compromise in order to allow for the model to be representative for flows at different Reynolds numbers. Since in a turbulent model the constants are linked together, the constants of the turbulent cascade model have to depend on the constants of the other parts of the general model. In this context, the value of C_{D1} was chosen in [47] using an approximation in the turbulent cascade model so that $\frac{2}{3}C_{D1}$ equals to C_{μ} , while for the latter the value 0.09 (Standard k- ϵ Model) was taken. However, the applicability of the k- ϵ turbulence model in low Reynolds number flows is limited [48]. Moreover, the choice of the numerical values for the EDC model constants, indeed, affects the local combustion-rate prediction [47].

The main difference between two turbulent flows with different Reynolds numbers but with the same integral length scale is the size of smallest eddies. A turbulent flow at a relatively low Reynolds number has a relatively “coarse” small-scale structure [49]. Hence, at low Reynolds flow conditions, where large and small scales of turbulence are very close to each other, the applicability of the EDC model should be revised.

The influence of the EDC model constants has been reported in a few recent works [13], [50], [51], [52], [53] and [54]. Rehm et. al [50] reported the capability of the EDC for gasification modelling. They found that C_τ had almost no impact, whereas C_γ had a strong impact on the mean reaction rate and their results were improved by increasing the C_γ constant. De et al. [13] performed a systematic EDC model sensitivity concerning the model constants. The outcomes of their study indicated that the EDC is not valid below a turbulent Reynolds number of 64. They performed a numerical investigation of turbulent natural gas combustion for a jet in a coflow of lean combustion products in the Delft-Jet-in-Hot-Coflow (DJHC) burner which emulates MILD (Moderate and Intense Low Oxygen Dilution) combustion at different jet Reynolds numbers ($Re = 4100$ and $Re = 8800$) and found too early ignition with the standard EDC model constants. They showed that the predictions could be improved if C_τ is increased to 3 and C_γ is decreased to 1.0. Graça et al. [51] made a simulation of turbulent natural gas combustion in a reversed flow small-scale combustor with the EDC and found a delayed ignition with the standard model constants. They demonstrated the dominating role of C_γ to improve the results in comparison with experiments. Shabaniyan et al. [52] confirmed the outcomes of De et al. [13] and used the modified C_τ constant proposed by [13], [53] and [54] for the simulation of an ethylene jet flame in diluted and heated oxidant stream combustion conditions. They displayed that a modified EDC leads to reasonable results with relatively low computational effort. Hence, when the EDC model is used in CFD calculations, it turns out that the constants C_τ and C_γ must be “tuned” within a wide range in order to obtain reasonable results for a particular problem.

Therefore, it is of interest to investigate the sensitivity and the validity of the EDC to the model constants C_τ and C_γ . The model constant C_τ appears as a multiplication factor in the EDC time scale (Eq. 2-11) as well as in the reaction rate term (Eq. 2-15). In the EDC, the reaction rate for the chemical species was assumed to be a linear function of the mass transfer between the fine structures and the surroundings [47]. However, it is clear from (Eq. 2-15) that the characteristic time scale in the EDC model is larger than τ_{EDC} :

$$\frac{1}{\tau_{mix}} = \frac{\gamma^2}{(1-\gamma^3)} \frac{1}{\tau_{EDC}} \quad \text{Eq. 2-16}$$

Now, by definition of the time scale ratio (T_{ratio}), Eq. 2-16 can be re-arranged as following:

$$T_{ratio} = \frac{\tau_{EDC}}{\tau_{mix}} = \frac{\gamma^2}{(1-\gamma^3)} \quad \text{Eq. 2-17}$$

From a physical point of view, the mixing time scale τ_{mix} should be greater than the EDC time scale. Therefore, for consistency, T (and γ) should be lower than one:

$$T_{ratio} = \frac{\gamma^2}{(1-\gamma^3)} < 1 \Rightarrow \gamma < 0.75 \quad \text{Eq. 2-18}$$

This implies that the fine scale length fraction (Eq. 2-7) should be less than 0.75. Now by re-arranging Eq. 2-7 in terms of turbulent Reynolds number (Eq. 2-10), the following expression can be obtained:

$$C_\gamma (\text{Re}_t)^{-1/4} < 0.75 \rightarrow \text{Re}_t > 64 \quad \text{Eq. 2-19}$$

Figure 2.1 shows the sensitivity of γ and the time scale ratio on the turbulent Reynolds number. It can be inferred from the figures that the model is limited to turbulent Reynolds numbers larger than 64. Besides, supposing that the maximum value for the fine scale length fraction is one (reaction takes place in the whole CFD computational cell), the model still has no value for the fine scale length fraction at turbulent Reynolds numbers lower than 20 (see Figure 2.1).

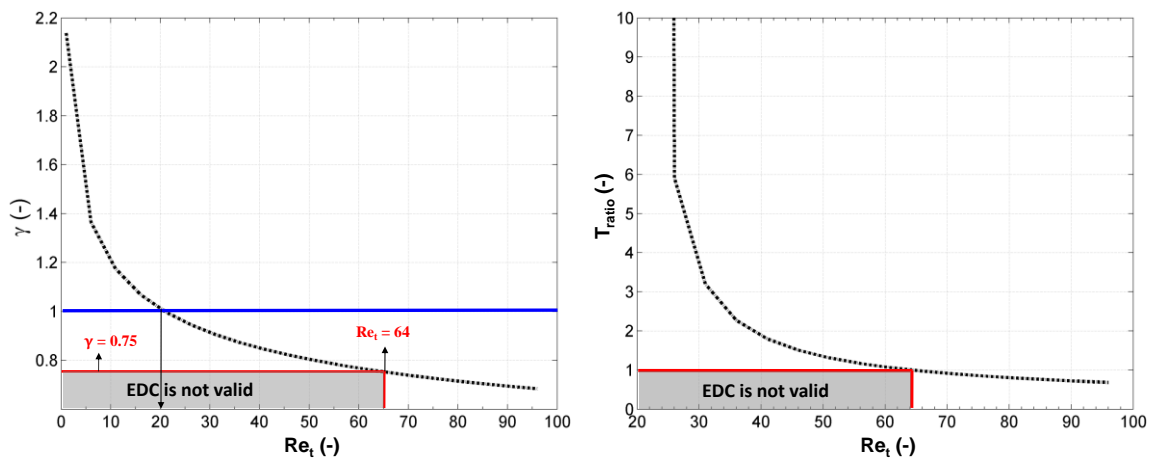


Figure 2.1: Dependence of γ (Eq. 2-10) (left) and T_{ratio} (Eq. 2-17) (right) on turbulent Reynolds number

As explained earlier, the assumptions of the EDC model at low turbulence flow are no longer valid. The model has no value for γ at turbulent Reynolds numbers lower than 64. Moreover, it is not an easy task to tune the model constants to be used universally since it might be changed for a particular application. Therefore, a general hybrid gas phase combustion model that is valid over a wide range of turbulent Reynolds numbers is proposed in section 2.2.2.

2.2.2 Bulk flow

Based on the outcomes of the EDC sensitivity analysis (see section 2.2.1), the necessity of a model which should be valid for all flow conditions is inevitable. The idea of such a reaction model which utilises the benefits of both the FRK and the EBU model first was proposed by Spalding [10]. The concept is to develop a hybrid reaction model to be sensitive to the local turbulent Reynolds number of flow. Therefore, a hybrid reaction model as a combination of both FRK as well as EDC models has been introduced based on the idea of Spalding [10]. In the hybrid model, the mean chemical reaction (second term in the right hand side of Eq. 2-1) is modelled as:

$$(R_i)_{hybrid} = \left(\frac{1}{1+Re_t} \right) (R_i)_{FRK} + \left(\frac{Re_t}{1+Re_t} \right) (R_i)_{EDC} \quad \text{Eq. 2-20}$$

where $(R_i)_{FRK}$ is the FRK mean reaction rate (Eq. 2-4) and the term $(R_i)_{EDC}$ is the mean reaction rate calculated by the EDC model (Eq. 2-15).

In the laminar range the reaction rate is calculated with pure finite rate kinetics and in the highly turbulent region with the EDC. In the transition region around $Re_t = 64$, the overall reaction rate is calculated as the sum of the weighted reaction rates of finite rate kinetics and the EDC. In other words, the overall reaction rate is determined as a linear combination of the two reaction rates.

The weighting factors $(1/(1+Re_t))$ and $(Re_t/(1+Re_t))$ are model parameters of a weight function which gave the best agreement with measurements for flames A, B and D (see *Paper I*). The effect of weighting factors in Eq. 2-20 on the reaction rate as a function of turbulent Reynolds number is shown in Figure 2.2. For instance, at zero turbulence ($Re_t \rightarrow 0$), the transition parameter $(Re_t/(1+Re_t) \rightarrow 0)$ while the transition parameter $(1/(1+Re_t) \rightarrow 1)$ and the reaction rate is controlled by the chemistry and vice versa.

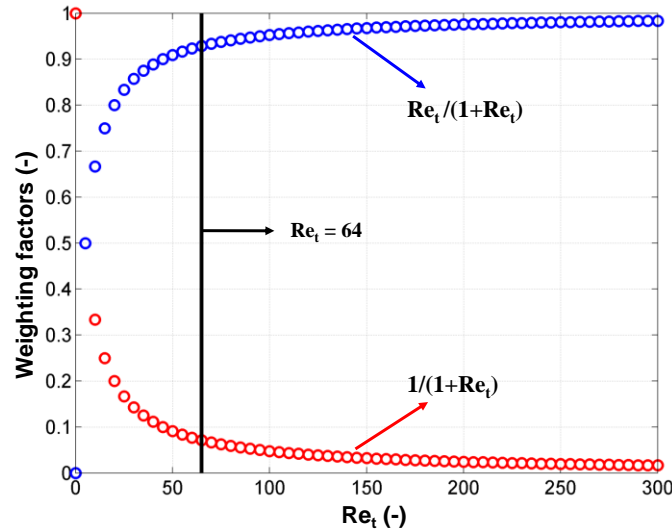


Figure 2.2: Effect of turbulent Reynolds number on the weighting factors in the hybrid model

2.2.3 Near wall combustion approach

In the hybrid gas phase reaction model, the overall reaction rate is calculated by a weighted reaction rate. The hybrid model gives results which are close to the FRK model when approaching the laminar regime, while the results are close to the EDC in the high turbulence region. The weighting factors in the hybrid model are a function of the turbulent Reynolds number of the flow. This imposes problems in the near wall region, when the flow cannot be sufficiently resolved, which is true in most of the real-scale combustion applications with wall-bounded flows involved. One challenge in CFD is how to treat the thin near-wall sublayer, where viscous effects are important. Generally, in

turbulent wall flows, two distinct zones exist near the wall. Firstly, the viscous sublayer which is completely dominated by viscous effects. The so-called “outer region” shows a nearly constant velocity with distance from the wall. Figure 2.3 (left) shows the distinct areas existing near the wall in turbulent wall flows. A non-dimensional wall distance (y^+) is used to differentiate the regions that exist near the wall. The y^+ can be interpreted as a local Reynolds number with the wall distance as length scale, so its magnitude defines also the relative importance of viscous and turbulent processes [55]. To support this hypothesis, Figure 2.3 (right) shows the fractional contributions of viscous and Reynolds stresses to the total stress in the near-wall region of a channel flow taken from [55] and [56]. When the stresses are plotted against y^+ , the profiles depicted for two Reynolds numbers almost collapse. The viscous contribution drops from 100% at the wall ($y^+=0$) to 50% at $y^+=12$ and is less than 10 at $y^+=50$.

Therefore, an accurate resolution of this layer can be crucial. This is due to the steep gradient of the mean values (e.g. transport of mean momentum and other parameters) that occur in the boundary layer. There are two approaches to model the near-wall-region. The most reliable way is to use modified turbulence models (e.g. low-Re-number turbulence models) to resolve viscosity-affected region (i.e. near wall regions) with a mesh which is fine enough to resolve the steep gradients near the wall, including the viscous sublayer. However, this can be computationally very expensive, particularly in 3D cases. Hence, the traditional industrial solution is to use wall-functions for flow modelling. Enhanced wall treatment is a near-wall modelling method that combines a two-layer model (i.e. linear (laminar) and logarithmic (turbulent)) with enhanced wall functions. The method formulates the law-of-the-wall as a single wall law for the entire wall region. ANSYS® FLUENT® achieves this by blending the linear (laminar) and logarithmic (turbulent) laws-of-the-wall using a function suggested by Kader [57] as follows:

$$u^+ = e^{\Gamma} u_{\text{laminar}}^+ + e^{\frac{1}{\Gamma}} u_{\text{turbulent}}^+ \quad \text{Eq. 2-21}$$

where Γ is a blending function in dependence of y^+ and is given by:

$$\Gamma = -\frac{0.01(y^+)^4}{1+5y^+} \quad \text{Eq. 2-22}$$

where u_{laminar}^+ and $u_{\text{turbulent}}^+$ are the dimensionless velocities.

The definitions of y^+ , u_{laminar}^+ and $u_{\text{turbulent}}^+$ can be found in [55]. Figure 2.4 shows the trend of the blending factors in dependence of the non-dimensional wall distance (y^+). This formula also guarantees the correct asymptotic behaviour for large and small values of y^+ and a reasonable representation of velocity profiles in the cases where y^+ falls inside the wall buffer layer.

In the hybrid combustion model defined in Eq. **2-20**, close to the wall, the turbulent Reynolds number of the flow approaches unity and the reaction rate is mainly calculated by the FRK model, despite the fact that the larger fraction of the flow in the wall near cell

is influenced by inertial forces (Reynolds stresses). Concluding, in reacting flows, it is also a problem of not sufficiently resolving the wall, which leads to the consideration of a flow regime when calculating the reacting rate, while in reality there is a rapid change of the flow regimes in the boundary layer. To avoid this, the reaction rate has to be weighted in dependence of the flow regime inside the wall cell. Therefore, the mean chemical reaction rate for the near wall cells can be adjusted by blending the FRK and EDC models using a function suggested by Kader [57] as follows:

$$(R_i)_{wall} = e^{\Gamma} (R_i)_{FRK} + e^{\frac{1}{\Gamma}} (R_i)_{EDC} \quad \text{Eq. 2-23}$$

where Γ is a blending function as defined in Eq. 2-22. The usage of y^+ in the blending function represents the concept of the local Reynolds number of the flow as earlier explained [55]. In this formulation, the FRK and the EDC are weighted according to the fractional contributions of the viscous and Reynolds stresses in the near-wall region and the overall reaction rate in the wall cell is calculated as the sum of the weighted reaction rates of the FRK and the EDC. As shown in Figure 2.4, in the laminar range ($y^+ < 5$) the reaction rate is calculated with the pure finite rate kinetics and in the turbulent region ($y^+ > 30$) with the EDC. In the transition region around $y^+ = 10$ (i.e. buffer layer), the contribution of viscous and Reynolds stresses is interchanging, therefore, the overall reaction rate in the wall cell is calculated by a combination of the two terms. Hence, the overall reaction rate is weighted by two terms as a function of y^+ .

This near wall combustion approach was implemented in the hybrid model (test and verification see **Paper II and III**).

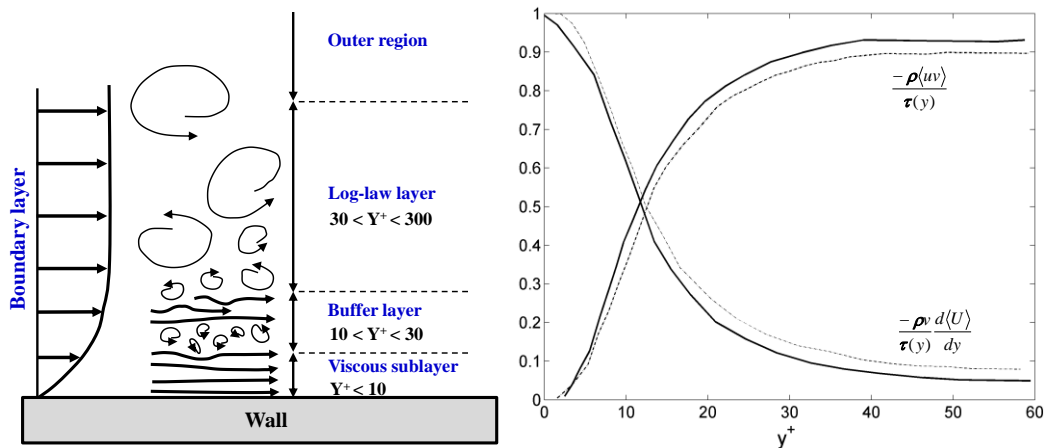


Figure 2.3: Areas of turbulent wall flows (left) and fractional contributions of viscous and Reynolds stresses to total stress in the near-wall region of a channel flow (right) (adapted from Chapter 7 in [55]) taken from [56] (dashed lines, $Re = 5600$; solid lines, $Re = 13750$)

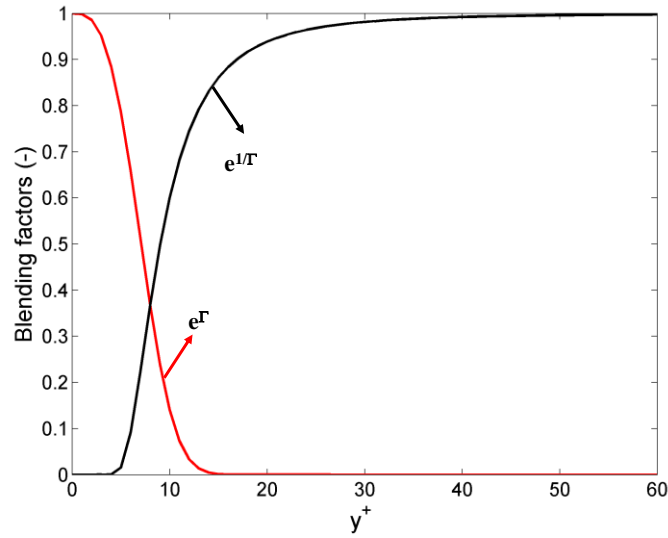


Figure 2.4: Trend of blending factors in dependence of y^+

2.3 Streak formation model

State-of-the-art packed bed models supply continuous concentration profiles as boundary conditions for subsequent CFD simulations of gas phase, leading to pre-mixed combustion conditions. However, in reality the “porous” nature of the packed bed leads to streak formation influencing gas mixing and combustion.

Therefore, in order to account for the influence of the streaks on gas phase combustion, a gas streak model based on a correlation between the local gas residence time and a mixing time has been developed based on numerical simulations. The model is based on a mixing time, where the gas streaks arising from the fuel bed are fully mixed and a correlation with the residence time of the flue gas released from the fuel bed. In order to describe the mixing process above the packed bed, a criterion has been defined to calculate the mixing state (MS) as follows:

$$MS = 1 - \frac{C_{fm} - C(t)}{C_{fm}} \quad \text{Eq. 2-24}$$

Here, C_{fm} is the tracer gas concentration (here CO_2) in the fully mixed gas and $C(t)$ is the local tracer gas (CO_2) concentration in dependence of the mixing time. The residence time which is necessary to reach the defined mixing state (here, $0.99 < MS < 1.01$ has been defined) is the mixing time t_{fm} . Finally, the mixing function (MF) is the combination of the mixing time t_{fm} and the gas residence time t_{gas} :

$$MF = \min\left(\frac{t_{gas}}{t_{fm}}; 1\right) \quad \text{Eq. 2-25}$$

where

MF = 0 (completely unmixed)

MF = 1 (completely mixed)

The mixing function provides information about the mixing quality of the volatiles and the primary air, it varies between 0 (no mixing) and 1 (fully mixed). The mixing time (t_{fm}) is derived from the packed bed case studies and is a constant value (see section 2.3.1). Therefore, Eq. 2-25 can be considered as a linear correlation of t_{gas} which is bounded between 0 and 1.

A user-defined scalar approach (UDS) is used to calculate the gas residence time inside the combustion unit. The approach proved to be valid for use in modelling heating, ventilation, air conditioning and hydraulic systems [58] and [59].

$$\frac{\partial}{\partial x_i} \left(\rho u_i \varphi_k - \Gamma_k \frac{\partial \varphi_k}{\partial x_i} \right) = S_{\varphi_k} \quad \text{Eq. 2-26}$$

where, Γ_k is the coefficient and S_{φ_k} is the source term.

The diffusivity of the UDS is defined to be the same as of the flue gas since the residence time is transported and mixed with the gas flow. Therefore, in turbulent combustion flows, the diffusivity of the UDS is a function of the binary diffusivity, the turbulent and laminar viscosity, and the turbulent Schmidt number and is defined as follows [59]:

$$\Gamma_k = D_b + \frac{\mu_l + \mu_t}{Sc_t} \quad \text{Eq. 2-27}$$

where, ρ is the density of the flue gas, D_b is the binary diffusivity of the flue gas (with a value of 2.88×10^{-5} which is also applied for the diffusion coefficient of each species in the mixture), μ_l and μ_t are the laminar and turbulent viscosities of the flue gas and Sc_t is the turbulent Schmidt number (with a value of 0.7 which is also applied for the species transport equation) is defined as:

$$Sc_t = \frac{\mu_t}{\rho D_t} \quad \text{Eq. 2-28}$$

where D_t is the turbulent diffusivity of the flue gas. The effect of turbulence fluctuations is taken into account in the calculation of residence time implicitly since the effect of turbulent viscosity is considered in the diffusivity of the scalar transport equation.

At time t the mass flowrate of a fluid into a cell is m^\bullet , therefore, the value of the scalar when it enters the cell is $m^\bullet t$. When the fluid leaves the cell, its age is increased by Δt , therefore, the value of the scalar when it leaves the cell is $m^\bullet (t + \Delta t)$. In order to find the time at which the fluid leaves, a source term is required equivalent to:

$$S_{\phi_k} = \frac{\dot{m} \Delta t}{V} \quad \text{Eq. 2-29}$$

where, \dot{m} is the mass flow rate and V is the volume of the computational cell.

The source term is divided by the cell volume since it is applied on a volumetric basis. Since neither the time nor the mass flow rate through the cell is known, the following relationship could be applied to simplify the source term:

$$\dot{m} = \rho A u = \rho V^* \quad \text{Eq. 2-30}$$

where A is the area of the cell and V^* is the volumetric flowrate.

By re-arranging Eq. 2-30 we have

$$V^* = \frac{\dot{m}}{\rho} \quad \text{Eq. 2-31}$$

and since

$$\Delta t = \frac{V}{V^*} \quad \text{Eq. 2-32}$$

by substituting Eq. 2-31 into Eq. 2-32 we have

$$\Delta t = \frac{V \rho}{\dot{m}} \quad \text{Eq. 2-33}$$

Now, by substituting Eq. 2-33 into Eq. 2-29, the source term can be found as follows:

$$S_{\phi_k} = \rho \quad \text{Eq. 2-34}$$

Eq. 2-26 has been implemented by a user-defined function (UDF) in ANSYS® FLUENT®.

Finally, the effective reaction rate is calculated by multiplying the mixing function, which defines the macro-mixing state, with the reaction rate, calculated by the hybrid combustion model as following:

$$(R_i)_{Hybrid-streak} = MF \times (R_i)_{Hybrid} \quad \text{Eq. 2-35}$$

Therefore, at positions where mixing is poor the rates of homogeneous reactions are damped which leads to streaks above the bed. The term “streaks” is used to represent the definition of the mixing function.

2.3.1 Derivation of streak formation model constants

A CFD study with an ideally packed bed with spheres as fuel particles and non-reacting flow has been performed in order to numerically derive the mixing time (i.e. t_{fm}). The SST k- ω low Reynolds turbulence model is applied to cover the whole range of flow conditions from laminar to turbulent flows in biomass grate furnaces. It should be noted that the SST k- ω low Reynolds turbulence model was applied as suitable turbulence model above the packed bed to predict the mixing time since the flow is weakly turbulent. In the furnace simulation, the mixing delay due to the streaks, which is assumed to be dominating over the turbulent mixing above the bed, is considered with the streak model. Moreover, the Realizable k- ϵ model gives considerably better results concerning the mixing of round jets in gas streams [5] and [60] than the SST k- ω model. Therefore, for the furnace simulations the Realizable k- ϵ model is used as a turbulence model.

The volatiles were represented by CO₂ released from the surface of the particles in the bed. The volatiles release rate from single particles was approximated by developed layer model [15] for the conversion of thermally thick biomass particles. In this parameter study, the following influencing parameters have been investigated for a packed bed: bed height, volatile mass flow rate and bulk flow velocity of primary air below the bed. The bed height was varied by particle layers from 5 to 15 layers. During typical biomass combustion conditions with air staging the most relevant components released are H₂O, CO₂, CO, H₂ and CH₄ [61], [62] and [63]. However, during packed bed combustion, the dominant gas volume flux comes from the primary air passing through the packed bed. In CFD simulations the density of the mixture is usually considered as incompressible ideal-gas (due to the low pressure changes) and mainly depends on the temperature inside the combustion chamber that influences the volume flow rate of the volatiles released from the biomass particles. Furthermore, to qualify the effect of mixing between primary air and volatiles the volatiles composition plays no role, while the released volume flow (which depends on temperature) is important. Moreover, since a non-reacting simulation is performed, for the release rates only an average value can be estimated. Therefore, a sensitivity analysis concerning the influence of the volatiles release rate was performed. In order to cover the possible range of released volume fluxes, the estimated value of the reference case was multiplied by a factor x . A typical volatiles release rate was estimated with the layer model; for the investigation of the sensitivity of the results on the release rates, this value has been varied between a factor of 1 to 1.7. It could be shown that the influence of the release rate is comparably low.

Bulk flow velocity of primary air below the bed was varied between 0.1 and 7 (m/s). In biomass grate furnaces, the flow above the fuel bed is typically in the low Re range. Usually, the primary air velocity fed below the grate may vary between 0.1 and 7 (m/s). The values are gained from developed empirical packed bed model [5] and [29]. Therefore, to cover all ranges of flow conditions for small to large-scale biomass combustion plants, a sensitivity analysis has been performed.

The diameter of the spheres was approximated based on the volume to surface area ratio of pellets according to the respective EU standard [64] and [65]. As mentioned, the study

has been performed for pellets as fuel. However, the simulation results can be applied for all particle sizes by applying the particle Reynolds number for the look-up table where the results are summarised. Here, three parameter studies with an ideally packed bed with the different bed heights and number of particle layers, respectively, were performed in order to calculate the mixing time in dependence of the influencing parameters. Figure 2.5 shows the CFD domain of the packed bed for 5 layers considered in this study. An unstructured computational grid with 2, 4 and 6 million cells in total was used for the simulation of the packed bed with 5, 10 and 15 numbers of layers, respectively. On the surface of the particles, a number of layers with prismatic grid (10 layers) are used to resolve the viscous sublayer. It has been assured that the first grid point (the thickness of the first layer of the prismatic cells was about 0.007 mm) is located in the viscous sublayer ($y^+ < 1$). The primary air was injected below the bed with an even distribution and the volatiles represented by CO_2 as tracer gas were released from the surface of the spheres. Moreover, different planes above the bed were defined to evaluate the mixing state and mixing time. In the definition of the packed bed, the reference plane and the other planes above it are fixed at a certain height for each number of layers studied. This means that all the layers are arranged below the reference plane (see also Figure 2.5).

A simulation matrix was built for each layer to derive the mixing time based on the primary air velocity and volatiles mass flow rate. The flow simulation was performed for all primary air velocities and volatile mass flow rates. Then, the mixing state was calculated at each plane defined above the bed. Finally, the mixing time was derived based on the estimated gas residence time which is necessary to reach the defined mixing state (here, $0.99 < \text{MS} < 1.01$).

Therefore, the mixing time can be represented by influencing parameters like primary air velocity and number of layers considered in the simulations. To make the model applicable for all fuel particle sizes, the mixing time can be represented as a function of the particle Reynolds number instead of the primary air velocity. The particle Reynolds number can be defined as follows:

$$\text{Re}_p = \frac{V_{\text{primary air}} d_v}{\nu_{\text{air}}} \quad \text{Eq. 2-36}$$

where $V_{\text{primary air}}$ is the primary air released below the particles, ν_{air} is the air kinematic viscosity and d_v is the volume diameter.

The volume diameter d_v [66] can be derived based on the diameter of a sphere having the same volume as the biomass particles. The biomass particle volume can be estimated from the average size of the biomass particles.

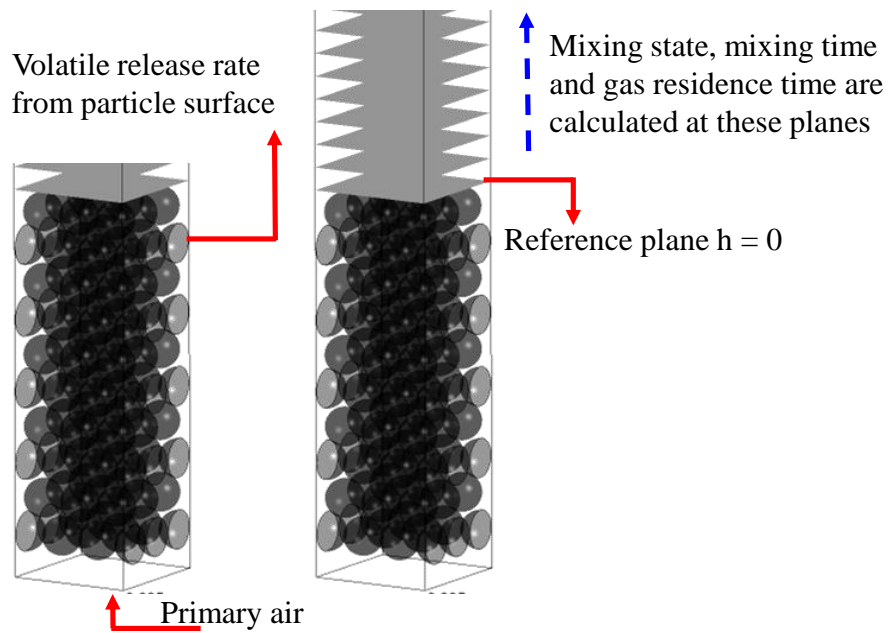


Figure 2.5: CFD domain and boundary conditions for the evaluation of the mixing time above a packed bed

An initial case study was performed to investigate the effect of the number of layers (bed height) on mixing. Figure 2.6 shows the mixing state (Eq. 2-24) variations in dependence of bed height for different numbers of layers. In the parametric case studies, the mixing state is calculated as a scalar field variable and evaluated in several planes defined above the packed bed. One can evaluate for each plane the maximum or minimum value of the tracer gas concentration for the definition of the mixing state. In the present study, the maximum value of the mixing state is determined at each plane. By doing this, the mixing state is derived in dependence of the height above the bed.

The results show a strong effect of the number of layers (bed height) on mixing. Hence, it was considered as an independent parameter. Afterwards, a simulation matrix was defined in order to investigate the effect of primary air velocity and volatiles mass flow rate variations on the mixing (mixing state) for each number of particle layers defined (5, 10 and 15 layers).

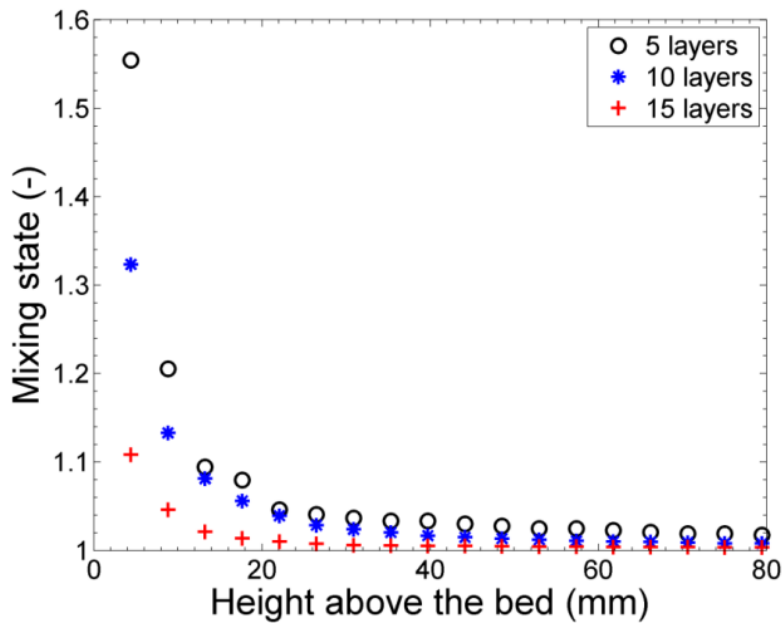


Figure 2.6: Maximum mixing state above the bed (-) evaluated for different numbers of layers

Figure 2.7 shows the mixing state in dependence of bed height for different volatiles mass flow rate variations at two selected primary air velocities and under consideration of 10 layers. The results confirm that the effect of volatiles is insignificant on the mixing in comparison to the effect of primary air mass flow rate since the fraction of the volatiles release rate to the primary air is low (e.g. 0.1-0.3). Because the mass flow of volatiles compared to the primary air mass flow is low and hence was expected to have an insignificant effect on mixing in comparison to the primary air flow rate, a value considerably higher than the reference value was investigated first. Since it showed nearly no difference to the results with the reference value, a reduction of the amount of flue gas below the reference value was expected to have even less effect and it was thus not investigated.

The effect of primary air velocity variations on the mixing state for different numbers of layers (10 and 15 layers) is shown in Figure 2.8. The results in Figure 2.8 are shown in dependence of particle Reynolds number instead of velocity. The results indicate that the mixing state strongly depends on the particle Reynolds number and, therefore, primary air velocity. The change of the slope in Figure 2.8 in the range of 15 -20 mm could be explained by a change in the flow regime from laminar to turbulent conditions (i.e. transition regime) in the range between $Re_p = 237 - 947$ (-) (i.e. the primary air velocity is in the range between 0.7 - 1 (m/s)). Hence, the length of the streaks in dependence of particle Reynolds number (defined by the criterion for fully mixed conditions) is oscillating in this range. As already explained, the mixing function is a linear correlation between the mixing time and the gas residence time. The mixing time is a constant, which is a value of the gas residence time at fully mixed conditions (MS = 1). Since the mixing state as a function of the height above the bed shows an asymptotic behaviour (fully mixed conditions with MS = 1 will never be reached) a certain tolerance has to be defined to achieve the mixing time. The tolerance has to be in a certain range in

order to minimize its influence. Therefore, on the one hand the value of the mixing state (for fully mixed conditions) has to be close to one. On the other hand (as can be seen in Figure 2.8) it should be on the branch of an individual curve with a rapid change of the mixing state, since on the flat branch the mixing time and hence the mixing function strongly changes when varying the tolerance and hence the mixing state. The evaluation of mixing time (t_{fm}) was done based on a certain error tolerance (here 1%) since the mixing state has asymptotic behaviour that means it never reaches the perfect mixing condition (i.e. $MS = 1$). The red line in Figure 2.8 represents the error tolerance used to derive the mixing time. It has been confirmed that 1% error tolerance is fine enough for all cases considered to derive the mixing time.

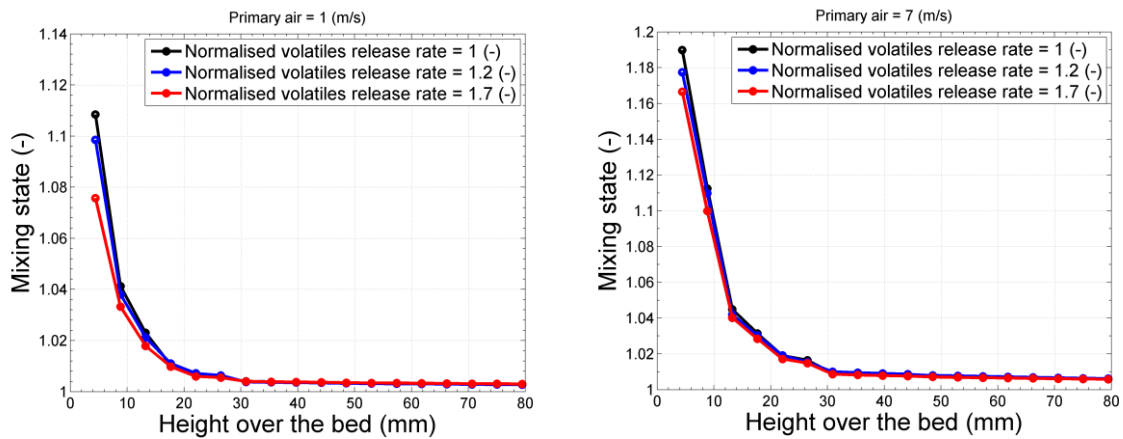


Figure 2.7: Maximum mixing state (-) evaluated for different volatiles release rates for 10 layers (left: primary air velocity 1 (m/s), right: primary air velocity 7 (m/s))

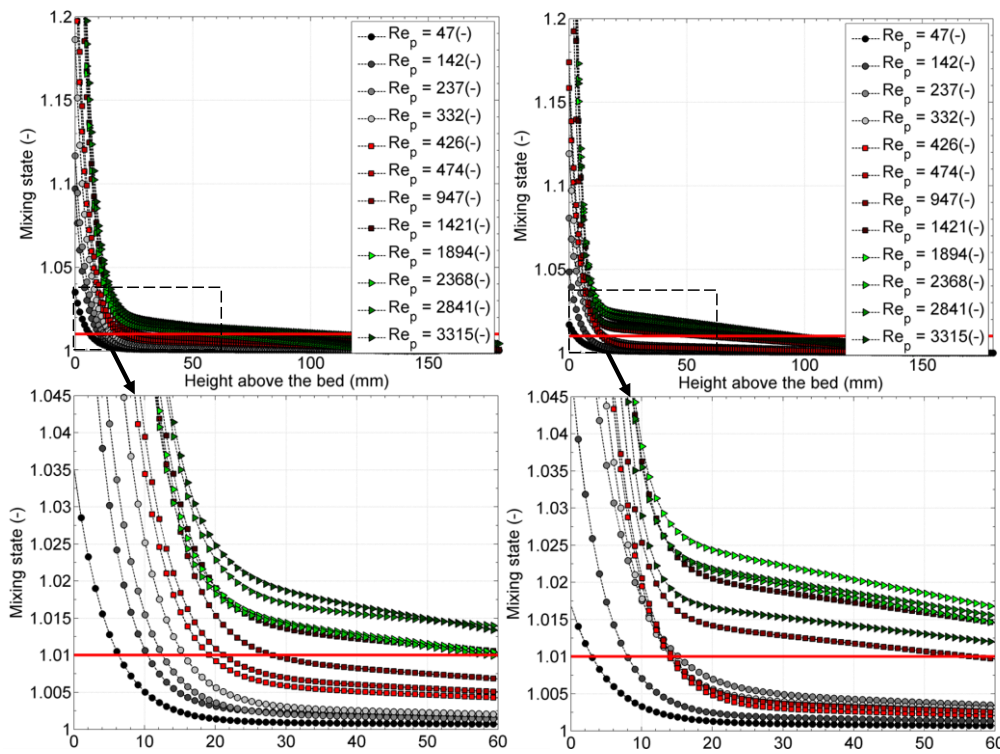


Figure 2.8: Maximum mixing state (-) evaluated for different primary air velocities (left: 10 layers, right: 15 layers)

Figure 2.9 shows the mixing time behaviour in dependence of the particle Reynolds number as well as the number of layers. For all layers considered, a trend concerning the mixing time in dependence of the particle Reynolds number was found. The non-monotonic behaviour in Figure 2.9 could also be explained by a change in flow regime from laminar to turbulent conditions (i.e. the transition regime) (see Figure 2.8). Hence, the length of the streaks in dependence of particle Reynolds number (defined by the criterion for fully mixed conditions) is oscillating in this range. The results showed that the mixing time of the streaks increases as the particle Reynolds number increases. Generally, at lower particle Reynolds numbers the mixing time is lower. This attributes to a higher residence time of the flue gas due to lower primary air velocities which results in a shorter streak length above the packed bed. The mixing time increases as the particle Reynolds number (i.e. primary air velocity) rises due to a higher streak length above the packed bed. Moreover, the mixing time for all particle Reynolds numbers is lower for a larger packed bed height since a higher residence time inside the packed bed improves mixing of primary air and volatile matter. The results of this case study serve as look-up table for the calculation of the mixing time in dependence of the different influencing parameters. For practical application (e.g. the furnace simulation with the streak formation model see **Paper II and Paper III**) the mixing time (t_{fm}) can be retrieved by a linear interpolation between the calculation points through an estimation of the local values of particle Reynolds number and the number of layers. The particle Reynolds number can be easily calculated from the velocity profile specified by the empirical packed bed model along the grate and the average particle diameter (e.g. volume diameter [66]). Furthermore, the number of layers can be estimated by the estimated initial height of the packed bed and the diameter of the fresh biomass fuel fed. The number of layers represents the number of particles that can be stacked in that length (e.g. length divided by the diameter of particles). Since the total number of particles on the bed remains constant on average for a certain operating condition, also the number of layers remains constant over the grate length. However, the entrainment of the particles from the grate and the fragmentation of the particles are neglected with this approach.

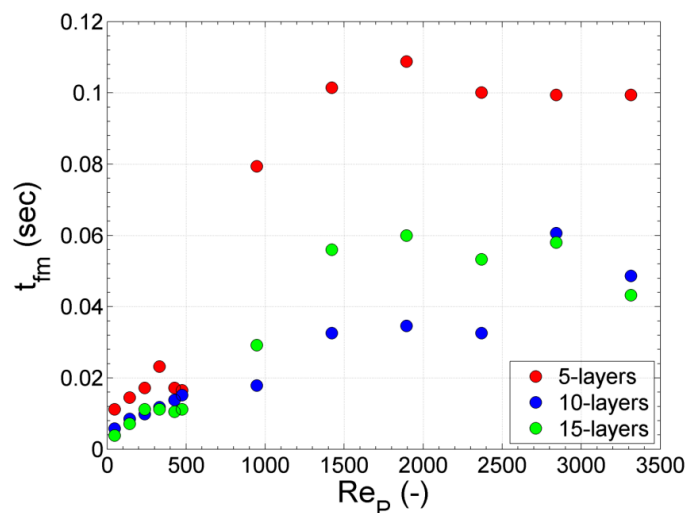


Figure 2.9: Mixing time (sec) for different particle Reynolds numbers and different number of particles

2.4 Routine for automatic CFD optimisation of biomass combustion plants

The classical way of biomass furnace design for industrial applications comprises as iteration between the design engineer and the measurement or computation department. Implementing automatic optimisation methods into the development process has the potential of shortening this iteration significantly. Such methods are based on a parametric geometry or frame work description of the plants and automatically yield a design that is optimal with respect to the desired properties and to the imposed constraints. In this context, an automatic optimisation routine has been developed for the optimisation of biomass combustion plants. The routine consists of parametrisation routines and an optimisation function that have been linked with an empirical packed bed combustion model and gas phase CFD models especially adapted for biomass combustion.

2.4.1 CFD model for biomass grate furnaces

CFD simulations are applied for the development and optimisation of furnaces and boilers. However, the simulation of biomass combustion plants is especially difficult due to highly complex and interacting processes of solid biomass combustion and the turbulent reacting flow in the combustion chamber. Therefore, BIOS together with researchers of Graz University and Technology have developed a CFD model for the development and optimisation of biomass grate furnaces [5] and [4]. The model comprise an in-house developed empirical fixed bed combustion model as well as CFD models especially adapted and validated for turbulent reactive flows in biomass combustion plants. The sub-models and the gas phase models together with the empirical packed bed combustion model have been experimentally validated [5] and [29] successfully applied for several plants.

An empirical model was used for the description of solid biomass combustion on the grate [5], [28] and [29]. The model describes the mass and energy fluxes on the grate as boundary conditions for the following CFD simulation of the turbulent reactive flow in the combustion chamber.

For the simulation of the gas phase, the Realizable k - ϵ Model for turbulence, the Discrete Ordinates Model for radiation and the EDM by Magnussen and Hjertager [11] in combination with a global methane 3-step mechanism (CH_4 , CO , H_2 , CO_2 , H_2O , O_2) [5] and [38] are applied. This approach is numerically robust and reasonably accurate for most industrial applications, especially, it is very fast in terms of calculation time which is very important at the initial stage of design process for furnace manufactures.

2.4.2 Optimisation function

Optimisation is a procedure of finding and comparing feasible solutions until no better solution can be found. Solutions are termed good and bad in terms of an optimisation variable (i.e. objective), which is often the cost of fabrication, amount of harmful gaseous emissions, efficiency of process or other factors. A significant portion of research and application in the field of optimisation considers a single optimisation variable, although

most real-world problems involve more than one optimisation variable. The presence of multiple optimisation variables (such as simultaneously minimising the CO emissions and minimising the pressure loss that is performed in this thesis) is natural in many problems and makes the optimisation problem interesting to solve.

Besides, identification of relevant system (design and operation) parameters is of high relevance since they have strong influences on the target optimisation variables. Usually, the design parameters are identified depending on the needs of the users. For example, In terms of biomass combustion plants optimisation, the design parameters can be the effect of primary air factor, total air factor, the biomass fuel type or the effect of geometric characteristics of the appliance.

As an example, the secondary air nozzles are identified as a design parameter in this thesis for the biomass grate furnace (nominal boiler load: 180 kW_{th}) studied. The secondary air nozzles are of special importance when designing and optimising a biomass furnace. They are the key factor for efficient air staging without backflow in the primary combustion zone (NO_x reduction by primary measures), for a good turbulent mixing and CO burnout, to reduce furnace volume and to lower the amount of excess air (increased efficiency). Therefore, the diameter and the angle of the secondary air nozzles have been selected as design parameters in order to achieve the best geometric configuration concerning low CO emissions and pressure losses over the secondary air nozzles.

A common difficulty with a multi-optimisation variables problem is the conflict between the optimisation variables. One of the most classical methods is the method of optimisation variables weighting. Therefore, a weight function is defined to combine the two optimisation variables (CO emissions and pressure loss over the secondary air nozzles) according to their relevance in a common function. While the energy demand of the fan linearly increases with the pressure loss over the secondary air nozzles, the relevance of the CO emissions substantially increases if a certain level of CO emissions is exceeded. **Eq. 2-37** shows the weight function:

$$W = A \cdot \left(\frac{1}{Y_{CO}} \right)^\gamma + B \cdot \Delta P \quad \text{Eq. 2-37}$$

where W is the weight function, Y_{CO} is the CO mole fraction (μLL^{-1}), A , γ and B are constant values and ΔP is the pressure loss (Pa).

Here, for the pressure drop a linear correlation to the weight function has been assumed (proportional to the energy demand of the fan). Regarding the CO emissions, a polynomial function with a strong increase at a chosen emission limit ($20 \mu\text{LL}^{-1}$ in the present case) was supposed. The constants A and B of the second order polynomial function ($\gamma = 2$) have been determined in a way to achieve roughly the same contribution of the pressure loss and the CO emission to the weight function at the respective limits of the output variables ($\Delta P = 2500$ Pa - maximum allowable pressure for fan design; CO emissions = $20 \mu\text{LL}^{-1}$ - emission limit). The values for the constants are given in Table 2.1.

Table 2.1: Values of the model constants used in the weight function

Constants	Value	Units
A	10	Consistent unit (mLL ⁻¹) ²
γ	-2	-
B	1	Consistent unit (Pa ⁻¹)

Within the optimisation process the design parameters are varied and the optimisation variables are evaluated using the weight function. The optimisation cycle for a selected combination of design parameters works as follows:

- Parameterisation of the geometry and definition of design points based on design parameters selected
- Automatic performance of CFD simulations with ANSYS FLUENT for the defined design points within the ANSYS Workbench
- Evaluation of the optimisation variables and calculation of the weight function for the design points
- Minimisation of the weight function to find the optimum geometric configuration (input parameters)

Figure 2.10 shows the entire workflow. The CAD was the only external step in the entire process whereas all the other steps were performed within the Workbench framework.

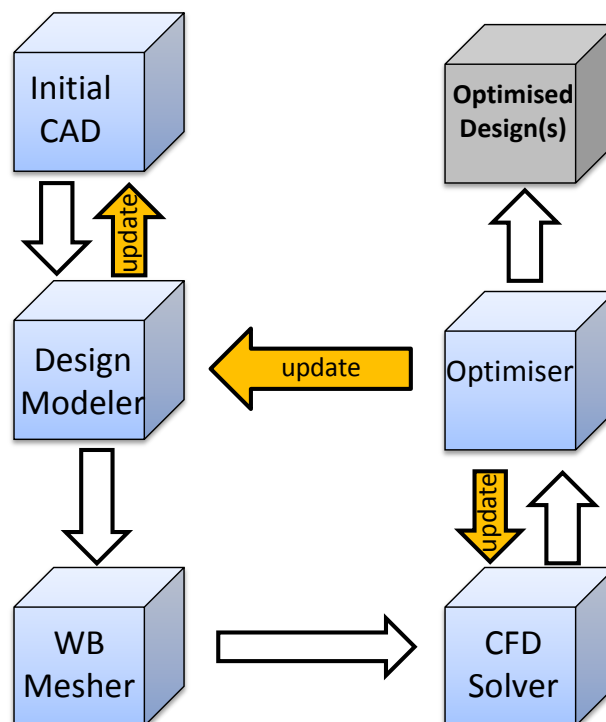


Figure 2.10: Workflow of a developed automatic optimisation routine

3 Modelling results – executive summary

The main contribution of this work is five papers which are published in peer-review journals and conferences. In this section, a summary of each paper is given.

3.1 Hybrid gas phase combustion model (Paper I)

In *paper I* the hybrid model validation was done based on the simulation of measured jet flames by Barlow et. al [67] covering laminar (flame A with a jet Re number of 1100), moderately turbulent (flame B with a jet Reynolds number of 8200), and highly turbulent flow conditions (Sandia flame D with a jet Reynolds number of 22400). The burner, consisting of a main round jet and a concentric pilot, was placed in a wind tunnel. The main jet consists of a mixture of CH₄ with air. The pilot is a lean fuel/air mixture and is active only for flame B and D for the purpose of flame stabilization. Detailed information concerning the operating conditions for flames A, B and D can be found in [67], [68], and [69].

A detailed description of the CFD boundary conditions and the models applied in the simulations can be found in *Paper I*.

3.1.1 Grid independency and effect of kinetic mechanisms

Two sets of structured grids with 4 and 10k elements are studied. The grids are refined close to the nozzle and in the axial direction. A modified version of the k- ϵ turbulence model with the constant $C_{\epsilon 1}$ set to 1.58 (instead of 1.44) is used for the simulation of flame D to compensate for the round jet anomaly [70], [71] and [53]. However, this modification leads to an over-prediction of the flame temperature in the axial direction of the flame. In this region, the temperature along the axis is determined by the mixing of the cold air with the post-combustion gases. So, it strongly depends on the spreading rate determined by the turbulence model applied [72], [73] and [60].

The results obtained with both grids exhibited the same performance (*Paper I*), therefore, the grid with 4k cells was selected in order to save calculation time for subsequent simulations (Flames A and B).

The influence of the reaction mechanism on the predictions for flame D was studied by using two different kinetic mechanisms. DRM-22 [74] is a reduced version of GRI1.2. [75]. It consists of 24 species and 104 reversible reactions. The mechanism GRI2.11 [76] is a full kinetic mechanism, which consists of 49 species and 277 reversible reactions.

The results showed that the performance of the DRM-22 mechanism (*Paper I*) is identical to the detailed GRI2.11 mechanism. Hence, the DRM-22 was used for the further simulations in order to save calculation time.

3.1.2 Molecular diffusion effect

In combustion at low Reynolds numbers the effect of molecular diffusion on mixing becomes comparable to the turbulent diffusion in certain regions in the flame. This is mainly due to the laminarisation of the flow caused by high temperatures in the reaction zones [77]. This is supposed to be caused by the following mechanism. The increase of kinematic viscosity due to high temperature decreases local turbulence Reynolds number in flames. The balance between generation and dissipation of turbulence existing in high Reynolds number regions is not preserved in low Reynolds number regions and the dissipation rate is superior to the generation rate, which results in suppression of turbulence. The effect of molecular diffusion becomes more important when there is H_2 in the fuel jet stream and the jet Reynolds number is lower than 10,000 [14]. In order to highlight the effect of differential diffusion on the accuracy of the prediction, the simulation of flame B (using EDC with DRM-22 mechanism) is performed with and without the effect of molecular diffusion. To account for the effect of differential diffusion in the simulation, diffusion coefficients for each species were represented as a fourth-order polynomial function of temperature. The results showed the significant role of differential diffusion in the accuracy of predictions (*Paper I*). As a result, the effect of differential diffusion at combustion of low and moderate Reynolds numbers cannot be disregarded. For all the simulations performed for the flame A and B, the effect of differential diffusion was taken in to account. In the next step, flame A and B were simulated with the EDC model to further verify and investigate the performance of the model at low Reynolds conditions.

3.1.3 Evaluation of the standard EDC at low Reynolds conditions

For the evaluation of the standard EDC at low and moderate Reynolds numbers, flame A (laminar) and B (moderately turbulent) were simulated. Flame A was chosen for the evaluation of the standard EDC due to its similar flow conditions prevailing above the fuel bed in biomass combustion plants. As explained, in the region above the fuel bed the gas phase mixing and reaction progress is highly influenced by laminar and low turbulent zones. As shown in 2.2.1, the standard EDC is not valid in regions with turbulent Reynolds number less than 64. Therefore, the standard EDC model can be tested for model evaluation at a low turbulent regime in case of flame A.

Figure 3.1 shows the simulation results for flame B in comparison with measurement data at $x/d = 15$ and $x/d = 30$, respectively. The mean mixture fraction is computed using Bilger's formula [78]. The results are in good agreement with measurement data at both heights. The results show that the standard EDC together with the differential diffusion approach gave satisfactorily results in comparison with experimental data even at moderate Reynolds number conditions.

For the simulation of flame A, the flame was piloted artificially by means of a small fluid zone attached to the nozzle outlet with a fixed high temperature value. This zone acted as an ignitor to establish the flame. However, flame A could not be simulated with the standard EDC even with artificial piloting. Figure 3.2 demonstrates the simulation results

obtained with the finite rate kinetics (FRK) model against experimental data for flame A. The results are in good agreement with experimental data even for minor species (H_2 and OH) profiles. This clearly indicates a good performance of the DRM-22 mechanism and the diffusion model used in this study. However, the flame temperature as well as species mass fraction profiles are somewhat over-predicted on the fuel lean side of the flame. The diffusion model plays, indeed, an important role to predict the flame characteristics properly.

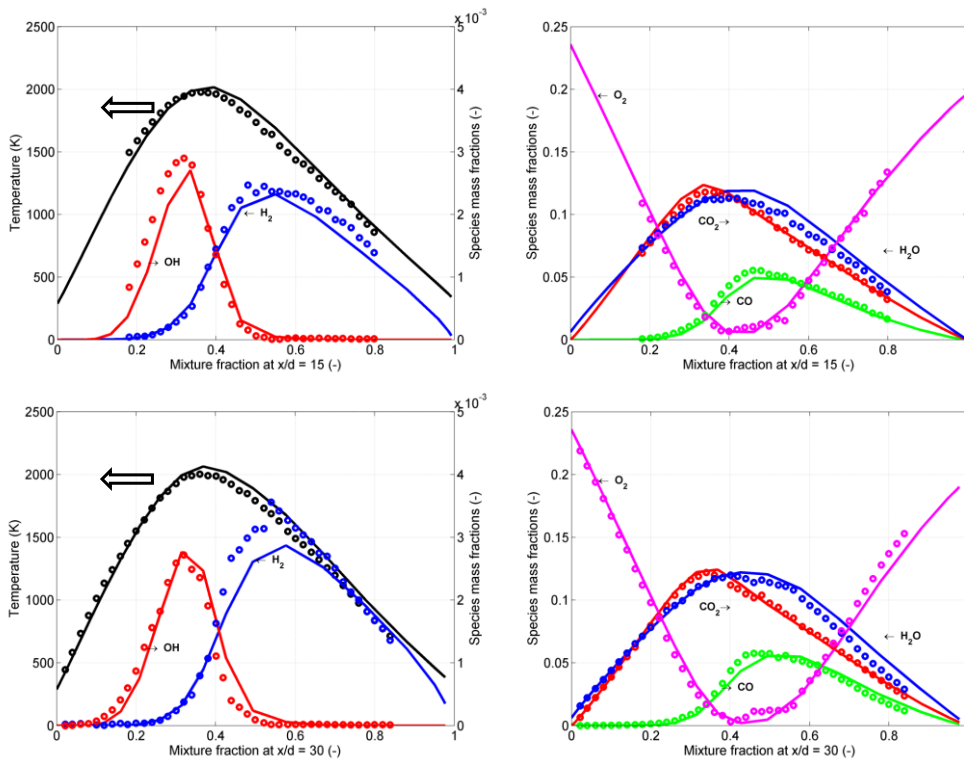


Figure 3.1: Radial profiles of temperature and species mass fractions at different normalised heights of flame B (the EDC model with modified $k-\epsilon$ turbulence model and DRM-22 mechanism, differential-diffusion effect included)

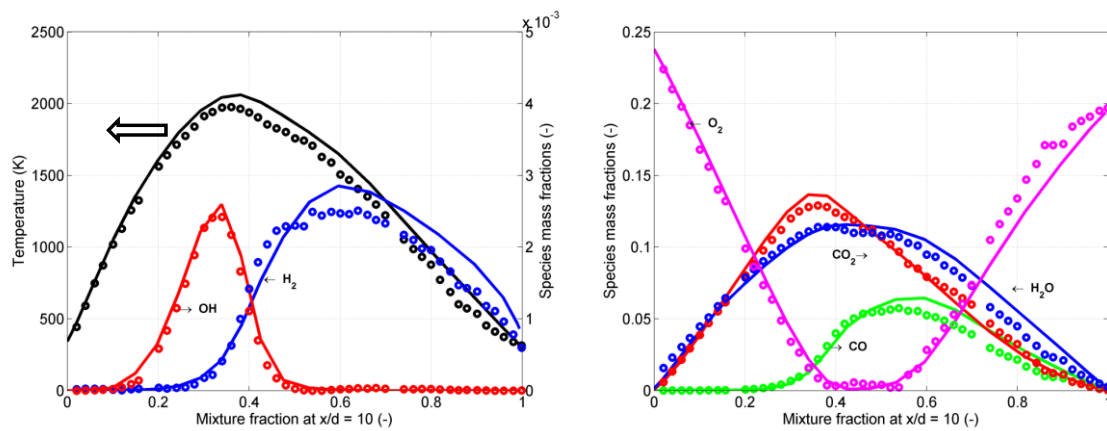


Figure 3.2: Radial profiles of temperature and species mass fractions for flame A at $x/d = 10$ (-) (FRK model with modified $k-\epsilon$ turbulence model and DRM-22 mechanism, differential-diffusion effect included)

3.1.4 Test of the hybrid combustion model

In this section the results of the simulation of flame A, B and D with the hybrid model are presented. Figure 3.3 shows the predicted temperature and species mass fraction profiles for flame A with the hybrid model in comparison with the pure FRK model as well as experimental data. The results obtained with the hybrid model are similar to the pure FRK model. This implies that at low Reynolds conditions the model performs approximately like the FRK model since the weight factor of the FRK model in the hybrid model has the main contribution in the overall reaction rate calculation in the hybrid model (*Paper I*).

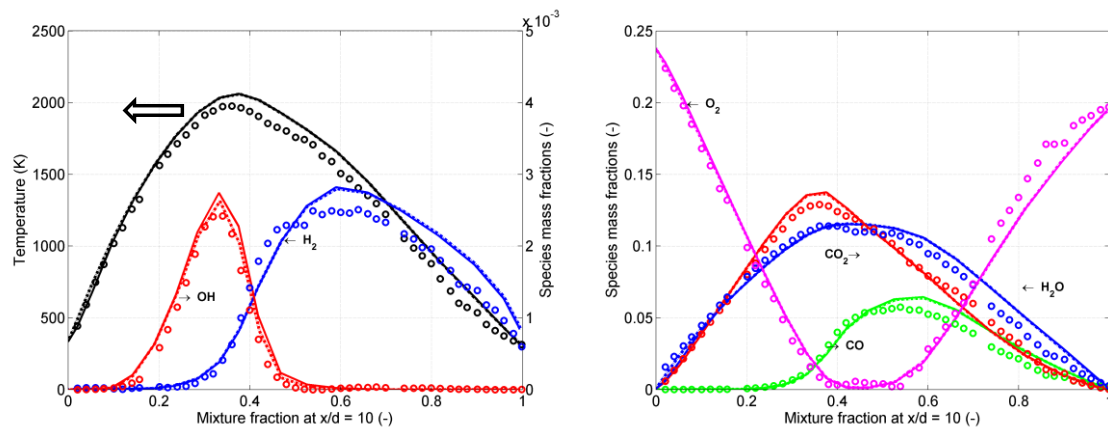


Figure 3.3: Radial profiles of temperature and species mass fractions for flame A at $x/d = 10$ (-) calculated with FRK and the hybrid model (modified $k-\epsilon$ turbulence model, DRM-22 mechanism and differential-diffusion effect included) Circles: experiment, solid lines: FRK model dashed dotted lines: hybrid model

The results predicted with the hybrid model for flame B at two different heights are shown in Figure 3.4. The results were also compared with the standard EDC and the FRK models. Generally, the predictions with the hybrid model lie between the FRK and the EDC results. The predictions with the hybrid model show a slightly better performance than the EDC model due to the sensitivity of the model to the locally too low turbulent Reynolds number of the flow (*Paper I*). Additionally, the predictions with the FRK model are quite similar to the predictions with the hybrid and the EDC except in terms of radical predictions.

The characteristics of reacting radicals are of high relevance for an in-depth understanding of the formation process of combustion emissions. Therefore, both reaction mechanism and gas phase reaction model play an important role for the better prediction of radicals in the combustion simulation.

The results show that both H_2 and OH mass fraction profiles at both heights are slightly improved with the hybrid model. This is mainly because of the lower turbulent Reynolds number than the critical value (*Paper I*) at these heights, therefore, the contribution of the FRK part in the hybrid model becomes more relevant. However, in case of FRK simulation results the radicals are better predicted since the effect of turbulence fluctuations are not considered in the model.

Figure 3.5 shows the evaluation of the hybrid model for flame D in comparison to the standard EDC as well as the FRK model along the normalised axial direction of the flame. The results show that the temperature and species mass fractions are over-predicted with the pure FRK model. The results with the EDC model indicate that by considering the effect of turbulence in the reaction rate calculation, the over-prediction of temperature and consequently the species mass fractions caused by the FRK model are suppressed. Although the turbulent Reynolds number is by far higher than $Re_t = 64$, the FRK part in the hybrid model has a small contribution to the reaction rate calculation due to the effect FRK weighting factor in the hybrid model (*Paper I*). The results obtained with the hybrid model show a slight improvement on the prediction. This is mainly due to the contribution of the FRK part in the overall reaction rate calculation, where the predicted CO and O₂ species are improved, respectively. The same behaviour is true also for the predicted CO₂ and H₂O species calculated with the hybrid model.

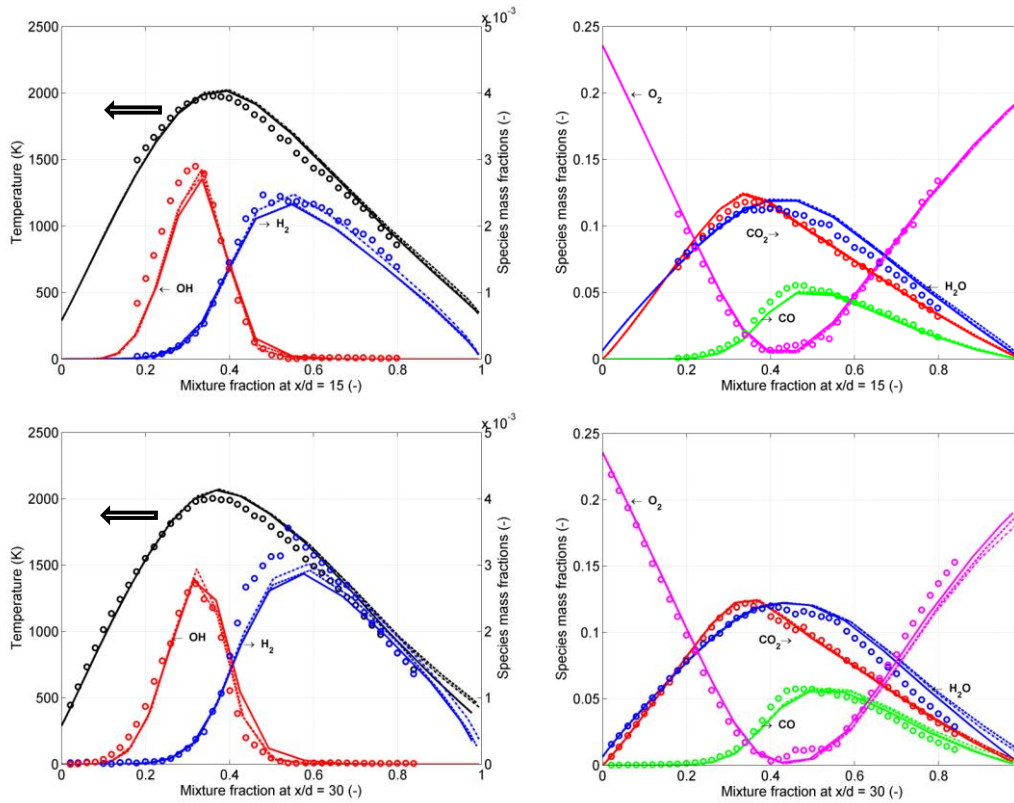


Figure 3.4: Radial profiles of temperature and species mass fractions for flame B at different heights calculated with EDC, FRK and the hybrid model (modified $k-\epsilon$ turbulence model, DRM-22 mechanism and differential-diffusion effect included) Circles: experiment, solid lines: EDC model, dashed lines: FRK and dashed dotted lines: hybrid model

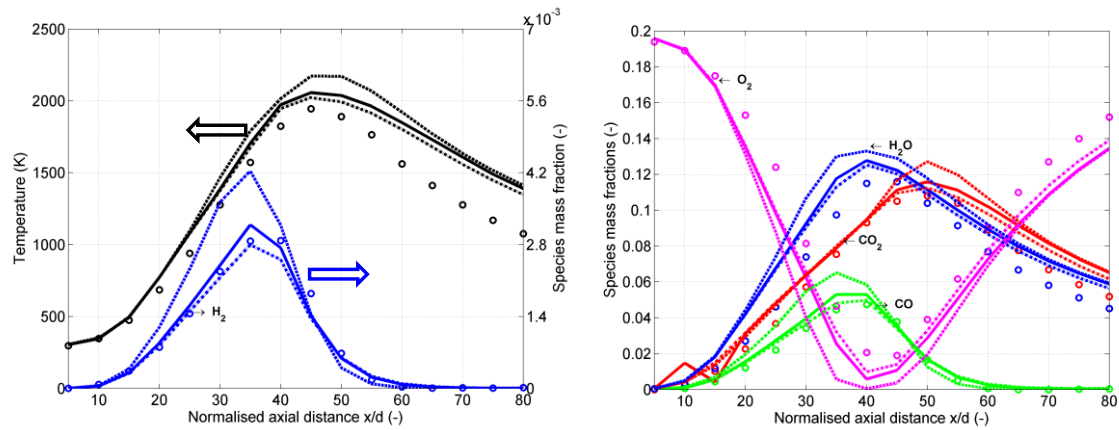


Figure 3.5: Temperature and species mass fractions predictions for flame D at different normalised axial distances calculated with EDC, FRK and hybrid model (modified $k-\epsilon$ turbulence model, DRM-22 mechanism) Circles: experiment, solid lines: EDC model, dashed lines: FRK model and dashed dotted lines: hybrid model

3.2 Development of a streak formation model for an improved prediction of gas phase combustion in biomass grate furnaces (Papers II and III)

In *paper II and III*, the streak formation model in order to account the effect of gas streaks arising from the packed bed influencing gas phase mixing and reaction progress was introduced. Moreover, the hybrid gas phase reaction model was further extended to account for the near wall combustion effect (*Paper III*) since the reaction progress in the near wall regions is mainly influenced by the contribution of the viscous and Reynolds stresses. Additionally, the streak formation model was linked with the hybrid gas phase reaction model. The link of the hybrid gas phase reaction model and the streak formation model was termed as hybrid-streak model in the papers and in the thesis. Therefore, the effective reaction rate in the hybrid model is achieved by multiplying the mixing function, which considers macro mixing, with the reaction rate predicted with the hybrid model (as described in section 2.3). Finally, the application and verification of the hybrid-streak model were performed for the simulation of a pilot-scale grate furnace (nominal boiler load: 150 kW_{th}) (*Paper II*) and an under-feed stoker furnace (nominal boiler load: 20 kW_{th}) (*Paper III*) in terms of gas phase combustion and NO_x formation. Under the assumption that NO_x formation reactions do not significantly influence the flow pattern in the furnace, a time saving 2-step approach is applied for CFD simulations. The basic gas phase combustion simulation has been performed using the hybrid and hybrid-streak combustion models with the C-H-O subset of the Skeletal Kilpinen97 mechanism (12 species and 25 reactions) [40], which has extensively been validated for grate furnaces [40]. The subsequent CFD simulation of gas phase fuel NO_x formation in a post-processing mode has been done using the hybrid and hybrid-streak models in combination with a detailed reaction mechanism (28 species and 102 reactions in total) [40]. In *Paper II and III*, for cases that consider the effect of streaks on combustion the particle Reynolds number and the number of layers (fuel bed thickness) are calculated from the velocity profile specified by the empirical packed bed model as well as the assumed height of the fuel bed, respectively. Then, to derive a mixing time

profile along the grate the values were retrieved from the look-up table for the mixing time (as describes in section 2.3.1). Finally, two transport equations were solved, one for the gas residence time and the other for the mixing time, to derive the local mixing function as defined in Eq. 2-25.

3.2.1 Model validation and application for a 150 kW_{th} grate furnace (paper II)

In *paper II*, the streak formation model to account for the effect of flue gas streaks arising from the packed bed on the gas phase mixing and reaction progress is presented. Additionally, to investigate and verify the influence of the streak formation model on gas phase mixing and reactions, a CFD simulation was performed for a pilot-scale moving grate furnace equipped with a hot water fire tube boiler (150 kW_{th}) using wood chips as fuel. The most relevant operating conditions, the fuel composition and description of the biomass combustion plant can be found in *Paper II*.

To see and to be able to evaluate the effect of streaks on the gas phase reactions concerning temperature and species (e.g. CO and NO_x formation), two simulations were performed, without and with the streak formation model. The hybrid gas phase combustion model applicable for laminar to turbulent flow situations was used for both simulations.

Figure 3.6 shows the contour plots of gas residence time (left) and the mixing function (right) derived from Eq. 2-25.

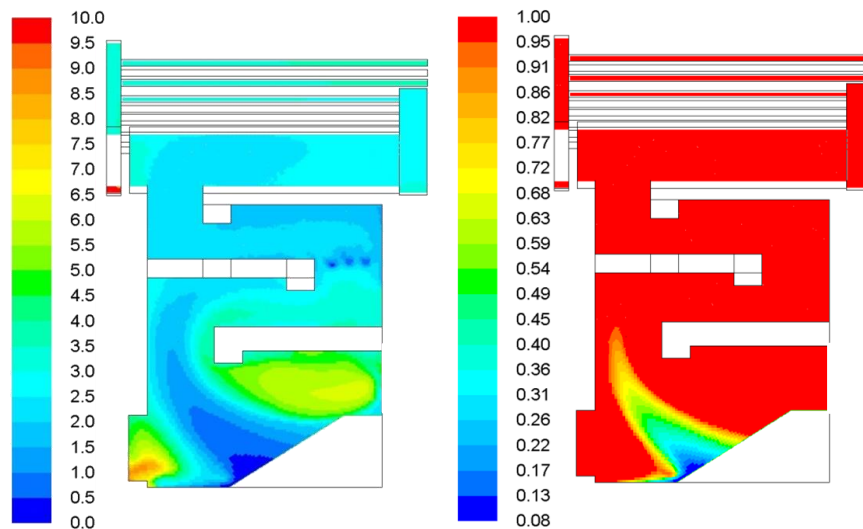


Figure 3.6: Gas residence time [sec] (left), and mixing function [-] (right)

The predicted O₂ mass fractions calculated with both models are depicted in Figure 3.7. The oxygen concentration above the bed is predicted slightly different in both cases. The O₂ concentrations are influenced by the streaks above the fuel bed especially in the locations where they are highlighted (location 1 and 2).

However, concerning the temperature and CO concentrations (*Paper II*), there are no big differences between the two models. This can be explained by a staged combustion with

($\lambda_{\text{primary combustion zone}} \ll 1$) and sufficient residence time in the primary combustion zone for a full consumption of O_2 and, hence a flue gas composition at the entrance to the secondary combustion zone, which is approximately independent from the combustion model. Furthermore, the reaction progress is not influenced by the streaks arising from the packed bed anymore and the residence time in the secondary combustion zone is high enough for an almost complete CO burnout. Therefore, the effect of streak formation on the combustion process (flue gas temperature and CO burnout) for this specific case is not distinctive. Moreover, in the present test case, the CO emissions measured at boiler outlet were very low. Therefore, in this specific case study, the influence of the models applied in the simulation (hybrid and hybrid-streak formation model) on CO emissions could not be validated. Therefore, further validation simulations were performed for other biomass combustion plants (*Paper III*), see section 3.2.2.

The characteristics of reacting radicals (e.g. OH and O) are of high relevance for an in-depth understanding of the combustion and NO_x formation processes [60], [79] and [80]. These radicals are of high relevance especially for the formation of NO_x . The calculated OH and O species with hybrid and hybrid-streak formation models are shown in Figure 3.8. The concentrations of OH and O species are generally predicted lower with the hybrid-streak formation model. This is mainly due to the contribution of the streak formation model (i.e. the spatial distribution of oxygen concentrations (see Figure 3.7) in which the rates of production or destruction of the species are slowed down by the streak formation model (see Eq. 2-35)). This could also be explained by a lower oxygen concentration in the primary combustion zone above the packed bed caused by the streak formation model.

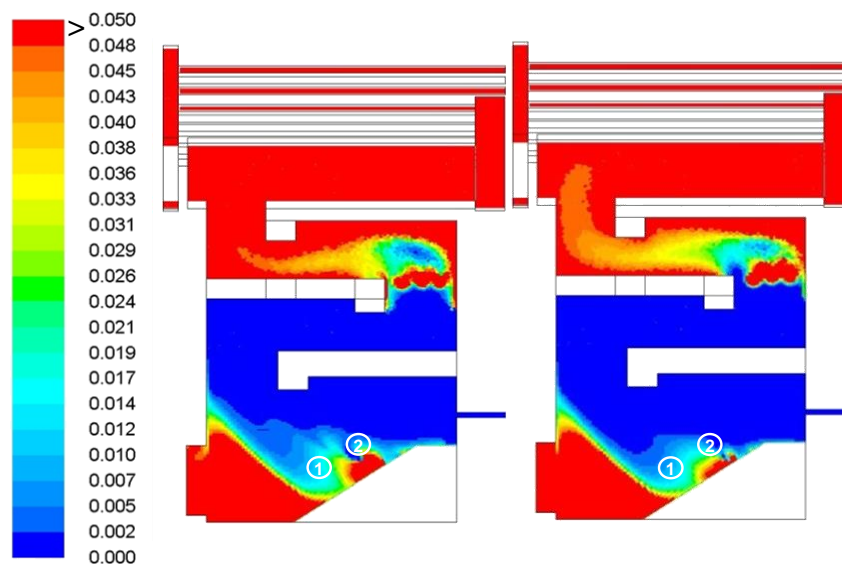


Figure 3.7: Iso-surfaces of the O_2 mass fraction [-] in the mid plane of the computational domain calculated with the hybrid model (left) and the hybrid-streak formation model (right)

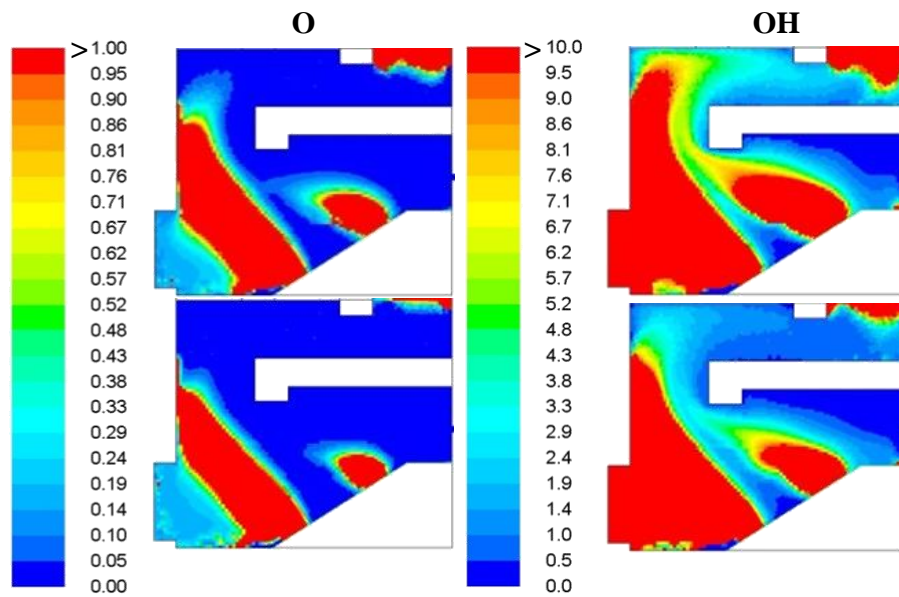


Figure 3.8 : Iso-surfaces of O concentration [ppmv] (left), and OH concentration [ppmv] (right) calculated with the hybrid (top) and the hybrid-streak formation model (bottom)

Figure 3.9 shows the NO_x profiles predicted with the hybrid and the hybrid-streak model. Table 3.1 provides the NO_x concentrations predicted with the hybrid and the hybrid-streak model in comparison with NO_x emission measurements at boiler outlet. The results indicate that the prediction is improved with the hybrid-streak formation model. This can be argued with the more accurate prediction of the species mixing process above the fuel bed and, therefore, of the radicals, that are important for the NO_x formation processes or for NO_x formation and reduction mainly in the primary combustion zone is of relevance.

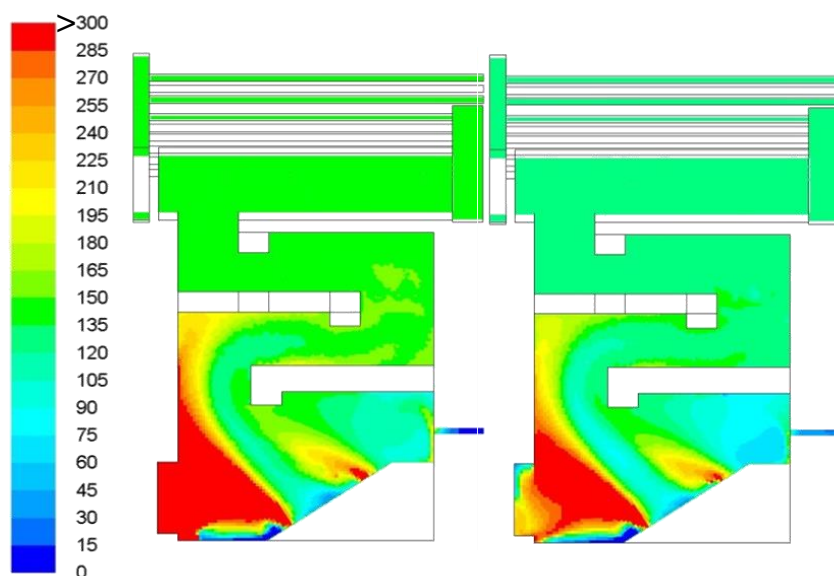


Figure 3.9: Iso-surfaces of NO_x concentration [mg/Nm³ d.b., 13 vol% O₂] calculated with the hybrid model (left) and the hybrid-streak formation model (right)

Table 3.1: Predicted NO_x concentrations with the hybrid and the hybrid-streak formation model in comparison to measurements

Parameter	Unit	Value	Deviation [%]
Experiment	[mg/Nm ³ d.b., 13 vol% O ₂]	129	-
Hybrid	[mg/Nm ³ d.b., 13 vol% O ₂]	141	9
Hybrid-streak	[mg/Nm ³ d.b., 13 vol% O ₂]	125	3

The results from the pilot-scale biomass grate furnace with and without the effect of streaks showed that in the present case, the streaks had no big influence on the combustion process including flue gas temperature and CO emissions but a certain improvement concerning NO_x formation prediction could be seen (*Paper II*). Therefore, further validation simulation was performed for a small scale grate furnace (see *Paper III*).

3.2.2 Model validation and application for a 20 kW_{th} under-feed stoker furnace (paper III)

In *paper III*, a detailed description of the streak formation model is given. Moreover, a further extension of the hybrid model to consider the effect of combustion in the near wall regions is discussed. As explained in section 3.2.1, since the effect of the streak formation model on the combustion process (temperature and CO emissions) had no big influence for the pilot-scale biomass grate furnace presented in *Paper II*, the simulation of a small-scale biomass under-feed stoker furnace was performed. The application of the streak formation model can be pronounced in small-scale packed bed biomass furnaces since the flow regime inside the primary combustion chamber is usually laminar or weakly turbulent which results to have a lower residence time that leads to streak formation. Again the hybrid gas phase combustion model suitable for laminar as well as moderately to highly turbulent combustion conditions was used as in small-scale biomass packed bed combustion applications gas phase mixing and reaction progress is highly influenced by laminar and low turbulence zones in the regions above the fuel bed.

In order to highlight the advantages of the hybrid model and the streak formation model for the simulation of small-scale furnaces in terms of combustion and emissions prediction, additional simulations were performed with different CFD gas phase reaction models like the EDM [11] and the EDC [12]. For the purpose of model evaluation, the simulation results were compared with CO and NO_x emission measurements.

The simulations were performed for two biomass fuels, wood pellets and straw pellets, for which experimental data concerning CO and NO_x emissions were available. The most

relevant operating conditions, the fuel composition and a description of the biomass combustion plant can be found in *Paper III*.

Figure 3.10 shows the contour plots of gas residence time (left) and the mixing function (right) derived from Eq. 2-25. The mixing function indicates that a major part of the reaction zone above the packed bed is influenced by streak formation. The mixing function as defined shows the degree of mixing above the grate. The value 0 means no mixing and 1 means fully mixed. As can be seen from Figure 3.10 (right), the mixing function varies between 0 and 1. Moreover, the main part of the primary combustion zone is influenced by streak formation (air lean region in the core).

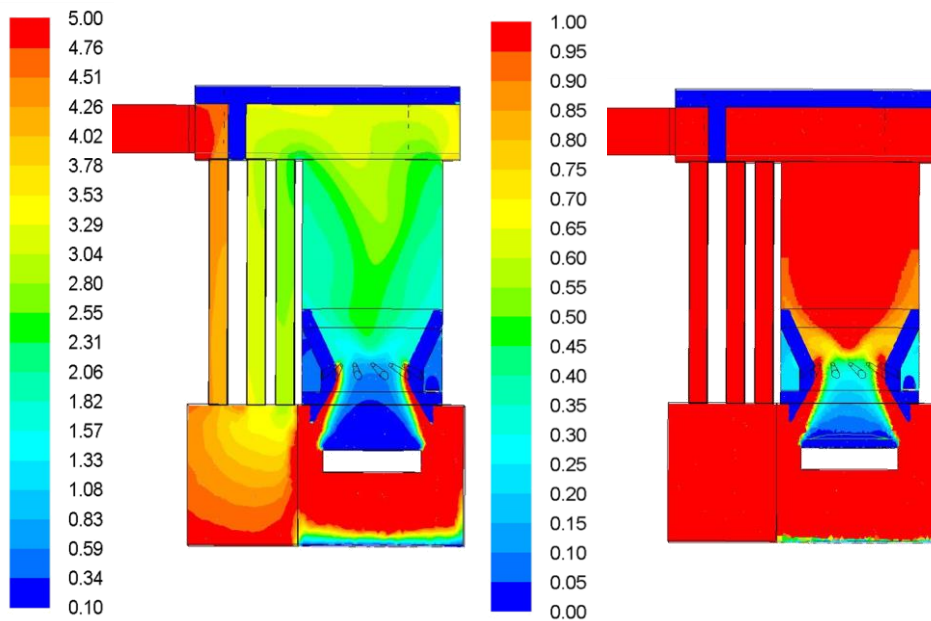


Figure 3.10: Gas residence time (sec) (left), and mixing function (-) (right) evaluated for wood pellets as fuel

Flue gas temperatures calculated with all models for both wood pellets (top) and straw pellets (bottom) are shown in Figure 3.11. The simulations show for both cases high flue gas temperatures (see Figure 3.11) in the major reaction zone above the fuel bed in the primary combustion zone as well as close to the secondary air injection. Here, also the peak flue gas temperatures can be observed.

The regions addressed correspond to increased combustion progress which is more pronounced in case of EDC and hybrid simulations than in case of the EDM simulation. The higher flue gas temperatures predicted with the EDC compared to the EDM are attributed to the Magnussen constant of the EDM model [11] which has been systematically adapted for biomass grate furnaces by a comparison with CO emission and temperature measurements [5] and [4]. Accordingly, a reduction of the mixing and the reaction rate compared to the original model is achieved. Therefore, the EDC, where no tuning is done, predicts higher reaction rates, which rise the temperatures. The higher

temperatures predicted with the hybrid model compared to the EDC are due to the influence of the selection of the combustion models (e.g. finite rate kinetics (FRK) or EDC model) by the hybrid model which depends on the local turbulent Reynolds number of the flow. Hence, it is of interest to investigate the flow regime in the combustion chamber. Figure 3.12 shows the flue gas temperatures and the turbulent Reynolds number obtained with different gas phase reaction models for wood pellets as fuel. The figure shows that the turbulent Reynolds number is lower than 64 in the major reaction zones that are indicated by high temperature zones above the fuel bed at the outer edge of the grate as well as close to secondary air injection and, therefore, the reaction rate in the hybrid model is calculated mostly with the FRK model in these regions. The flue gas temperatures predicted with the hybrid-streak model are somewhat different. It can be seen that the major part of the reaction zone above the packed bed is also influenced by streak formation (i.e. the mixing function) (see Figure 3.10). It is clear that the combustion progress is slowed down by the hybrid-streak model in the regions where the streaks exist (above the grate).

Significant differences can also be observed in the prediction of CO concentrations with the EDM, the EDC, the hybrid model and the hybrid-streak model as shown in Figure 3.13. Generally, the EDC and hybrid model resulted in a much faster CO oxidation, especially in the regions of intense mixing in the primary combustion zone and in the region directly after the secondary air injection, while the EDM with the mixing parameter applied leads to a generally slower CO oxidation. Therefore, EDC and hybrid led to significantly lower CO levels further downstream in the secondary combustion zone and at boiler inlet. Moreover, the slight differences in the CO concentrations between the EDC and the hybrid model are mainly due to a higher reaction rate caused by a higher contribution of the FRK model, where micro-mixing plays no role (see Table 3.2 and Table 3.3). The CO prediction with the hybrid-streak model is higher than for the EDC and the hybrid model since the combustion progress is delayed due to the presence of streaks (see Figure 3.10) mainly in the primary combustion zone. The predicted CO concentrations at boiler outlet for both wood and straw pellets are given in Table 3.2 and Table 3.3. For wood pellets (see Table 3.2), the calculated CO value predicted with the hybrid-streak model is in best agreement with the measured values. The better prediction with the hybrid-streak model can be explained by a delay in the CO oxidation, since the net reaction rate in the hybrid-streak model is multiplied by the mixing function, therefore, the regions above the major flue gas release zone and the reaction fronts are mainly influenced by mixing function.

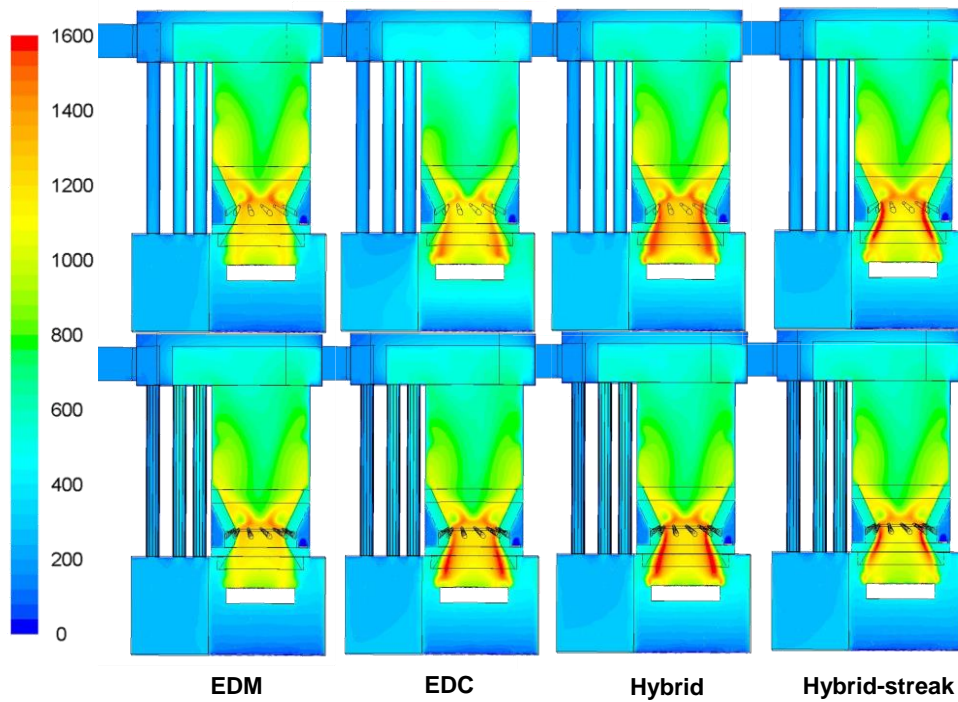


Figure 3.11: Iso-surfaces of flue gas temperatures (°C) in a vertical cross-section of the furnace for wood pellets (top) and straw pellets (bottom)

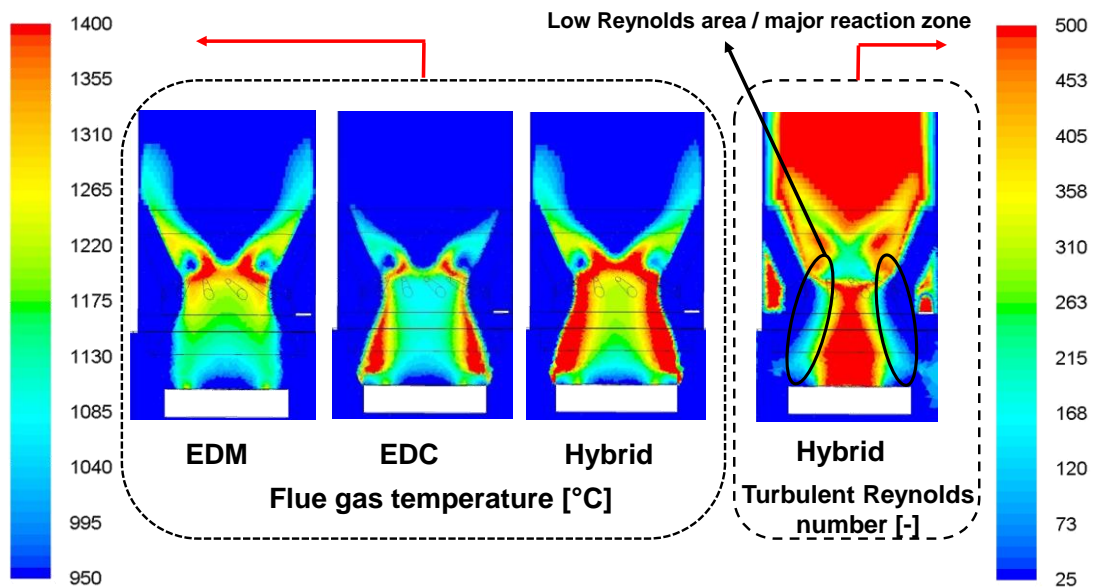


Figure 3.12: Iso-surfaces of flue gas temperatures (°C) predicted with different gas phase reaction models (left) and turbulent Reynolds number (-) (right) in a vertical cross section of the furnace (up to the upper edge of the refractory lining) evaluated for wood pellets as fuel

The CO values calculated with the EDC model are in better agreement with measured values than the hybrid and the EDM model. The hybrid model results in a much faster CO oxidation, since the major part of the reaction progress is calculated with the FRK, while in the EDM the reaction rate is mainly controlled by the mixing constant, A_{mag} [8] which is tuned [5] and [4]. In case of straw pellets, the CO values predicted with the hybrid-streak

model are in better agreement than the EDC and hybrid model (i.e. the deviation with respect to the measured value is positive) due to a more accurate prediction of mixing processes above the packed bed. The CO values predicted with the EDC and hybrid model are too low in comparison with the measured values. The EDM gives the best agreement with the measured CO values. As already explained, the eddy dissipation rate is directly proportional to the value of the modelling constant A_{mag} [11] and to the mean eddy lifetime, k/ε where the value of A_{mag} is lowered from the originally proposed value, $A_{mag} = 4$, to $A_{mag} = 0.8$ for the simulation of small-scale biomass combustion plants [11] and [14]. Besides, there is no explicit modelling of streaks with the EDM model and the model is valid for highly turbulent flows which means the best agreement in this case is due to good tuning for grate combustion plants but a model which can predict reliable CO burnout rates without tuning would be preferable. A clear drawback of the EDM in combination with global reaction mechanisms is that it is not able to describe complex interactions of turbulence and multi-step reaction kinetics. Besides, when modelling gas phase combustion with the EDM basically we are already tuning the model constant A_{mag} by nearly an order of magnitude. This is actually not satisfactory since tuning of model constants over such a wide range may lead to a limited validity range linked with wrong predictions under deviating conditions (e.g. the effect of mixing may be overestimated especially in kinetically limited zones). In order to avoid this, the EDC and the Hybrid model, which provide a more fundamental prediction of gas phase reactions, have been applied. However, they are more sensitive to the boundary conditions at the surface of the fuel bed (turbulence and mixing degree) and hence need an additional model, which explicitly considers the effects of streaks on the mixing. By introducing this model, no tuning of the gas phase combustion model to fixed bed combustion is necessary.

In a next step, NO_x simulations have been performed in a post-processing approach based on the solution obtained from the combustion simulations. The distribution of the NH_3 , HCN and NO profiles show that streak formation has a strong influence on the spatial distributions of these species (see *Paper III*). Figure 3.14 shows the NO_x profiles predicted with the different models for wood pellets (top) and straw pellets (bottom). The predicted NO_x concentrations at boiler outlet for both wood pellets and straw pellets are given in Table 3.4 and Table 3.5. According to the hybrid model, the major part of the reaction zones is located above the grate as well as in front of the secondary air jets, where the turbulent Reynolds number is lower than 64. Therefore, the reaction progress is mainly calculated with the FRK model, whereas micro-mixing plays no important role. This causes a higher net reaction rate of NO in these regions (see *Paper III*). However, in the EDC, the reaction progress is always influenced by micro-mixing. According to this model, the fluid is in any case mixed on a micro-scale and the reactions finally take place in the fine structures [12] of the fluid, where the reactants are mixed on a molecular level. Hence, the EDC fails to predict reactive flows in laminar and moderately turbulent situations. Therefore, in this case, the EDC leads to a higher NO_x reduction (see *Paper III*), since NO_x formation in the outer air-rich zone in the primary combustion zone is stronger decreased than the NO_x reduction in the air lean zone of the primary combustion zone (see Table 3.4 and Table 3.5). The NO_x formation processes according to the hybrid-streak model are completely different from the EDC and the hybrid model. Here, it is shown that

the spatial distributions of NO, NH₃ and HCN are different especially above the fuel bed (see *Paper III*). These differences are mainly attributed to the different oxygen and radical (O and OH) concentrations (see *Paper III*) that are influenced by streak formation (i.e. mixing function). A detailed discussion on the NO_x formation and reduction processes predicted with different gas phase reaction models has been given in *Paper III*. The results for both cases show that the predictions are improved with the hybrid-streak model.

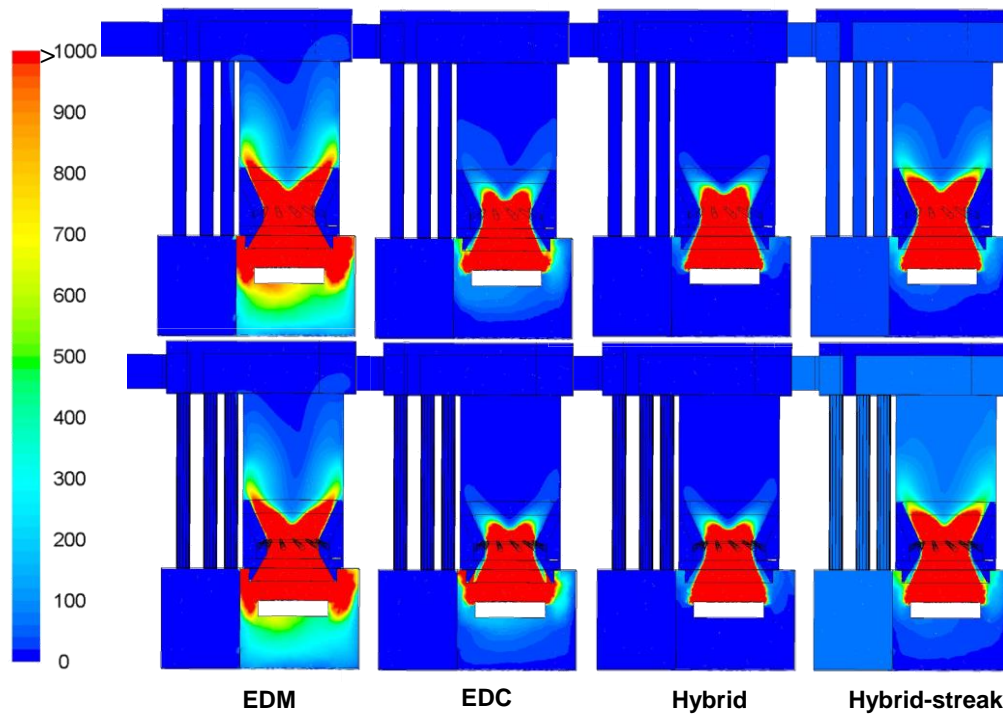


Figure 3.13: Iso-surfaces of CO concentrations (ppmv) in a vertical cross-section of the furnace for wood pellets (top) and straw pellets (bottom)

Table 3.2: Predicted CO concentrations with the EDM, EDC, hybrid and hybrid-streak model in comparison to measurements for wood pellets

		Simulations				
Average CO concentration	Unit	EDM	EDC	Hybrid	Hybrid-	Measurement
Boiler outlet	[ppm dry]	16	19	5	30	38
Boiler outlet	[mg/Nm ³ 13 Vol% O ₂ dry]	10	15	3	22	29
Deviation (percentage error with respect to measured value)	[%]	-65	-48	-89	-24	

Table 3.3: Predicted CO concentrations with the EDM, EDC, hybrid and hybrid-streak model in comparison to measurements for straw pellets

Average CO concentration	Unit	Simulations				Measurement
		EDM	EDC	Hybrid	Hybrid-	
Boiler outlet	[ppm dry]	13	4	3	29	16
Boiler outlet	[mg/Nm ³ 13 Vol% O ₂ dry]	10	3	2	27	13
Deviation (percentage error with respect to measured value)	[%]	-23	-76	-84	107	

Table 3.4: Predicted NO_x concentrations with the EDC, hybrid and hybrid-streak model in comparison to measurements for wood pellets as fuel

Average NO _x concentration	Unit	Simulations			Measurement
		EDC	Hybrid	Hybrid-	
Boiler outlet	[ppm dry]	118	132	110	105
Boiler outlet	[mg/Nm ³ 13 Vol% O ₂ dry]	146	165	135	130
Deviation (percentage error with respect to measured value)	[%]	12	26	5	

Table 3.5: Predicted NO_x concentrations with the EDC, hybrid and hybrid-streak model in comparison to measurements for straw pellets as fuel

Average NO _x concentration	Unit	Simulations			Measurement
		EDC	Hybrid	Hybrid-	
Boiler outlet	[ppm dry]	167	186	352	286
Boiler outlet	[mg/Nm ³ 13 Vol% O ₂ dry]	220	247	466	380
Deviation (percentage error with respect to measured value)	[%]	-41	-34	23	

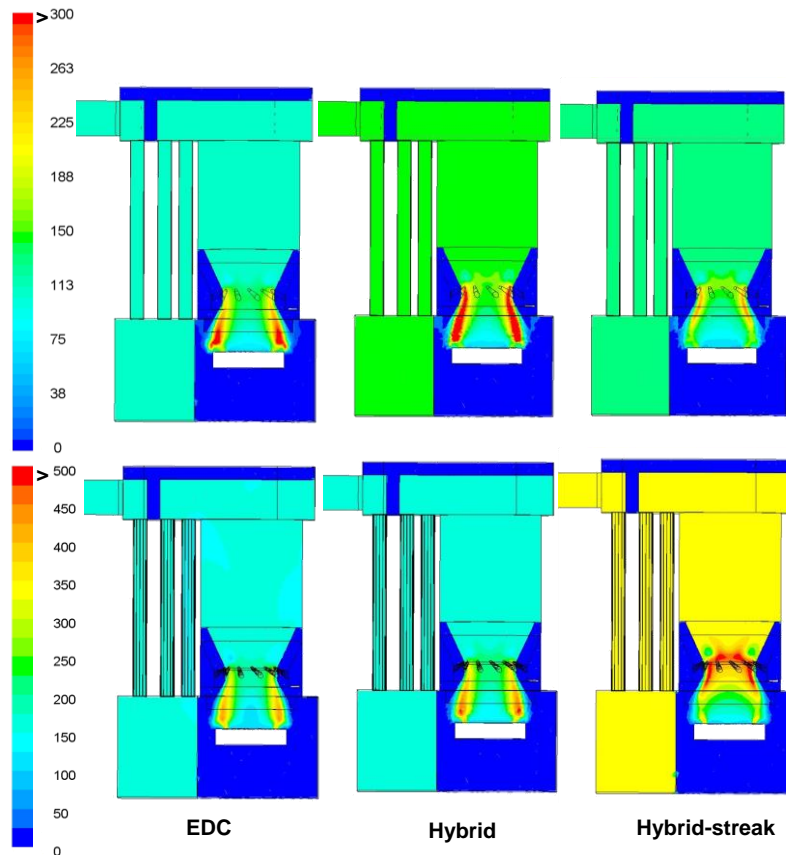


Figure 3.14: Iso-surfaces of NO_x concentrations (ppmv dry) in a vertical cross-section of the furnace for wood pellets (top) and straw pellets (bottom)

3.3 Automatic CFD optimisation of biomass combustion plants (Papers IV and V)

In *Paper IV and V*, an automatic optimisation routine is developed for the optimisation of biomass combustion plants. The routine consists of parametrisation routines and an optimisation function that have been linked with a developed empirical packed bed combustion model as well as gas phase CFD models especially adapted for the optimisation of biomass grate furnaces. The CFD models applied for the simulation of turbulent reactive flow include: the Realizable $k-\epsilon$ Model for turbulence, the Discrete Ordinates Model for radiation and the Eddy Dissipation Model (EDM) in combination with a global methane 3-step mechanism [5], [27] and [4]. The EDM is used as a gas phase combustion model in the present optimisation study instead of the Eddy Dissipation Concept (EDC) or hybrid models since it is numerically robust and reasonably accurate for most industrial applications especially, it is very fast in terms of calculation time which is very important at the initial stage of design process for furnace manufactures. Besides, in the present case study since the CO emissions and pressure losses (i.e. target variables) should be evaluated over a wide range of secondary air nozzle diameter and angle variations therefore a qualitative representation (i.e. trend identification) of the target

variables would be sufficient and thus the EDM combustion model is applied in the simulations.

To investigate the efficiency of the method developed as described in section 2.4, a design optimisation for a pilot-scale moving grate furnace equipped with a hot water fire tube boiler (nominal boiler load: 180 kW_{th}) using Miscanthus as fuel has been carried out. The most relevant operating conditions, the fuel composition and a description of the biomass combustion plant can be found in **Paper IV and V**. The diameter and angle of the secondary air nozzle were parametrised as design parameters. The variation range of the design parameters is shown in Table 3.6.

Table 3.6: Design parameters and their variation range

Design parameter	Range
Diameter (mm)	10-35
Angle (deg)	1-30

To verify the efficiency of the optimisation strategy concerning the reduction of the overall time for the performance of the case study in comparison to conventional manual methods, at first a manual optimisation run was carried out (as a reference). Since this method is very time-consuming, only the diameter of the nozzles has been changed (for 10 design points). A computational grid with 700,000 cells in total was used in the manual optimisation study. In the next step, the automatic optimisation routine was performed for the two selected design parameters for 80 design points. The number of computational cells was about 1 million for the automatic optimisation study using the tetrahedral cell type. Figure 3.15 and Figure 3.16 show the calculated results concerning CO emissions and pressure losses for the manual and the automatic optimisation method. The black circles in the diagrams represent the evaluated design points within the automatic CFD simulations for each pair of design parameters (diameter and angle). The red line in the diagrams represents the results obtained with the manual optimisation method. Based on the results of the automatic CFD simulation (black circles), a response surface was created by a second order polynomial fit. The trends for both methods generally are in good agreement for comparable design points.

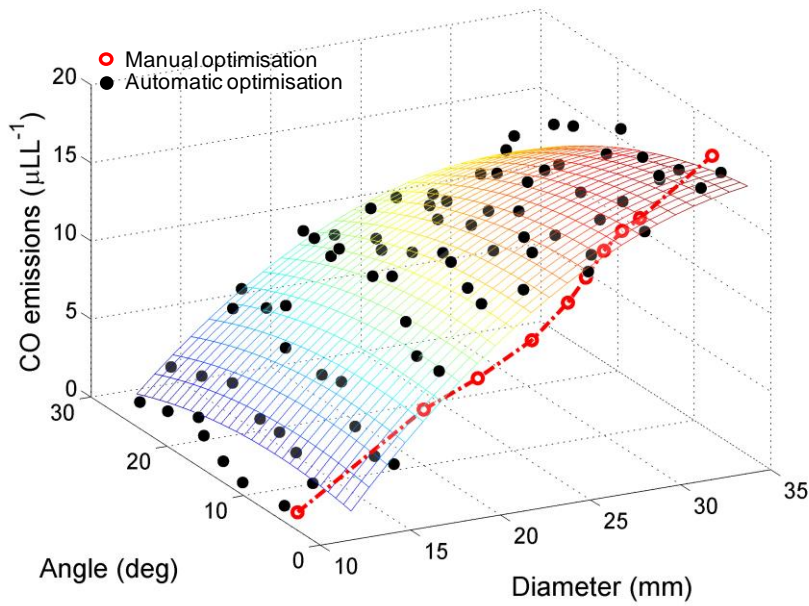


Figure 3.15: Response surface plot of CO emissions calculated with the automatic optimisation method (Explanation: [mLL⁻¹] corresponds to [ppmv] in non-SI unit)

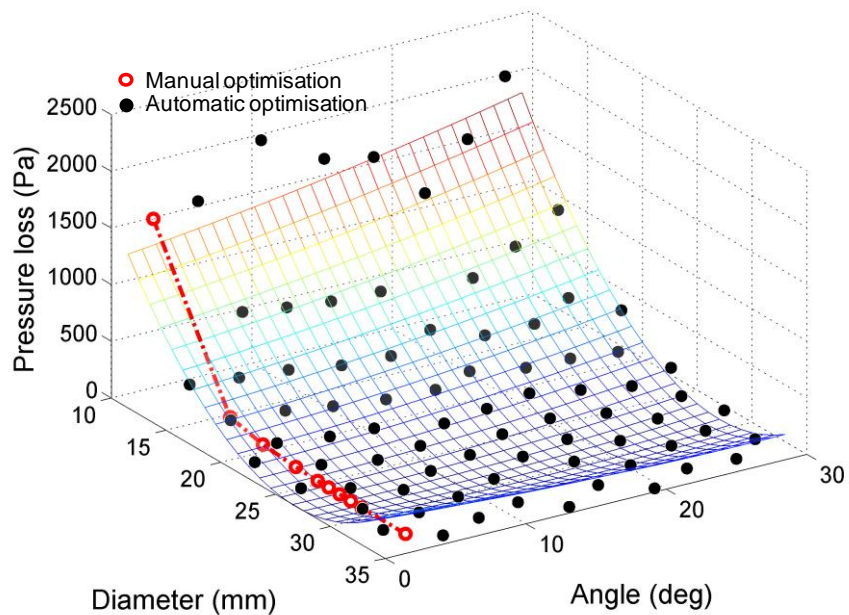


Figure 3.16: Response surface plot of pressure losses calculated with the automatic optimisation method

Figure 3.17 shows the values of the weight function calculated according to Eq. 2-37 for different combinations of nozzle angles and diameters. By screening through the weight surface, many local minima can be detected. These local minima represent the smallest values in a certain investigated area, while the global minimum represents the smallest value within the total definition range of the variation parameters. The absolute minimum represents the optimum combination of nozzle diameter and nozzle angle (15 mm diameter and 5° nozzle angle in the present case). While in the automatic

optimisation study the whole parameter range is investigated systematically, only a few simulations based on trial-and-error can be performed during a manual optimisation study. Therefore, the automatic optimisation provides a considerably higher possibility to find the global optimum.

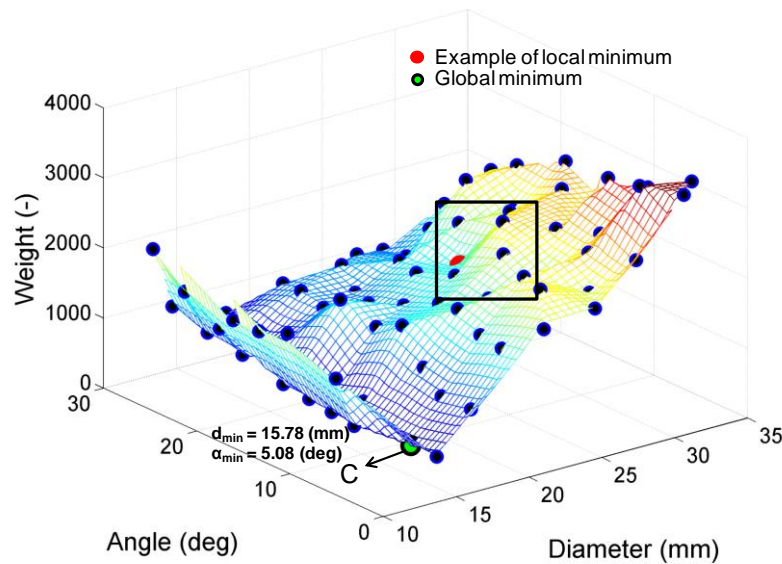


Figure 3.17: Weight surface from automatic optimisation calculations based on 80 design points (tetrahedral mesh type with 1 million grid cells)

In Figure 3.18 the CO emissions are plotted against the pressure loss for all design points. Here, the Pareto front represents the design points which have the lowest CO emission for a chosen pressure loss and the lowest pressure loss for a chosen CO emission, respectively. Hence, by the Pareto front not only the global optimum can be found but also the best possible design for a certain restriction e.g. concerning the pressure loss or CO emissions.

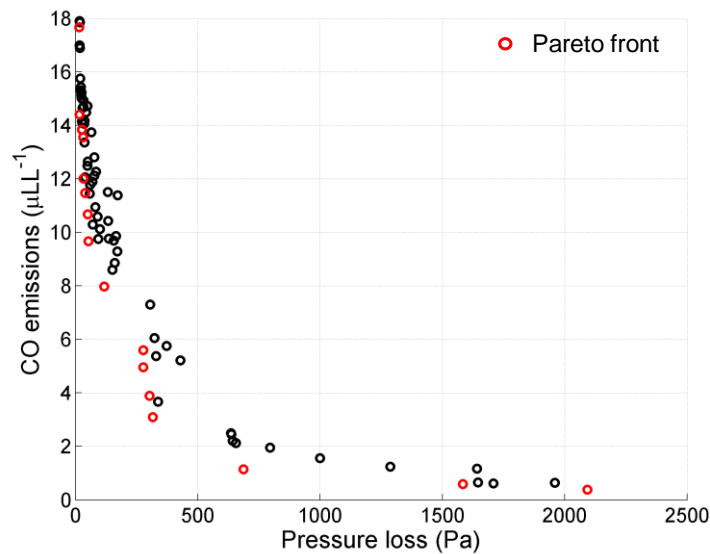


Figure 3.18: Results for design points with Pareto front (Explanation: $[mLL^{-1}]$ corresponds to $[ppmv]$ in non-SI unit)

Additionally, a further automatic parameter study has been carried out to investigate the influence of the grid type on computation time and accuracy. For this purpose, two sets of grid have been studied: a tetrahedral mesh and a polyhedral mesh. While the first grid type has been used as reference grid with 1 million cells (high resolution), the polyhedral type was generated by a conversion of the tetrahedral mesh type. This method reduces the number of mesh cells to approximately 250,000 cells.

The influence of the different grids on the results is shown in Figure 3.19. The CO emissions calculated with the polyhedral mesh show deviations from results which have been achieved with the tetrahedral mesh for diameters larger than 20 mm, since the penetration of the secondary air is underestimated due to large cell sizes in the region of the nozzles. The calculated weight function for the different meshes is shown in Figure 3.20. While for a diameter of approximately 15 mm the pressure drop is below 200 Pa, the CO concentrations at the outlet of the secondary combustion chamber are still below 8 (μLL^{-1}) (see Figure 3.19). Although the CO emissions calculated with the polyhedral mesh show deviations from the values calculated with the tetrahedral mesh, the optimum of the weight function (point H) is located approximately at the same position (point G) (see Figure 3.20). The main reason for the difference between the obtained global minimum from the manual optimisation study (point K) in comparison to the automatic optimisation studies (points G and H) is due to the effect of angle variations which has not been considered in the manual study.

In case of the tetrahedral mesh type the overall optimisation time took one month under consideration of two optimisation parameters (diameter and angle for 80 design points). By using the polyhedral mesh, the optimum of the parameter study was found within 6 days. In contradiction, a manual design study would need approximately 8 months due to the comprehensive number of person-hours to create the numerical grid and to set-up the calculations for each design point.

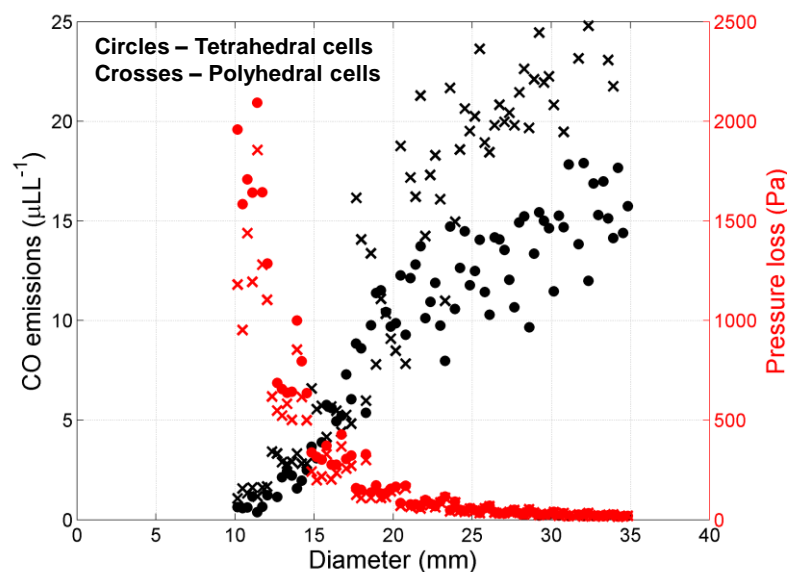


Figure 3.19: Effect of mesh type on the calculated CO emissions and pressure losses for the pilot-scale grate furnace (Explanation: [mLL^{-1}] corresponds to [ppmv] in non-SI unit)

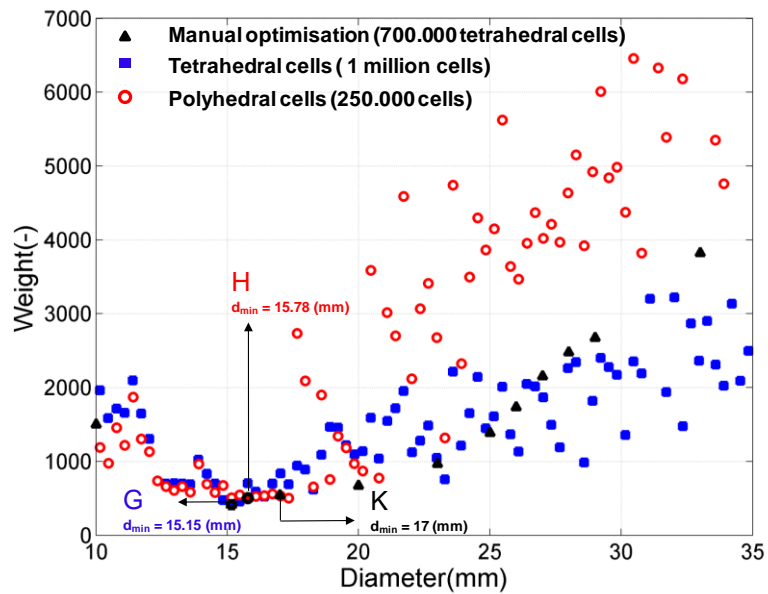


Figure 3.20: Weight function for different mesh types

Despite deviations in CO emission predictions from the referenced grid, the polyhedral mesh shows a great potential to accelerate the optimisation cycle. A local mesh refinement in the region of secondary air jets is needed for an improved CO prediction and is expected to just slightly increase the mesh size and hence computation time.

The developed routine has proved the applicability of the automatic optimisation procedures in the context of biomass furnace industry by using CFD for the furnace simulation and optimisation. The integration of the automatic CFD-based optimisation routine developed in the design phase allows engineers to interact with the other design groups without excessive delays. Moreover, the reduction of industrial costs is significant since it is no longer needed to build many different models to be tested for an optimised model building with respect to the optimisation targets.

The new automatic CFD-based optimisation routine has demonstrated to work effectively in terms of qualitative representation of targeted optimisation variables (e.g. CO emissions) when state-of-the-art EDM combustion model is applied in the simulations. However, it is possible to couple the optimisation routine with a newly developed gas phase combustion models (e.g. the hybrid and hybrid-streak model) when the quantitative representation of the optimisation variables are of high relevance like in case of NO_x formation processes.

4 Summary and conclusions

The present work aimed at the development and validation of CFD-based design tools for an improved simulation of gas phase related processes as well as CFD-based simulations coupled with optimisation routines to find the optimal design in biomass packed bed furnaces.

As far as the gas phase related processes are concerned, the gas phase combustion models play an important role as predictive models concerning flow, temperature and gaseous emission prediction. The well-known Eddy Dissipation Model (EDM) and Eddy Dissipation Concept (EDC) are the most prevalent gas phase combustion models usually being applied for the simulation of biomass packed bed furnaces. However, both models are developed for high Reynolds flows and the constants of the models need to be tuned for particular applications. In biomass grate furnaces, in particular above the fuel bed, the flow is in low Reynolds range. Here, the flue gas velocity varies from 0.5 to 2 (m/s). Moreover, in small-scale combustion plants even the exit Reynolds number of the secondary air jets may be in the laminar to transition region. Therefore, the prediction of the flue gas species and temperature strongly depends on the CFD gas phase combustion model applied. Here, it is important to simulate the combustion progress by the pure finite rate kinetics model. It was shown that the EDC is not valid for turbulent Reynolds numbers lower than 64 which makes the model impractical to be used in laminar and weakly turbulent regions. Besides, it is not an easy task to tune the EDC model constants to be used universally since it might be changed for a particular application. Therefore, a general hybrid gas phase combustion model which is valid in low and high turbulent Reynolds numbers is developed and verified. The hybrid model is a combination of finite rate kinetics (FRK) and EDC models, where the reaction rate is weighted by the local turbulent Reynolds number of the flow. The lower the turbulent Reynolds number of the flow, the greater the contribution of the FRK model to the overall reaction rate calculation in the hybrid model and vice versa. The hybrid model was extensively validated for a series of diffusion methane jet flames covering laminar (flame A with a jet Reynolds number 1100), moderately turbulent (flame B with a jet Reynolds number 8200), and highly turbulent (Sandia flame D with a jet Reynolds number 22400) flow conditions. The CFD results obtained for flames A and B showed that the differential diffusion has profound effect on the accuracy of the predictions at low Reynolds combustion flows. Moreover, it was found that the EDC was not able to establish flame A, where most of the reaction zones were located outside of the validity range of the EDC model (see *Paper I*). The results with the hybrid model for all flames showed good agreements with measurement data. The results obtained with the hybrid and the FRK models for flame A outlined that the hybrid model performed very similarly to the FRK model, since the reaction zones for this flame were out of the EDC validity range. The simulation results for flame B with the EDC model showed good agreements with experimental data. However, the simulation with the hybrid model exhibited better performance to predict the radicals (e.g. OH and H₂). The better performance of the hybrid model in case of flame B can be explained by a greater contribution of the FRK model to the overall reaction rate calculation (see *Paper I*). Moreover, the simulated

results with the hybrid model for flame D showed a better performance of the hybrid model in comparison to the EDC and the FRK models.

In the hybrid combustion model, close to the wall, the turbulent Reynolds number of the flow approaches unity and the reaction rate is mainly calculated by the FRK model, despite the fact that the larger fraction of the flow in the wall near cells is influenced by inertial forces (Reynolds stresses). Thus, in reacting flows, the reaction rate prediction in the boundary layer should be controlled depends on the contribution of viscous or inertial forces. Therefore, the hybrid model was further extended to account for the near wall combustion conditions. In this context, the mean chemical reaction rate for the near wall cells was adjusted by blending the FRK and the EDC models using weighting factors (see *Paper III*).

Concluding, the hybrid model shows a great potential for the application in all ranges of flow conditions (i.e. from laminar to turbulent flow) and can be applied for an improved prediction of gas phase combustion in biomass combustion plants. The model can also be applied for an improved NO_x prediction since it captures radicals with better accuracy than the EDC model.

The streak formation from the packed bed is another gas phase related process that needs to be considered when modelling biomass packed bed furnaces when no detailed simulations of the biomass conversion in the packed bed are considered but release profiles from the bed are defined as boundary conditions. State-of-the-art packed bed models calculate profiles of partially premixed flue gas compositions not considering spatial concentration gradients of oxygen and volatiles since the fuel particles and the surrounding space cannot be resolved. However, in reality, the amount and distribution of combustibles and oxidiser in the gas released from the biomass particles in the fuel bed are locally strongly differing. Therefore, the “porous” nature of the packed bed leads to streak formation influencing gas mixing and combustion, which is not described by state-of-the-art CFD-based packed bed models. Therefore, a streak formation model was developed to account for the effects of gas streaks arising from the fuel bed on gas mixing and reactions. The streak formation model was based on a correlation between the local gas residence time and a mixing time in which the latter is the necessary time to reach the fully mixed condition in the gas phase above the fuel bed.

A mixing state definition was introduced in order to evaluate the degree of mixing above the packed bed. The gas residence time introduced in the streak formation model is obtained by solving a scalar transport equation. A series of packed bed CFD case study simulations were carried out to derive the mixing time introduced in the streak formation model. The primary air velocity, volatile mass flow rate and number of particles (bed thickness) were identified as influencing parameters for the derivation of the mixing time. The results of the CFD packed bed case study serves as look-up table for the calculation of the mixing time in dependence of the different influencing parameters. The mixing time can be retrieved by a linear interpolation between the calculation points in dependence of the particle Reynolds number and the number of fuel layers. Then, the streak formation model was linked with the hybrid gas phase reaction model. The link of

the hybrid gas phase reaction model and the streak formation model was termed as hybrid-streak model. Therefore, the effective reaction rate in the hybrid model is achieved by multiplying the mixing function, which considers macro mixing, with the reaction rate predicted with the hybrid model. Furthermore, application and verification of the hybrid-streak model were performed by the simulations of a pilot-scale grate furnace (nominal boiler load: 150 kW_{th}) (**Paper II**) and an under-feed stoker furnace (nominal boiler load: 20 kW_{th}) (**Paper III**) regarding gas phase combustion and NO_x formation.

The results from the pilot-scale biomass grate furnace (**Paper II**) showed that the streaks had no big influence on the combustion process including flue gas temperature and CO emissions. The low oxygen concentrations in the primary combustion zone (i.e. $\lambda_{\text{primary combustion zone}} \ll 1$) and rather high flue gas residence time in the primary combustion chamber resulted in a full CO burnout at furnace exit as well as a full conversion of oxygen before the secondary combustion zone. However, the formation of reacting radicals (e.g. O and OH), especially, in the region above the fuel bed were influenced by the streak formation model since the reaction progress was delayed caused by the incomplete mixing. Moreover, the distribution of NH₃, HCN and NO profiles showed that the streak formation model has a strong influence on the spatial distribution of these species which is mainly due to the slowdown of the reaction rate predictions caused by the streak formation model.

The second verification of the streak formation model was done for a small-scale under-feed stoker furnace (nominal boiler load: 20 kW_{th}) for two biomass fuels (**Paper III**). The EDM, EDC, hybrid gas phase reaction models as well as the new hybrid-streak model were used for the simulation of turbulent reactive flow in the combustion chamber. The results from the under-feed stoker case studies showed that for both fuels investigated, the streaks has a relevant influence on the combustion process regarding flue gas temperature, O₂ distribution and CO emissions. Moreover, the formation of radicals (e.g. O and OH), especially in the region above the bed is influenced by the mixing of the streaks which delays the reaction progress. The NO_x emissions calculated with the hybrid-streak model show the best agreement with measured values.

Concluding, the streak formation model in combination with the hybrid gas phase combustion model shows a clear potential for an improved NO_x prediction since it considers species mixing and reaction processes above the fuel bed with a higher accuracy.

Finally, a basic CFD-based design tool for the automatic performance of parameter studies for the optimisation of biomass combustion plants was developed. The routine consists of parametrisation routines and optimisation functions that have been linked with an empirical packed bed combustion model and gas phase CFD models especially adapted for biomass combustion. For the simulation of the gas phase, the Realizable k- ϵ turbulence model for turbulence, the Discrete Ordinate Model for radiation and state-of-the-art EDM gas phase combustion model in combination with a global 3-step mechanism are used. The approach is numerically robust and computationally fast for

engineering applications which is important in the design phase for biomass furnace industry when trend identifications of targeted optimisation variables are necessary. However, the optimisation routines could also be coupled with the newly developed hybrid-streak model in future for better evaluation of NO_x formation processes. To test and verify the model developed, it was applied for the optimisation of a pilot-scale biomass grate furnace (nominal boiler load: 180 kW_{th}) with the main objective to minimise the CO emissions at an acceptable pressure loss by changing the diameter and angle of the secondary air nozzles. A common difficulty with a multi-optimisation variables problem is the conflict between the optimisation variables. One of the most classical methods is the method of optimisation variables weighting. Therefore, a weight function is defined to combine the two optimisation variables (CO emissions and pressure loss over the secondary air nozzles) according to their relevance in a common function. For the biomass grate furnace studied, a linear correlation to the weight function has been assumed (proportional to the energy demand of the fan) for the pressure drop. Regarding the CO emissions, a polynomial function with a strong increase at a chosen emission limit (20 µLL⁻¹ in the present case) was supposed.

The sensitivity analysis performed underlines the high impact of the nozzle diameter on the pressure losses and CO emissions in comparison to the nozzle angle (**Paper IV and V**). The parameter variation performed automatically is by far more efficient than the manual case study due to the considerably lower simulation time and personnel demand. The overall simulation time for the calculation of 80 design points could be reduced by a factor of 8 in case of the tetrahedral mesh type and by a factor of 32 in case of the polyhedral mesh type (**Paper IV and V**). Although the CO emission trends were slightly differing for the two studied grid types, the global minima are located nearly at the same positions (**Paper IV and V**). The new CFD optimisation routine proofed to work efficiently in terms of nozzle design optimisation and time demand. Concluding, the new automatic CFD optimisation routine works well and shows a large potential concerning targeted geometry optimisation of biomass furnaces as well as a substantial reduction of manpower needed.

To sum up, the thesis contributes with two relevant inputs to the improved simulation of packed bed biomass combustion plants. On the one hand with a development of an advanced hybrid gas phase combustion model that is valid over a wide range of turbulent Reynolds numbers as well as a streak formation model to account for the effect of streaks from the packed bed when state-of-the-art packed bed models are used to describe the release profiles of the bed as boundary conditions and no detailed simulations of the biomass conversion in the packed bed are considered. On the other hand with a development of automatic CFD-based optimisation routines and optimisation functions linked with the CFD models adapted for biomass combustion for an optimised model building with respect to the input optimisation parameters and constraints which are specified by the users.

Bibliography

- [1] K. Görner and T. Klasen, "Modelling, simulation and validation of the solid biomass combustion in different plants," *Progress in Computational Fluid Dynamics*, vol. 6, no. 4-5, pp. 225-234, 2006.
- [2] S. K. Kær, "Numerical modelling of a straw-fired grate boiler," *Fuel*, vol. 83, no. 9, pp. 1183-1190, 2004.
- [3] J. Larfeldt, L. Tao and N. Berge, "Development of an engineering tool for design and optimisation of biomass combustion in grate-fired boilers," in *Proceedings of the 5th European Conference on Industrial Furnaces and Boilers*, Porto, Portugal, 2000.
- [4] R. Scharler, T. Fleckl and I. Obernberger, "Modification of a Magnussen Constant of the Eddy Dissipation Model for biomass grate furnaces by means of hot gas in-situ FT-IR absorption spectroscopy," *Progress in Computational Fluid dynamics*, vol. 3, no. 2-4, pp. 102-111, 2003.
- [5] R. Scharler, "Entwicklung und Optimierung von Biomasse-Rostfeuernungen durch CFD-Analyse," PhD Thesis, Graz University of Technology, 2001.
- [6] M. Mancini, R. Weber and U. Bollettini, "Predicting NOx emissions of a burner operated in flameless oxidation mode," *Proceedings of the Combustion Institute*, vol. 29, no. 1, pp. 1155-1163, 2002.
- [7] A. A. F. PETERS and R. WEBER, "Mathematical Modeling of a 2. 25 MWt Swirling Natural Gas Flame. Part 1: Eddy Break-up Concept for Turbulent Combustion; Probability Density Function Approach for Nitric Oxide Formation," *Combustion Science and Technology*, Vols. 110-111, no. 1, pp. 67-101, 1995.
- [8] H. Xue, J. Ho and Y. Cheng, "Comparison of different combustion models in enclosure fire simulation," *Fire Safety Journal*, vol. 36, no. 1, pp. 37-54, 2001.
- [9] S. Yaxin, C. Chen and A. Su, "Simulation of High Temperature Air Combustion with modified Eddy-Break-Up combustion model," *Energy Procedia*, vol. 14, pp. 127-132, 2012.
- [10] D. Spalding, "Mixing and chemical reaction in steady confined turbulent flames," *Symposium (International) on Combustion*, vol. 13, no. 1, pp. 649-657, 1971.
- [11] B. F. Magnussen and B. H. Hjertager, "On mathematical modeling of turbulent combustion with special emphasis on soot formation and combustion," in *the 16th Symp. (Int.) on Combustion*, Pittsburgh, 1976.

- [12] B. F. Magnussen, "On the structure of turbulence and a generalized eddy dissipation concept for chemical reaction in turbulent flow," in *19th AIAA aerospace science meeting*, St. Louis, Missouri, USA, 1981.
- [13] A. De, E. Oldenhof, P. Sathiah and D. Roekaerts, "Numerical Simulation of Delft-Jet-in-Hot-Coflow (DJHC) Flames Using the Eddy Dissipation Concept Model for Turbulence–Chemistry Interaction," *Flow, Turbulence and Combustion*, vol. 87, no. 4, pp. 537-567, 2011.
- [14] R. Barlow, J. Frank, A. Karpetis and J.-Y. Chen, "Piloted methane/air jet flames: Transport effects and aspects of scalar structure," *Combustion and Flame*, vol. 143, no. 4, pp. 433-449, 2005.
- [15] R. Mehrabian, S. Zahirović, R. Scharler, I. Obernberger, S. Kleditzsch, S. Wirtz, V. Scherer, H. Lu and L. L. Baxter, "A CFD model for thermal conversion of thermally thick biomass particles," *Fuel Processing Technology*, vol. 95, no. 0, pp. 96-108, 2012.
- [16] H. Safikhani, M. Akhavan-Behabadi, N. Nariman-Zadeh and M. M. Abadi, "Modeling and multi-objective optimization of square cyclones using CFD and neural networks," *Chemical Engineering Research and Design*, vol. 89, no. 3, pp. 301-309, 2011.
- [17] K. Elsayed and C. Lacor, "Modeling, analysis and optimization of air cyclones using artificial neural network, response surface methodology and CFD simulation approaches," *Powder Technology*, vol. 212, no. 1, pp. 115-133, 2011.
- [18] H. Safikhani, A. Hajiloo and M. Ranjbar, "Modeling and multi-objective optimization of cyclone separators using CFD and genetic algorithms," *Computers & Chemical Engineering*, vol. 35, no. 6, pp. 1064-1071, 2011.
- [19] K. Elsayed and C. Lacor, "Optimization of the cyclone separator geometry for minimum pressure drop using mathematical models and CFD simulations," *Chemical Engineering Science*, vol. 65, no. 22, pp. 6048-6058, 2010.
- [20] S. Park, "Optimization of combustion chamber geometry and engine operating conditions for compression ignition engines fueled with dimethyl ether," *Fuel*, vol. 97, no. 0, pp. 61-71, 2012.
- [21] S. W. Park, "Optimization of combustion chamber geometry for stoichiometric diesel combustion using a micro genetic algorithm," *Fuel Processing Technology*, vol. 91, no. 11, pp. 1742-1752, 2010.
- [22] S. Derakhshan, B. Mohammadi and A. Nourbakhsh, "Incomplete sensitivities for 3D radial turbomachinery blade optimization," *Computers & Fluids*, vol. 37, no. 10, pp. 1354-1363, 2008.

- [23] S. Derakhshan, B. Mohammadi and A. Nourbakhsh, "The comparison of incomplete sensitivities and Genetic algorithms applications in 3D radial turbomachinery blade optimization," *Computers & Fluids*, vol. 39, no. 10, pp. 2022-2029, 2010.
- [24] K.-Y. KIM and S.-J. SEO, "Application of Numerical Optimization Technique to Design of Forward-Curved Blades Centrifugal Fan," *JSME International Journal Series B Fluids and Thermal Engineering*, vol. 49, no. 1, pp. 152-158, 2006.
- [25] X. Huai, W. Xu, Z. Qu, Z. Li, F. Zhang, G. Xiang, S. Zhu and G. Chen, "Analysis and optimization of municipal solid waste combustion in a reciprocating incinerator," *Chemical Engineering Science*, vol. 63, no. 12, pp. 3100-3113, 2008.
- [26] K. Shah, R. Vuthaluru and H. Vuthaluru, "CFD based investigations into optimization of coal pulveriser performance: Effect of classifier vane settings," *Fuel Processing Technology*, vol. 90, no. 9, pp. 1135-1141, 2009.
- [27] R. Scharler, C. Benesch, K. Schulze and I. Obernberger, "CFD simulations as efficient tool for the development and optimisation of small-scale biomass furnaces and stoves.," in *the 19th European Biomass Conference & Exhibition*, Berlin, Germany, 2011.
- [28] E. Widmann, "Modellbildung zum Abbrandverhalten von Biomasse unter besonderer Berücksichtigung der N-Freisetzung am Beispiel einer Rostfeuerung," MSc Thesis, Graz University of Technology, Graz, 2002.
- [29] R. Scharler, E. Widmann and I. Obernberger, "CFD modeling of NO_x formation in biomass grate furnaces with detailed chemistry," in *Science in thermal and chemical biomass conversion*, Victoria, Canada, 2004.
- [30] I. Obernberger, E. Widmann and R. Scharler, "Entwicklung eines Abbrandmodells und eines NO_x-Postprozessors zur Verbesserung der CFD-Simulation von Biomasse-Festbettfeuerungen," Ministry for Transport, Innovative and Technology, Vienna, Austria, 2003.
- [31] G. Stubenberger, R. Scharler, S. Zahirovic and I. Obernberger, "Experimental investigation of nitrogen species release from different solid biomass fuels as a basis for release models," *Fuel*, vol. 87, no. 6, pp. 793-806, 2008.
- [32] Y. B. Yang, H. Yamauchi, V. Nasserzadeh and J. Swithenbank, "Effects of fuel devolatilisation on the combustion of wood chips and incineration of simulated municipal solid wastes in a packed bed," *Fuel*, vol. 82, no. 18, p. 2205-2221, 2003.
- [33] H. Zhou, A. D. Jensen, P. Glarborg and A. Kavaliauskas, "Numerical modeling of straw combustion in a fixed bed," *Fuel*, vol. 84, no. 4, p. 389-403, 2005.

- [34] B. Peters, "Measurements and Application of a Discrete Particle Model (DPM) to Simulate Combustion of a Packed Bed of Individual Fuel Particles," *Combustion and Flame*, vol. 131, no. 1-2, pp. 132-146, 2002.
- [35] R. Scharler, C. Benesch, A. Neudeck and I. Obernberger, "CFD based design and optimisation of wood log fired stoves," in *17th European biomass conference & exhibition*, Hamburg, Germany, 2009.
- [36] R. Scharler, M. Forstner, M. Braun, T. Brunner and I. Obernberger, "Advanced CFD analysis of large fixed bed biomass boilers with special focus on the convective section," in *2nd World conference and exhibition on biomass for energy, industry and climate protection*, Rome, Italy, 2004.
- [37] R. Scharler and I. Obernberger, "CFD analysis of air staging and flue gas recirculation in biomass grate furnaces," in *1st World conference on biomass for energy and industry*, Sevilla, Spain, 2000.
- [38] A. Brink, "Eddy Break-Up based models for industrial diffusion flames with complex gas phase chemistry," PhD Thesis, Abo Akademi University, 1998.
- [39] P. Kilpinen.
- [40] S. Zahirović, R. Scharler, P. Kilpinen and I. Obernberger, "A kinetic study on the potential of a hybrid reaction mechanism for prediction of NO_x formation in biomass grate furnaces," *Combustion Theory and Modelling*, vol. 15, no. 5, pp. 645-670, 2011.
- [41] T. F. Smith, Z. F. Shen and J. N. Friedman, "Evaluation of Coefficients for the Weighted Sum of Gray Gases Model," *Journal of Heat Transfer*, vol. 104, no. 4, pp. 602-608, 1982.
- [42] S. Pope, "Computationally efficient implementation of combustion chemistry using in situ adaptive tabulation," *Combustion Theory and Modelling*, vol. 1, no. 1, pp. 41-63, 1997.
- [43] H. Magel, U. Schnell and K. Hein, "Simulation of detailed chemistry in a turbulent combustor flow," *Symposium (International) on Combustion*, vol. 26, no. 1, pp. 67-74, 1996.
- [44] I. R. GRAN and B. F. MAGNUSSEN, "A Numerical Study of a Bluff-Body Stabilized Diffusion Flame. Part 2. Influence of Combustion Modeling And Finite-Rate Chemistry," *Combustion Science and Technology*, vol. 119, no. 1-6, pp. 191-217, 1996.
- [45] I. R. Gran, "Mathematical Modeling and Numerical Simulations of Chemical Kinetics

in Turbulent Combustions,” Ph.D. Thesis, Dept. of Applied Mechanics, Thermodynamics and Fluid Dynamics, Norwegian University of Science and Technology, Trondheim, Norway, 1994.

- [46] J. P. Jessee, R. Gansman and W. Fiveland, “Calculation of chemically reacting flows using finite rate kinetics,” *Heat Transfer in Fire and Combustion System*, vol. 250, pp. 43-53, 1993.
- [47] I. S. ERTESVAG and B. F. MAGNUSSEN, “The Eddy Dissipation Turbulence Energy Cascade Model,” *Combustion Science and Technology*, vol. 159, no. 1, pp. 213-235, 2000.
- [48] J. B. Perot and S. M. D. B. Kops, “Modeling turbulent dissipation at low and moderate Reynolds numbers,” *Journal of Turbulence*, vol. 7, p. N69, 2006.
- [49] H. Tennekes and J. L. Lumley, *A first course in turbulence*, MIT Press, 1972.
- [50] M. Rehm, P. Seifert and B. Meyer, “Theoretical and numerical investigation on the EDC-model for turbulence and chemistry interaction at gasification conditions,” *Computers & Chemical Engineering*, vol. 33, no. 2, pp. 402-407, 2009.
- [51] M. Graça, A. Duarte, P. Coelho and M. Costa, “Numerical simulation of a reversed flow small-scale combustor,” *Fuel Processing Technology*, vol. 107, no. 0, pp. 126-137, 2013.
- [52] S. R. Shabanian, P. R. Medwell, M. Rahimi, A. Frassoldati and A. Cuoci, “Kinetic and fluid dynamic modeling of ethylene jet flames in diluted and heated oxidant stream combustion conditions,” *Applied Thermal Engineering*, vol. 52, no. 2, pp. 538-554, 2013.
- [53] J. Aminian, C. Galletti, S. Shahhosseini and L. Tognotti, “Key modeling issues in prediction of minor species in diluted-preheated combustion conditions,” *Applied Thermal Engineering*, vol. 31, no. 16, pp. 3287-3300, 2011.
- [54] J. Aminian, C. Galletti, S. Shahhosseini and L. Tognotti, “Numerical Investigation of a MILD Combustion Burner: Analysis of Mixing Field, Chemical Kinetics and Turbulence-Chemistry Interaction,” *Flow, Turbulence and Combustion*, vol. 88, no. 4, pp. 597-623, 2012.
- [55] S. . B. Pope, *Turbulent Flows*, Cambridge University Press, 2000.
- [56] J. Kim, P. Moin and R. Moser, “Turbulence statistics in fully developed channel flow at low Reynolds number,” *Journal of Fluid Mechanics*, vol. 177, pp. 133-166, 4 1987.
- [57] B. Kader, “Temperature and concentration profiles in fully turbulent boundary

- layers," *International Journal of Heat and Mass Transfer* , vol. 24, no. 9, pp. 1541-1544, 1981.
- [58] M. Bartak, M. Cermak, J. A. Clarke, J. Denev and F. Drkal, "Experimental and numerical study of local mean age-of-air," in *7th International Building performance Simulation Association Conference*, Rio de Janeiro, Brazil, 2001.
- [59] D. A. Eggar, M. G. Faram, T. O'Doherty, D. A. Phipps and N. Syred, "Computational fluid dynamic prediction of the residence time distribution of a prototype hydrodynamic vortex separator operating with a base flow component," *Part E Journal of Process Mechanical Engineering*, vol. 219, no. 1, pp. 53-67, 2005.
- [60] S. Zahirović, R. Scharler, P. Kilpinen and I. Obernberger, "Validation of flow simulation and gas combustion sub-models for the CFD-based prediction of NO_x formation in biomass grate furnaces," *Combustion Theory and Modelling*, vol. 15, no. 1, pp. 61-87, 2010.
- [61] D. Neves, H. Thunman, A. Matos, L. Tarelho and A. Gómez-Barea, "Characterization and prediction of biomass pyrolysis products," *Progress in Energy and Combustion Science*, vol. 37, no. 5, pp. 611-630, 2011.
- [62] M. L. Boroson, J. B. Howard, J. P. Longwell and W. A. Peters, "Product yields and kinetics from the vapor phase cracking of wood pyrolysis tars," *AIChE Journal*, vol. 35, no. 1, pp. 120-128, 1989.
- [63] R. Graham, M. Bergougnou and R. Overend, "Fast pyrolysis of biomass," *Journal of Analytical and Applied Pyrolysis* , vol. 6, no. 2, pp. 95-135, 1984.
- [64] ÖNORM.M7135, Compressed wood or compressed bark in natural state, pellets and briquettes. Requirements and test specifications, Vienna, Austria: Österreichisches, 2003.
- [65] A. Garcia-Maraver, V. Popov and M. Zamorano, "A review of European standards for pellet quality," *Renewable Energy*, vol. 36, no. 12, pp. 3537-3540, 2011.
- [66] S. Hamel, *On the Packing Properties of Fixed Beds for Thermal Fuel Conversion*, Germany: Shaker verlag, 2010.
- [67] R. Barlow and J. Frank, "Effects of turbulence on species mass fractions in methane/air jet flames," *Symposium (International) on Combustion* , vol. 27, no. 1, pp. 1087-1095, 1998.
- [68] C. Schneider, A. Dreizler, J. Janicka and E. Hassel, "Flow field measurements of stable and locally extinguishing hydrocarbon-fuelled jet flames," *Combustion and Flame*, vol. 135, no. 1-2, pp. 185-190, 2003.

- [69] R. S. Barlow and J. H. Frank. [Online]. Available: www.sandia.gov/TNF/DataArch/Flamed.html.
- [70] A. Morse, "Axisymmetric turbulent shear flows with and without swirl," Ph.D. thesis, England, London University, 1977.
- [71] S. B. POPE, "An explanation of the turbulent round-jet/plane-jet anomaly," *AIAA Journal*, vol. 16, no. 3, pp. 279-281, 1978.
- [72] B. Merci, E. Dick, J. Vierendeels, D. Roekaerts and T. W. J. Peeters, "Application of a new cubic turbulence model to piloted and bluff-body diffusion flames," *Combustion and Flame*, vol. 126, no. 1-2, pp. 1533-1556, 2001.
- [73] B. Merci and E. Dick, "Influence of computational aspects on simulations of a turbulent jet diffusion flame," *International Journal of Numerical Methods for Heat & Fluid Flow*, vol. 13, no. 7, pp. 887-898, 2003.
- [74] A. Kazakov and M. Frenklach. [Online]. Available: www.me.berkeley.edu/drm/.
- [75] M. Frenklach, H. Wang, C. Yu, M. Goldenberg, C. Bowman and R. Hanson. [Online]. Available: www.me.berkeley.edu/gri_mech/.
- [76] C. Bowman, R. Hanson, D. Davidson, W. Gardiner, V. Lissianski and G. Smith. [Online]. Available: www.me.berkeley.edu/gri_mech/.
- [77] F. Christo and B. Dally, "Modeling turbulent reacting jets issuing into a hot and diluted coflow," *Combustion and Flame*, vol. 142, no. 1-2, pp. 117-129, 2005.
- [78] R. Bilger, S. Starner and R. Kee, "On reduced mechanisms for methane air combustion in nonpremixed flames," *Combustion and Flame*, vol. 80, no. 2, pp. 135-149, 1990.
- [79] A. Mardani and S. Tabejamaat, "NO_x Formation in H₂-CH₄ Blended Flame Under MILD Conditions," *Combustion Science and Technology*, vol. 184, no. 7-8, pp. 995-1010, 2012.
- [80] S. R. Turns, "Understanding NO_x formation in nonpremixed flames: Experiments and modeling," *Progress in Energy and Combustion Science*, vol. 21, no. 5, pp. 361-385, 1995.

Annex

Paper I



Development of a gas phase combustion model suitable for low and high turbulence conditions



Ali Shiehnejadhesar^{a,b,*}, Ramin Mehrabian^{a,b}, Robert Scharler^{a,b,c}, Graham M. Goldin^d, Ingwald Obernberger^{a,b,c}

^a BIOENERGY 2020+ GmbH, Inffeldgasse 21b, 8010 Graz, Austria

^b Institute for Process and Particle Engineering, Graz University of Technology, Inffeldgasse 21b, 8010 Graz, Austria

^c BIOS BIOENERGIESYSTEME GmbH, Inffeldgasse 21b, 8010 Graz, Austria

^d ANSYS, Inc., 10 Cavendish Court, Lebanon, NH 03766, USA

HIGHLIGHTS

- The limitation of the EDC combustion model in low turbulence conditions is argued.
- A hybrid combustion model applicable over the whole Reynolds range is introduced.
- The importance of molecular diffusion at low Reynolds number is shown.
- The simulation results are in good agreement with experimental data.

ARTICLE INFO

Article history:

Received 18 November 2013
Received in revised form 17 February 2014
Accepted 18 February 2014
Available online 12 March 2014

Keywords:

Combustion
Eddy Dissipation Concept
Finite rate kinetics
Differential diffusion
Hybrid model

ABSTRACT

A novel hybrid gas phase combustion model suitable for low as well as high turbulent combustion conditions is proposed. In particular, in the region above the fuel bed of small-scale biomass combustion plants, gas phase mixing is highly influenced by laminar and low turbulence zones. Here, the eddy break-up combustion models are not valid because they were originally developed for highly turbulent flows. Therefore, a CFD gas phase reaction model applicable over the whole Reynolds range from laminar to turbulent flows is developed. It is a hybrid Eddy Dissipation Concept/finite rate kinetics model which calculates the effective reaction rate from laminar finite rate kinetics and the turbulent reaction rate and weights them depending on the local turbulent Reynolds number of the flow. To validate the proposed model, comparisons are made with experimental data for a series of jet flames covering laminar, transitional, and turbulent flow conditions. The simulation results show that the prediction of flame can be improved with the proposed hybrid combustion model.

© 2014 Elsevier Ltd. All rights reserved.

1. Introduction

The production and supply of energy is one of the greatest concerns of human society. With regard to the facts that the fossil fuel resources are depleting rapidly, the necessity to find new energy resources is indispensable. During recent decades, the share of energy production by biomass combustion plants has been growing, because biomass is a CO₂ neutral source of energy in a sustainable agriculture/forestry system [1]. CFD modelling is

becoming increasingly important for the development and optimisation of biomass combustion plants. Here, gas phase combustion models play a key role concerning predictions of flow, temperature, and gaseous emissions (e.g. CO).

The eddy break-up models (EBU) are the most prevalent Reynolds Averaged Navier–Stokes (RANS) based combustion models which have been successfully applied for a variety of combustion plants [2–4]. The popularity of the EBU combustion models come from their low computational costs especially for industrial applications in the context of RANS simulations. However, the empirical constants in the EBU models are not universally valid and need to be adapted depending on the application [5,6]. The EBU model first was proposed by Spalding [7] and later modified by Magnussen and Hjertager [8]. The main assumption of the EBU model is based on infinitely fast chemistry and assumes that the reaction rate is

* Corresponding author at: Institute for Process and Particle Engineering, Graz University of Technology, Inffeldgasse 21b, 8010 Graz, Austria. Tel.: +43 316 8739230; fax: +43 316 8739202.

E-mail addresses: ali.shiehnejadhesar@gmail.com, ali.shiehnejad@bioenergy2020.eu (A. Shiehnejadhesar).

Nomenclature

$C_{j,r}$	molar concentration of each reactant and product species j in reaction r (kg mol m^{-3})	T_r	time scale ratio (-)
C_γ	EDC model constant (-)	Y_i	mass fraction of species i (-)
C_{D1}	EDC model constant (-)	<i>Greek symbols</i>	
C_{D2}	EDC model constant (-)	ε	turbulent dissipation rate ($\text{m}^2 \text{s}^{-3}$)
C_τ	EDC model constant (-)	γ	length fraction of EDC fine scales (-)
d	jet diameter (m)	ν	kinematic viscosity ($\text{m}^2 \text{s}^{-1}$)
$D_{i,m}$	diffusion coefficient for species i in the mixture ($\text{m}^2 \text{s}^{-1}$)	$\nu'_{i,r}$	stoichiometric coefficient for reactant i in reaction r (-)
D_t	turbulent diffusivity ($\text{m}^2 \text{s}^{-1}$)	$\nu''_{i,r}$	stoichiometric coefficient for product i in reaction r (-)
\vec{J}_i	diffusion flux of species i ($\text{kg m}^{-1} \text{s}^{-1}$)	ρ	density (kg m^{-3})
$K_{f,r}$	forward rate constant for reaction r (s^{-1})	τ_{EDC}	EDC time scale (s)
$K_{b,r}$	backward rate constant for reaction r (s^{-1})	\vec{v}	velocity vector (m s^{-1})
k	turbulent kinetic energy ($\text{m}^2 \text{s}^{-2}$)	μ_t	turbulent viscosity ($\text{kg m}^{-1} \text{s}^{-1}$)
$M_{w,i}$	molecular weight (kg kmol^{-1})	<i>Subscript</i>	
N	number of species	b,r	backward reaction
N_R	number of reactions	EDC	Eddy Dissipation Concept
Re	Reynolds number (-)	FRK	finite rate kinetics
Re_t	turbulent Reynolds number (-)	f, r	forward reaction
R_i	net rate of production of species i by chemical reaction ($\text{kg m}^{-3} \text{s}^{-1}$)	i	species index
$\bar{R}_{i,r}$	molar rate of creation/destruction of species i in reaction r ($\text{kg mol m}^{-3} \text{s}^{-1}$)	r	reaction
S_{ct}	Schmidt number (-)	t	turbulent
T	temperature (K)		

controlled by turbulent mixing [8]. The Eddy Dissipation Concept (EDC) is an extended version of EBU model developed by Magnussen [9] which can incorporate detailed chemistry calculations in turbulent combustion. However, in the region above the fuel bed and in small-scale biomass combustion applications (size-range < 500 kWth), the gas phase mixing and reaction progress is highly influenced by laminar and low turbulence zones. Here, the EBU gas phase combustion models, which are originally developed for highly turbulent flows, are not valid, leading to wrong predictions of the reaction progress and wrong concentrations of gas species (CO, NO_x species, etc.).

The EDC, which enables the consideration of the complex interaction of turbulence and detailed reaction kinetics, was taken as a basis for the development of a general gas phase combustion model applicable for the entire Reynolds-number range of flows. However, gas phase combustion models like the EDC are originally developed for high-Reynolds-number conditions. The EDC is based on the turbulent energy cascade, which means that larger eddies break up into smaller eddies, and the reactions take place in the so-called fine structures, where the fluid is mixed on a micro-scale.

In biomass grate furnaces, in particular above the fuel bed, the flow is in the low Re range. Here, the flue gas varies from 0.5 to 2 (m/s). Moreover, in small-scale combustion plants (up to 100 kW), even the exit Reynolds number of the secondary air jets may be in the laminar to transition region. Therefore, the prediction of the flue gas species and temperature strongly depends on the CFD gas phase combustion model applied. In the EDC, the prediction mainly depends on the turbulent quantities k and ε , where a large error on the predictions is imposed when the flow approaches low Reynolds conditions. Here, it is important to simulate the combustion progress by the pure finite rate kinetics model.

Therefore, an advanced gas phase reaction model has to be developed which is sensitive regarding local flow conditions. The model should reliably distinguish between the mixing or kinetically dominated zones. Hence, a novel hybrid gas phase

combustion model which utilizes combined finite rate kinetics and EDC combustion models is presented in this work. The hybrid model was implemented in ANSYS® FLUENT®.

The model development was done based on the simulation of measured jet flames by Barlow and Frank [10] (Sandia flame D as well as flame A with a jet Re number of 1100 and flame B with a jet Re number of 8200). Since it is well-known that k - ε models over-predict the spreading rate of round jets, the model constants were modified in order to minimize additional effects influencing gas phase combustion modelling. Furthermore, at low-turbulent combustion regimes the description of the reaction kinetics is of high relevance since it has a considerable influence on the simulation results.

During typical biomass combustion conditions with air staging the most relevant components released are H₂O, CO₂, CO, H₂, and CH₄ [11–13]. All these species are also relevant during Methane combustion [14,15]. Moreover, the combustion model developed can be applied together with any reaction mechanisms, which of course has to be validated for the target application. Currently, the Skeletal Kilpinen97 mechanism [16] which has extensively been validated for biomass combustion conditions is being applied [17] for biomass grate furnaces. Hence, the reduced DRM-22 reaction mechanism [15] was selected based on the simulation of Sandia flame D.

At low-Re conditions the influence of molecular diffusion on mixing becomes comparable to the influence of turbulent diffusion. Therefore, the diffusion of each gas species in the mixture was taken into account and compared with the conventional approach (constant value for the diffusion of the species in the mixture) for the simulation of flame A (Re = 1100) and B (Re = 8200). While the EDC together with the differential-diffusion (diff-diff) approach gave a good agreement with measurements for flame B with moderate turbulence, it failed to predict the laminar flame A. With finite rate kinetics (FRK) good results could be achieved for flame A. Since it could be shown that the EDC is not valid below turbulent Reynolds number of 64 [18], a hybrid EDC/FRK model is introduced. The model calculates the reaction rates with the FRK

and the EDC and finally an effective reaction rate is calculated with weight functions in dependence of the turbulent Reynolds number.

2. Methodology

Since the hybrid model is a combination of the FRK and the EDC model, a brief description of both models is given first. Next, the limitation of the EDC especially at low turbulent conditions is investigated. Finally, the hybrid model is introduced which combines the FRK and the EDC model with a weighting factor in dependence of the local turbulent Reynolds number of the flow.

2.1. Finite-rate kinetics

The FRK model computes the chemical source terms using Arrhenius expressions, and ignores the effects of turbulent fluctuations [19]. For a multi-component system, the species mass conservation equation is defined as follows;

$$\frac{\partial}{\partial t}(\rho Y_i) + \nabla \cdot (\rho \vec{v} Y_i) = -\nabla \cdot \vec{J}_i + R_i \quad (1)$$

where ρ is the mixture density, Y_i is the mass fraction of species i , \vec{v} is the velocity vector, \vec{J}_i is the diffusion flux of species i due to concentration gradients, and R_i is the net rate of production of species i by the chemical reactions. The net reaction source of chemical species i is computed as the sum of the Arrhenius reaction sources over the N_R reactions that the species participates in [19]:

$$(R_i)_{\text{FRK}} = M_{w,i} \sum_{r=1}^{N_R} \bar{R}_{i,r} \quad (2)$$

where $M_{w,i}$ is the molecular weight of species i and $\bar{R}_{i,r}$ is the Arrhenius molar rate of creation/destruction of species i in reaction r .

The molar rate of creation/destruction of species i in reaction r ($\bar{R}_{i,r}$ in Eq. (2)) is determined:

$$\bar{R}_{i,r} = (v'_{i,r} - v''_{i,r}) \left[k_{f,r} \prod_{j=1}^N [C_{j,r}]^{\eta'_{j,r}} - k_{b,r} \prod_{j=1}^N [C_{j,r}]^{\eta''_{j,r}} \right] \quad (3)$$

where N is the number of chemical species in the system, $v'_{i,r}$ is the stoichiometric coefficient for reactant i in reaction r , $v''_{i,r}$ is the stoichiometric coefficient for product i in reaction r , $k_{f,r}$ is the forward rate constant for reaction r , $k_{b,r}$ is the backward rate constant for reaction r , $C_{j,r}$ is the molar concentration of species j in reaction r , and $\eta'_{j,r}$ is the rate exponent for reactant species j in reaction r .

2.2. EDC gas phase combustion model

The EDC is based on the turbulent energy cascade, which means that larger eddies break up into smaller eddies and the reactions take place in the so-called fine structures, where the fluid is mixed on a micro-scale. In the EDC the fluid is divided into the volume fraction of the fine structures $\gamma^* = \gamma^3$, where the reactions take place and the volume fraction $\gamma_0 = (1 - \gamma^3)$ of the surroundings, which are considered as inert.

The length fraction γ of fine scales is modelled as:

$$\gamma = C_\gamma \left(\frac{v\varepsilon}{k^2} \right)^{0.25} \quad (4)$$

where C_γ is

$$C_\gamma = \left(\frac{3C_{D2}}{4C_{D1}^2} \right)^{0.25} = 2.1377, \quad \text{with } C_{D1} = 0.134, \quad C_{D2} = 0.5 \quad (5)$$

The time scale for the mass transfer from the fine structures to the surrounding fluid (and the residence time in the fine scales) is:

$$\tau_{\text{EDC}} = C_\tau \left(\frac{v}{\varepsilon} \right)^{0.25} \quad \text{with } C_\tau = \left(\frac{C_{D2}}{3} \right)^{1/2} = 0.4082 \quad (6)$$

Here, v is the kinematic viscosity; ε is the turbulent dissipation rate and k the turbulent kinetic energy.

The length fraction and the time scale sizes in terms of turbulent Reynolds number ($\text{Re}_t = k^2/v\varepsilon$) can be written as following:

$$\gamma = C_\gamma (\text{Re}_t)^{-1/4} \quad (7)$$

and

$$\tau_{\text{EDC}} = C_\tau \text{Re}_t^{-1/2} \frac{k}{\varepsilon} \quad (8)$$

There are two different approaches for the mean average reaction rate. The first one is γ^3/τ [9], while the expression γ^2/τ has been used in recent papers [20,21]. The later expression is derived assuming that the fine structures exchange mass mainly with fine structure regions and not with the whole surrounding flow [20]. Therefore, the source term in the species mass conservation equation (Eq. (1)) for the mean species i based on the recent formulation is modelled as [20];

$$(R_i)_{\text{EDC}} = \rho \frac{\gamma^2 \chi}{\tau_{\text{EDC}}} (Y_i^* - Y_i^0) \quad (9)$$

where the term χ is a parameter that expresses the probability that the conditions are suitable for reaction to occur in the fine structures. Y^0 is the surrounding mass fraction of species i and Y^* is the fine structure mass fraction of species i . Gran [20–22] proposed that by setting the value of $\chi = 1$, the amount of reaction is controlled by the chemistry. The relation between the mass-averaged state and the surrounding species mass fraction is computed as [20]:

$$\bar{Y}_i = \gamma^3 Y_i^* + (1 - \gamma^3) Y_i^0 \quad (10)$$

The surrounding species mass fraction can be obtained from Eq. (10) as following:

$$Y_i^0 = \frac{\bar{Y}_i - \gamma^3 \chi Y_i^*}{(1 - \gamma^3 \chi)} \quad (11)$$

Now by substituting the surrounding species mass fraction (Eq. (11)) into Eq. (9), the final expression for the mean chemical reaction rate can be re-written as following:

$$(R_i)_{\text{EDC}} = \frac{\rho \gamma^2}{\tau_{\text{EDC}} (1 - \gamma^3)} (Y_i^* - \bar{Y}_i) \quad (12)$$

The reactor condition in (Eq. (12)), is found from the mean values of mass fractions and enthalpy, assuming no pressure changes between surrounding and fine structure [23]. In the original formulation of the EDC [8,9] the fine structures are treated as well stirred reactors (WSR). This circumstance may lead to convergence problems during the iterative solution of the high non-linear algebraic equation system and causes a considerable numerical effort. It was shown [23] that a plug flow reactor (PFR) model can be implemented in the EDC instead of a WSR, which leads to a considerable simplification of the numerical solution process. An integration of the reaction rates over the residence time (or reaction time) in the fine structures via a time-stepping method can then be used for the calculation of the fine structure values. This is the current formulation of the EDC implemented in the CFD code ANSYS® FLUENT®.

2.3. EDC model sensitivity analysis

The EDC was originally developed for high Reynolds combustion flows. The main assumption of the model is that the reaction takes place in the so-called fine structures, which are in the order

of the Kolmogorov eddy scale, where the dissipation occurs. The EDC model was derived based on the cascade model for highly turbulent flows. Magnussen [8,9] presented the EDC cascade model with a characteristic frequency or strain rate, whereas the mechanical energy transfers from the mean flow to heat. In the EDC cascade model for the transport of mechanical energy and thermal energy from preceding level to the following one, a constant [24] has been introduced. However, for simplicity, the model assumed all constants at each level are the same. Besides, the numerical values for the model constants are derived based on an analogy with the $k-\varepsilon$ turbulence model constants [24]. However, the applicability of the $k-\varepsilon$ turbulence model in low Reynolds number flows is with uncertainties [25]. Thus, the choice of numerical values for the EDC model constants, indeed, affects the local combustion-rate predictions [24].

The main difference between two turbulent flows with different Reynolds numbers but with the same integral scale is the size of smallest eddies. A turbulent flow at a relatively low Reynolds number has a relatively “coarse” small-scale structure [26]. Hence at low Reynolds flow conditions, where large and small scales of turbulence are very close to each other, the applicability of the EDC model should be revised.

The influence of the EDC model constants has been reported in a few recent works [18,27–30]. Rehm et al. [27] reported the capability of the EDC for gasification modelling. They found that C_τ had almost no impact whereas the C_γ had a strong impact on the mean reaction rate and their results were improved by increasing of the C_γ constant. De et al. [18] performed a systematic EDC model sensitivity concerning the model constants. The outcomes of their study indicated that the EDC is not valid below the turbulent Reynolds number of 64. They simulated a jet in a hot co-flow and found too early ignition with the standard EDC model constants. They showed that the predictions could be improved if the C_τ is increased to 3 and C_γ is decreased to 1.0. Graça et al. [28] simulated a reversed flow small-scale combustor with the EDC and found a delayed ignition with the standard model constants. They demonstrated the dominating role of C_γ to improve the results in comparison with experiments. Shabaniyan et al. [29] confirmed the outcomes of De et al. [18] and used the modified C_τ constant proposed by [18,30] for the simulation of an ethylene jet flame in diluted and heated oxidant stream combustion conditions. They displayed that a modified EDC leads to reasonable results with relatively low computational effort.

Therefore, based on the above explanation, it is of interest to investigate the sensitivity of the predicted reaction rate to the model constants C_τ and C_γ . The model constant C_τ appears as a multiplication factor in the EDC time scale (Eq. (6)) as well as in the reaction rate term (Eq. (12)). In the EDC model, the reaction rate for the chemical species was assumed to be a linear function of the mass transfer between fine structures and surroundings

[24]. However, it is clear from (Eq. (12)) that the characteristic time scale in the EDC model is larger than τ_{EDC} :

$$\frac{1}{\tau_{mix}} = \frac{\gamma^2}{(1-\gamma^3)} \frac{1}{\tau_{EDC}} \quad (13)$$

Now, by definition of the time scale ratio (T_{ratio}), Eq. (13) can be rearranged as following:

$$T_{ratio} = \frac{\tau_{EDC}}{\tau_{mix}} = \frac{\gamma^2}{(1-\gamma^3)} \quad (14)$$

From a physical point of view, the mixing time scale τ_{mix} should be greater than the EDC time scale. Therefore, for consistency, T (and γ) should be lower than one:

$$T_{ratio} = \frac{\gamma^2}{(1-\gamma^3)} < 1 \Rightarrow \gamma < 0.75 \quad (15)$$

This implies that the fine scale length fraction (Eq. (4)) should be less than 0.75. Now by re-arranging Eq. (4) in terms of turbulent Reynolds number (Eq. (7)), the following expression can be obtained:

$$C_\gamma(\text{Re}_t)^{-1/4} < 0.75 \rightarrow \text{Re}_t > 64 \quad (16)$$

Fig. 1 shows the sensitivity of γ and the time scale ratio on the turbulent Reynolds number. It can be inferred from the figures that the model is limited to turbulent Reynolds numbers larger than 64. Besides, supposing that the maximum value for the fine scale length fraction is one (reaction takes place in the whole CFD computational cell), the model still has no value for the fine scale length fraction at turbulent Reynolds numbers lower than 20 (see Fig. 1 left).

As explained earlier, the assumptions of the EDC model at low turbulence flow are no longer valid. The model has no value for γ at turbulent Reynolds numbers lower than 64.

2.4. Hybrid gas phase combustion model

Based on the outcomes of the EDC sensitivity analysis, the necessity of a model which should be valid for all flow conditions is inevitable. The idea of such a reaction model which utilises the benefits of both the FRK and the EBU model first was proposed by Spalding [7]. The concept is to develop a hybrid reaction model to be sensitive to the local turbulent Reynolds number of flow. Therefore, a hybrid reaction model as a combination of both FRK as well as EDC models has been introduced. In the hybrid model, the mean chemical reaction (second term in the right hand side of Eq. (1)) is modelled as:

$$(R_i)_{Hybrid} = \left(\frac{1}{1 + \text{Re}_t} \right) (R_i)_{FRK} + \left(\frac{\text{Re}_t}{1 + \text{Re}_t} \right) (R_i)_{EDC} \quad (17)$$

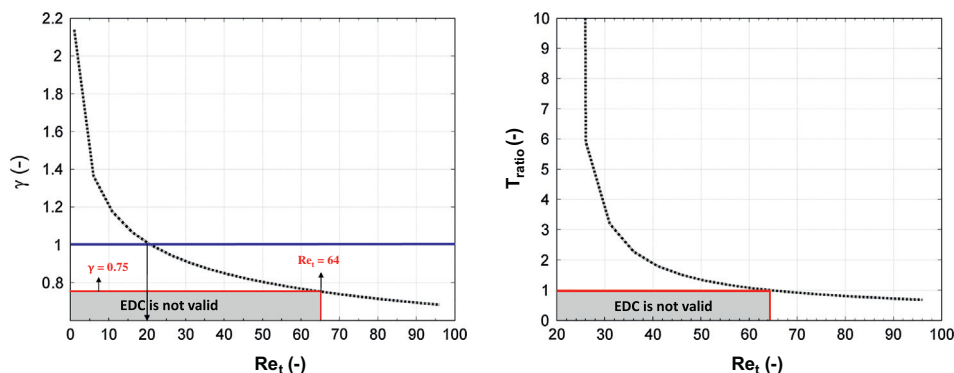


Fig. 1. Dependence of γ (Eq. (7)) (left) and T_{ratio} (Eq. (14)) (right) on turbulent Reynolds number.

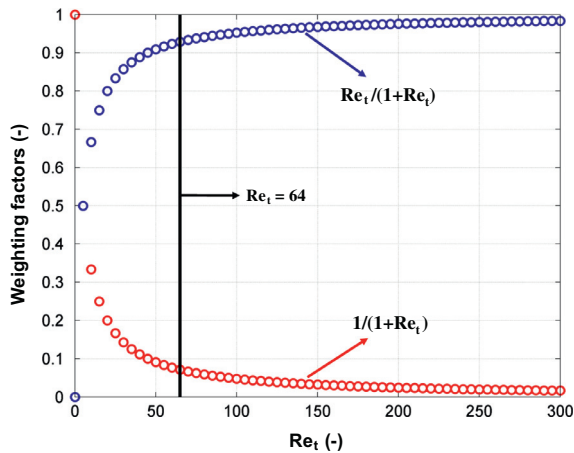


Fig. 2. Effect of turbulent Reynolds number on the weighting factors in the hybrid model.

where $(R_i)_{FRK}$ is the FRK mean reaction rate (Eq. (2)) and the term $(R_i)_{EDC}$ is the mean reaction rate calculated by the EDC model (Eq. (12)).

In the laminar range the reaction rate is calculated with pure finite rate kinetics and in the highly turbulent region with the EDC. In the transition region around $Re_t = 64$, the overall reaction rate is calculated as the sum of the weighted reaction rates of finite rate kinetics and the EDC. In other words, the overall reaction rate is determined as a linear combination of the two reaction rates.

The weighting factors $((1/1 + Re_t)$ and $(Re_t/1 + Re_t))$ are model parameters of a weight function which gave the best agreement with measurements for flames A, B and D.

The effect of weighting factors in Eq. (17) on each reaction rate as a function of turbulent Reynolds number is shown in Fig. 2.

For instance, at zero turbulence ($Re_t = 0$), the transition parameter $(Re_t/1 + Re_t = 0)$ while the transition parameter $(1/1 + Re_t = 1)$ and the reaction rate is controlled by the chemistry and vice versa.

3. Validation cases and numerical set-up

Three round jet flames are chosen for model validations which were measured by Barlow and Frank [10]. The flames cover laminar (flame A), transition (flame B) and turbulent (flame D) combustion conditions. The burner, consisting of a main round jet and a concentric pilot, was placed in a wind tunnel. The main jet consists of a mixture of CH_4 with air. The pilot is a lean fuel/air mixture which is active just for flames B and D for the purpose of flame stabilization, while there is no mass flow rate through the pilot for flame A. A detailed information concerning the operating conditions for flames A, B and D can be found in [10,31,32].

For all simulations, a 2D axisymmetric domain was used due to the symmetry of the burner. The computational domain extended from $10d$ behind the nozzle exit plane to $100d$ in the axial direction and $50d$ in the radial direction, where d is the main jet diameter. In order to estimate the velocity and turbulence quantity profiles at inlet boundaries (main jet and pilot) according to the experiments, the nozzle with a length of $10d$ was included in the computational domain. The applied CFD boundary conditions as well as the flame configuration are shown in Fig. 3.

The governing equations consist of incompressible Favre-averaged transport equations of continuity, momentum, energy, species conservation and the standard $k-\epsilon$ equations. The discrete ordinates (DO) radiation model [33] together with the Weighted-Sum-of-Gray-Gases (WSGG) method was used to solve the radiative heat transfer equation. A second-order upwind discretisation

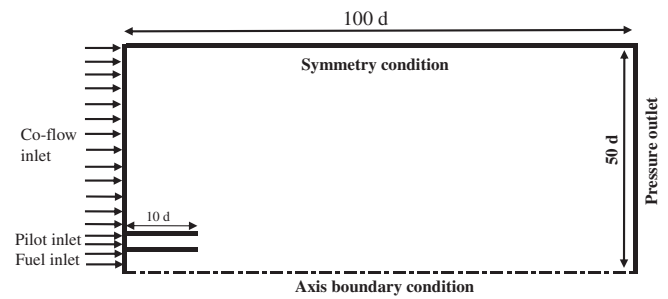


Fig. 3. Numerical model geometry and applied boundary conditions.

scheme was used to solve all governing equations. Solution convergence has been determined by two criterions. Firstly, all the residuals of the solved equations fall below the value of 10^{-6} . The second convergence criterion is to monitor the concentration of some species (e.g. CO concentration) at a specified location in the computational domain which has to be stabilised and does not change with iterations. The direct integration (DI) of the stiff ODE system of Eqs. (2) and (12) is very time-consuming due to the disparity of time-scales involved in the reaction mechanism. Therefore the In-Situ Adaptive Tabulation (ISAT) algorithm by Pope [34] has been used to speed-up the CPU-intensive treatment of the detailed reaction kinetics. In the calculations reported here the ISAT error tolerance was set to 10^{-5} .

4. Results and discussion

The simulation results for flames A, B and D are presented in this section. Firstly, flame D is used for validating the CFD grid as well as the reaction mechanism applied for the subsequent simulations. The importance of differential (molecular) diffusion at low Reynolds turbulent flames is explained later. Then, it is shown that flame A could not be simulated with the standard EDC model. The validity range of the EDC for the simulation of flames A and B is discussed and finally the simulation results with the hybrid model for all flames are shown.

4.1. Grid independence and effect of kinetic mechanisms

Two sets of structured grids of 4 and 10 k elements are studied. The grids are refined close to the nozzle and in the axial direction. A modified version of the $k-\epsilon$ turbulence model with the constant $C_{\epsilon 1}$ set to 1.58 (instead of 1.44) is used for the simulation of flame D to compensate for the round jet anomaly [35–37]. However, this modification leads to an over prediction of the flame temperature in the axial direction of the flame (see Fig. 4). In this region, the temperature along the axis is determined by the mixing of the cold air with the post combustion gases. So, it strongly depends on the spreading rate determined by the turbulence model applied [38–40].

The results obtained with both grids exhibited the same performance (not shown here), therefore, the grid with 4 k cells was selected to guarantee computational accuracy and to save calculation time for subsequent simulations (flames A and B).

The influence of the reaction mechanism on the predictions for flame D is studied by using two different kinetic mechanisms. DRM-22 [15] is a reduced version of the GRI1.2. [41]. It consists of 24 species and 104 reversible reactions. The GRI2.11 [14] is a full kinetic mechanism, which consists of 49 species and 277 reversible reactions.

Fig. 4 exhibits the results obtained for flame D with both reaction mechanisms. The results are obtained with the EDC on the

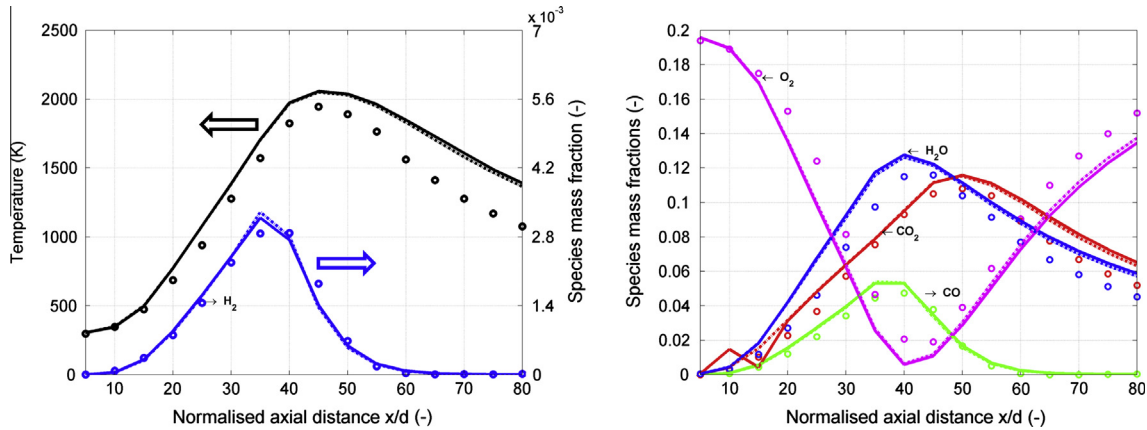


Fig. 4. Effect of chemical mechanism on the accuracy of prediction for flame D. Circles: experiment, solid lines: GRI 2.11 mechanism, dashed dotted lines: DRM-22 mechanism.

benchmark CFD grid (4k cells) with a modified $k-\epsilon$ turbulence model. The results show that the performance of the DRM-22 mechanism is identical to the detailed GRI2.11 mechanism. Hence, the DRM-22 is used for the further simulations.

4.2. 2Molecular diffusion effect

In turbulent flows the turbulent diffusion generally overwhelms laminar diffusion, and the specification of detailed laminar diffusion properties in turbulent flows is usually not necessary. The diffusion flux (J_i) in Eq. (1) is defined as

$$J_i = -\left(\rho D_{i,m} + \frac{\mu_t}{Sc_t}\right) \nabla Y_i \tag{18}$$

where the first term on the right-hand side of Eq. (18) is molecular diffusion and the second term expresses the turbulent diffusion. The term, $D_{i,m}$ is the mass diffusion coefficient for species i in the mixture, and $Sc_t = \mu_t / \rho D_t$ is the turbulent Schmidt number (where μ_t is the turbulent viscosity and D_t is the turbulent diffusivity). However, under combustion conditions at low Reynolds numbers the effect of molecular diffusion on mixing becomes comparable to the turbulent diffusion at certain regions in the flame. This is mainly due to the laminarisation of the flow caused by high temperatures in the reaction zones [42]. The effect of molecular diffusion becomes more important when there is H_2 in the fuel jet stream and the jet Reynolds number is lower than 10,000 [43]. In order to highlight the effect of differential

Table 1 Modified $C_{\epsilon 1}$ values used in the simulations for flames A and B.

Flame	A	B
$C_{\epsilon 1}$	11	4

diffusion (diff-diff) on the accuracy of the predictions, the simulation of flame B (using EDC with DRM-22 mechanism) is performed with and without the effect of molecular diffusion. To account for the effect of differential diffusion in the simulation, diffusion coefficients for each species were represented as a fourth-order polynomial function of temperature. Fig. 5 shows the temperature and species mass fraction profiles which have been compared with experimental data at $x/d = 30$. The mean mixture fraction is computed using Bilger’s formula [44]. The results show the significant role of differential diffusion in the accuracy of predictions. It is evident that the flame temperature is underestimated considerably (25%) in case of complete exclusion of molecular diffusion in the simulation. The minor species (H_2 and OH) mass fraction predictions are remarkably improved by more than 80% when the molecular diffusion is considered in the simulation. Ignoring differential diffusion has also caused peak H_2O and CO values being under-predicted by 20% and 60%, respectively. As a result, the effect of differential diffusion at combustion of low and moderate Reynolds numbers cannot be disregarded.

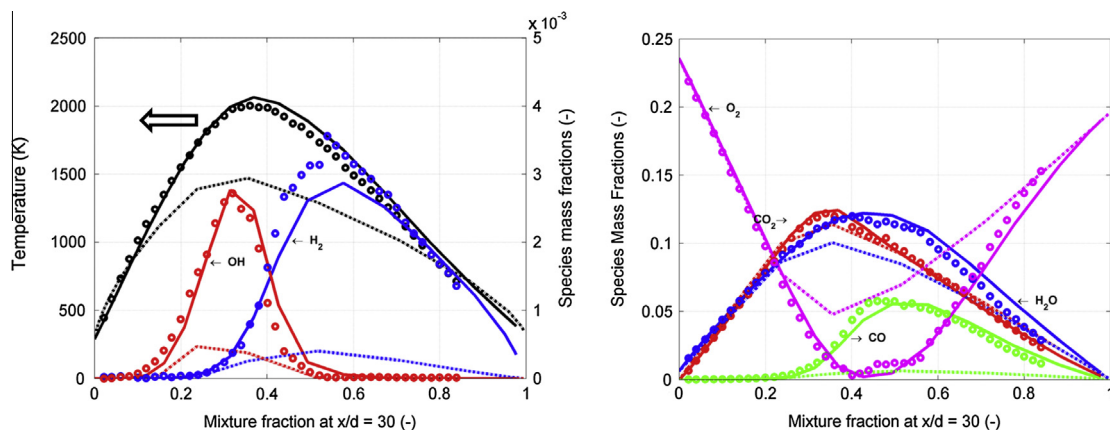


Fig. 5. Effect of differential diffusion (diff-diff) on the prediction of temperature and species mass fractions for flame B at $x/d = 30$ (-) (EDC with modified $k-\epsilon$ turbulence model and DRM-22 mechanism). Circles: experiment, solid lines: diff-diff effect included, dashed dotted lines: diff-diff effect excluded in the simulation.

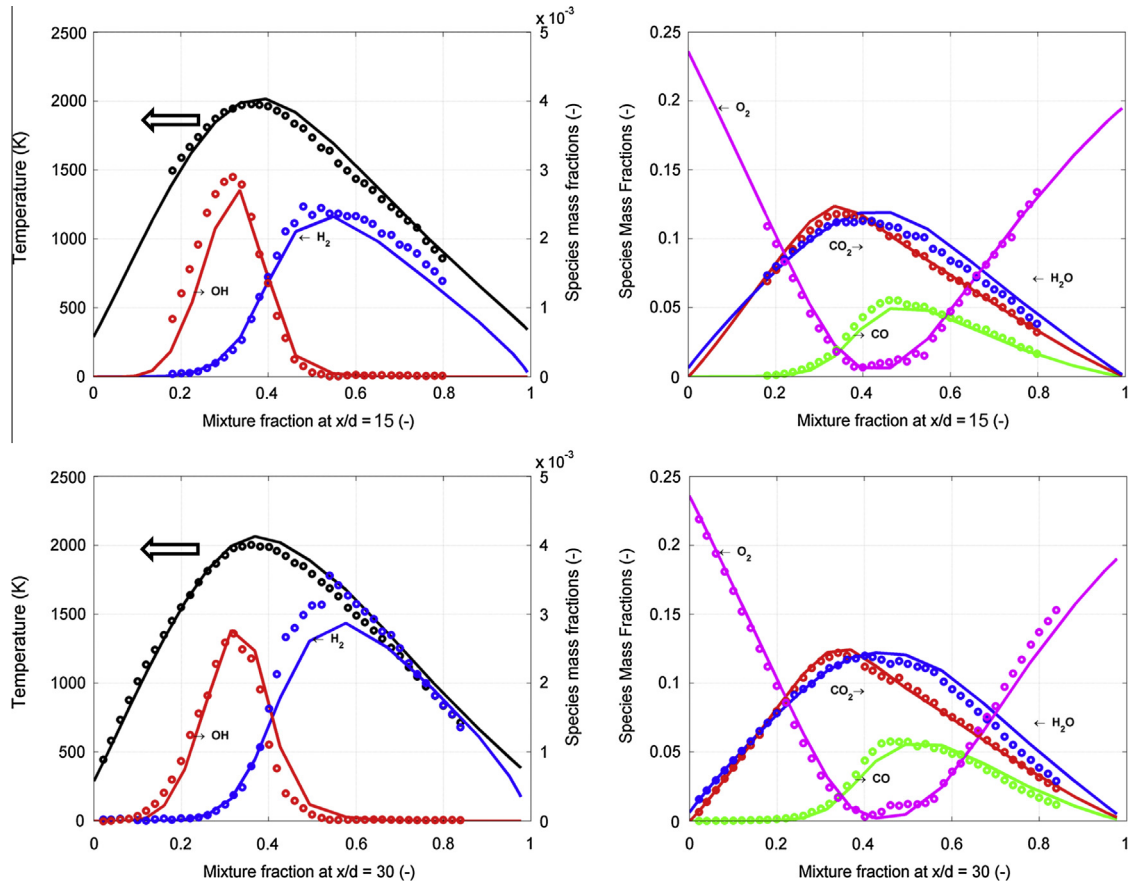


Fig. 6. Radial profiles of temperature and species mass fractions at different normalised heights of flame B (the EDC model with modified $k-\epsilon$ turbulence model and DRM-22 mechanism, diff-diff effect included).

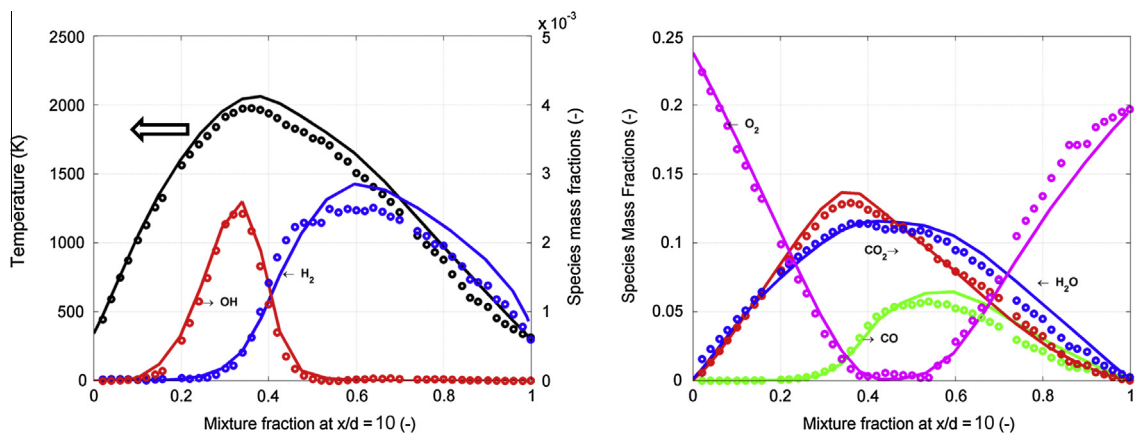


Fig. 7. Radial profiles of temperature and species mass fractions for flame A at $x/d = 10$ (-) (FRK model with modified $k-\epsilon$ turbulence model and DRM-22 mechanism, diff-diff effect included).

4.3. Evaluation of the standard EDC at low Reynolds conditions

For the evaluation of the standard EDC at low and moderate Reynolds number, the simulation results for flames A (laminar) and B (transitional) are presented. Flame A was mainly chosen for the evaluation of the standard EDC due to its similar flow conditions prevailing above the fuel bed in biomass combustion plants. As explained, in the region above the fuel bed the gas phase mixing and reaction progress is highly influenced by laminar and low turbulent zones. As shown in Section 2.3, the stan-

dard EDC model is not valid in regions with turbulent Reynolds number less than 64. Therefore, the standard EDC model can be tested for model evaluation at a low turbulent regime in case of flame A.

It is worth mentioning, that the experimental data were available at only two different positions ($x/d = 15$ and $x/d = 30$) for flame B and at one position for flame A ($x/d = 10$) including the temperature and species mass fraction profiles [10]. The standard $k-\epsilon$ turbulence model with a modified $C_{\epsilon 1}$ constant is used in the simulations. The modified constants are given in Table 1.

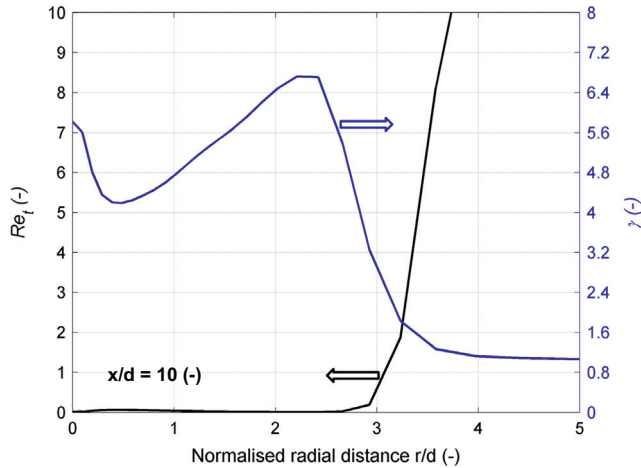


Fig. 8. Radial profiles of Re_t (left vertical axis) and, γ (Eq. (7)) (right vertical axis) for flame A at $x/d = 10$ (-) (FRK model with modified $k-\varepsilon$ turbulence model and DRM-22 mechanism, diff-diff effect included).

Fig. 6 shows the simulation results for flame B in comparison with measurement data at $x/d = 15$ and $x/d = 30$, respectively. The results are in good agreements with measurement data at both heights. The results show that the standard EDC together with the differential diffusion approach gave satisfactory results in

comparison with experimental data even in moderate Reynolds number conditions.

For the simulation of flame A, the flame was piloted artificially by means of a small fluid zone attached to the nozzle outlet with a fixed high temperature value. This zone acted as an ignitor to establish the flame. However, flame A could not be simulated with the standard EDC even with artificial piloting. Fig. 7 demonstrates the simulation results obtained with the FRK model against experimental data for flame A. The results are in good agreement with experimental data even for minor species (H_2 and OH) profiles. This clearly indicates a good performance of the DRM-22 mechanism and the diffusion model used in this study. However, the flame temperature as well as species mass fraction profiles are somewhat over-predicted on the fuel lean side of the flame. The diffusion model plays, indeed, an important role to predict the flame characteristics properly.

The EDC sensitivity analysis presented in Section 2.3 confirmed that the model is not valid below the turbulent Reynolds number of 64. Therefore, flames A and B are chosen to analyse the validity range of the model. Fig. 8 shows the distribution of the turbulent Reynolds number (Re_t) and the fine scale length fraction γ (Eq. (4)) in radial direction at $x/d = 10$ for flame A. Since flame A could not be simulated with EDC, the fine scale length fraction was calculated according to Eq. (4) from the turbulent quantities k and ε (simulation with the FRK model together with the modified $k-\varepsilon$ turbulence model). It is obvious that for flame A Re_t is lower than 64 in the whole reaction zone, therefore, the EDC is not valid.

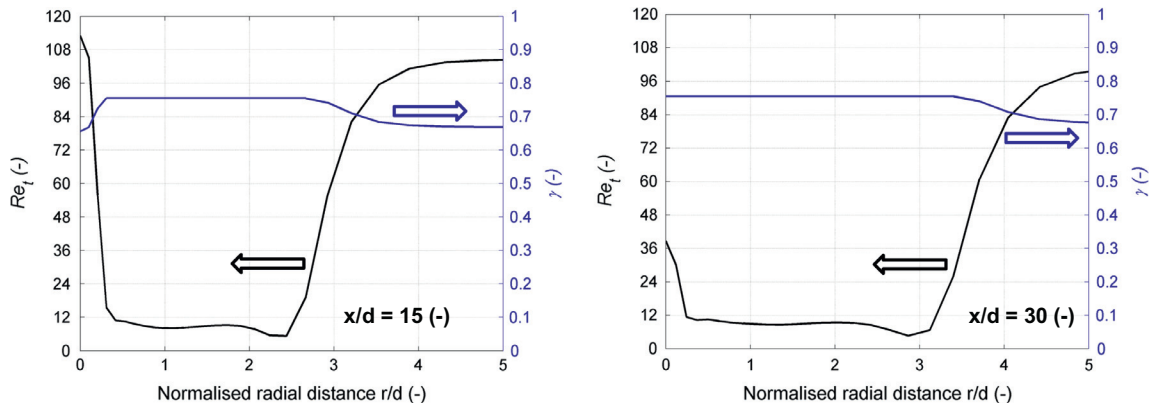


Fig. 9. Radial profiles of Re_t (left vertical axis) and, γ (Eq. (7)) (right vertical axis) for flames B (EDC with modified $k-\varepsilon$ turbulence model and DRM-22 mechanism, diff-diff effect included).

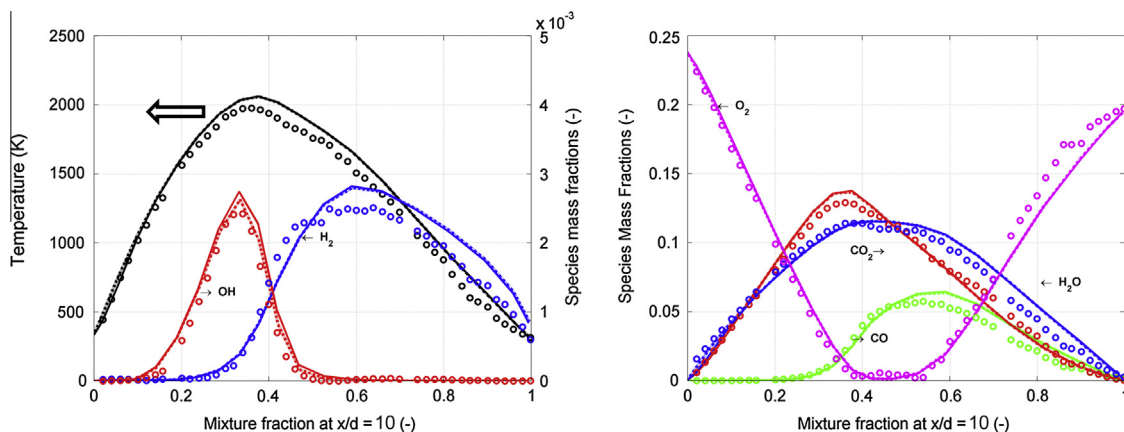


Fig. 10. Radial profiles of temperature and species mass fractions for flame A at $x/d = 10$ (-) calculated with FRK and the hybrid model (modified $k-\varepsilon$ turbulence model, DRM-22 mechanism and diff-diff effect included). Circles: experiment, solid lines: FRK model, dashed dotted lines: hybrid model.

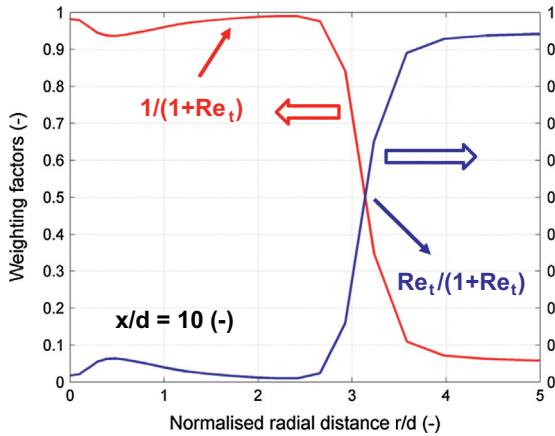


Fig. 11. Effect of weighting factors on the reaction rate calculation for flame A at $x/d = 10$ (-).

The distribution of both turbulent Reynolds number (Re_t) and the fine scale length fraction at two different heights are also presented in Fig. 9 for flame B. The turbulent Reynolds number even for flame B is generally low. Furthermore, it could be shown that the implemented EDC model in ANSYS® FLUENT® truncates the fine scale length fraction value to 0.75 for any value of Re_t lower than 64, in order to avoid non-physical values of this quantity.

It can be concluded that the standard EDC model performs well even in moderate turbulence regimes. However, the results for flame B showed that the unphysical behaviour of the mean

reaction rate is prevented by clipping the fine scale length fraction to 0.75. This behaviour of the EDC model is also reported in [18], whereas the jet Reynolds number is lower than 5000.

In case of flame A, the EDC model even cannot simulate the flame since the whole reaction domain is out of the EDC validity range.

4.4. Test of the hybrid combustion model

Fig. 10 shows the predicted temperature and species mass fraction profiles for flame A with the hybrid model in comparison with the pure FRK model as well as experimental data. The results obtained with the hybrid model are similar to the pure FRK model. This implies that at low Reynolds conditions the model performs approximately as the FRK model.

The effect of weighting factors on the reaction rate calculations is also shown in Fig. 11 at $x/d = 10$ for flame A. The figure shows that the term $(1/(1 + Re_t))$ in the reaction zone takes the value of unity, therefore, the reaction rate is calculated based on the FRK part in the hybrid model.

The results predicted with the hybrid model for flame B at two different heights are shown in Fig. 12. The results were also compared with the standard EDC and the FRK models. The predictions with the hybrid model show better performance than the EDC model due to the sensitivity of the model to the locally too low turbulent Reynolds number of the flow.

The characteristics of reacting radicals are of high relevance for an in-depth understanding of the formation process of combustion emissions. Therefore, both reaction mechanism and gas phase

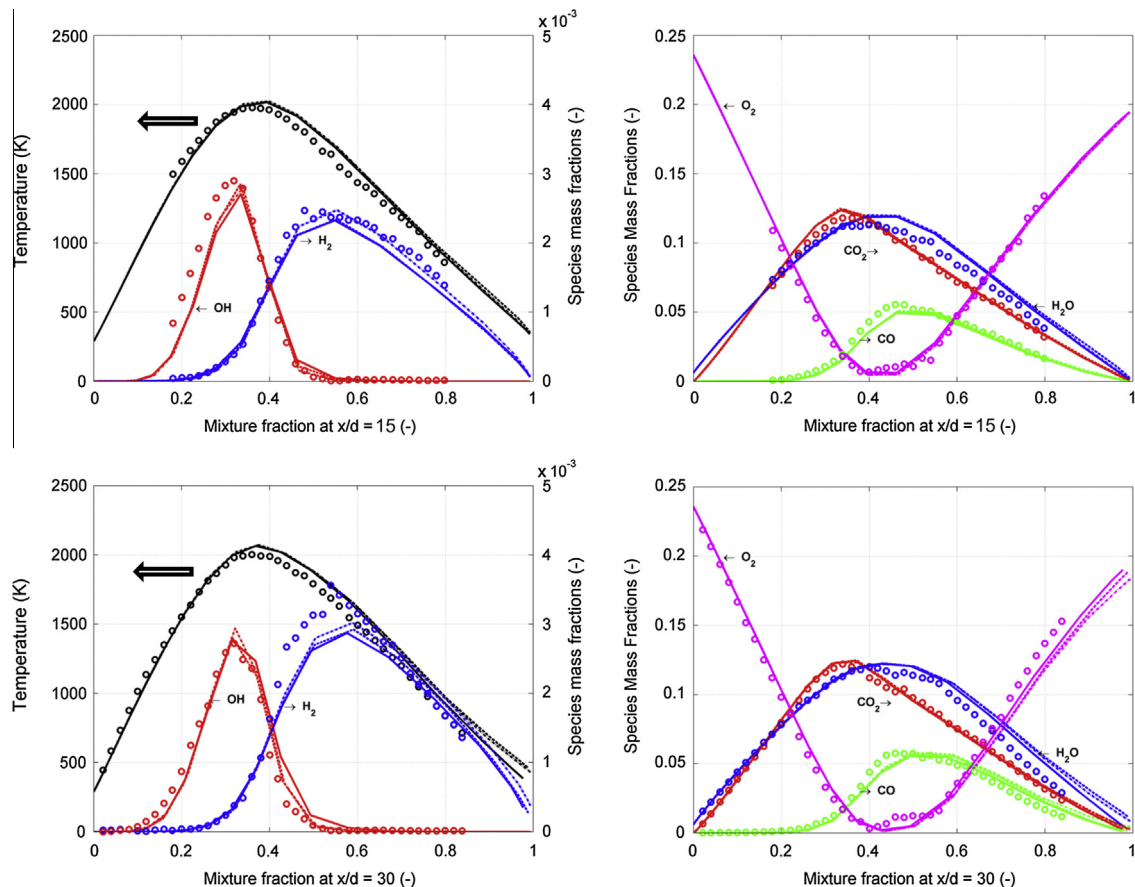


Fig. 12. Radial profiles of temperature and species mass fractions for flame B at different heights calculated with EDC, FRK and the hybrid model (modified $k-\epsilon$ turbulence model, DRM-22 mechanism and diff-diff effect included). Circles: experiment, solid lines: EDC model, dashed lines: FRK and dashed dotted lines: hybrid model.

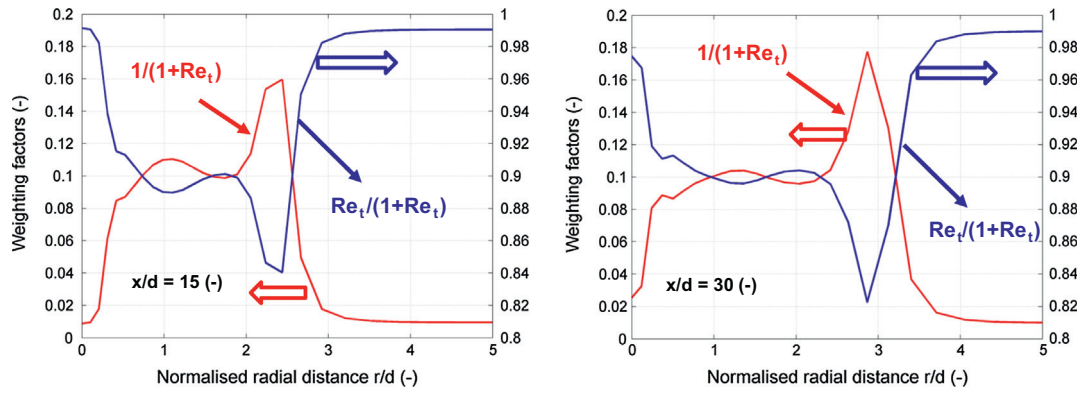


Fig. 13. Effect of weighting factors on the reaction rate calculation for flame B at different heights.

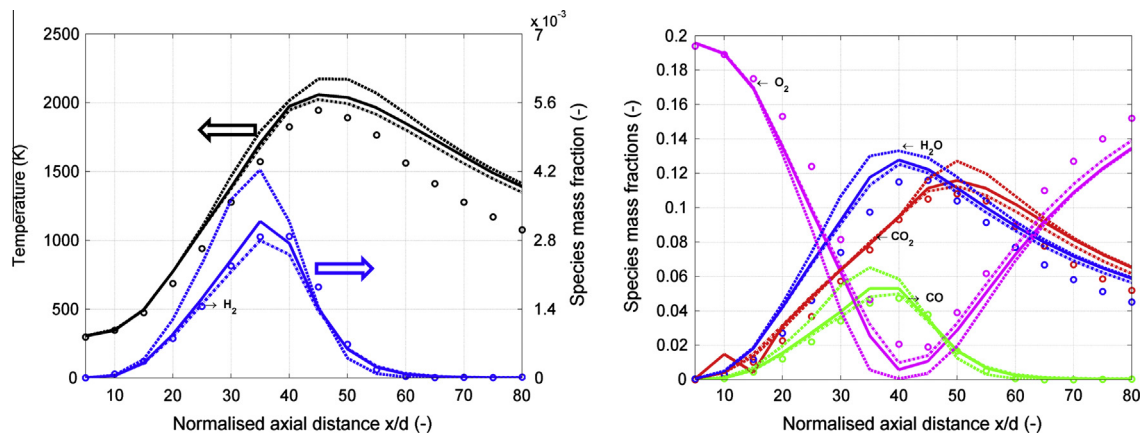


Fig. 14. Temperature and species mass fractions predictions for flame D at different normalised axial distances calculated with EDC, FRK and hybrid model (modified $k-\epsilon$ turbulence model, DRM-22 mechanism). Circles: experiment, solid lines: EDC model, dashed lines: FRK model and dashed dotted lines: hybrid model.

reaction model play an important role for the better prediction of radicals in the combustion simulation.

The results show that both H_2 and OH mass fraction profiles at both heights are slightly improved with the hybrid model. This is mainly because of the lower turbulent Reynolds number than the critical value (see Fig. 9) at these heights, therefore, the contribution of the FRK part in the hybrid model becomes more relevant. The effect of weighting factors on the reaction rate calculation is also presented in Fig. 13 for flame B at two different heights. The figure shows that the FRK weighting term ($1/(1 + Re_t)$) has a small effect (maximum value of 0.12 at the height of $x/d = 15$ and 0.18 at the height of $x/d = 30$) on the overall reaction rate calculation at both heights.

Fig. 14 shows the evaluation of the hybrid model for flame D in comparison to the standard EDC as well as the FRK model along the normalised axial direction of the flame. The results show that the temperature and species mass fractions are over-predicted with the pure FRK model. The obtained results with the EDC model indicate that by considering the effect of turbulence in the reaction rate calculation, the over-prediction of temperature and consequently the species mass fractions caused by the FRK model are suppressed. Although the turbulent Reynolds number is by far higher than $Re_t = 64$, the FRK part in the hybrid model has a small contribution to the reaction rate calculation. The results obtained with the hybrid model show a slight improvement on the predictions. This is mainly due to a contribution of the FRK part in the overall reaction rate calculation, where the predicted CO and O_2 species are improved, respectively. The same behaviour is true also for the predicted CO_2 and H_2O species calculated with the hybrid model.

5. Summary and conclusion

A new hybrid gas phase combustion model suitable from laminar to turbulent combustion flows is presented. The hybrid model is a combination of FRK and EDC models, where the reaction rate is weighted by the local turbulent Reynolds number of the flow. The lower the turbulent Reynolds number of the flow, the greater the contribution of the FRK model to the overall reaction rate calculation in the hybrid model and vice versa. The hybrid model was programmed in C and coupled with ANSYS® FLUENT®. Also, the limitation of the EDC at low Reynolds turbulent combustion was shown. The EDC sensitivity analysis regarding model constants showed that the EDC is not valid for turbulent Reynolds numbers lower than 64. Furthermore, the CFD results obtained for flames A ($Re = 1100$) and B ($Re = 8200$) confirmed that the differential diffusion has a profound effect on the accuracy of predictions at low Reynolds combustion flows. It was found that the standard EDC was not able to establish flame A, where most of the reaction zones are located outside of the validity range of the EDC model. The results with the hybrid model for all flames showed good agreements with measurement data. The results obtained with hybrid and FRK models for flame A outline that the hybrid model performs very similarly to the pure FRK model, since the reaction zones for this flame are out of the EDC validity range.

The simulation results for flame B with the standard EDC model show good agreements with experimental results. However, the simulation with the hybrid model exhibited better performance to predict the radicals (e.g. OH and H_2). The better performance of the hybrid model in case of flame B can be explained by a greater

contribution of the FRK model to the overall reaction rate calculation. Moreover, the simulated results with the hybrid model for flame D show a better performance of the hybrid model in comparison to the EDC and the pure FRK models.

Concluding, the hybrid model displayed a great potential for application in all ranges of flow conditions and can be applied for an improved prediction of gas phase combustion in biomass combustion plants. The model can also be applied for an improved NO_x prediction since it captures radicals with better accuracy than the standard EDC model.

Acknowledgement

The author wishes to thank Dr. Barlow at Sandia National Laboratories for providing the data for flames A and B on request and helpful comments on the manuscript.

References

- [1] Mehrabian R, Zahirovic S, Scharler R, Obernberger I, Kleditzsch S, et al. A CFD model for thermal conversion of thermally thick biomass particles. *Fuel Process Technol* 2012;95:96–108.
- [2] Mancini M, Weber R, Bolletini U. Predicting NO_x emissions of a burner operated in flameless oxidation mode. *Proc Combust Inst* 2002;29(1):1115–63.
- [3] Peters AAF, Weber R. Mathematical modeling of a 2.25 MWt swirling natural gas flame. Part 1: Eddy break-up concept for turbulent combustion; probability density function approach for nitric oxide formation. *Combust Sci Technol* 1995;110–111:67–101.
- [4] Xue H, Ho JC, Cheng YM. Comparison of different combustion models in enclosure fire simulation. *Fire Saf J* 2001;36(1):37–54.
- [5] Scharler R, Fleckl T, Obernberger I. Modification of a Magnussen constant of eddy dissipation model for biomass grate furnaces by means of hot gas in-situ FT-IR absorption spectroscopy. *Prog Comput Fluid Dyn Int J* 2003;3:102–11.
- [6] Yaxin S, Cuiwu C, Along S. Simulation of high temperature air combustion with modified eddy-break-up combustion model. *Energy Proc* 2012;14:127–32. <http://dx.doi.org/10.1016/j.egypro.2011.12.90>.
- [7] Spalding DB. Mixing and chemical reaction in steady confined turbulent flames. *Symp (Int) Combust* 1971;13:649–57.
- [8] Magnussen BF, Hjertager BH. On mathematical modeling of turbulent combustion with special emphasis on soot formation and combustion. *Proc Combust Inst* 1977;16(1):719–29. [http://dx.doi.org/10.1016/S0082-0784\(77\)80366-4](http://dx.doi.org/10.1016/S0082-0784(77)80366-4).
- [9] Magnussen BF. On the structure of turbulence and a generalized eddy dissipation concept for chemical reaction in turbulent flow. In: 19th AIAA aerospace science meeting, St. Louis, Missouri, USA; 1981.
- [10] Barlow RS, Frank JH. Effects of turbulence on species mass fractions in methane/air jet flames. *Proc Combust Inst* 1998;27:1087–95.
- [11] Neves D, Thunman H, Matos A, Tarelho L, Gomez-Barea A. Characterization and prediction of biomass pyrolysis products. *Prog Energy Combust* 2011;37:611–30.
- [12] Boroson ML, Howard JB, Longwell JP, Peters WA. Product yields and kinetics from the vapor phase cracking of wood pyrolysis tars. *AIChE J* 1989;35:120–8.
- [13] Graham RG, Bergougnou MA, Overend RP. Fast pyrolysis of biomass. *J Anal Appl Pyrol* 1984;6:95–135.
- [14] Bowman CT, Hanson RK, Davidson DF, Gardiner WC, Lissianski V, Smith GP, et al. <http://www.me.berkeley.edu/gri_mech/>.
- [15] Kazakov A, Frenklach M. <<http://www.me.berkeley.edu/drm/>>.
- [16] Kilpinen P. pia.kilpinen@uku.fi or pia.kilpinen@abo.fi.
- [17] Zahirovic S, Scharler R, Kilpinen P, Obernberger I. A kinetic study on the potential of a hybrid reaction mechanism for prediction of NO_x formation in biomass grate furnaces. *Combust Theor Model* 2011;15:645–70.
- [18] De A, Oldenhof E, Sathiah P, Roekaerts DJEM. Numerical simulation of delft-jet in-hot-coflow (DJHC) flames using the eddy dissipation concept model for turbulence-chemistry interaction. *Flow Turbul Combust* 2011;87:537–67.
- [19] ANSYS® Academic Research. Release 14.0. Help System, FLUENT User Guide, ANSYS Inc.
- [20] Gran IR, Magnussen BF. Numerical study of a bluff-body stabilized diffusion flame, Part 2. Influence of combustion modeling and finite-rate chemistry. *Combust Sci Technol* 1996;119:191–217.
- [21] Magel HC, Schnell U, Hein KRG. Simulation of detailed chemistry in a turbulent combustor flow. *Symp (Int) Combust* 1996;26(1):67–74. [http://dx.doi.org/10.1016/S0082-0784\(96\)80201-3](http://dx.doi.org/10.1016/S0082-0784(96)80201-3).
- [22] Gran IR. Mathematical modeling and numerical simulation of chemical kinetics in turbulent combustion. Ph.D. thesis, Dept. of Applied Mechanics, Thermodynamics and fluid dynamics, Norwegian University of Science and Technology, Trondheim, Norway; 1994.
- [23] Jessee JP, Gansman RF, Fiveland WA. Calculation of chemically reacting flows using finite rate kinetics. *Heat Transfer in Fire and Combustion System (ASME ed.)* 1993;250:43–53.
- [24] Etesvåg IS, Magnussen BF. The eddy dissipation turbulence energy cascade model. *Combust Sci Technol* 2000;159(1):213–35.
- [25] Perot JB, Bruyn Kops S de. Modeling turbulent dissipation at low and moderate Reynolds numbers. *J Turbul* 2006;7(69):1–14.
- [26] Tennekes H, Lumley JL. A first course in turbulence. USA: MIT Press; 1972. p. 21–2.
- [27] Rehm M, Seifert P, Meyer B. Theoretical and numerical investigation on the EDC model for turbulence-chemistry interaction at gasification conditions. *Comput Chem Eng* 2009;33:402–7.
- [28] Graça M, Duarte A, Coelho PJ, Costa M. Numerical simulation of a reversed flow small-scale combustor. *Fuel Process Technol* 2012;107:126–37.
- [29] Shabanian SR, Medwell PR, Rahimi M, Frassoldati A, Cuoci A. Kinetic and fluid dynamic modeling of ethylene jet flames in diluted and heated oxidant stream combustion conditions. *Appl Therm Eng* 2013;52:538–54.
- [30] Aminian J, Galletti C, Shahhosseini S, Tognotti L. Numerical investigation of a MILD combustion burner: analysis of mixing field, chemical kinetics and turbulence-chemistry interaction. *Flow Turbul Combust* 2012;88:597–623.
- [31] Schneider Ch, Dreizler A, Janicka J. Flow field measurements of stable and locally extinguishing hydrocarbon-fuelled jet flames. *Combust Flame* 2003;135(1–2):185–90.
- [32] Barlow RS, Frank JH. SandiaPilotDoc21.pdf. <<http://www.sandia.gov/TNF/DataArch/FlameD.html>>.
- [33] Smith TF, Shen ZF, Friedman JN. Evaluation of coefficients for the weighted sum of gray gases model. *J Heat Transf* 1982;104:602–8.
- [34] Pope SB. Computationally efficient implementation of combustion chemistry using in situ adaptive tabulation. *Combust Theor Model* 1997;1:41–63.
- [35] Morse AP. Axisymmetric turbulent shear flows with and without swirl. Ph.D. thesis. England: London University; 1977.
- [36] Pope SB. An explanation of the turbulent round-jet/plane-jet anomaly. *AIAA J* 1978;16(3):279–81.
- [37] Aminian J, Galletti C, Shahhosseini S, Tognotti L. Key modeling issues in prediction of minor species in diluted-preheated combustion conditions. *Appl Therm Eng* 2011;31:3287–300.
- [38] Merci B et al. Application of a new cubic turbulence model to piloted and bluff-body diffusion flames. *Combust Flame* 2001;126:1533–56.
- [39] Merci B, Dick E. Influence of computational aspects on simulations of a turbulent jet diffusion flame. *Int J Numer Method H* 2003;13(7):887–98.
- [40] Zahirovic S, Scharler R, Kilpinen P, Obernberger I. Validation of flow simulation and gas combustion sub-models for the CFD-based prediction of NO_x formation in biomass grate furnaces. *Combust Theor Model* 2010;15(1):61–87.
- [41] Frenklach M, Wang H, Yu CL, Goldenberg M, Bowman CT, Hanson RK, et al. <http://www.me.berkeley.edu/gri_mech/>.
- [42] Christo FC, Dally BB. Modeling turbulent reacting jets issuing into a hot and diluted coflow. *Combust Flame* 2005;142:117–29.
- [43] Barlow RS, Frank JH, Karpets AN, Chen JY. Piloted methane/air jet flames: transport effects and aspects of scalar structure. *Combust Flame* 2005;143:433–49.
- [44] Bilger RW, Starnner SH, Kee RJ. On reduced mechanisms for methane/air combustion in nonpremixed flames. *Combust Flame* 1990;80:135–49.

Paper II

Development of a streak formation model for an improved prediction of gas phase combustion in biomass grate furnaces

Ali Shiehnejadhesar^{1,2}, Ramin Mehrabian², Robert Scharler^{1,2,3}, Ingwald Obernberger^{1,3}

¹ Graz University of Technology, Institute for Process and Particle Engineering, Inffeldgasse 21B, 8010 Graz, Austria; Tel: +43(0)3168739230; Fax: +43(0)3168739202; Email: Ali.shiehnejad@bioenergy2020.eu

² BIOENERGY 2020+ GmbH, Inffeldgasse 21B, 8010 Graz, Austria

³ BIOS BIOENERGIESYSTEME GmbH, Inffeldgasse 21B, 8010 Graz, Austria

Abstract

State-of-the-art packed bed models supply continuous concentration profiles as boundary conditions for subsequent CFD simulations of gas phase, leading to pre-mixed combustion conditions. However, in reality the “porous” nature of the packed bed leads to streak formation influencing gas mixing and combustion. Therefore, in the present work, in order to account for the influence of the streaks on gas phase combustion, a gas streak model based on a correlation between the local gas residence time and a mixing time has been developed based on numerical simulations and tested for a real-scale grate furnace. The streak model is based on the mixing function to describe the mixing process above the fuel bed. The mixing function is a combination of the mixing time, the necessary residence time to reach the fully mixed condition, and the flue gas residence time in the region above the fuel bed.

A CFD case study with an ideally packed bed with spheres as fuel particles and non-reacting flow was performed to numerically derive the mixing time. The particle diameter was derived from the volume to surface area ratio of pellets according to Austrian standard. The volatiles were represented by CO₂ released from the surface of the particles. The volatiles release rate from a single particle was approximated by the value of an in-house developed model for single particle conversion. The influence of relevant parameters, like bed height, volatiles mass flow rate and particle Reynolds number (calculated with the bulk flow velocity of primary air below the bed and the particle diameter), on mixing time was investigated.

The results showed a strong influence of the number of layers (bed height) on mixing. Hence, it was considered as independent parameter. As a next step, three different heights with different numbers of particle layers (5, 10 and 15 layers) were chosen to investigate the influence of particle Reynolds number and volatiles release rates. The results show a negligible effect of the volatiles release rate on mixing. However, the particle Reynolds number has a significant effect on the mixing time. For all layers considered, a trend concerning the mixing time in dependence of the particle Reynolds number was found. The results of this study serve as look-up table for the calculation of the mixing time in dependence of the different influencing parameters.

Finally, the model was linked with an in-house developed hybrid gas phase combustion model suitable for low as well as highly turbulent combustion conditions and tested for a 180 kW_{th} pilot-scale grate furnace. The results in comparison with a simulation without the streak formation model show, that the temperature and flue gas species prediction can be improved with the proposed streak formation model. Especially, in the region above the fuel bed (in the primary combustion chamber), this is of special importance for NO_x reduction by primary measures.

Keywords

CFD modelling, biomass, combustion, grates furnace, streak formation model, hybrid model

1. Introduction and objectives

CFD modelling is becoming increasingly important for the development and optimisation of biomass grate furnaces. Here, gas phase combustion models play a key role concerning predictions of flow, temperature, and gaseous emissions (e.g. CO and NO_x).

The mode of gas combustion in a grate furnace can be classified as partially premixed with a locally different mixing degree of oxidiser and fuel, whereas in this context the combustible gases released from the solid biomass fuel bed are to be understood as (gaseous) fuel.

An empirical packed-bed model developed by TU Graz in cooperation with BIOS [1] is usually being used at BIOENERGY 2020+ for the calculation of composition, temperature and flue gas leaving the surface of the solid biomass fuel bed. The empirical packed-bed model, as most of the common packed bed models, calculates profiles of partially premixed flue gas compositions not considering spatial concentration gradients of oxygen and volatiles since the fuel particles and the surrounding space cannot be resolved. However, in reality, the amount and distribution of combustibles and oxidiser in the gas released from the biomass particles in the fuel bed are locally strongly differing. Therefore, the “porous” nature of the packed bed leads to streak formation influencing gas mixing and combustion, which is not described by state-of-the-art CFD-based packed bed models.

Therefore, in this paper a model which accounts for the influence of the streaks on gas phase mixing and reactions (combustion, NO_x formation) is introduced. The streak model is based on a correlation between the local gas residence time and mixing time, whereas the mixing time is defined as the necessary residence time to reach the fully mixed condition. The mixing time was derived based on a series of numerical simulations with an ideally packed bed with spheres representing the biomass particles.

Finally, the streak model was linked with an in-house developed hybrid gas phase combustion model suitable for laminar to highly turbulent combustion conditions and applied for a pilot-scale grate furnace (180 kWth) of BE2020+ concerning the simulation of gas phase combustion and NO_x formation. For the purpose of model evaluation, the simulation results were compared with CO and NO_x emission measurements and simulations without the application of the streak formation model.

2. Methodology

The paper is structured as following: Firstly, an overview of the models applied for the case studies is given in the modelling part. Then, the non-reacting packed bed simulations to derive the streak formation parameters are described. Finally, the case study (pilot-scale grate furnace of BE2020+) for the application of the streak formation model is introduced.

2.1 Modelling

In this chapter, all the models used for the non-reacting packed bed simulations as well as the grate furnace simulations are explained. Then, the hybrid gas phase combustion model which is utilised for the grate furnace simulations is introduced. Finally, the streak formation model is presented.

2.1.1 Model overview

For the derivation of streak formation parameters, non-reacting multi-species simulations with an ideally packed bed with spheres have been performed. The SST $k-\omega$ low Reynolds turbulence model is applied to cover the whole range of flow conditions from laminar to turbulent flows in biomass grate furnaces. The primary air is injected uniformly below the fuel particles whereas the grate has been neglected. CO₂ is taken as trace species representing the volatiles release through the particle surface. To estimate the degree of mixing, a mixing state is defined (see section 2.1.3). The mixing time is evaluated based on an estimated residence time to achieve a certain degree of mixing. The gas residence time is calculated by solving a scalar transport equation.

For the simulation of the pilot-scale grate furnace of BE2020+, the following models have been applied: an empirical model developed by TU Graz in cooperation with BIOS [1] is used to describe the thermal decomposition of the solid biomass fuel. The model consists mainly of three parts. The

definition of one-dimensional profiles along the grate concerning the degradation of the fuel components as well as fuel drying (part 1 based on assumptions and experimental data forms the basis). In combination with the definition of conversion parameters (based on assumptions as well as experimental and literature data), which describe the formation of the most important flue gas components CH₄, CO, CO₂, H₂, H₂O O₂ as well as NH₃, HCN and NO (part 2), the stepwise balancing of mass and energy fluxes released from the fuel bed is possible (part 3) [1, 2, and 3]. The calculation results are used as boundary profiles for subsequent CFD simulations of the turbulent reactive flow in the furnace. For modelling of the turbulent reactive flow in the combustion chamber the Realizable k-ε model (turbulence), the Discrete Ordinates Model (radiation) as well as the Hybrid model (gas phase combustion) have been applied. Together with the Realizable k-ε model, the enhanced wall treatment model is used, which covers a two-layer turbulence approach combined with enhanced wall functions [4]. The model is valid throughout the near-wall region (i.e., laminar sub-layer, buffer region, and fully-turbulent outer region). Therefore, the model is supposed to be valid for low and high Reynolds wall-bounded flows.

Under the assumption that NO_x formation reactions do not significantly influence the flow pattern in the furnace, a time saving 2-step approach is applied for CFD simulations. The basic gas phase combustion simulation has been performed using the hybrid combustion model (two simulations without and with the effect of streaks) with a C-H-O subset of the Skeletal Kilpinen97 mechanism (12 species and 25 reactions) [5], which has extensively been validated for grate furnaces [6]. The subsequent CFD simulation of gas phase fuel NO_x formation in a post-processing mode has been done using the hybrid model in combination with a detailed reaction mechanism (28 species and 102 reactions in total) [6].

2.1.2 Hybrid gas phase reaction model

An in-house developed hybrid gas phase reaction model suitable for laminar to highly turbulent flows has been applied for the simulation of the reacting gas flow. In particular, in the region above the fuel bed and in small-scale biomass combustion plants, gas phase mixing is highly influenced by laminar and low turbulence zones. Here, the Eddy Break-Up combustion models are not valid because they were originally developed for highly turbulent flows. Therefore, a hybrid Eddy Dissipation Concept (EDC) / Finite Rate Kinetics model (FRK) has been developed, which calculates the effective reaction rate from laminar finite rate kinetics and the turbulent reaction rate and weights them depending on the local turbulent Reynolds number of the flow.

For a multi-component system, the species mass conservation equation is defined as follows;

$$\frac{\partial}{\partial t}(\rho Y_i) + \nabla \cdot (\rho \bar{u} Y_i) = -\nabla \cdot \bar{J}_i + R_i \quad (1)$$

Where ρ is the mixture density, Y_i is the mass fraction of species i , \bar{u} is the velocity vector, \bar{J}_i is the diffusion flux of species i due to concentration gradients, and R_i is the net rate of production of species i by chemical reactions.

In the hybrid model, the mean chemical reaction (second term in the right hand side of Eq. (1)) is modelled as:

$$(R_i)_{\text{Hybrid}} = \left(\frac{1}{1 + Re_t} \right) (R_i)_{\text{FRK}} + \left(\frac{Re_t}{1 + Re_t} \right) (R_i)_{\text{EDC}} \quad (2)$$

where $(R_i)_{\text{FRK}}$ is the FRK mean reaction rate, the term $(R_i)_{\text{EDC}}$ is the mean reaction rate calculated by the EDC model and Re_t is the turbulent Reynolds number ($Re_t = \frac{\rho k^2}{\nu \varepsilon}$). The hybrid model has been extensively validated for a series of diffusion jet flames covering laminar, transitional, and turbulent flow conditions. A detail description of the hybrid gas phase reaction model can be found in [7].

2.1.3 Streak formation model

A streak formation model has been developed. The model is based on a mixing time, where the gas streaks arising from the fuel bed are fully mixed, and a correlation with the residence time of the flue gas released from the fuel bed. In order to describe the mixing process above the packed bed, a criterion has been defined to calculate the mixing state (MS) as following:

$$MS = \left(1 - \frac{C_{fm} - C(t)}{C_{fm}} \right) \quad (3)$$

Here, C_{fm} is the tracer gas concentration (here CO_2) in the fully mixed gas and $C(t)$ is the local tracer gas (CO_2) concentration in dependence of the mixing time. The residence time which is necessary to reach the defined mixing state (here, $0.99 < MS < 1.01$ has been defined) is the mixing time t_{fm} . Finally, the mixing function (MF) is the combination of the mixing time t_{fm} and the gas residence time t_{gas} :

$$MF = \text{MIN} \left(\frac{t_{gas}}{t_{fm}}; 1 \right) \quad (4)$$

where

MF = 0 (completely unmixed)

MF = 1 (completely mixed)

A scalar transport equation has been solved to calculate the gas residence time as following [8]:

$$\frac{\partial}{\partial x_i} \rho u_i \phi - \bar{J} \frac{\partial \phi}{\partial x_i} = \rho, \quad (\bar{J} = -\rho(D_m + D_t) \frac{\partial \phi}{\partial x_i}) \quad (5)$$

Here, ρ and \bar{u} are density and velocity of the flue gas; \bar{J} is a component of diffusion flux; D_m and

$D_t = \left(\frac{\mu_t}{\rho Sc_t} \right)$ are molecular and turbulent diffusivity; where, μ_t is the turbulent viscosity and Sc_t is the

turbulent Schmidt number (with a value of 0.7 which is also applied for the species transport equation). After the flow field is solved with CFD simulations, the values of residence time are approximated by solving Eq. (5). The first and second terms on the left hand side of Eq. (5) represent the convection and diffusion fluxes, the density on the right hand side represents the source term. The later means, that the residence time in each computing cell will be added to the residence time calculated by the transport equation. Eq. (5) has been implemented by a user-defined function (UDF) in ANSYS FLUENT.

As a first approximation, a linear correlation between the gas residence time t_{gas} and the mixing function MF has been chosen. A CFD-based case study with an ideally packed bed has been defined in order to numerically derive the mixing time (t_{fm}).

Finally, the effective reaction rate is calculated by multiplying the mixing function, which defines the macro-mixing state, with the reaction rate, calculated by the hybrid combustion model as following:

$$(R_i)_{\text{Hybrid-streak formation}} = MF \times (R_i)_{\text{Hybrid}} \quad (6)$$

2.2 Case study for the derivation of the streak formation model constants

A CFD-based case study with an ideally packed bed with spheres as fuel particles and non-reacting flow has been performed in order to numerically derive the mixing time. The volatiles were represented by CO_2 released from the surface of the particles in the bed. The volatiles release rate from single particles was approximated by an in-house developed layer model [9] for the conversion of thermally

thick biomass particles. In this parameter study, the following influencing parameters have been investigated for a packed bed:

- Bed heights: variation by particle layers (from 5 to 15 layers)
- Volatiles mass flow rate: During typical biomass combustion conditions with air staging the most relevant components released are H₂O, CO₂, CO, H₂ and CH₄ [10, 11 and 12]. However, during packed bed combustion, the dominant gas volume flux is from the primary air passing through the packed bed. In CFD simulations the density of the mixture is usually considered as incompressible (due to the low pressure changes) and mainly depends on the temperature inside the combustion chamber that influences the volume flow rate of the volatiles released from the biomass particles. Moreover, since a non-reacting simulation is performed, for the release rates only an average value can be estimated. Therefore, a sensitivity analysis concerning the influence of the volatiles release rate was performed. In order to cover the possible range of released volume fluxes, the estimated value of the reference case was multiplied by a factor x . A typical volatiles release rate was estimated with the layer model; for the investigation of the sensitivity of the results on the release rates, this value has been varied between a factor from 1 to 1.7. It could be shown that the influence of the release rate is comparably low.
- Bulk flow velocity of primary air below the bed (0.1 -7 m/s): In biomass grate furnaces, the flow above the fuel bed is typically in the low Re range. Which primary air velocities varying from 0.1 to 3 (m/s). The values are gained from an in-house developed empirical packed bed model of TU Graz and BIOS. Therefore, to cover all ranges of flow conditions for small to large-scale biomass combustion plants, the sensitivity analysis has been performed.

The diameter of the spheres was approximated based on the volume to surface area ratio of pellets according to the respective EU standard. As mentioned, the study has been performed for pellets as fuel. However, the simulation results can be applied for all particle sizes by applying the particle Reynolds number for the look-up table where the results are summarised. Here, three parameter studies with an ideally packed bed were performed in order to calculate the mixing time in dependence of the influencing parameters. Figure 1 shows the CFD domain of the packed bed for 5 layers considered in this study. The primary air was injected below the bed with an even distribution and the volatiles represented by CO₂ as tracer gas were released from the surface of the spheres. Moreover, different planes above the bed were defined to evaluate the mixing state and mixing time. A simulation matrix was built for each layer to derive the mixing time based on the primary air velocity and volatiles mass flow rate. The flow simulation was performed for all primary air velocities and volatile mass flow rates. Then, the mixing state was calculated at each plane defined above the bed. Finally, the mixing time was derived based on the estimated gas residence time which is necessary to reach the defined mixing state (here, $0.99 < MS < 1.01$).

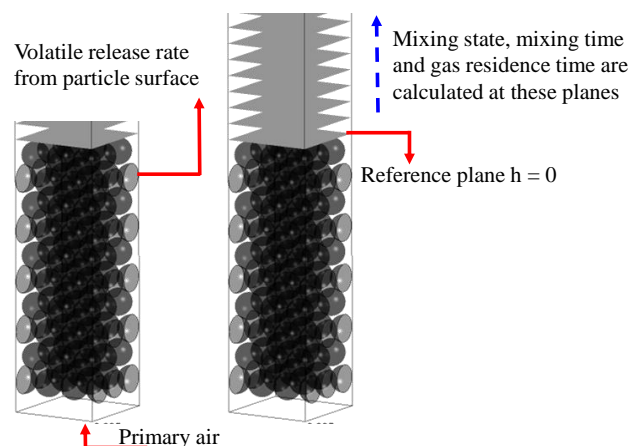


Figure 1: CFD domain and boundary conditions for the evaluation of the mixing time above the packed bed

Therefore, the mixing time can be represented by influencing parameters like primary air velocity and number of layers considered in the simulations. To make the model applicable for all fuel particle sizes, the mixing time can be represented as function of the particle Reynolds number instead of primary air velocity. The particle Reynolds number can be defined as particle diameter times primary air velocity divided by the kinematic viscosity of air ($Re_p = \frac{V_{\text{primary air}} d_v}{\nu_{\text{air}}}$). The volume diameter d_v [13] can be derived based on the diameter of a sphere having the same volume as the biomass particles. The biomass particle volume can be estimated from the average size of the biomass particles.

2.3 Test and verification of the streak formation model

To investigate and verify the influence of the streak formation model on gas phase mixing and reactions, a CFD simulation was performed for a pilot-scale moving grate furnace equipped with a hot water fire tube boiler (180 kW_{th}) using wood chips as fuel. Table 1 provides the most relevant operating conditions of the furnace and the fuel composition.

The pilot-scale moving grate furnace used for the test of the streak formation model is shown in Figure 2. The simulation domain comprises the combustion chamber above the fuel bed till the exit of the hot water fire tube boiler. Recirculated flue gas can be supplied below the grate and through six nozzles above the fuel bed. The furnace has been designed to switch between a short and a long primary combustion zone. The short primary combustion chamber is achieved by activating the first secondary air nozzle row and closing the second secondary air nozzle row and vice versa for the long primary combustion zone.

In this case study the first secondary air nozzles (eight nozzles) were closed and secondary air was injected through six nozzles at the entrance to the third horizontal duct. Besides, there was no flue gas recirculation applied neither below the grate nor through the flue gas recirculation nozzles. False air leaking into the combustion chamber due to non-perfect sealing of the fuel feeding system was injected via the fuel supply. A certain amount of leakage air (10% of primary air), obtained from the measurements during the test run, was taken into account in the simulation as false air. Due to the symmetry of the furnace, only half of the furnace was simulated. Therefore, the symmetry boundary condition was used in the mid plane of the furnace.

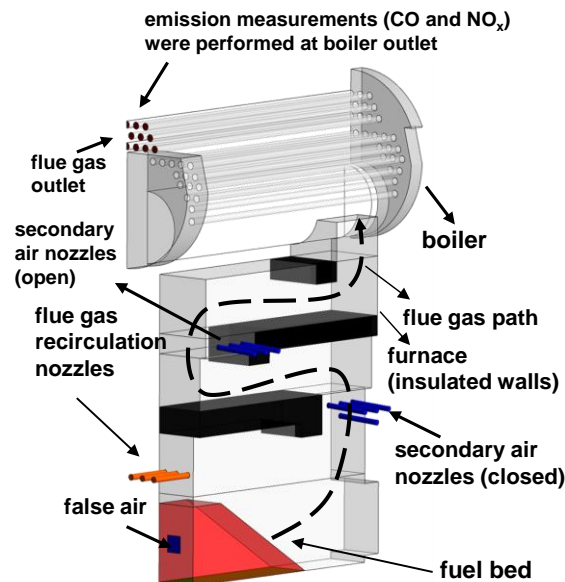


Figure 2: Geometry of the pilot-scale moving grate biomass furnace of BIOENERGY2020+ with a fire-tube hot water boiler

The water side of the fire tube boiler walls was not included in the simulation. A convection boundary condition with 85°C (average water temperature) and a typical heat transfer coefficient for water in forced convection (6000 W/m²K) was used for the fire tube boiler walls.

Table 1: Operating conditions and fuel characteristics of the pilot-scale grate furnace

Operating conditions	Unit	Value
Nominal boiler load	kW	155
Adiabatic flame temperature	°C	1325
Flue gas recirculation ratio	-	0
λ_{Prim}	-	0.52
λ_{total}	-	1.41
Fuel composition	Unit	Value
Ash	Mass fraction d.b.	0.76
C	Mass fraction d.b.	49.70
H	Mass fraction d.b.	6.00
O	Mass fraction d.b.	43.50
N	Mass fraction d.b.	0.08
S	mg/kg d.b.	62.00
Moisture content	Mass fraction w.b.	41.90
GCV	MJ/kg d.b.	19.9
NCV	MJ/kg w.b.	9.8

Explanations: **w.b.**: wet basis; **d.b.**: dry basis; **GCV**: gross calorific value; **NCV**: net calorific value; λ_{prim} : primary air ratio related to primary air supplied below the grate; λ_{total} : total air ratio related to total amount of air supplied

3. Discussion of results

3.1 Derivation of streak formation model constants

An initial case study showed a strong effect of the number of layers (bed height) on mixing (not shown here). Hence, it was considered as an independent parameter. Afterwards, a simulation matrix was defined in order to investigate the effect of primary air velocity and volatiles mass flow rate variations on the mixing (mixing state) for each number of particle layers defined (5, 10 and 15 layers). Moreover, to reduce the number of independent parameters (here, particle diameter and primary air velocity) from two to one, the particle Reynolds number was defined (see section 2. 2).

The results showed a negligible effect of the volatiles release on mixing (not shown here). However, the primary air velocity and particle Reynolds number respectively, had a significant effect on mixing. Figure 3 shows the mixing time behaviour in dependence of the particle Reynolds number as well as the number of layers. For all layers considered, a trend concerning the mixing time in dependence of the particle Reynolds number was found. The results showed that the mixing time of the streaks increases as the particle Reynolds number increases. Generally, at lower particle Reynolds numbers the mixing time is lower. This attributes to a higher residence time of the flue gas due to lower primary air velocities that improve the mixing of primary air and volatile matter. The mixing time increases as the particle Reynolds number (i.e. primary air velocity) rises. moreover, the mixing time at all particle Reynolds numbers is lower for a packed bed with larger height since a higher residence time inside the packed bed improves mixing of primary air and volatile matter. The results of this case study serve as look-up table for the calculation of the mixing time in dependence of the different influencing parameters. For practical application (e.g. the furnace simulation with the streak formation model - see section 3. 2) the mixing time (t_{fm}) can be retrieved by a linear interpolation between the calculation points through an estimation of the particle Reynolds number and the number of layers. The particle Reynolds number can be easily calculated from the velocity profile specified by the empirical packed

bed model along the grate and the particle diameter (e.g. volume diameter [13]). Besides, the number of layers can be estimated by the initial estimated height of the packed bed and the diameter of the fresh biomass fuel fed. The number of layers represents the number of particles that can be stacked in that length (e.g. length divided by the diameter of particles). Since the total number of particles on the bed remains constant on an average, also the number of layers remains constant over the grate length.

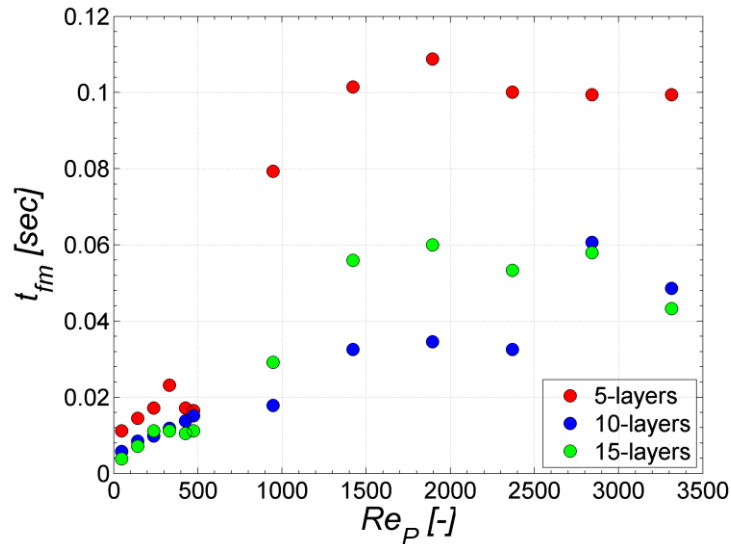


Figure 3: Mixing time [sec] for different particle Reynolds numbers and different numbers of particle layers

3. 2 Test of the streak formation model for a biomass grate furnace

In this section, the results for the simulation of the 180 kW biomass grate furnace of BIOENERGY 2020+ are shown. To see the effect of streaks on the gas reactions concerning temperature and species (e.g. CO and NO_x formation), two simulations were performed, without and with the streak formation model. Figure 4 (left) shows the calculated particle Reynolds number as well as the number of layers along the grate. The particle Reynolds number was calculated based on the velocity profile calculated with the empirical packed bed model (the maximum primary air velocity is about 0.5 [m/s] in the present case). The particle diameter was estimated from the volume diameter (see section 2. 2) (the wood chips particles were assumed as spheres with a $d_v = 25$ [mm]). Besides, the number of layers can be estimated by the initial estimated height of the packed bed and the diameter of the fresh wood chips fed. To derive a mixing time profile along the grate, (Figure 4 [right]) the values were retrieved from the look-up table for the mixing time (as described in section 3. 1).

The shrinkage of particles was implicitly considered in the simulations by the assumption of the shape of the fuel bed and the assumption of a constant number of particle trajectories along the grate length. For example, the particle size changes as the particles move along the grate (i.e. the diameter of particles decreases). However, the number of particles remains constant during the conversion processes along the grate which is considered in the simulations. Hence, the particle size variation affecting the particle Reynolds number along the grate is considered in the simulations.

Finally, two transport equations were solved, one for the gas residence time and the other for the mixing time, to derive the local mixing function defined in Eq. 4. Figure 5 shows the contour plots of gas residence time (left) and the mixing function (right) derived from Eq. 4.

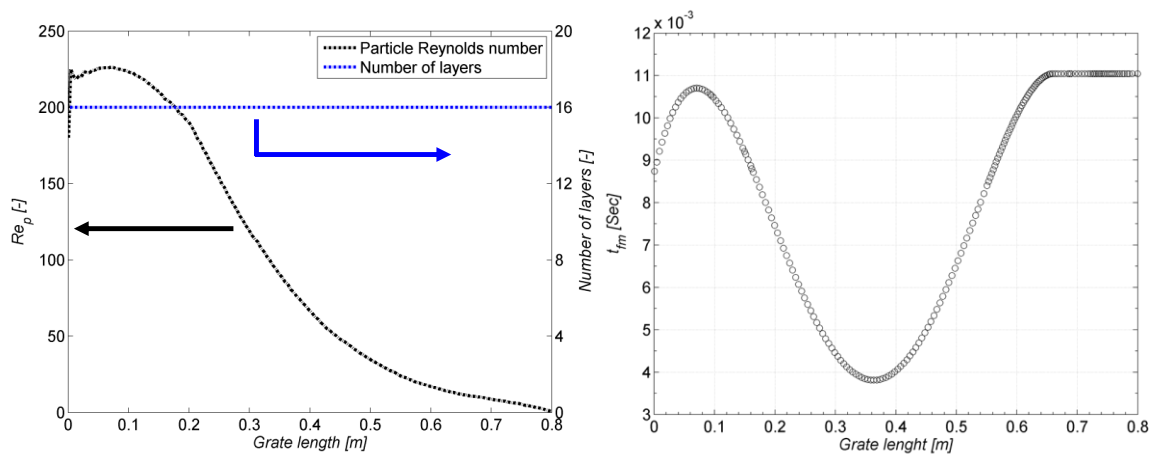


Figure 4: Particle Reynolds number [-] and number of particle layers [-] (left) as well as estimated mixing time [sec] interpolated from calculation points of Figure 3 (right)

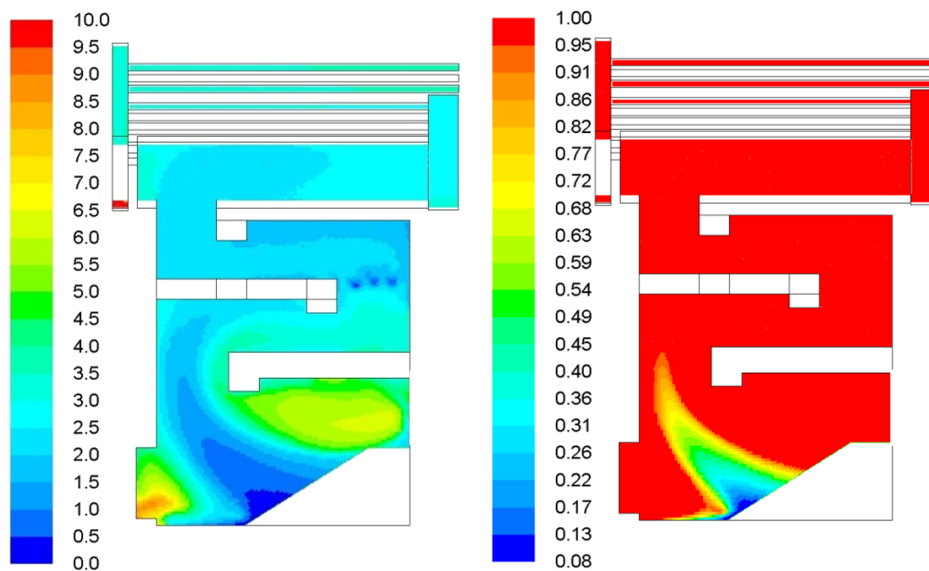


Figure 5: Gas residence time [sec] (left), and mixing function [-] (right)

Figure 6 shows the flue gas temperature predicted with the hybrid model (left) and the hybrid-streak formation model (right). The calculated CO concentrations for both hybrid and hybrid-streak formation model are shown in Figure 7. As can be seen from both figures (temperature and CO concentrations), there are no big differences between the two models. This can be explained by a staged combustion with $\lambda_{PCZ} < 1$ and sufficient residence time in the primary combustion zone for a full consumption of O_2 and, hence a flue gas composition at the entrance to the secondary combustion zone, which is approximately independent from the combustion model. Furthermore, the reaction progress is not influenced by the streaks from the packed bed anymore and the residence time in the secondary combustion zone is high enough for an almost complete CO burnout. Therefore, the effect of streak formation on the combustion process (flue gas temperature and CO burnout) for this specific case is not distinctive. Moreover, in the present test case, the CO emission's measured at boiler outlet was very low. Therefore, in this specific case study, the influence of the models applied in the simulation (hybrid and hybrid-streak formation model) on CO emissions could not be validated. Therefore, further validation simulations are currently being performed for other cases. The predicted O_2 mass fraction calculated with both models is depicted in Figure 8. The oxygen concentration above the bed is predicted slightly different in both cases. The O_2 concentrations are influenced by the streaks above the fuel bed especially in the locations where they are highlighted (location 1 and 2). The

characteristics of reacting radicals (e.g. OH and O) are of high relevance for an in-depth understanding of the combustion and NO_x formation processes [14]. These radicals are of high relevance especially for the formation of NO_x. The calculated OH and O species with hybrid and hybrid-streak formation models are shown in Figure 9. The OH and O species are generally lower predicted with the hybrid-streak formation model.

This is mainly due to the contribution of the streak formation model (i.e. the spatial distribution of oxygen concentrations (see Figure 8)) in which the rates of production or destruction of the species are slowed down by the streak formation model (see Eq. 6). Since the net reaction rate in the streak formation model is multiplied by the mixing function, the region above the major flue gas release zone and the adjacent shear layers / reaction fronts are mainly influenced by mixing of the streaks.

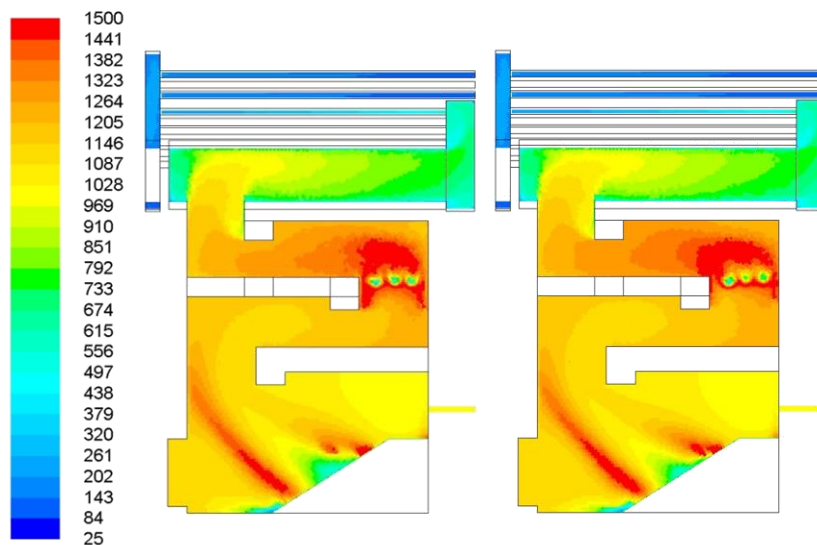


Figure 6: Flue gas temperature field calculated by the hybrid model [°C] (left) and the hybrid-streak formation model (right)

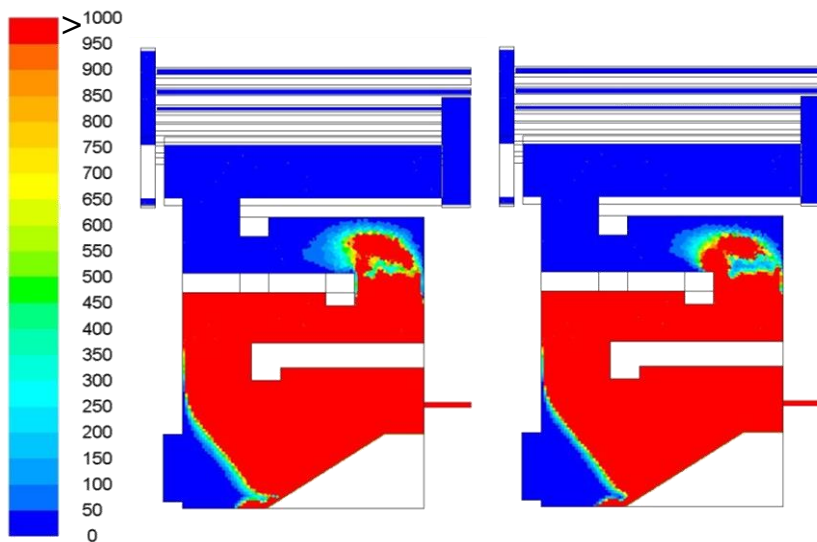


Figure 7: Iso-surfaces of CO concentration [ppmv] in the mid plane of the computational domain calculated by the hybrid model (left) and the hybrid-streak formation model (right)

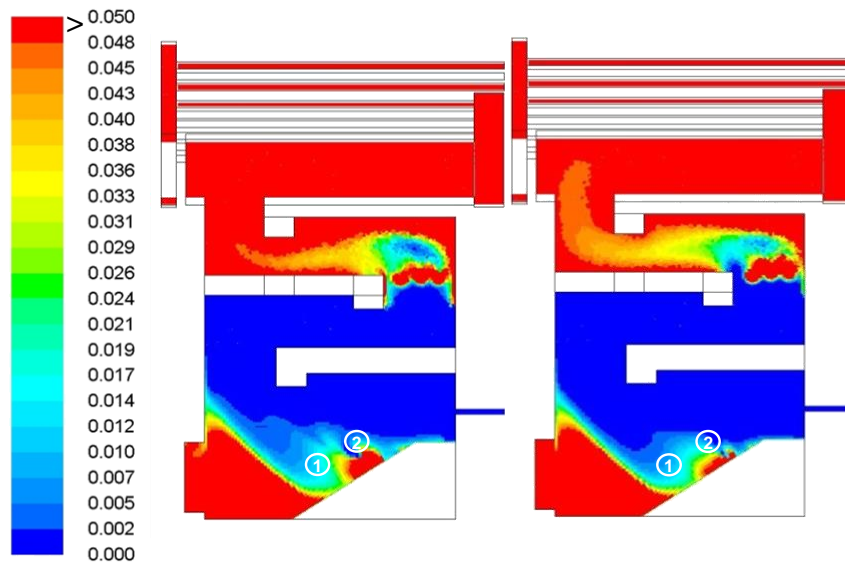


Figure 8: Iso-surfaces of the O₂ mass fraction [-] in the mid plane of the computational domain calculated with the hybrid model (left) and the hybrid-streak formation model (right)

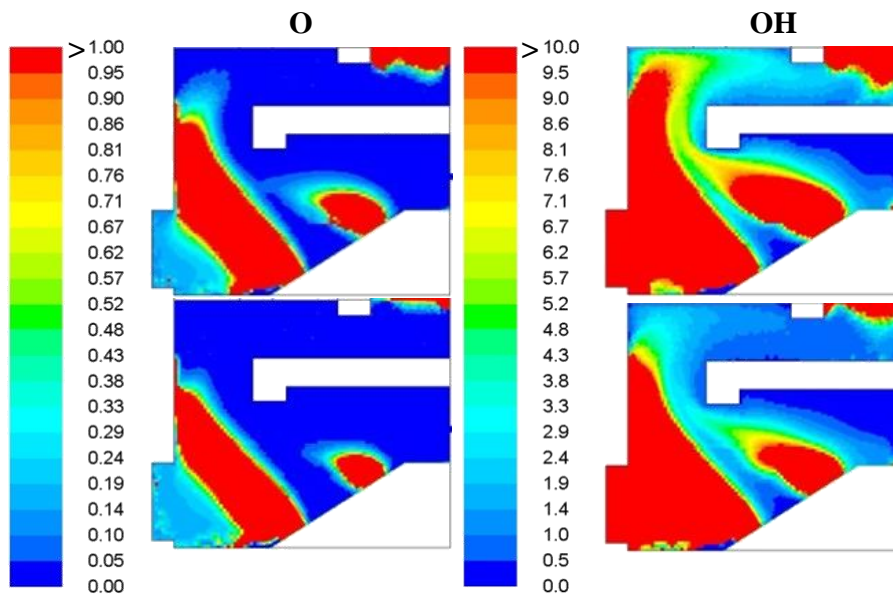


Figure 9: Iso-surfaces of O concentration [ppmv] (left), and OH concentration [ppmv] (right) calculated with the hybrid (top) and the hybrid-streak formation model (bottom)

As already mentioned, a skeletal reaction mechanism (28 species and 102 reactions in total) was applied [6] for the simulation of the NO_x formation process, whereas the simulation was performed in a post-processing step. The initial conditions were taken from the previous solution data (combustion simulation with hybrid and hybrid-streak formation model, respectively).

Experimental data of the combustion and release behaviour for a variety of solid biomass fuels have been gained through several measurement campaigns in a lab-scale pot furnace reactor (packed bed batch reactor) [15, 16]. These experimental data include the concentration profiles of the N containing species NO, NH₃, HCN, NO₂ and N₂O over time. The measured profiles are utilised for the derivation

of release functions for the most relevant NO_x precursors measured. The release functions of fuel nitrogen depend on the local air ratio (λ) and the nitrogen content of the fuel. The most important NO_x precursor detected above the fuel bed under fuel rich conditions is NH₃, while HCN is almost insignificant. NO is detected mainly under air rich conditions. Furthermore, the experimental data are utilised to derive release functions for the relevant NO_x precursors NO, NH₃ and HCN. The release functions were implemented in an in-house empirical packed bed combustion model [15 and 16], which serves as a basis for the subsequent CFD gas phase simulation of N species conversion. Figure 10 shows the NO, NH₃ and HCN profiles calculated with the hybrid and the hybrid-streak formation model. Generally, distinct areas can be observed, where the release of NO, HCN and NH₃ takes place. NO is released in the air-rich zones at the beginning and the end of the fuel bed. NO is formed in regions of simultaneously high temperature and high concentrations of O and OH radicals [17 and 18]. The locations, where the NO has been released are in line with the high concentrations of O and OH radicals above the bed (see Figure 9). In contrast, NH₃ and HCN are primarily released from the main in-bed devolatilisation/gasification zone. These differences result from the local differences in the in-bed availability of oxidiser (see Figure 8), which in turn depends on the distribution of the primary air under the grate as well as on the in-bed thermal conversion processes. At the beginning and at the end of the fuel bed high in-bed availability of oxygen primarily leads to the release of the fuel-bound nitrogen in form of NO (see Figure 8), while NH₃ and HCN are formed at low in-bed availability of oxygen in the main in-bed devolatilisation/gasification zone. The distribution of the N-containing species in the gas phase results from the simultaneous formation and reduction processes, taking place in different regions of the combustion chamber and depending on many factors. Here, by taking into account the effect of the streak formation model, it can be seen that the spatial distribution of NO and NH₃, specially, above the fuel bed are different (see Figure 10). These differences are mainly attributed to the different oxygen and radical (O and OH) concentrations that are influenced by the streak formation model (see Figure 8 and Figure 9). Figure 11 shows the NO_x profiles predicted with the hybrid and the hybrid-streak model. Table 2 provides the NO_x concentrations predicted with the hybrid and the hybrid-streak model in comparison with NO_x emission measurements at boiler outlet. The results indicate that the prediction is improved with the hybrid-streak formation model. This can be argued with the more accurate prediction of the species mixing process above the fuel bed and, therefore, of the radicals, that are important for the NO_x formation processes.

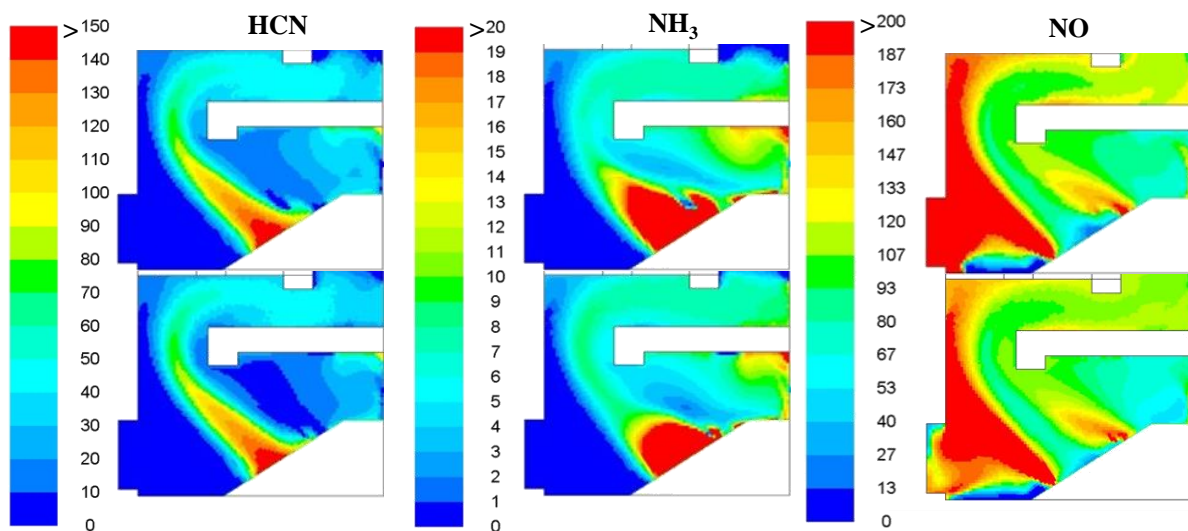


Figure 10: Iso-surfaces of HCN concentration [ppmv] (left), NH₃ concentration [ppmv] (middle) and NO concentration [ppmv] (right) calculated with the hybrid model (top) and the hybrid-streak formation model (bottom)

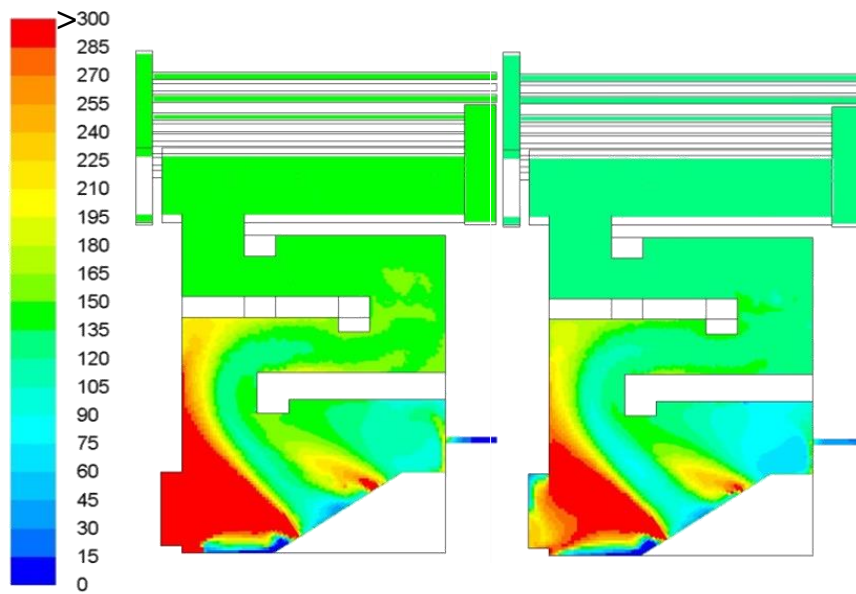


Figure 11: Iso-surfaces of NO_x concentration [mg/Nm³ d.b., 13 vol% O₂] calculated with the hybrid model (left) and the hybrid-streak formation model (right)

Table 2: Predicted NO_x concentrations with the hybrid and the hybrid-streak formation model in comparison to measurements

Parameter	Unit	Value	Deviation [%]
Experiment	[mg/Nm ³ d.b., 13 vol% O ₂]	129	-
Hybrid	[mg/Nm ³ d.b., 13 vol% O ₂]	141	9
Hybrid-streak	[mg/Nm ³ d.b., 13 vol% O ₂]	125	3

4. Summary and conclusions

A streak formation model has been developed to account for the effects of gas streaks arising from the fuel bed on gas mixing and reactions. The streak formation model is based on a correlation between the local gas residence time and a mixing time in which the mixing time is the necessary time to reach the fully mixed condition above the packed bed. A mixing state definition was introduced in order to evaluate the degree of mixing and the fully mixed condition, respectively, above the packed bed. The gas residence time introduced in the streak formation model was obtained by solving a scalar transport equation. A series of packed bed CFD case study simulations has been carried out to derive the mixing time introduced in the streak formation model. The primary air velocity, volatile mass flow rate and number of particles (bed thickness) were identified as influencing parameters for the derivation of mixing time. The number of layers was considered as independent parameter since it had considerable influence on the mixing. Then, the effect of primary air velocity and volatile mass flow rate variations on the mixing were studied for a defined number of layers (5, 10 and 15 layers). The results showed a negligible effect of the volatile release rates on mixing. However, the primary air velocity and particle Reynolds number, respectively, had a significant effect on mixing. The particle Reynolds number definition was applied in terms of particle diameter and primary air velocity. This definition helped to reduce the number of independent parameters and to make the model applicably for any fuel particle size. The results of the CFD packed bed case study served as look-up table for the calculation of the mixing time in dependence of the different influencing parameters. The mixing time can be retrieved by a linear interpolation between the calculation points in dependence of the particle Reynolds number and the number of fuel layers. Furthermore, the application of the streak formation model has been verified for a pilot-scale grate furnace. Two simulations have been

performed, with and without the effect of the streak formation model. An in-house developed hybrid gas phase combustion model applicable for laminar to turbulent flow situations was used for both simulations (hybrid model). For the case that considers the effect of streaks on combustion, the particle Reynolds number and the number of layers (fuel bed thickness) have been calculated from the velocity profile specified by the empirical packed bed model as well as the assumed height of the fuel bed, respectively. The mixing time profile for the pilot-scale grate furnace was then evaluated by an interpolation through the values retrieved as a function of the particle Reynolds number and the bed height. Two scalar transport equations have been solved for gas residence time as well as mixing time to derive the local mixing function defined in the streak formation model. The effective reaction rate within the hybrid model was achieved by multiplying the mixing function, which considers macro-mixing, with the reaction rate predicted with the hybrid model. The results from the pilot-scale biomass grate furnace with and without the effect of streaks showed that in the present case, the streaks had no big influence on the combustion process including flue gas temperature and CO emissions. The low oxygen concentrations in the primary combustion zone and high flue gas residence time result in a full CO burnout at furnace exit as well as a full conversion of oxygen before the secondary combustion zone. However, the formation of reacting radicals (e.g. O and OH), especially, in the region above the bed are influenced by the streak formation model since the reaction progress is delayed caused by the incomplete mixing.

In the next step, NO_x simulations have been performed in a post-processing approach based on the solution obtained from the combustion simulations. The NO_x precursor species release profiles have been calculated with an empirical packed bed model. The distribution of the NH₃, HCN and NO profiles showed that the streak formation model has a strong influence on the spatial distributions of the aforementioned species. This is mainly due to the slowdown of the reaction rate predictions caused by the streak formation model. Finally, the NO_x emissions calculated with the streak formation model showed a better agreement with measured values due to the superiority of the model for the prediction of the reacting radicals above the packed bed. Concluding, the streak formation model in combination with the hybrid gas phase combustion model displayed a potential for an improved NO_x prediction since it considers species mixing and reaction processes above the fuel bed with a higher accuracy. In the future, extensive validation simulations for real-scale plants are foreseen in order to validate and evaluate the model in more detail and for different framework conditions.

5. Literature

1. Scharler R. Entwicklung und Optimierung von Biomasse-Rostfeuerungen durch CFD-Analyse. PhD Thesis. Graz University of Technology; 2001.
2. R. Scharler, E. Widmann, I. Obernberger CFD modeling of NO_x formation in biomass grate furnaces with detailed chemistry A.V. Bridgwater, D.G.B. Boocock (Eds.), Science in thermal and chemical biomass conversion; Sept 2004, CPL Press, Victoria; Canada. UK (2006), pp. 284–300
3. A. Shiehnejadhesar, K. Schulze, R. Scharler, I. Obernberger A new innovative CFD-based optimisation method for biomass combustion plants Biomass & Bioenergy, 53 (2013), pp. 48–53
4. B. Kader. Temperature and Concentration Profiles in Fully Turbulent Boundary Layers. Int. J. Heat Mass Transfer, 24(9):1541-1544, 1981.
5. Kilpinen P. pia.kilpinen@uku.fi or pia.kilpinen@abo.fi.
6. S. Zahirovic, R. Scharler, P. Kilpinen, I. Obernberger A kinetic study on the potential of a hybrid reaction mechanism for prediction of NO_x formation in biomass grate furnaces Combust Theor Model, 15 (2011), pp. 645–670
7. A. Shiehnejadhesar, R. Mehrabian, R. Scharler, I. Obernberger Development of a gas phase combustion model suitable for low and high turbulence conditions Fuel, 126 (2014), pp. 177-187.

8. M. Bartak, M. Cermak, J. A. Clarke, J. Denev, F. Drkal, et al. Experimental and numerical study of local mean age-of-air. In proc. 7th International Building performance Simulation Association Conference, IBPSA. ISBN 85-901939-3-4 (2001).
9. R. Mehrabian, S. Zahirovic, R. Scharler, I. Obernberger, S. Kleditzsch, et al. A CFD model for thermal conversion of thermally thick biomass particles Fuel Process Technol, 95 (2012), pp. 96–108
10. D. Neves, H. Thunman, A. Matos, L. Tarelho, A. Gomez-Barea. Characterization and prediction of biomass pyrolysis products. Prog Energy Combust 2011;37:611-30.
11. M.L. Boroson, J.B. Howard, J.P. Longwell, W.A. Peters. Product yields and kinetics from the vapor phase cracking of wood pyrolysis tars. AIChE J 1989;35:120–8
12. R.G. Graham, M.A. Bergougnou, R.P. Overend. Fast pyrolysis of biomass. J Anal Appl Pyrol 1984;6:95–135
13. S. Hamel, On the Packing Properties of Fixed Beds for Thermal Fuel Conversion, Germany: Shaker verlag; 2010, pp. 74-75.
14. S. Zahirovic, R. Scharler, P. Kilpinen, I. Obernberger Validation of flow simulation and gas combustion sub-models for the CFD-based prediction of NO_x formation in biomass grate furnaces Combust Theor Model, 15 (1) (2011), pp. 61–87
15. I. Obernberger, E. Widmann, R. Scharler. Entwicklung eines Abbrandmodells und eines NO_x-Postprozessors zur Verbesserung der CFD-Simulation von Biomasse-Festbettfeuerungen. Report from energy and environment research, report No. 31/2003, Ministry for Transport, Innovative and Technology (Ed.), Vienna, Austria.
16. G. Stubenberger, R. Scharler, S. Zahirovic, I. Obernberger. Experimental investigation of nitrogen species release from different solid biomass fuels as a basis for release models Fuel, 87(6) (2008), pp. 793-806
17. S.R. Turns, Understanding NO_x formation in non-premixed flames: experiments and modeling, Prog. Energy Combust. Sci. 21 (1995), pp. 361–385.
18. A. Mardani, S. Tabejamaat NO_x Formation in H₂-CH₄ Blended Flame Under MILD Conditions, Combust Sci Technol, 184:7-8 (2012), pp. 995-1010

Paper III



Development and validation of CFD models for gas phase reactions in biomass grate furnaces considering gas streak formation above the packed bed



Ali Shiehnejadhesar^{a,b,*}, Robert Scharler^{a,b,c}, Ramin Mehrabian^b, Ingwald Obernberger^{a,c}

^a Institute for Process and Particle Engineering, Graz University of Technology, Inffeldgasse 21b, 8010 Graz, Austria

^b BIOENERGY 2020+ GmbH, Inffeldgasse 21b, 8010 Graz, Austria

^c BIOS BIOENERGIESYSTEME GmbH, Inffeldgasse 21b, 8010 Graz, Austria

ARTICLE INFO

Article history:

Received 22 April 2015

Received in revised form 3 July 2015

Accepted 24 July 2015

Available online 5 August 2015

Keywords:

CFD modelling

Biomass

Combustion

Grate furnace

Streak formation model

Hybrid model

ABSTRACT

State-of-the-art packed bed models supply continuous concentration profiles as boundary conditions for subsequent CFD simulations of gas phase, leading to pre-mixed combustion conditions. However, in reality the “porous” nature of the packed bed leads to streak formation influencing gas mixing and combustion. Therefore, in the present work, in order to account for the influence of the streaks on gas phase combustion, a gas streak model based on a correlation between the local gas residence time and a mixing time has been developed based on numerical simulations. Finally, the streak model was linked with an in-house developed hybrid gas phase combustion model suitable for laminar to highly turbulent flow conditions and applied for an under-feed pellet stoker furnace (20 kW_{th}) concerning the simulation of gas phase combustion and NO_x formation. The results in comparison with a simulation without the streak formation model show that the flue gas species prediction can be improved with the proposed streak formation model. Especially, in the region above the fuel bed (in the primary combustion chamber), this is of special importance for NO_x reduction by primary measures.

© 2015 Elsevier B.V. All rights reserved.

1. Introduction and objectives

CFD modelling is becoming increasingly important for the development and optimisation of biomass grate furnaces. Here, gas phase combustion models play a key role concerning predictions of flow, temperature, and gaseous emissions (e.g. CO and NO_x).

The mode of gas combustion in a grate furnace can be classified as partially premixed with a locally differing mixing degree of oxidiser and fuel, whereas in this context the reactive gases released from the combusting biomass particles in the fuel bed are to be understood as (gaseous) fuel.

An empirical packed bed model developed by BIOS in cooperation with TU Graz [1–3] is usually being used at BIOENERGY 2020+ for the calculation of composition, temperature and velocity of the flue gas leaving the fuel bed. The empirical packed bed model, as most of the common packed bed models, calculates profiles of partially premixed flue gas compositions not considering spatial concentration gradients of oxygen and volatiles, since the fuel particles and the surrounding space cannot be resolved. However, in reality, the amount and distribution of combustibles and oxidiser in the gas released from the biomass

particles in the fuel bed are locally strongly differing, which is termed here as streak formation, influencing gas mixing and combustion.

Therefore, in this paper, a model which accounts for the influence of the streaks on gas phase mixing and reactions (e.g. combustion and NO_x formation) is introduced. The streak model is based on a correlation between the gas residence time and mixing time above the fuel bed, whereas the mixing time is defined as the necessary residence time to reach the fully mixed condition.

To derive the mixing time, a CFD case study with an ideally packed bed with spheres as fuel particles and non-reacting flow was performed to numerically derive the mixing time in dependence of relevant influencing parameters. The particle diameter was derived from the volume to surface area ratio of pellets according to EU standard [4,5]. The volatiles were represented by CO₂ released from the surface of the particles. The volatile release rate from a single particle was approximated with an in-house developed model [6] for single particle conversion. The influence of relevant parameters, like bed height, volatile mass flow rate and particle Reynolds number (calculated with the bulk flow velocity of primary air below the bed and the particle diameter), on mixing time was investigated.

In the next step, the model was linked with an in-house developed hybrid gas phase combustion model suitable for laminar as well as moderately to highly turbulent combustion conditions [7] and tested for a 20 kW_{th} under-feed pellet stoker furnace concerning the simulation of gas phase combustion and NO_x formation. The gas phase mixing and

* Corresponding author at: Institute for Process and Particle Engineering, Graz University of Technology, Inffeldgasse 21b, 8010 Graz, Austria.

E-mail addresses: ali.shiehnejadhesar@gmail.com, ali.shiehnejad@bioenergy2020.eu (A. Shiehnejadhesar).

reaction progress is highly influenced by laminar and low turbulence zones in the regions above the fuel bed and in small-scale biomass combustion applications in general. Therefore, the application of the hybrid model is relevant.

In order to highlight the advantages of the hybrid model and the streak formation model for the simulation of small-scale furnaces in terms of combustion and emission predictions, additional simulations were performed with different CFD gas phase reaction models like the eddy dissipation model (EDM) [8] and the eddy dissipation concept (EDC) [9]. All the simulations were performed with ANSYS® FLUENT® release 15.0. For the purpose of model evaluation, the simulation results were compared with CO and NO_x emission measurements.

2. Methodology

Firstly, an overview of the models applied for the case studies is given in the modelling section. Then, the non-reacting packed bed simulations for the derivation of the parameters of the streak formation model are described. Finally, the case study with the under-feed pellet stoker grate furnace for the test and evaluation of the streak formation model is introduced.

2.1. Modelling

In this chapter, the models used for the non-reacting packed bed simulations as well as the grate furnace simulations are explained. Then, the hybrid gas phase combustion model which is utilised for the grate furnace simulations is introduced. Finally, the streak formation model is presented.

2.1.1. Model overview

2.1.1.1. Case study with ideally packed bed. For the derivation of streak formation parameters, non-reacting multi-species simulations with an ideally packed bed with spheres have been performed. The SST $k-\omega$ low Reynolds turbulence model is applied to cover the whole range of flow conditions from laminar to turbulent flows in biomass grate furnaces. The primary air is injected uniformly below the fuel particles whereas the grate has been neglected. CO₂ is taken as trace species representing the volatiles release through the particle surface. To estimate the degree of mixing, a mixing state is defined (see Section 2.1.3). The mixing time is evaluated based on an estimated residence time to achieve a certain degree of mixing. The gas residence time is calculated by solving a scalar transport equation.

2.1.1.2. Furnace simulation. For the simulation of the under-feed stoker furnace, the following models have been applied: an empirical model developed by BIOS in cooperation with TU Graz [1–3] is used to describe the thermal decomposition of the solid biomass fuel. The model consists mainly of three parts. The definition of one-dimensional profiles along the grate concerning the degradation of the fuel components as well as fuel drying (part 1: based on assumptions and experimental data from test runs). In combination with the definition of conversion parameters (based on assumptions as well as experimental and literature data), which describe the formation of the most important flue gas components CH₄, CO, CO₂, H₂, H₂O, and O₂ as well as the NO_x precursors NH₃, HCN and NO (part 2), the stepwise balancing of mass and energy fluxes released from the fuel bed is possible (part 3) [1–3]. The calculation results are used as boundary profiles for subsequent CFD simulations of the reactive flow in the furnace.

The EDM, the EDC and hybrid gas phase reaction models were used for the simulations of turbulent reactive flow in the combustion chamber. The solution of the EDM simulation, which is specially adapted for biomass grate furnaces with a global 3-step reaction mechanism [1,10,11], was used as starting solution for the subsequent EDC and hybrid model simulations. In the case of the hybrid model, an additional

simulation was performed by taking into account the effect of streak formation. The latter will be referred to as hybrid-streak model throughout the paper.

The In-Situ Adaptive Tabulation (ISAT) algorithm by Pope [12] has been used to speed-up the CPU-intensive treatment of the detailed reaction kinetics for the EDC, hybrid and hybrid-streak simulations. The discrete ordinate model (DOM) model was applied to simulate radiative heat transfer in the furnace. A domain based weighted-sum of gray-gases model (WSGGM) was used to calculate the absorption coefficient of the gas phase. Since the temperature and flue gas species specified by the empirical packed bed model are fixed at the surface of the fuel bed, there is no feedback from the freeboard on the bed model. The Realizable $k-\varepsilon$ turbulence model was used for turbulence. Together with the Realizable $k-\varepsilon$ model, the enhanced wall treatment model is used, which is a two-layer turbulence approach combined with enhanced wall functions [13]. The model is valid throughout the near-wall region (i.e., laminar sub-layer, buffer region, and fully-turbulent outer region). Therefore, the model is supposed to be valid for low and high Reynolds wall-bounded flows. It should be noted that the SST $k-\omega$ low Reynolds turbulence model was applied as suitable turbulence model above the packed bed to predict the mixing time since the flow is weakly turbulent. In the furnace simulation, the mixing delay due to the streaks, which is assumed to be dominating over the turbulent mixing above the bed, is considered with the streak model. Moreover, the Realizable $k-\varepsilon$ model gives considerably better results concerning the mixing of round jets in gas streams [1,14] than the SST $k-w$ model. The governing equations consist of incompressible Favre-averaged transport equations of continuity, momentum, energy, radiation, turbulence and species conservation equations. A second-order upwind discretisation scheme was used to solve all governing equations. Mass diffusion coefficients are required whenever species transport equations in multi-component flows are solved. The constant dilute approximation method with a value of 2.88×10^{-5} was used for the diffusion coefficient of each species in the mixture. An overview of the solution algorithm used for the furnace simulations with different gas phase reaction models is shown in Fig. 1. Under the assumption that NO_x formation reactions do not significantly influence the flow pattern in the furnace, a time saving 2-step approach is applied for CFD simulations. The basic gas phase combustion simulation has been performed using the EDC, hybrid and hybrid-streak combustion models with the C—H—O subset of the Skeletal Kilpinen97 mechanism (12 species and 25 reactions) [15], which has extensively been validated for grate furnaces [15]. The subsequent CFD simulation of gas phase fuel NO_x formation in a post-processing mode has been done using the EDC, hybrid and hybrid-streak models in combination with a detailed reaction mechanism (28 species and 102 reactions in total) [15]. Here, it is worth to mention that, the EDM in combination with global reaction mechanisms is not able to describe complex interactions of turbulence and multi-step reaction kinetics as given in the case of NO_x formation in biomass combustion plants. Therefore, the NO_x simulations reported in this paper were only performed with the EDC, the hybrid and the hybrid-streak model.

2.1.2. Hybrid gas phase reaction model

2.1.2.1. Bulk flow. An in-house developed hybrid gas phase reaction model, suitable for laminar to highly turbulent flows, has been applied for the simulation of the reacting gas flow. In particular, in the region above the fuel bed and in small-scale biomass combustion plants, gas phase mixing is highly influenced by laminar and low turbulence zones. Here, the eddy break-up combustion models are not valid because they were originally developed for highly turbulent flows. Therefore, a hybrid eddy dissipation concept (EDC)/finite rate kinetics model (FRK) has been developed, which calculates the effective reaction rate from laminar finite rate kinetics and the turbulent reaction rate and weights them depending on the local turbulent Reynolds number of the flow.

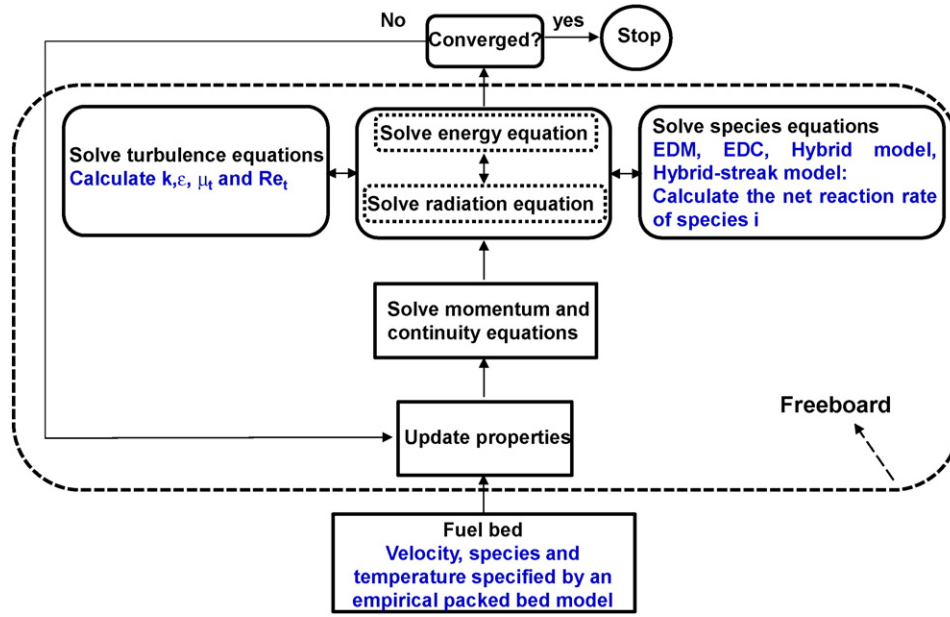


Fig. 1. Overview of the solution algorithm.

For a multi-component system, the species mass conservation equation is defined as follows;

$$\frac{\partial}{\partial t}(\rho Y_i) + \nabla \cdot (\rho \vec{v} Y_i) = -\nabla \cdot \vec{J}_i + R_i \quad (1)$$

where ρ is the mixture density, Y_i is the mass fraction of species i , \vec{v} is the velocity vector, \vec{J}_i is the diffusion flux of species i due to concentration gradients, and R_i is the net rate of production of species i by chemical reactions.

In the hybrid model, the mean chemical reaction (second term in the right hand side of Eq. (1)) is modelled as:

$$(R_i)_{\text{Hybrid}} = \left(\frac{2}{1 + Re_t} \right) (R_i)_{\text{FRK}} + \left(\frac{Re_t - 1}{1 + Re_t} \right) (R_i)_{\text{EDC}} \quad (2)$$

where $(R_i)_{\text{FRK}}$ is the FRK mean reaction rate, the term $(R_i)_{\text{EDC}}$ is the mean reaction rate calculated by the EDC model and Re_t is the turbulent Reynolds number which is defined as follows:

$$Re_t = \frac{\rho k^2}{\nu \varepsilon} \quad (3)$$

In the laminar range, the reaction rate is calculated with pure finite rate kinetics and in the highly turbulent region with the EDC. In the transition region around $Re_t = 64$, the overall reaction rate is calculated as the sum of the weighted reaction rates of finite rate kinetics and the EDC. In other words, the overall reaction rate is determined as a linear combination of the two reaction rates. The hybrid model has been extensively validated for a series of diffusion jet flames covering laminar, transitional, and turbulent flow conditions. A detail description of the hybrid gas phase reaction model can be found in [7].

2.1.2.2. Near-wall combustion. In the hybrid gas phase reaction model, the overall reaction rate is calculated by a weighted reaction rate. The hybrid model gives results which are close to the FRK model when approaching the laminar regime, while the results are close to the EDC in the high turbulence region. The weighting factors in the hybrid model are a function of the turbulent Reynolds number of the flow. This imposes problems in the near wall region, when the flow cannot be sufficiently resolved, which is true in most of the real-scale combustion

applications with wall-bounded flows involved. One challenge in CFD is how to treat the thin near-wall sublayer, where viscous effects are important. Generally, in turbulent wall flows, two distinct zones exist near the wall. Firstly, the viscous sublayer which is completely dominated by viscous effects. The so-called “outer region” shows a nearly constant velocity with distance from the wall. Fig. 2 (left) shows the distinct areas existing near the wall in turbulent wall flows. A non-dimensional wall distance (y^+) is used to differentiate the regions that exist near the wall. The y^+ can be interpreted as a local Reynolds number with the wall distance as length scale, so its magnitude defines also the relative importance of viscous and turbulent processes [16]. To support this hypothesis, Fig. 2 (right) shows the fractional contributions of viscous and Reynolds stresses to the total stress in the near-wall region of a channel flow taken from [16,17]. When the stresses are plotted against y^+ , the profiles depicted for two Reynolds numbers almost collapse. The viscous contribution drops from 100% at the wall ($y^+ = 0$) to 50% at $y^+ = 12$ and is less than 10 at $y^+ = 50$.

Therefore, an accurate resolution of this layer can be crucial. This is due to the steep gradient of the mean values (e.g. transport of mean momentum and other parameters) that occur in the boundary layer. There are two approaches to model the near-wall-region. The most reliable way is to use modified turbulence models (e.g. low-Re-number turbulence models) to resolve viscosity-affected region (i.e. near wall regions) with a mesh which is fine enough to resolve the steep gradients near the wall, including the viscous sublayer. However, this can be very computationally expensive, particularly in 3D cases. Hence, the traditional industrial solution is to use wall-functions for flow modelling. Enhanced wall treatment is a near-wall modelling method that combines a two-layer model (i.e. linear (laminar) and logarithmic (turbulent)) with enhanced wall functions. The method formulates the law-of-the-wall as a single wall law for the entire wall region. ANSYS® FLUENT® achieves this by blending the linear (laminar) and logarithmic (turbulent) laws-of-the-wall using a function suggested by Kader [13] as follows:

$$u^+ = e^{\Gamma} u_{\text{laminar}}^+ + e^{1-\Gamma} u_{\text{turbulent}}^+ \quad (4)$$

where Γ is a blending function in dependence of y^+ and is given by:

$$\Gamma = -\frac{0.01(y^+)^4}{1 + 5y^+} \quad (5)$$

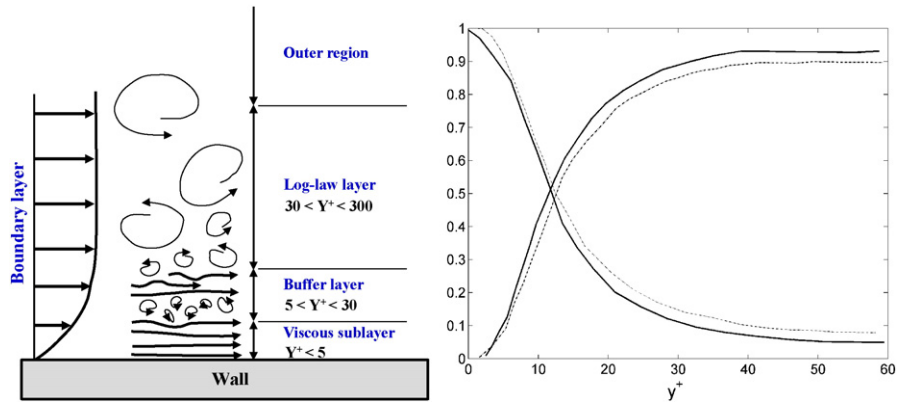


Fig. 2. Areas of turbulent wall flows (left) and fractional contributions of viscous and Reynolds stresses to total stress in the near-wall region of a channel flow (right) (adapted from Chapter 7 in [16]) taken from [17] (dashed lines, $Re = 5600$; solid lines, $Re = 13,750$).

where u^+ laminar and u^+ turbulent are the dimensionless velocities. The definitions of y^+ , u^+ laminar and u^+ turbulent can be found in [16]. Fig. 3 shows the trend of the blending factors in dependence of the non-dimensional wall distance (y^+). This formula also guarantees the correct asymptotic behaviour for large and small values of y^+ and reasonable representation of velocity profiles in the cases where y^+ falls inside the wall buffer layer.

In the hybrid combustion model, close to the wall, the turbulent Reynolds number of the flow approaches zero and the reaction rate is mainly calculated by the FRK model, despite the fact that the larger fraction of the flow in the wall near cell is influenced by inertial forces (Reynolds stresses). In conclusion, in reacting flows, it is also a problem of not sufficiently resolving the wall, which leads to the consideration of flow regime when calculating the reacting rate, while in reality there is a rapid change of the flow regimes in the boundary layer. To avoid this, the reaction rate has to be weighted in dependence of the flow regime inside the wall cell. Therefore, the mean chemical reaction rate for the near wall cells can be adjusted by blending the FRK and EDC models using a function suggested by Kader [13] as follows:

$$(R_i)_{wall} = e^\Gamma (R_i)_{FRK} + e^{1-\Gamma} (R_i)_{EDC} \quad (6)$$

where Γ is a blending function as defined in Eq. (5). The usage of y^+ in the blending function represents the concept of local Reynolds number of the flow as earlier explained [16]. In this formulation, the FRK and the EDC are weighted according to the fractional contributions of the

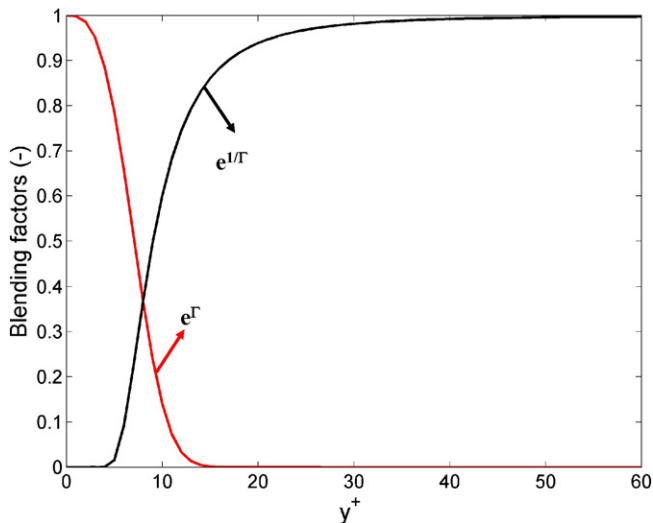


Fig. 3. Trend of blending factors in dependence of y^+ .

viscous and Reynolds stresses in the near-wall region and the overall reaction rate in the wall cell is calculated as the sum of the weighted reaction rates of the FRK and the EDC. As shown in Fig. 3, in the laminar range ($y^+ < 5$) the reaction rate is calculated with pure finite rate kinetics and in the turbulent region ($y^+ > 30$) with the EDC. In the transition region around $y^+ = 10$ (i.e. buffer layer), the contribution of viscous and Reynolds stresses is interchanging. Therefore, the overall reaction rate in the wall cell is calculated by a combination of the two terms. Hence, the overall reaction rate is weighted by two terms as a function of y^+ .

This near wall combustion approach was implemented in the hybrid model. The cases that have been simulated with the hybrid and the hybrid-streak model in this paper utilise the near wall combustion approach embedded in the hybrid model.

2.1.3. Streak formation model

A streak formation model has been developed. The model is based on a mixing time, where the gas streaks arising from the fuel bed are fully mixed, and a correlation with the residence time of the flue gas released from the fuel bed. In order to describe the mixing process above the packed bed, a criterion has been defined to calculate the mixing state (MS) as follows:

$$MS = 1 - \frac{C_{fm} - C(t)}{C_{fm}} \quad (7)$$

Here, C_{fm} is the tracer gas concentration (here CO_2) in the fully mixed gas and $C(t)$ is the local tracer gas (CO_2) concentration in dependence of the mixing time. The residence time which is necessary to reach the defined mixing state (here, $0.99 < MS < 1.01$ has been defined) is the mixing time t_{fm} . Finally, the mixing function (MF) is the combination of the mixing time t_{fm} and the gas residence time t_{gas} :

$$MF = \min\left(\frac{t_{gas}}{t_{fm}}, 1\right) \quad (8)$$

where

- MF = 0 (completely unmixed)
- MF = 1 (completely mixed).

The mixing function provides information about the mixing quality of the volatiles and the primary air, it varies between 0 (no mixing) and 1 (fully mixed). The mixing time (t_{fm}) is derived from the packed bed case studies and is a constant value. Therefore, Eq. (8) can be considered as a linear correlation of t_{gas} which is bounded between 0 and 1.

A user-defined scalar approach (UDS) is used to calculate the gas residence time inside the combustion unit. The approach proved to be

valid for use in modelling heating, ventilation, air conditioning and hydraulic systems [18,19].

For an arbitrary scalar, φ_k (here gas residence time), the steady state transport equation to be solved is given by [18,19]:

$$\frac{\partial}{\partial x_i} \left(\rho u_i \varphi_k - \Gamma_k \frac{\partial \varphi_k}{\partial x_i} \right) = S_{\varphi_k} \quad (9)$$

where, Γ_k is the diffusion coefficient and S_{φ_k} is the source term.

The diffusivity of the UDS is defined to be the same as of the flue gas since the residence time is transported and mixed with the gas flow. Therefore, in turbulent combustion flows, the diffusivity of the UDS is a function of the binary diffusivity, the turbulent and laminar viscosities, and the turbulent Schmidt number and is defined as follows [19]:

$$\Gamma_k = D_b \rho + \frac{\mu_l + \mu_t}{Sc_t} \quad (10)$$

where, ρ is the density of the flue gas, D_b is the binary diffusivity of the flue gas (with a value of 2.88×10^{-5} which is also applied for the diffusion coefficient of each species in the mixture), μ_l and μ_t are the laminar and turbulent viscosities of the flue gas and Sc_t is the turbulent Schmidt number (with a value of 0.7 which is also applied for the species transport equation) defined as:

$$Sc_t = \frac{\mu_t}{\rho D_t} \quad (11)$$

where D_t is the turbulent diffusivity of the flue gas. The effect of turbulence fluctuations is taken into account in the calculation of residence time implicitly since the effect of turbulent viscosity is considered in the diffusivity of the scalar transport equation.

At time t the mass flow rate of a fluid into a cell is m^* , therefore, the value of the scalar when it enters the cell is m^*t . When the fluid leaves the cell, its age is increased by Δt , therefore, the value of the scalar when it leaves the cell is $m^*(t + \Delta t)$. In order to find the time at which the fluid leaves, a source term is required equivalent to:

$$S_{\varphi_k} = \frac{m^* \Delta t}{V} \quad (12)$$

where, m^* is the mass flow rate and V is the volume of the computational cell.

The source term is divided by the cell volume since it is applied on a volumetric basis. Since neither the time nor the mass flow rate through the cell is known, the following relationship could be applied to simplify the source term:

$$m^* = \rho A u = \rho V^* \quad (13)$$

where A is the area of the cell and V^* is the volumetric flow rate.

By rearranging Eq. (13) we have

$$V^* = \frac{m^*}{\rho} \quad (14)$$

and since

$$\Delta t = \frac{V}{V^*} \quad (15)$$

by substituting Eq. (14) into Eq. (15) we have

$$\Delta t = \frac{V \rho}{m^*} \quad (16)$$

Now, by substituting Eq. (16) into Eq. (12), the source term can be found as follows:

$$S_{\varphi_k} = \rho \quad (17)$$

A second-order upwind discretisation scheme was used to solve Eq. (9). Eq. (9) has been implemented by a user-defined function (UDF) in ANSYS® FLUENT®.

Finally, the effective reaction rate is calculated by multiplying the mixing function, which defines the macro-mixing state, with the reaction rate, calculated by the hybrid combustion model as follows:

$$(R_i)_{\text{Hybrid-streak}} = MF \times (R_i)_{\text{Hybrid}} \quad (18)$$

Therefore, at positions where mixing is poor the rates of homogeneous reactions are damped which leads to streaks above the bed. The term “streaks” is used to represent the definition of the mixing function.

2.2. Case study for the derivation of the streak formation model

A CFD study with an ideally packed bed with spheres as fuel particles and non-reacting flow has been performed in order to numerically derive the mixing time. The volatiles were represented by CO_2 released from the surface of the particles in the bed. The volatile release rate from single particles was approximated by an in-house developed layer model [6] for the conversion of thermally thick biomass particles. In this parameter study, the following influencing parameters have been investigated for a packed bed: bed height, volatile mass flow rate and bulk flow velocity of primary air below the bed. The bed height was varied by particle layers from 5 to 15 layers. During typical biomass combustion conditions with air staging the most relevant components released are H_2O , CO_2 , CO , H_2 and CH_4 [20–22]. However, during packed bed combustion, the dominant gas volume flux is from the primary air passing through the packed bed. In CFD simulations the density of the mixture is usually considered as incompressible ideal-gas (due to the low pressure changes) and mainly depends on the temperature inside the combustion chamber that influences the volume flow rate of the volatiles released from the biomass particles. Furthermore, to qualify the effect of mixing between primary air and volatiles the volatile composition plays no role, while the released volume flow (which depends on temperature) is important. Moreover, since a non-reacting simulation is performed, for the release rates only an average value can be estimated. Therefore, a sensitivity analysis concerning the influence of the volatile release rate was performed. In order to cover the possible range of released volume fluxes, the estimated value of the reference case was multiplied by a factor x . A typical volatile release rate was estimated with the layer model; for the investigation of the sensitivity of the results on the release rates, this value has been varied between a factor of 1 to 1.7. It could be shown that the influence of the release rate is comparably low.

Bulk flow velocity of primary air below the bed was varied between 0.1 and 7 (m s^{-1}). In biomass grate furnaces, the flow above the fuel bed is typically in the low Re range. Usually, the primary air velocity fed below the grate may vary between 0.1 and 7 (m s^{-1}). The values are gained from an in-house developed empirical packed bed model [1–3]. Therefore, to cover all ranges of flow conditions for small to large-scale biomass combustion plants, a sensitivity analysis has been performed.

The diameter of the spheres was approximated based on the volume to surface area ratio of pellets according to the respective EU standard [4,5]. As mentioned, the study has been performed for pellets as fuel. However, the simulation results can be applied for all particle sizes by applying the particle Reynolds number for the look-up table where the results are summarised. Here, three parameter studies with an ideally packed bed with the different bed heights and number of particle layers, respectively, were performed in order to calculate the mixing

time in dependence of the influencing parameters. Fig. 4 shows the CFD domain of the packed bed for 5 layers considered in this study. An unstructured computational grid with 2, 4 and 6 million cells in total was used for the simulation of the packed bed with 5, 10 and 15 numbers of layers, respectively. On the surface of the particles, a number of layers with prismatic grid (10 layers) are used to resolve the viscous sublayer. It has been assured that the first grid point (the thickness of the first layer of the prismatic cells was about 0.007 mm) is located in the viscous sublayer ($y^+ < 1$). The primary air was injected below the bed with an even distribution and the volatiles represented by CO₂ as tracer gas were released from the surface of the spheres. Moreover, different planes above the bed were defined to evaluate the mixing state and mixing time. In the definition of the packed bed, the reference plane and the other planes above it are fixed at a certain height for each number of layers studied. This means that all the layers are arranged below the reference plane (see also Fig. 4).

A simulation matrix was built for each layer to derive the mixing time based on the primary air velocity and volatile mass flow rate. The flow simulation was performed for all primary air velocities and volatile mass flow rates. Then, the mixing state was calculated at each plane defined above the bed. Finally, the mixing time was derived based on the estimated gas residence time which is necessary to reach the defined mixing state (here, $0.99 < MS < 1.01$).

Therefore, the mixing time can be represented by influencing parameters like primary air velocity and number of layers considered in the simulations. To make the model applicable for all fuel particle sizes, the mixing time can be represented as function of the particle Reynolds number instead of the primary air velocity. The particle Reynolds number can be defined as follows:

$$Re_p = \frac{V_{\text{primary air}} d_v}{\nu_{\text{air}}} \quad (19)$$

where $V_{\text{primary air}}$ is the primary air released below the particles, ν_{air} is the air kinematic viscosity and d_v is the volume diameter.

The volume diameter d_v [23] can be derived based on the diameter of a sphere having the same volume as the biomass particles. The biomass particle volume can be estimated from the average size of the biomass particles.

2.3. Test and verification of the streak formation model for small-scale biomass under-feed stoker furnaces

To investigate and verify the influence of the streak formation model on gas phase mixing and reactions, a CFD simulation was performed for an under-feed stoker furnace (20 kW_{th}).

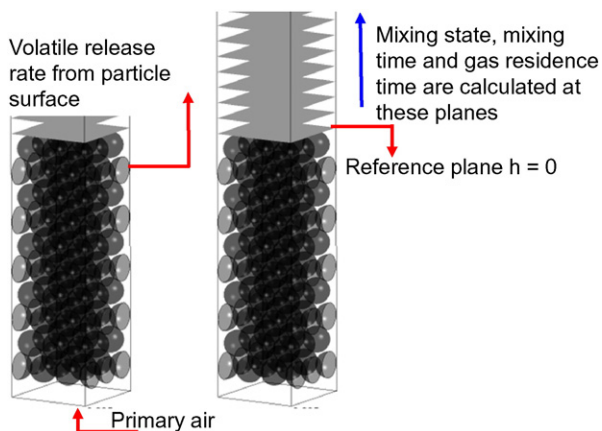


Fig. 4. CFD domain and boundary conditions for the evaluation of the mixing time above a packed bed.

The under-feed stoker furnace used for the test of the streak formation model is shown in Fig. 5. The simulation domain comprises the combustion chamber above the fuel bed till the exit of the hot water fire tube boiler. For the furnace simulation, an unstructured computational grid with 2 million cells in total was used while 7 layers are used with prismatic grid with initial prism height of 2 mm to resolve the viscous sublayer. It is necessary to resolve the viscous sublayer for small-scale plants since the low Reynolds regions are of high relevance. However, in larger plants the flow is fully turbulent and it is not economic to resolve the viscous sublayer due to high computational costs. The fuel is fed on the grate from below and is transported towards the outer edge of the grate. Primary air is supplied through the grate by nozzles at the bottom which form a concentric ring with the fuel feeding tube in the centre. The secondary air is injected through the secondary air inlet channel and is distributed in annular space of secondary air supply (see Fig. 6). There are twelve secondary air nozzles located on the circumference of the burner. However, every third nozzle is blocked and only eight nozzles are open in this case study. The secondary combustion zone is located after the secondary air is introduced. Moreover, there is no flue gas recirculation considered in this case study. Moreover, false air supply into the combustion chamber due to the ash removal system is considered. A certain amount of leakage air (10% of primary air), obtained from measurements during test runs, was taken into account in the simulation as false air.

The water side of the fire tube boiler walls was not included in the simulation. A convection boundary condition with 75 °C (average water temperature) and a typical heat transfer coefficient for water in forced convection (2000 W/m² K) are used as framework conditions for the fire tube boiler walls.

The simulations were performed for two biomass fuels, wood pellets and straw pellets, for which the experimental data concerning CO and NO_x emissions were available. Table 1 provides the most relevant operating conditions of the furnace and fuel composition.

3. Discussion of the results

3.1. Derivations of the streak formation model constants

An initial case study was performed to investigate the effect of the number of layers (bed height) on mixing. Fig. 7 shows the mixing state (Eq. (7)) variations in dependence of bed height for different numbers of layers. In the parametric case studies, the mixing state is calculated as a scalar field variable and evaluated in several planes defined above the packed bed. One can evaluate for each plane the maximum or minimum value of the tracer gas concentration for the definition of

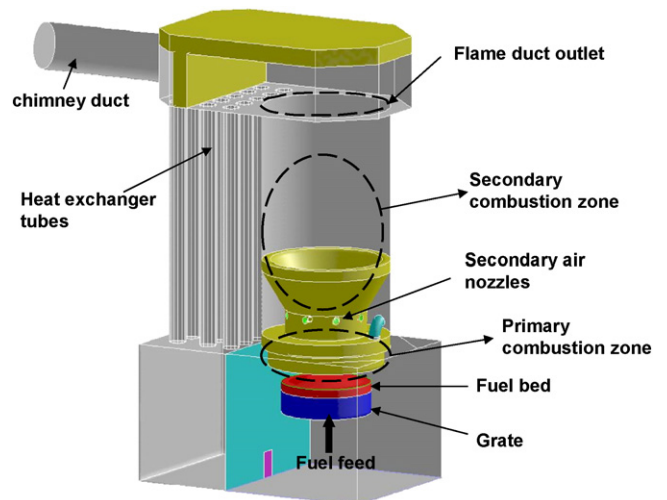


Fig. 5. Geometry of the under-feed stoker furnace with a fire-tube hot water boiler.

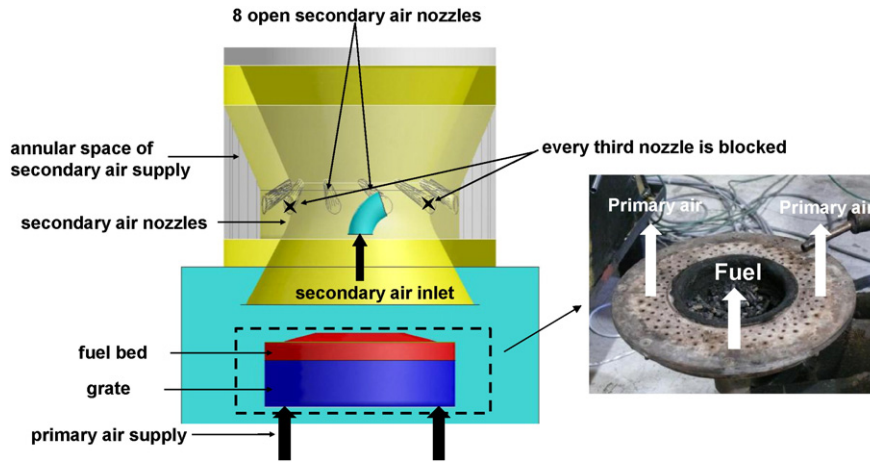


Fig. 6. Close-up of the primary and secondary air supplies.

the mixing state. In the present study, the maximum value of the mixing state is determined at each plane. By doing this, the mixing state is derived in dependence of the height above the bed.

The results show a strong effect of the number of layers (bed height) on mixing. Hence, it was considered as an independent parameter. Afterwards, a simulation matrix was defined in order to investigate the effect of primary air velocity and volatile mass flow rate variations on the mixing (mixing state) for each number of particle layers defined (5, 10 and 15 layers).

Fig. 8 shows the mixing state in dependence of bed height for different volatile mass flow rate variations at two selected primary air velocities and under consideration of 10 layers. The results confirm that the effect of volatiles is insignificant on the mixing in comparison to the effect of primary air mass flow rate since the fraction of the volatile release rate to the primary air is low (e.g. 0.1–0.3). Because the mass flow of volatiles compared to the primary air mass flow is low and hence was expected to have an insignificant effect on mixing in comparison to the primary air flow rate, a value considerably higher than the reference value was investigated first. Since it showed nearly no difference to the results with the reference value, a reduction of the amount of flue gas below the reference value was expected to have even less effect and it was thus not investigated.

The effect of primary air velocity variations on the mixing state for different numbers of layers (10 and 15 layers) is shown in Fig. 9. The results in Fig. 9 are shown in dependence of particle Reynolds number instead of velocity. The results indicate that the mixing state strongly

depends on the particle Reynolds number and, therefore, primary air velocity. The change of the slope in Fig. 9 in the range of 15–20 mm could be explained by a change in the flow regime from laminar to turbulent conditions (i.e. transition regime) in the range between $Re_p = 237\text{--}947$ (–) (i.e. the primary air velocity is in the range between 0.7 and 1 (m s^{-1})). Hence, the length of the streaks in dependence of particle Reynolds number (defined by the criterion for fully mixed conditions) is oscillating in this range. As already explained, the mixing function is a linear correlation between the mixing time and the gas residence time. The mixing time is a constant, which is a value of the gas residence time at fully mixed conditions ($MS = 1$). Since the mixing state as a function of the height above the bed shows an asymptotic behaviour (fully mixed conditions with $MS = 1$ will never be reached) a certain tolerance has to be defined to achieve the mixing time. The tolerance has to be in a certain range in order to minimise its influence. Therefore, on the one hand the value of the mixing state (for fully mixed conditions) has to be close to one. On the other hand (as can be seen in Fig. 9) it should be on the branch of an individual curve with a rapid change of the mixing state, since on the flat branch the mixing time and hence the mixing function strongly changes when varying the tolerance and hence the mixing state. The evaluation of mixing time (t_{fm}) was done based on a certain error tolerance (here 1%) since the mixing state has asymptotic behaviour that means it never reaches the perfect mixing condition (i.e. $MS = 1$). The red line in Fig. 9 represents the error tolerance used to derive the mixing time. It has been

Table 1
Operating conditions and fuel characteristics of the furnace.

Operating conditions	Unit	Wood pellets	Straw pellets
Nominal boiler load	kW	21	19
Adiabatic flame temperature	°C	1501	1360
Flue gas recirculation ratio	–	0	0
λ_{Prim}	–	0.64	0.69
λ_{total}	–	1.58	1.71
Fuel composition	Unit	Wood pellets	Straw pellets
Ash	Mass fraction d.b.	0.40	7.30
C	Mass fraction d.b.	50.10	46.10
H	Mass fraction d.b.	5.70	5.80
O	Mass fraction d.b.	43.77	40.20
N	Mass fraction d.b.	0.07	0.54
S	Mass fraction d.b.	0.0	0.17
Moisture content	Mass fraction w.b.	8.10	8.10
GCV	MJ/kg d.b.	20.24	18.56
NCV	MJ/kg w.b.	17.24	15.69

Explanations: w.b.: wet basis; d.b.: dry basis; GCV: gross calorific value; NCV: net calorific value; λ_{prim} : primary air ratio related to primary air supplied below the grate including the false air; λ_{total} : total air ratio related to total amount of air supplied.

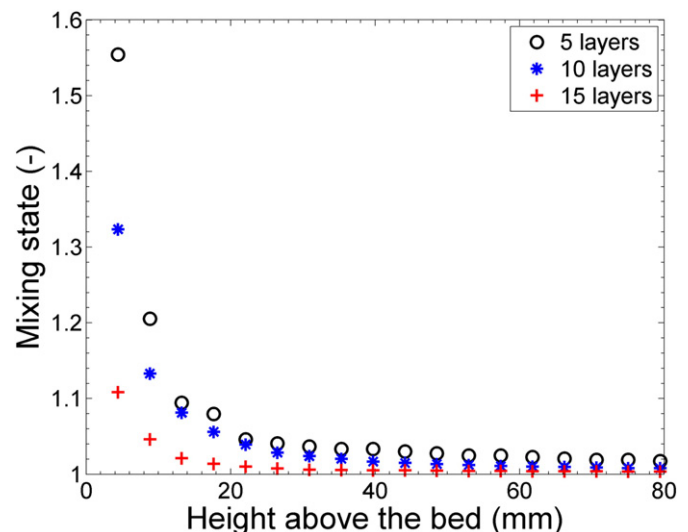


Fig. 7. Maximum mixing state above the bed (–) evaluated for different numbers of layers.

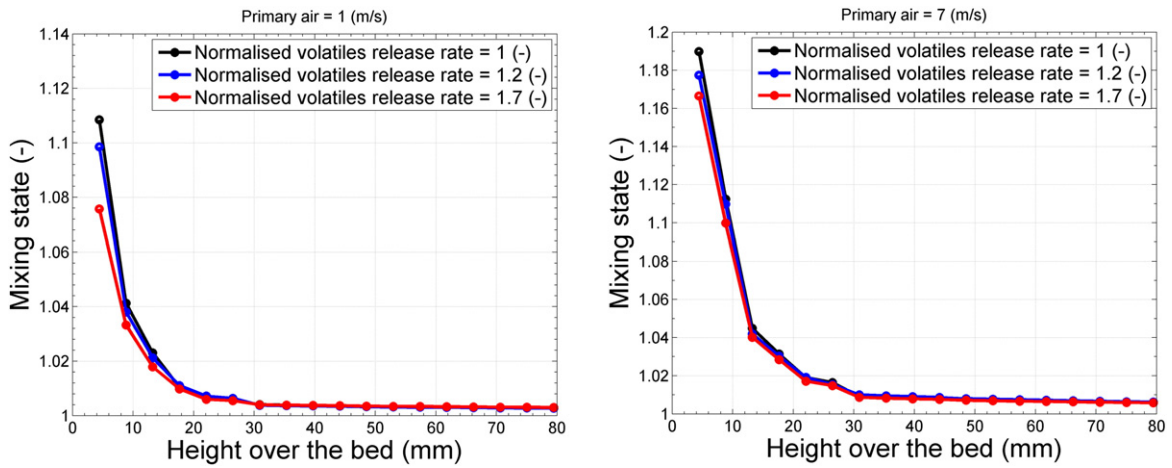


Fig. 8. Maximum mixing state (-) evaluated for different volatile release rates for 10 layers (left: primary air velocity 1 m s^{-1} , right: primary air velocity 7 m s^{-1}).

confirmed that 1% error tolerance is fine enough for all cases considered to derive the mixing time.

Fig. 10 shows the mixing time behaviour in dependence of the particle Reynolds number as well as the number of layers. For all layers considered, a trend concerning the mixing time in dependence of the particle Reynolds number was found. The non-monotonic behaviour in Fig. 10 could also be explained by a change in flow regime from laminar to turbulent conditions (i.e. the transition regime) (see Fig. 9). Hence, the length of the streaks in dependence of particle Reynolds number (defined by the criterion for fully mixed conditions) is oscillating in this range. The results showed that the mixing time of the streaks increases as the particle Reynolds number increases. Generally, at lower particle Reynolds numbers the mixing time is lower. This attributes to a higher residence time of the flue gas due to lower primary air velocities

which results in a shorter streak length above the packed bed. The mixing time increases as the particle Reynolds number (i.e. primary air velocity) rises due to a higher streak length above the packed bed. Moreover, the mixing time for all particle Reynolds numbers is lower for a larger packed bed height since a higher residence time inside the packed bed improves mixing of primary air and volatile matter. The results of this case study serve as look-up table for the calculation of the mixing time in dependence of the different influencing parameters. For practical application (e.g. the furnace simulation with the streak formation model – see Section 3.2) the mixing time (t_{fm}) can be retrieved by a linear interpolation between the calculation points through an estimation of the particle Reynolds number and the number of layers. The particle Reynolds number can be easily calculated from the velocity profile specified by the empirical packed bed model along the grate and the

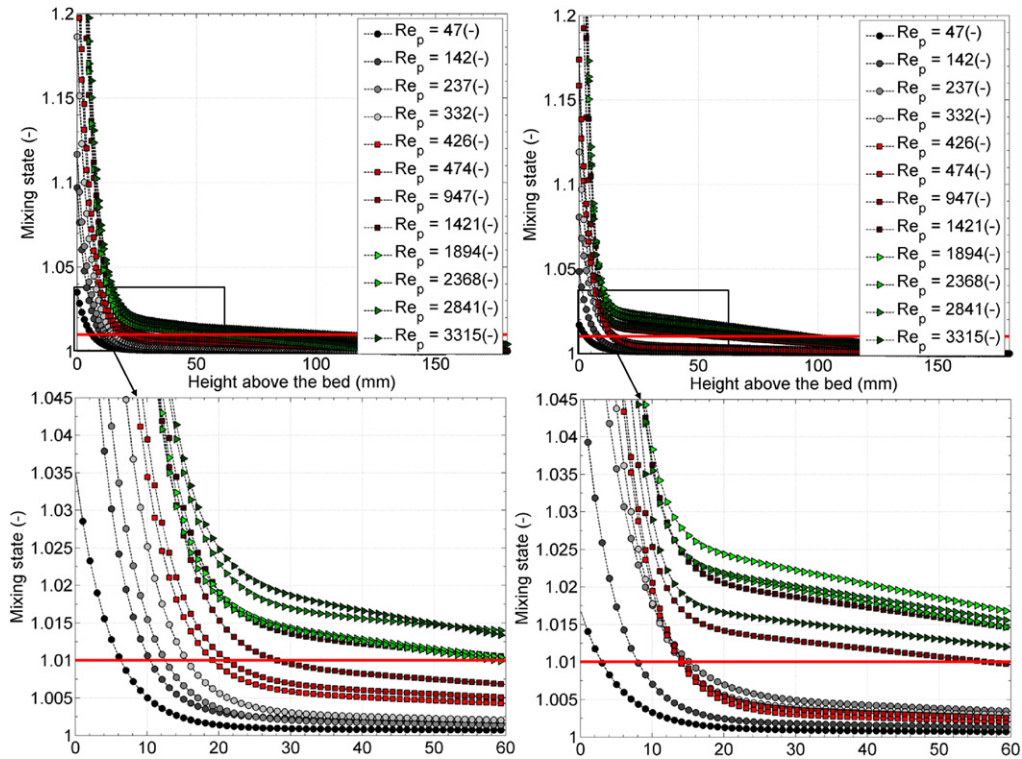


Fig. 9. Maximum mixing state (-) evaluated for different particle Reynolds numbers (left: 10 layers, right: 15 layers).

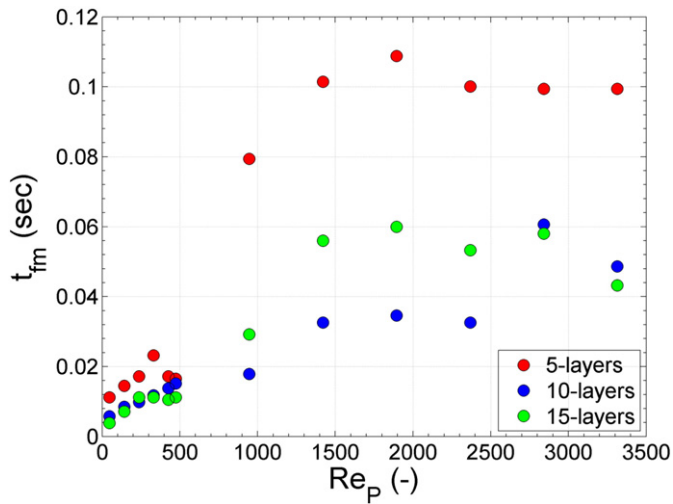


Fig. 10. Mixing time (s) for different particle Reynolds numbers and different numbers of particles.

average particle diameter (e.g. volume diameter [23]). Also, the number of layers can be estimated by the initial estimated height of the packed bed and the diameter of the fresh biomass fuel fed. The number of layers represents the number of particles that can be stacked in that length (e.g. length divided by the diameter of particles). Since the total number of particles on the bed remains constant on average for a certain operating condition, also the number of layers remains constant over the grate length.

3.2. Test of the steak formation model for a biomass under-feed stoker furnace

In this section, the results for the simulation of the 20 kW biomass under-feed stoker furnace are shown. The mixing function needs to be evaluated for the present case to investigate the effect of the streak formation model on the combustion simulation. Therefore, the mixing function evaluation is presented for the case wood pellets. However, the same approach was applied to derive the mixing function for straw pellets (not shown here). Fig. 11 (left) shows the calculated particle Reynolds number as well as the number of layers along the grate for wood pellets as fuel. The particle Reynolds number was calculated based on the velocity profile calculated with the empirical packed bed model (the maximum primary air velocity was about $2.5 \text{ [m s}^{-1}]$ in the present case). The particle diameter was estimated from the volume

diameter (see Section 2.2) (the wood pellet particles were assumed as spheres with a $d_v = 6 \text{ [mm]}$). The number of layers can be estimated by the initially estimated height of the packed bed and the diameter of the fresh wood pellets fed. The kinematic viscosity of the flue gas was taken from the CFD simulation results stored in the centre of the cells along the grate surface. A tetrahedral mesh was applied, which results in different distances from the grate surface (boundary of the simulation domain). Since the temperature profile values calculated with the empirical packed bed model and applied as boundary condition of the CFD simulation are not the same as the gas temperatures stored in the centre of the adjacent cells, the varying cell centre distances from the surface of the grate causes fluctuations in gas temperature and, therefore, of the viscosity as a function of the gas temperature. Therefore, the particle Reynolds number profile shows disturbances (Fig. 11 (left)). To derive a mixing time profile along the grate (Fig. 11 (right)) the values were retrieved from the look-up table for the mixing time (as described in Section 3.1). In the present case the mixing time could also be simplified by a constant value. But since using release profiles with varying influencing parameters on the mixing time, the range of the mixing time is not known in advance. Therefore, a method is needed for the calculation of mixing time profiles. Hence, the profile of the mixing time is used as an initial boundary condition at the surface of the fuel bed. Then a transport equation is solved to obtain the mixing time as a field variable in the CFD domain. Therefore, the mixing time has a higher relevance in comparison to the initial conditions.

The shrinkage of the particles along the grate is implicitly considered in the simulations since the shape of the fuel bed and the path of particles along the grate is assumed based on visual observation. Furthermore, it is assumed, that the number of particles (i.e. 5) and the horizontal velocity on the grate remain constant along the grate, since the initial values of mass flux, particle size and particle density are held constant, and moreover, the entrainment of particles from the grate and the fragmentation of the particles are neglected. With the information of the locally assumed bed height and the initial values of particle density, porosity and particle mass flux, the local particle volume and shrinkage respectively, can be estimated (the diameter change is thus implicitly considered).

Finally, two transport equations were solved, one for the gas residence time and the other for the mixing time, to derive the local mixing function defined in Eq. (8). Fig. 12 shows the contour plots of gas residence time (left) and the mixing function (right) derived from Eq. (8).

Finally, the mixing function defined is linked with the hybrid combustion model. The mixing function indicates that a major part of the reaction zone above the packed bed is influenced by streak formation. The mixing function as defined shows the degree of mixing above the grate. The value 0 means no mixing and 1 means fully mixed. As can be seen from Fig. 12 (right), the mixing function varies between 0 and 1. The

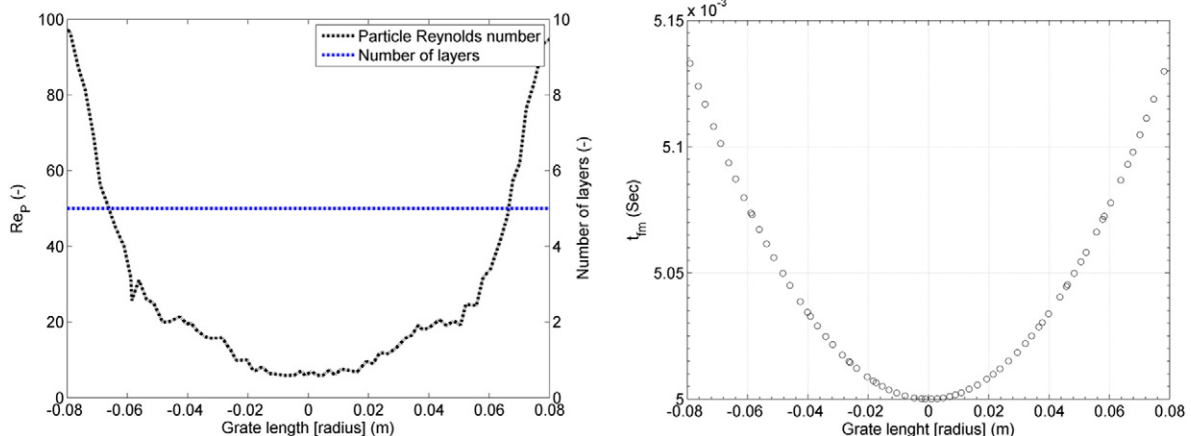


Fig. 11. Particle Reynolds number (–) and number of particle layers (–) (left) as well as estimated mixing time (s) interpolated from calculation points of Fig. 10 (right).

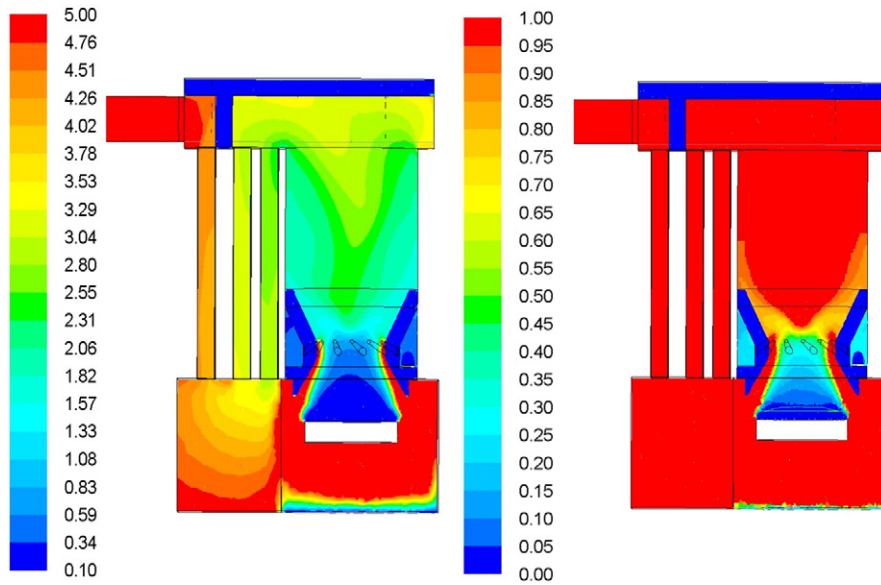


Fig. 12. Gas residence time (s) (left), and mixing function (-) (right) evaluated for wood pellets as fuel.

mixing function is non-uniform, especially, above the grate up to the secondary air nozzles.

Flue gas temperature and O₂ concentrations calculated with all models for both wood pellets (top) and straw pellets (bottom) are shown in Figs. 13 and 14, respectively. The simulations show for both cases low O₂ concentrations (see Fig. 14) and high flue gas temperatures (see Fig. 13) in the major reaction zone above the fuel bed in the primary combustion zone as well as close to the secondary air injection. Here, also the peak flue gas temperatures can be observed.

The regions addressed correspond to increased combustion progress which is more pronounced in the case of EDC and hybrid simulations than in the case of the EDM simulation. The higher flue gas temperatures predicted with the EDC compared to the EDM are attributed to the Magnussen constant of the EDM model [8] which is systematically adapted for biomass grate furnaces by a comparison with CO emission

and temperature measurements [11,14]. Accordingly, a reduction of the mixing and the reaction rate compared to the original model is achieved. Therefore, the EDC, where no tuning is done, predicts higher reaction rates, which rise the temperatures. The higher temperatures predicted with the hybrid model compared to the EDC are pertaining to influence of the combustion models (e.g. FRK or EDC model) in the hybrid model which depend on the local turbulent Reynolds number of the flow. Hence, it is of interest to investigate the flow regime in the combustion chamber. Fig. 15 shows the flue gas temperatures and the turbulent Reynolds number obtained with different gas phase reaction models for wood pellets as fuel. The figure shows that the turbulent Reynolds number is lower than 64 in the major reaction zones that are indicated by high temperature zones above the fuel bed at the outer edge of the grate as well as close to secondary air injection and, therefore, the reaction rate in the hybrid model is calculated mostly with the FRK model in these regions.

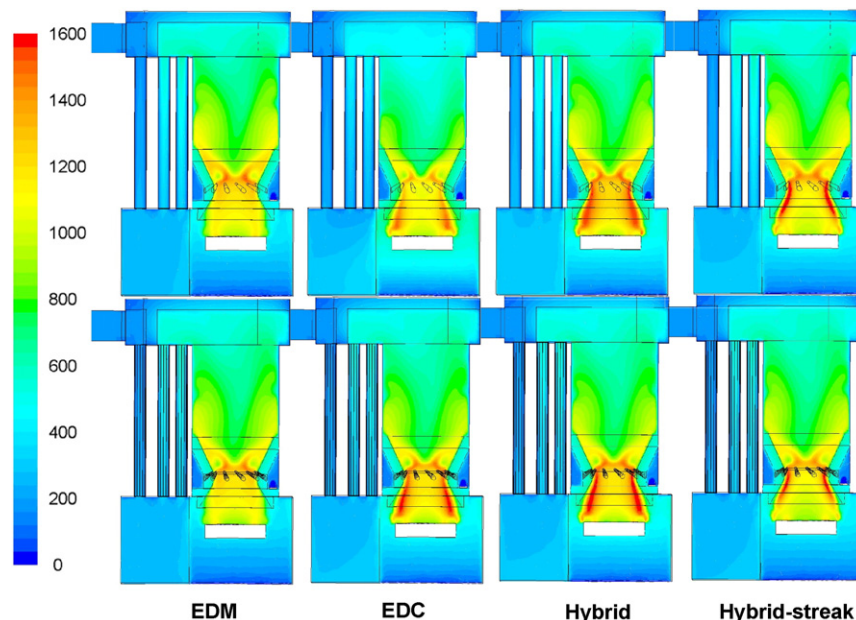


Fig. 13. Iso-surfaces of flue gas temperatures (°C) in a vertical cross-section of the furnace for wood pellets (top) and straw pellets (bottom).

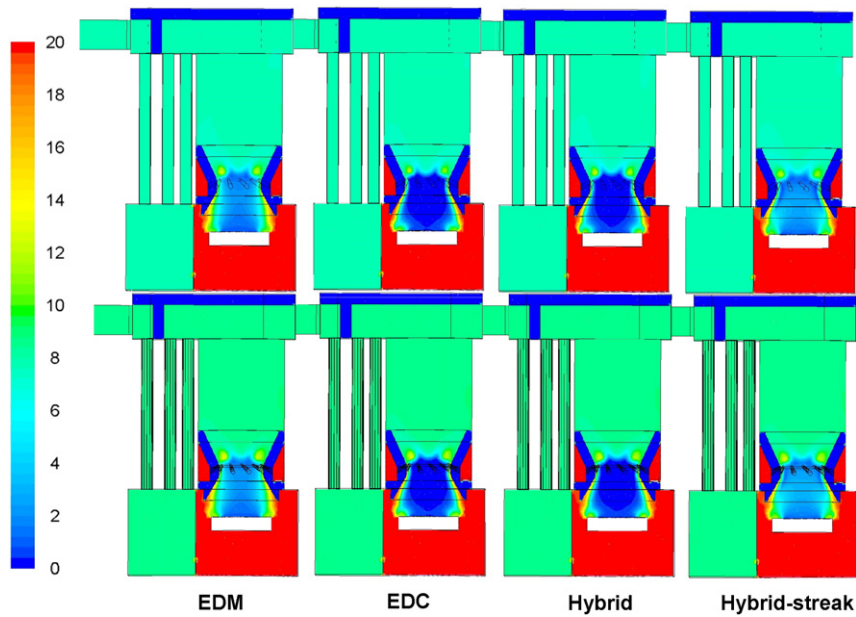


Fig. 14. Iso-surfaces of O_2 concentrations (vol.% dry) in a vertical cross-section of the furnace for wood pellets (top) and straw pellets (bottom).

The flue gas temperatures predicted with the hybrid-streak model are somewhat different. It was shown that the major part of the reaction zone above the packed bed is also influenced by streak formation (i.e. the mixing function) (see Fig. 12). It is clear that the combustion progress is slowed down by the hybrid-streak model in the regions where the streaks exist (above the grate). The same trend can be found for the O_2 concentration fields. As can be seen from Fig. 14, the O_2 concentrations calculated with the hybrid-streak model are higher, especially in the primary combustion zone, because the combustion progress is delayed due to a poor mixing caused by the presence of streaks.

Significant differences can also be observed in the prediction of CO concentrations with the EDM, the EDC, the hybrid model and the hybrid-streak model as shown in Fig. 16. Generally, the EDC and hybrid model resulted in a much faster CO oxidation, especially in the regions of intense mixing in the primary combustion zone and in the region directly after the secondary air injection, while the EDM with the mixing parameter applied leads to a generally slower CO oxidation. Therefore,

EDC and hybrid led to significantly lower CO levels further downstream in the secondary combustion zone and at boiler inlet.

Moreover, the slight differences in the CO concentrations between the EDC and the hybrid model are mainly due to a higher reaction rate caused by a higher contribution of the FRK model, where micro-mixing plays no role (see Tables 2 and 3).

The CO prediction with the hybrid-streak model is higher than for the EDC and the hybrid model since the combustion progress is delayed due to the presence of streaks (see Fig. 12) mainly in the primary combustion zone. The predicted CO concentrations at boiler outlet for both wood and straw pellets are given in Tables 2 and 3. For wood pellets (see Table 2), the calculated CO value predicted with the hybrid-streak model is in best agreement with the measured values. The better prediction with the hybrid-streak model can be explained by a delay in the CO oxidation, since the net reaction rate in the hybrid-streak model is multiplied by the mixing function, therefore, the regions above the major flue gas release zone and the reaction fronts are mainly

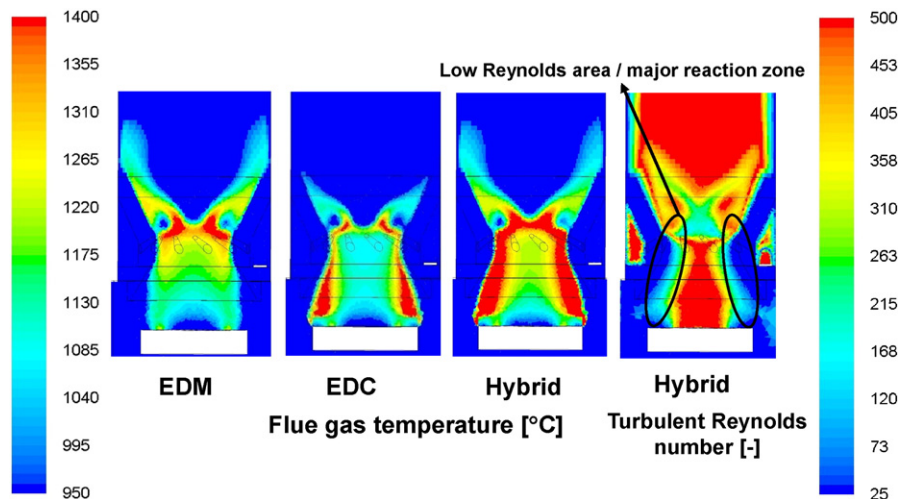


Fig. 15. Iso-surfaces of flue gas temperatures ($^{\circ}C$) (left) and turbulent Reynolds number (-) (right) in a vertical cross-section of the furnace (up to the upper edge of the refractory lining) evaluated for wood pellets as fuel.

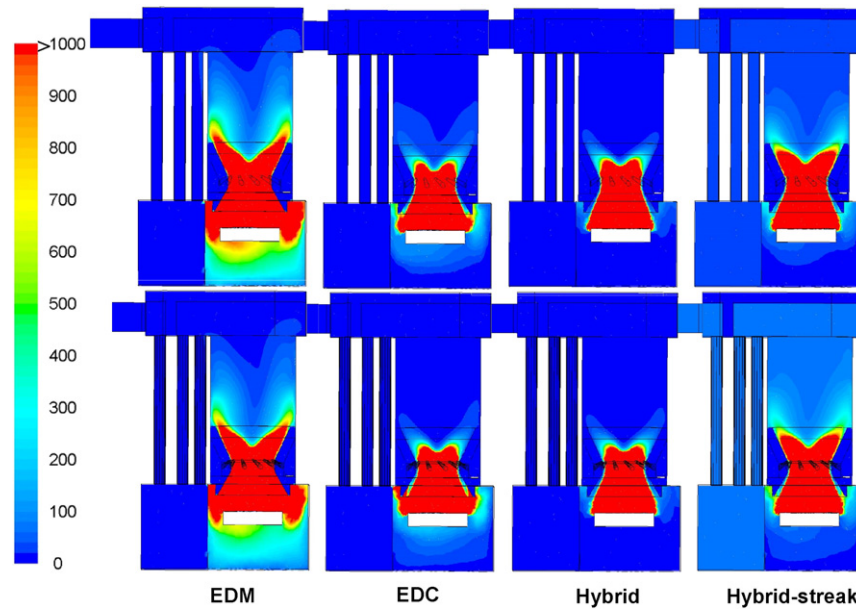


Fig. 16. Iso-surfaces of CO concentrations (ppmv) in a vertical cross-section of the furnace for wood pellets (top) and straw pellets (bottom).

influenced by mixing function. The CO values calculated with the EDC model are in better agreement with measured values than the hybrid and the EDM model. The hybrid model results in a much faster CO oxidation, since the major part of the reaction progress is calculated with the FRK, while in the EDM the reaction rate is mainly controlled by the mixing constant, A_{mag} [8] which is tuned [11,14]. In the case of straw pellets, the CO values predicted with the hybrid-streak model are in better agreement than the EDC and hybrid model due to a more accurate prediction of mixing processes above the packed bed. The CO values predicted with the EDC and hybrid model are too low in comparison with the measured values. The EDM gives the best agreement with the measured CO values. As already explained, the eddy dissipation rate is directly proportional to the value of the modelling constant A_{mag} [8] and to the mean eddy lifetime, k/ϵ where the value of A_{mag} is lowered from the originally proposed value, $A_{mag} = 4$, to $A_{mag} = 0.8$ for the simulation of small scale biomass combustion plants [11,14]. Besides, there is no explicit modelling of streaks with the EDM model and the model is valid for highly turbulent flows which mean that the best agreement in this case is due to good tuning for grate combustion plants but a model which can predict reliable CO burnout rates without tuning would be preferable. A clear drawback of the EDM in combination with global reaction mechanisms is that it is not able to describe complex interactions of turbulence and multi-step reaction kinetics. Besides, when modelling gas phase combustion with the EDM basically we are already tuning the model constant A_{mag} by nearly an order of magnitude. This is actually not satisfactory since tuning of model constants over such a wide range may lead to a limited validity range linked with wrong predictions under deviating conditions (e.g. the effect of mixing may be overestimated especially in kinetically limited zones). In order to

avoid this, the EDC and the Hybrid model, which provide a more fundamental prediction of gas phase reactions, have been applied. However, they are more sensitive to the boundary conditions at the surface of the fuel bed (turbulence and mixing degree) and hence need an additional model, which explicitly considers the effects of streaks on the mixing. By introducing this model, no tuning of the gas phase combustion model to fixed bed combustion is necessary.

The characteristics of reacting radicals (e.g. OH and O) are important for an in-depth understanding of the combustion and NO_x formation processes [14]. These radicals are of high relevance especially for the formation of NO_x . The OH and O species calculated with the EDC, hybrid and hybrid-streak model for straw pellets are shown in Fig. 17. The OH and O species are generally predicted highest with the hybrid-streak model since the rates of production or destruction of the species are slowed down due to multiplication of the mixing function (see Eq. (18)).

As known from already performed research [24,25], NO_x formation in fixed bed biomass combustion plants is dominated by fuel NO_x . Moreover, NO is the clearly dominating species formed [25].

As already mentioned, a skeletal reaction mechanism (28 species and 102 reactions in total) was applied [15] for the simulation of NO_x formation, and the simulation was performed in a post-processing step.

Experimental data of the combustion and release behaviour for a variety of solid biomass fuels have been gained through several measurement campaigns in a lab-scale packed bed pot furnace reactor [24,25]. These experimental data include the concentration profiles of the N containing species NO, NH_3 , HCN, NO_2 and N_2O released from the fuel bed over time. The measured profiles are utilised for the derivation of release functions for the most relevant NO_x precursors measured. The

Table 2

Predicted CO concentrations with the EDM, EDC, hybrid and hybrid-streak models in comparison to measurements for wood pellets.

Average CO concentration	Unit	Simulations				Measurement
		EDM	EDC	Hybrid	Hybrid-streak	
Boiler outlet	[ppm dry]	16	19	5	30	38
Boiler outlet	[mg/Nm ³ 13 vol.% O ₂ dry]	10	15	3	22	29
Deviation (percent error)	[%]	−65	−48	−89	−24	

Table 3

Predicted CO concentrations with the EDM, EDC, hybrid and hybrid-streak models in comparison to measurements for straw pellets.

Average CO concentration	Unit	Simulations				Measurement
		EDM	EDC	Hybrid	Hybrid-streak	
Boiler outlet	[ppm dry]	13	4	3	29	16
Boiler outlet	[mg/Nm ³ 13 vol.% O ₂ dry]	10	3	2	27	13
Deviation (percent error)	[%]	−23	−76	−84	107	

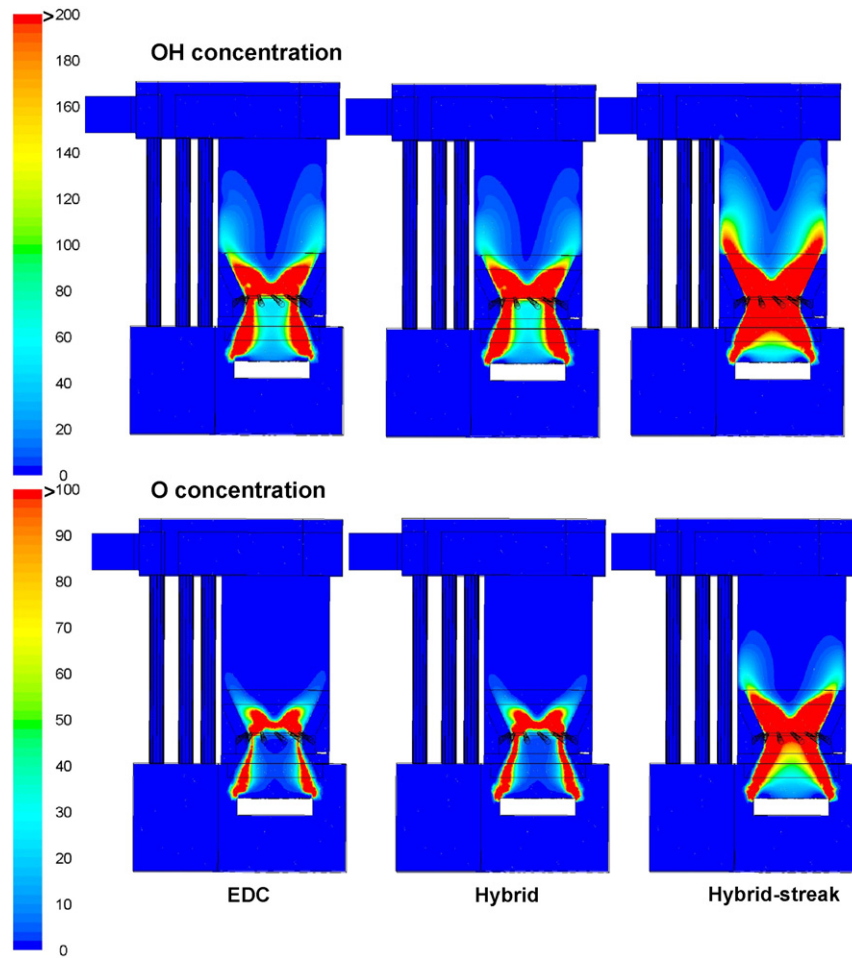


Fig. 17. Iso-surfaces of OH concentration (ppmv dry) (top) and O concentration (ppmv dry) (bottom) for straw pellets in a vertical cross-section of the furnace.

release functions of fuel nitrogen depend on the local air ratio (λ), the nitrogen content of the fuel as well as the N binding in the fuel (the kind of biomass fuel). The most important NO_x precursor detected above the fuel bed for wood (spruce) and straw pellets under fuel rich conditions is NH_3 , while HCN is almost insignificant. NO is detected mainly under air rich conditions (charcoal burnout) [25]. Furthermore,

the experimental data are utilised to derive release functions for the relevant NO_x precursors NO, NH_3 and HCN. The release functions were implemented in an in-house developed empirical packed bed combustion model [24,25], which serves as a basis for the subsequent CFD gas phase simulation of N species conversion. Figs. 18 and 19 show the NO, NH_3 and HCN profiles calculated with the EDC, hybrid and the hybrid-

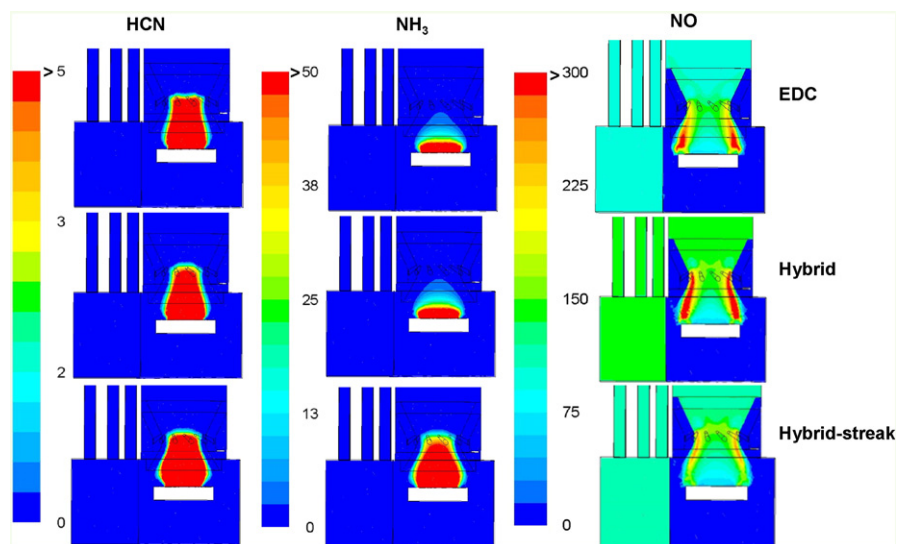


Fig. 18. Iso-surfaces of HCN concentrations (ppmv) (left), NH_3 concentrations (ppmv) (middle) and NO concentrations (ppmv) (right) calculated with the EDC model (top), the hybrid model (middle) and the hybrid-streak model (bottom) for wood pellets.

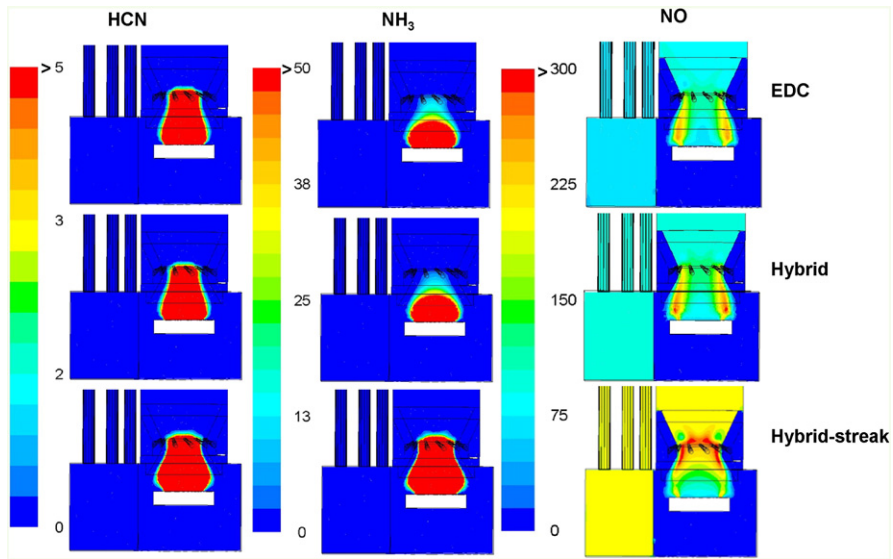


Fig. 19. Iso-surfaces of HCN concentrations (ppmv) (left), NH₃ concentrations (ppmv) (middle) and NO concentrations (ppmv) (right) calculated with the EDC model (top), the hybrid model (middle) and the hybrid-streak model (bottom) for straw pellets.

streak model for wood pellets and straw pellets, respectively. Generally, distinct areas can be observed, where the release of NO, HCN and NH₃ takes place. NO is released in the air-rich zone towards the outer edge of the grate. NO is formed in regions where high temperatures and high concentrations of O and OH radicals prevail [26,27]. The locations, where the NO has been released are co-located with high concentrations of O and OH radicals above the bed (see Fig. 17 for straw pellets). In contrast, NH₃ and HCN are primarily released from the main in-bed devolatilisation/gasification zone. These differences result from the local differences in the in-bed availability of the oxidiser (see Fig. 14), which in turn depends on the amount and distribution of primary air under the grate as well as on the in-bed thermal conversion processes. The distribution of N-containing species in the gas phase results from the simultaneous formation and reduction processes, taking place in different regions of the combustion chamber and depends on many factors.

The regions, where NO reduction takes place in the combustion chamber, can be observed by looking at reaction $N_2 + O \rightleftharpoons NO + N$

[14] (NO reduction) as shown in Figs. 20 and 21 for both wood pellets and straw pellets. Generally, NO released from the fuel bed as well as locally formed in the gas phase is primarily consumed in the primary combustion zone (see Fig. 13, O₂ distribution). Here, products of NH₃ (and HCN) breakdown act as reducing agents, as can be seen by comparing profiles of NO, NH₃ and HCN (see Figs. 18 and 19) and the kinetic reaction rate of N₂ (see Figs. 20 and 21 (left)). The regions of high NH₃ concentrations and low availability of O₂ overlap with the regions of an increased NO reduction. Simultaneously, NO is locally produced in the primary combustion zone in the outer grate zones, above the fuel bed, as well as in front of the secondary air jets at the oxygen rich side of the flame (see Fig. 13). Processes related to NO formation and reduction are also relevant close to the area affected by the injection of secondary air.

Generally, the higher NO formation in the case of straw pellets (see Tables 4 and 5), especially in the primary combustion zone, is mainly attributed to the higher fuel nitrogen content (approximately seven times higher than wood pellets) (see Table 1). Fig. 22 shows the NO_x

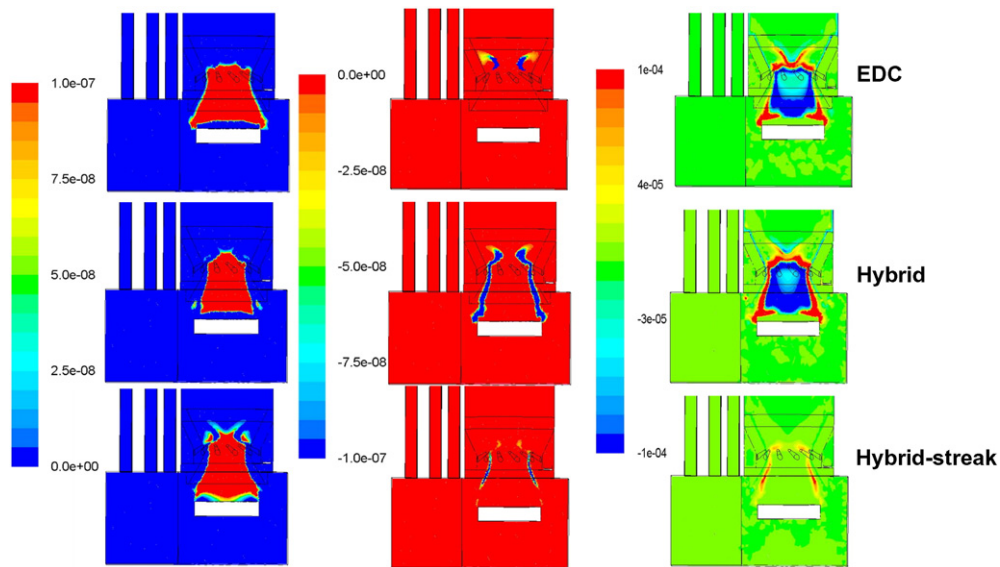


Fig. 20. Iso-surfaces of reaction rates for the reaction $N + NO \rightarrow N_2 + O$ (reduction to N₂) (kmol/(m³ s)) (left), for the reaction $N_2 + O \rightarrow N + NO$ (NO formation from N₂) (kmol/(m³ s)) (middle) and for the net reaction rate of NO formation (kg/(m³ s)) (right) calculated with the EDC model (top), the hybrid model (middle) and the hybrid-streak model (bottom) for wood pellets as fuel.

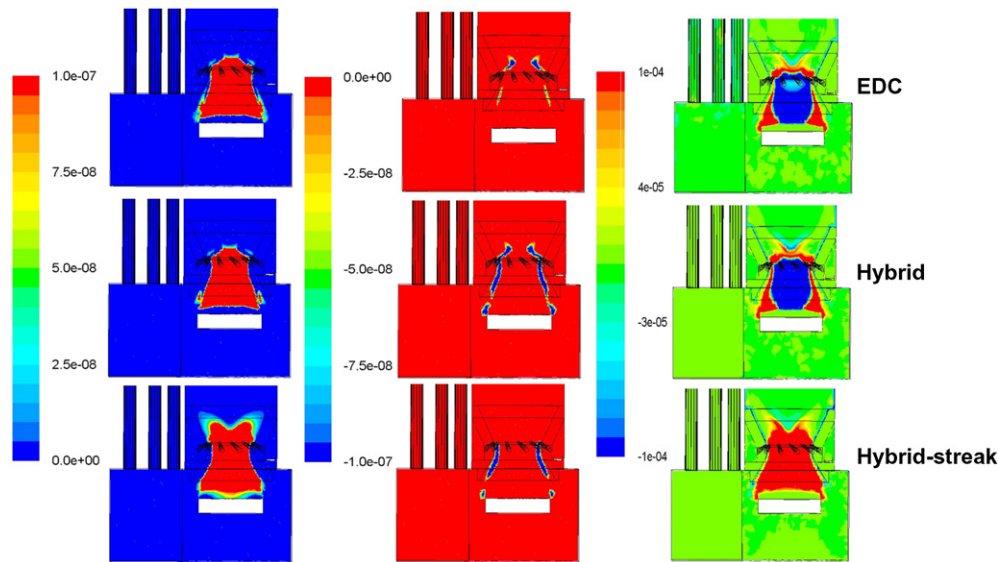


Fig. 21. Iso-surfaces of reaction rates for the reaction $N + NO \rightarrow N_2 + O$ (reduction to N_2) ($\text{kmol}/(\text{m}^3 \text{ s})$) (left), for the reaction $N_2 + O \rightarrow N + NO$ (NO formation from N_2) ($\text{kmol}/(\text{m}^3 \text{ s})$) (middle) and for the net reaction rate of NO formation ($\text{kg}/(\text{m}^3 \text{ s})$) (right) calculated with the EDC model (top), the hybrid model (middle) and the hybrid-streak model (bottom) for straw pellets as fuel.

emissions in dependence of the fuel nitrogen content for different biomass fuels. The experimental data are from different plants fired with different fuels [28,29]. The intention is to show the trends of NO_x emissions in dependence of different biomass fuels used with varying fuel nitrogen contents and to check if the simulated values predicted are in the correct range. The simulation results (NO_x simulation with the hybrid-streak model) are also provided in the figure. The results indicate that a higher N content of the fuel leads to higher NO_x emissions in the gas phase during the combustion process.

The simulation results with the EDC, the hybrid and the hybrid-streak model show substantial differences in terms of NO_x profiles for wood pellets and straw pellets. Fig. 23 shows the NO_x profiles predicted with the different models for wood pellets (top) and straw pellets (bottom). The predicted NO_x concentrations at boiler outlet for both wood pellets and straw pellets are given in Tables 4 and 5. According to the hybrid model, the major part of the reaction zones is located above the grate as well as in front of the secondary air jets, where the turbulent Reynolds number is lower than 64. Therefore, the reaction progress is mainly calculated with the FRK model, whereas micro-mixing plays no important role. This causes a higher net reaction rate of NO in these regions (see Figs. 20 and 21 (middle)). However, in the EDC, the reaction progress is always influenced by micro-mixing. According to this model, the fluid is in any case mixed on a micro-scale and the reactions finally take place in the fine structures [9] of the fluid, where the reactants are mixed on a molecular level. Hence, the EDC fails to predict reactive flows in laminar and moderately turbulent situations. Therefore, in this case, the EDC leads to a higher NO_x reduction, since NO_x formation in the outer air-rich zone in the primary combustion zone is stronger decreased than the NO_x reduction in the air lean zone of the

primary combustion zone (see Tables 4 and 5). Furthermore, the NO_x formation processes according to the hybrid-streak model are completely different from the EDC and the hybrid model.

Here, it can be seen that the spatial distributions of NO, NH_3 and HCN are different especially above the fuel bed (see Figs. 18 and 19). These differences are mainly attributed to the different oxygen and radical (O and OH) concentrations that are influenced by streak formation (i.e. mixing function).

The results for both cases show that the predictions are improved with the hybrid-streak model. This can be explained with the more accurate prediction of the species mixing process above the fuel bed and, therefore, of the radicals, that are important for NO_x formation processes. This means that in the case for straw pellets with a high fuel nitrogen content, where the NO_x formation is dominated by the reaction progress in the reduction zone, which is slowed down by the mixing function since it is multiplied by the net reaction rate in the hybrid-streak model, higher NO_x emissions are predicted than with the other models. For wood pellets with a very low nitrogen content and hence a low concentration of the NO_x reducing agent NH_3 , the overall NO_x reaction progress is dominated by the NO_x formation in the air rich zone of the primary combustion zone, which is again slowed down by the presence of streaks, leading to lower NO_x emissions than for the other models.

4. Summary and conclusions

A streak formation model has been developed to account for the effects of gas streaks arising from the fuel bed of grate combustion plants on gas mixing and reactions. The streak formation model is based on a correlation between the local gas residence time and a mixing time in

Table 4

Predicted NO_x concentrations with the EDC, hybrid and hybrid-streak models in comparison to measurements for wood pellets as fuel.

Average NO_x concentration	Unit	Simulations			Measurement
		EDC	Hybrid	Hybrid-streak	
Boiler outlet	[ppm dry]	118	132	110	105
Boiler outlet	[mg/Nm^3 13 vol.% O_2 dry]	146	165	135	130
Deviation (percent error)	[%]	12	26	5	

Table 5

Predicted NO_x concentrations with the EDC, hybrid and hybrid-streak models in comparison to measurements for straw pellets as fuel.

Average NO_x concentration	Unit	Simulations			Measurement
		EDC	Hybrid	Hybrid-streak	
Boiler outlet	[ppm dry]	167	186	352	286
Boiler outlet	[mg/Nm^3 13 vol.% O_2 dry]	220	247	466	380
Deviation (percent error)	[%]	-41	-34	23	

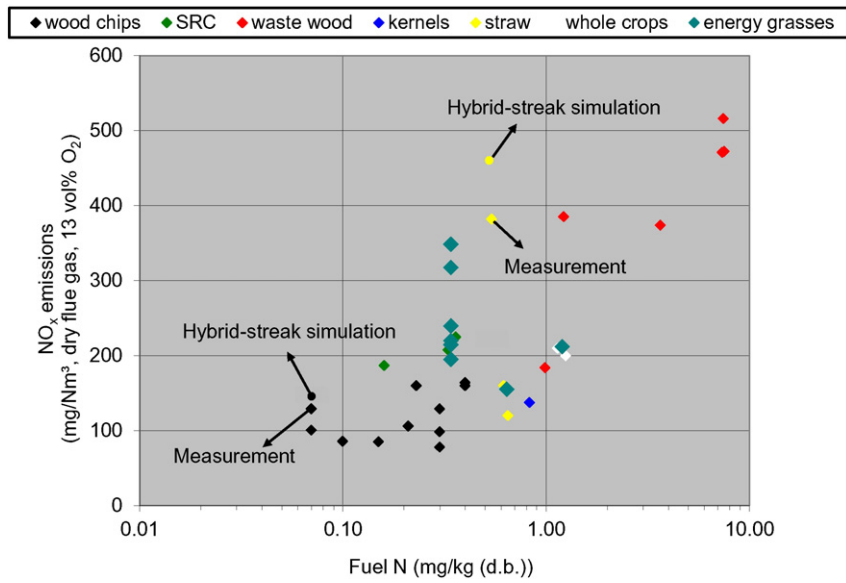


Fig. 22. NO_x emissions in dependence of the fuel nitrogen content for different biomass fuels [25,28,29]. Explanations: SRC: short rotation coppice.

which the mixing time is the necessary time to reach the fully mixed condition in the flue gas. A mixing state definition is introduced in order to evaluate the degree of mixing above the packed bed. The gas residence time introduced in the streak formation model is obtained by solving a scalar transport equation. A series of packed bed CFD case

study simulations has been carried out to derive the mixing time to be considered in the streak formation model. The primary air velocity, volatile mass flow rate and number of particles (bed thickness) were identified as influencing parameters for the derivation of the mixing time. The results of the CFD packed bed case study serves as look-up table

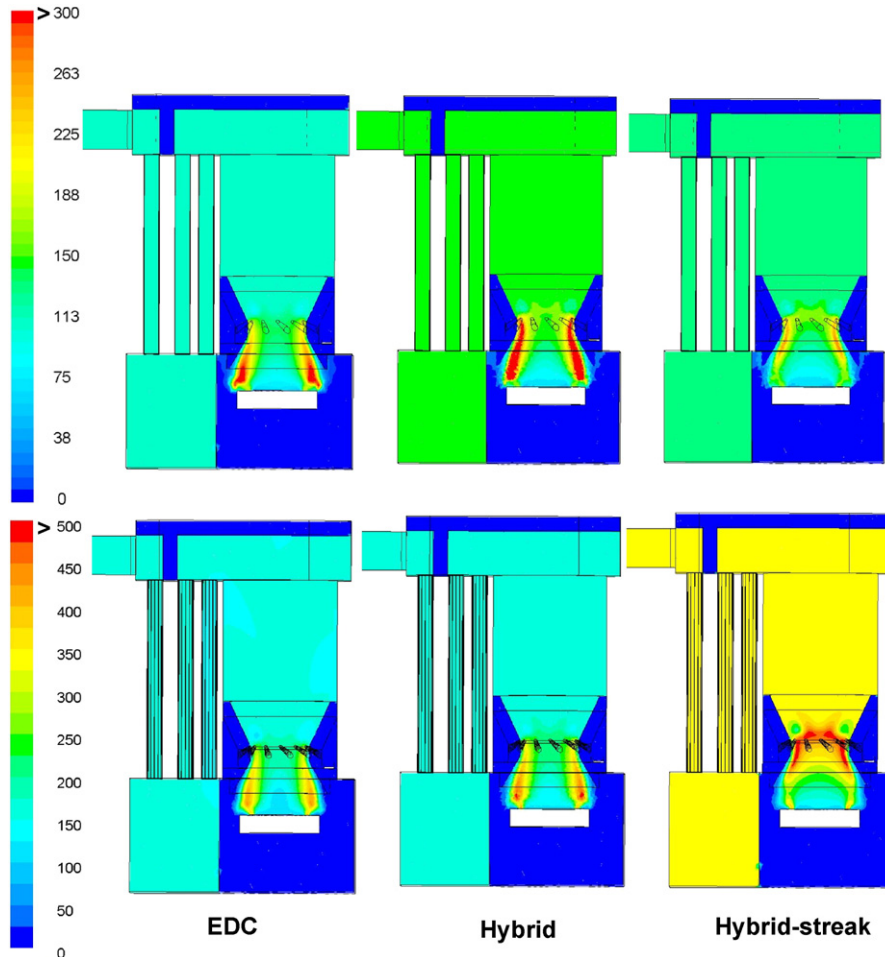


Fig. 23. Iso-surfaces of NO_x concentrations (ppmv dry) in a vertical cross-section of the furnace for wood pellets (top) and straw pellets (bottom).

for the calculation of the mixing time in dependence of the different influencing parameters. The mixing time can be retrieved by a linear interpolation between the calculation points in dependence of the particle Reynolds number and the number of fuel layers. Furthermore, the application of the streak formation model has been verified for an under-feed stoker grate furnace for wood and straw pellets.

The EDM, EDC and hybrid gas phase reaction models are used for the simulation of turbulent reactive flow in the combustion chamber. In the case of the hybrid model, an additional simulation has been performed where, the hybrid and streak formation model have been coupled.

The results from the under-feed stoker case studies show that for both fuels investigated, the streaks have relevant influence on the combustion process regarding flue gas temperature, O₂ distribution and CO emissions. Moreover, the formation of reacting radicals (e.g. O and OH), especially, in the region above the bed are influenced by streak formation since the reaction progress is delayed caused by the incomplete mixing.

In a next step, NO_x simulations have been performed in a post-processing approach based on the solution obtained from the combustion simulations. The distribution of the NH₃, HCN and NO profiles shows that streak formation has a strong influence on the spatial distributions of the aforementioned species. This is mainly due to the slow-down of the reaction rate predictions caused by the streaks. The NO_x emissions calculated with the hybrid-streak model show the best agreement with measured values. In conclusion, the streak formation model in combination with the hybrid gas phase combustion model shows a clear potential for an improved NO_x prediction since it considers species mixing and reaction processes above the fuel bed with a higher accuracy. In the future, extensive validation simulations for real-scale plants are foreseen in order to validate and evaluate the model in more detail and for different framework conditions.

References

- [1] R. Scharler, Entwicklung und Optimierung von Biomasse-Rostfeuerungen durch CFD-Analyse (PhD Thesis) Graz University of Technology, 2001.
- [2] R. Scharler, E. Widmann, I. Obernberger, CFD modeling of NO_x formation in biomass grate furnaces with detailed chemistry, in: A.V. Bridgwater, D.G.B. Boocock (Eds.), Science in Thermal and Chemical Biomass Conversion; Sept 2004, CPL Press, Victoria, Canada; UK 2006, pp. 284–300.
- [3] A. Shiehnejadhesar, K. Schulze, R. Scharler, I. Obernberger, A new innovative CFD-based optimisation method for biomass combustion plants, Biomass Bioenergy 53 (2013) 48–53.
- [4] ÖNORM M 7135, Compressed Wood or Compressed Bark in Natural State, Pellets and Briquettes. Requirements and Test Specifications, Österreichisches, Vienna, Austria, 2003.
- [5] A. García-Maraver, V. Popov, M. Zamorano, A review of European standards for pellet quality, Renew. Energy 36 (2011) 3537–3540.
- [6] R. Mehrabian, S. Zahirovic, R. Scharler, I. Obernberger, S. Kleditzsch, et al., A CFD model for thermal conversion of thermally thick biomass particles, Fuel Process. Technol. 95 (2012) 96–108.
- [7] A. Shiehnejadhesar, R. Mehrabian, R. Scharler, G.M. Goldin, I. Obernberger, Development of a gas phase combustion model suitable for low and high turbulence conditions, Fuel 126 (2014) 177–187.
- [8] B.F. Magnussen, B.H. Hjertager, On mathematical modeling of turbulent combustion with special emphasis on soot formation and combustion, Proc. Combust. Inst. 16 (1) (1977) 719–729, [http://dx.doi.org/10.1016/S0082-0784\(77\)80366-4](http://dx.doi.org/10.1016/S0082-0784(77)80366-4).
- [9] B.F. Magnussen, On the structure of turbulence and a generalized eddy dissipation concept for chemical reaction in turbulent flow, 19th AIAA Aerospace Science Meeting, St Louis, Missouri, USA, 1981.
- [10] A. Brink, Eddy Break-up Based Models for Industrial Diffusion Flames With Complex Gas Phase Chemistry (PhD Thesis) Abo Akademi University, 1998.
- [11] R. Scharler, T. Fleckl, I. Obernberger, Modification of a Magnussen Constant of the eddy dissipation model for biomass grate furnaces by means of hot gas in-situ FT-IR absorption spectroscopy, Prog. Comput. Fluid Dyn. Int. J. 3 (2003) 102–111.
- [12] S.B. Pope, Computationally efficient implementation of combustion chemistry using in situ adaptive tabulation, Combust. Theory Model. 1 (1997) 41–63.
- [13] B. Kader, Temperature and concentration profiles in fully turbulent boundary layers, Int. J. Heat Mass Transfer 24 (9) (1981) 1541–1544.
- [14] S. Zahirovic, R. Scharler, P. Kilpinen, I. Obernberger, Validation of flow simulation and gas combustion sub-models for the CFD-based prediction of NO_x formation in biomass grate furnaces, Combust. Theory Model. 15 (1) (2011) 61–87.
- [15] S. Zahirovic, R. Scharler, P. Kilpinen, I. Obernberger, A kinetic study on the potential of a hybrid reaction mechanism for prediction of NO_x formation in biomass grate furnaces, Combust. Theory Model. 15 (5) (2011) 645–670.
- [16] S.B. Pope, Turbulent Flow, Cambridge University Press, Cambridge, UK, 2001.
- [17] J. Kim, P. Monin, R. Moser, Turbulence statistics in fully developed channel flow at low Reynolds number, J. Fluid Mech. 177 (1987) 133–166.
- [18] M. Bartak, M. Cermak, J.A. Clarke, J. Denev, F. Drkal, et al., Experimental and numerical study of local mean age-of-air, Proc. 7th International Building performance Simulation Association Conference, IBPSA, ISBN: 85-901939-3-4, 2001.
- [19] D.A. Egarr, M.G. Faram, T. O'Doherty, D.A. Phipps, N. Syred, Computational fluid dynamic prediction of the residence time distribution of a prototype hydrodynamic vortex separator operating with a base flow component, Proc. Inst. Mech. Eng. E J. Process Mech. Eng. 219 (1) (2005) 53–67.
- [20] D. Neves, H. Thunman, A. Matos, L. Tarelho, A. Gomez-Barea, Characterization and prediction of biomass pyrolysis products, Prog. Energy Combust. Sci. 37 (2011) 611–630.
- [21] M.L. Boroson, J.B. Howard, J.P. Longwell, W.A. Peters, Product yields and kinetics from the vapor phase cracking of wood pyrolysis tars, AIChE J. 35 (1989) 120–128.
- [22] R.G. Graham, M.A. Bergougou, R.P. Overend, Fast pyrolysis of biomass, J. Anal. Appl. Pyrol. 6 (1984) 95–135.
- [23] S. Hamel, On the Packing Properties of Fixed Beds for Thermal Fuel Conversion, Shaker Verlag, Germany, 2010. 74–75.
- [24] I. Obernberger, E. Widmann, R. Scharler Entwicklung eines Abbrandmodells und eines NO_x-Postprozessors zur Verbesserung der CFD-Simulation von Biomasse-Festbettfeuerungen, Report from energy and environment research, report No. 31/2003, Ministry for Transport, Innovative and Technology (Ed.), Vienna, Austria.
- [25] G. Stubenberger, R. Scharler, S. Zahirovic, I. Obernberger, Experimental investigation of nitrogen species release from different solid biomass fuels as a basis for release models, Fuel 87 (6) (2008) 793–806.
- [26] S.R. Turns, Understanding NO_x formation in non-premixed flames: experiments and modeling, Prog. Energy Combust. Sci. 21 (1995) 361–385.
- [27] A. Mardani, S. Tabejamaat, NO_x formation in H₂-CH₄ blended flame under mild conditions, Combust. Sci. Technol. 184 (7–8) (2012) 995–1010.
- [28] I. Obernberger, Strategy for the application of novel characterization methods for biomass fuels: case study of straw, Energy Fuel 28 (2) (2014) 1041–1052.
- [29] T. Hesch, F. Biedermann, T. Brunner, I. Obernberger, Reduction of NO_x and PM1 emissions from automated boilers by advanced air staging, in: M. Faulstich (Ed.), 19th European Biomass Conference & Exhibition, June 2011, Berlin, Germany, ETA-Renewable Energies, Florence, Italy 2011, pp. 874–879.

Nomenclature

- C_{fm} : tracer gas concentration in the fully mixed gas (–)
 $C_{(i)}$: local tracer gas (–)
 D_b : molecular diffusivity (m² s⁻¹)
 D_t : turbulent diffusivity (m² s⁻¹)
 d_p : volume diameter (m)
 J_i : diffusion flux of species *i* (kg m⁻¹ s⁻¹)
 \dot{m} : mass flow rate (kg s⁻¹)
 MS : mixing state (–)
 MF : mixing function (–)
 Re_p : particle Reynolds number (–)
 Re_t : turbulent Reynolds number (–)
 R_i : net rate of production of species *i* by chemical reaction (kg m⁻³ s⁻¹)
 $S_{c_{i0}}$: source term (kg m⁻³)
 Sc_i : Schmidt number (–)
 t : residence time (s)
 Δt : time step (s)
 u : fluid velocity (m s⁻¹)
 UDF : user-defined function
 UDS : user-defined scalar
 V : volume (m³)
 V : volumetric flow rate (m³ s⁻¹)
 Y_i : mass fraction of species *i* (–)

Greek symbols

- ϵ : turbulent dissipation rate (m² s⁻³)
 ν : kinematic viscosity (m² s⁻¹)
 ρ : density (kg m⁻³)
 \vec{v} : velocity vector (m s⁻¹)
 φ_k : scalar quantity (residence time) (s)
 Γ_k : diffusion coefficient (m² s⁻¹)
 μ_t : turbulent viscosity (kg m⁻¹ s⁻¹)
 μ : laminar viscosity (kg m⁻¹ s⁻¹)

Subscript

- EDC: eddy dissipation concept
 FRK: finite rate kinetics
i: species index
t: turbulent

Paper IV

Available online at www.sciencedirect.com

SciVerse ScienceDirect

<http://www.elsevier.com/locate/biombioe>

A new innovative CFD-based optimisation method for biomass combustion plants



Ali Shiehnejadhesar^{a,b,*}, Kai Schulze^a, Robert Scharler^{a,b,c},
Ingwald Obernberger^{a,b,c}

^a Bioenergy 2020+GmbH, Inffelgasse 21b, 8010 Graz, Austria

^b Institute for Process and Particle Engineering, Graz University of Technology, Inffeldgasse 21b, 8010 Graz, Austria

^c BIOS BIOENERGIESYSTEME GmbH, Inffeldgasse 21b, 8010 Graz, Austria

ARTICLE INFO

Article history:

Received 27 June 2012

Received in revised form

29 January 2013

Accepted 3 February 2013

Available online 11 March 2013

Keywords:

CFD

Optimisation

Combustion

Biomass

Emission reduction

ABSTRACT

In this paper, the work on the development and test of a basic design tool for the automatic performance of parameter studies for the optimisation of biomass combustion plants is presented. The model consists of parameterisation and optimisation routines linked with an in-house developed empirical packed bed combustion model as well as gas phase CFD models especially adapted for biomass grate furnaces.

To test and verify the routine developed, it has been applied to the optimisation of a 180 kW_{th} pilot-scale grate furnace. The main focus was on the minimisation of CO emissions and the pressure loss by changing the diameter and angle of the secondary air nozzles. The simulation results show that the time of the optimisation process can be reduced considerably by the automatic routine developed and the evaluation of several independent design parameters is possible. This new procedure forms an important milestone towards automatic CFD-based furnace and boiler optimisations in the future.

© 2013 Elsevier Ltd. All rights reserved.

1. Introduction

CFD models are being successfully applied for the simulation of biomass combustion plants in order to design and improve the plants with respect to lower CO emissions, the reduction of flue gas temperature peaks, additionally increased plant efficiencies. However, even experienced scientific personnel needs a large number of time-consuming simulations during a CFD-based design cycle. A “real” optimum typically cannot be found due to the complex interactions of the influencing parameters in the plant. While automatic CFD-optimisation methods have been applied for the design of cyclones [1–4], the combustion chamber of engines [5,6] and in the field of turbo machinery [7–9], only manual optimisation methods have been applied in the field of biomass combustion plants

[10–12] due to the high degree of complexity of the processes in the plant and thus the high number of influencing parameters.

Therefore, at BIOENERGY 2020+ a tool for the automatic CFD-optimisation of biomass grate furnaces has been developed. The model consists of parameterisation and optimisation routines linked with an in-house developed model for biomass grate furnaces (empirical packed bed combustion model and gas phase CFD models especially adapted for biomass combustion). In order to test and verify the efficiency of the routine developed, the procedure has been applied to a pilot-scale grate furnace (180 kW_{th}). The main focus was on the minimisation of carbon monoxide emissions and the energy demand of the secondary air fan by changing the diameter and angle of the secondary air nozzles.

* Corresponding author. Institute for Process and Particle Engineering, Graz University of Technology, Inffeldgasse 21b, 8010 Graz, Steiermark, Austria. Tel.: +43 316 8739230; fax: +43 316 8739202.

E-mail addresses: ali.shiehnejadhesar@gmail.com, ali.shiehnejad@bioenergy2020.eu (A. Shiehnejadhesar).

0961-9534/\$ – see front matter © 2013 Elsevier Ltd. All rights reserved.

<http://dx.doi.org/10.1016/j.biombioe.2013.02.005>

2. Methodology

As already explained, parameterisation routines and optimisation functions have been linked with an in-house developed model for biomass grate furnaces (empirical packed bed combustion model and gas phase CFD models especially adapted for biomass combustion).

2.1. CFD model for biomass grate furnaces

An empirical model was developed for the description of solid biomass combustion on the grate [13–15]. The model describes the mass and energy fluxes on the grate as boundary conditions for the following CFD simulation of the turbulent reactive flow in the combustion chamber. The empirical packed bed combustion model consists of three parts:

- 1D-profiles along the grate, which describe fuel drying and the thermal degradation of the fuel components C, H, O as well as profiles of the primary air and re-circulated flue gas supplied below the grate are the basis of the model.
- By the definition of conversion parameters based on literature data and experiments, which describe the conversion of the fuel components C, H, and O to the flue gas components CH₄, CO, CO₂, H₂, H₂O and O₂ which are dependent on the local fuel composition and the stoichiometric air ratio on the grate. Then the local composition of the flue gas released from the packed bed can be described. Nitrogen species have not been considered since the CFD simulation of NO_x formation was not within the scope of this work.
- Finally, the local mass and energy profiles and hence, the profiles of flue gas velocity, temperature and composition along the grate are calculated.

The results of the simulation applications (e.g. Refs. [13,16–19]) showed that the empirical packed bed combustion model is sufficiently accurate for the calculation of the boundary conditions for the CFD simulation of flow and gas phase combustion in the furnace. However, it is noted that the processes of solid biomass combustion on the grate cannot be described by the empirical packed bed combustion model. For the simulation of the gas phase, the Realizable $k-\epsilon$ Model for turbulence, the Discrete Ordinates Model for radiation and the Eddy Dissipation Model (EDM) by Magnussen and Hjertager [20] in combination with a global methane 3-step mechanism (CH₄, CO, H₂, CO₂, H₂O, O₂) [21] are applied. The sub-models and the gas phase models together with the empirical packed bed combustion model have been experimentally validated [13,15] and successfully applied for several plants.

2.2. Selection of the design parameters

The secondary air nozzles are of special importance when designing and optimising a biomass furnace. They are the key factor for efficient air staging without backflow in the primary combustion zone (NO_x reduction by primary measures), for a good turbulent mixing and CO burnout, to reduce furnace volume and to lower the amount of excess air (increased

efficiency). Therefore, the diameter and the angle of the secondary air nozzles have been selected as design parameters in order to achieve the best geometric configuration concerning low CO emissions and pressure losses over the secondary air nozzles.

2.3. Optimisation function

A weight function has to be defined to combine the two optimisation variables (CO emissions and pressure loss over the secondary air nozzles) according to their relevance in a common function. While the energy demand of the fan linearly increases with the pressure loss over the secondary air nozzles, the relevance of the CO emissions substantially increases if a certain level of CO emissions is exceeded. Equation (1) shows the weight function:

$$W = A \cdot \left(\frac{1}{Y_{CO}} \right)^\gamma + B \cdot \Delta P \quad (1)$$

where W is the weight function, Y_{CO} is the CO mole fraction ($\mu\text{L L}^{-1}$), A , γ and B are constant values and ΔP is the pressure loss (Pa).

Here, for the pressure drop a linear correlation to the weight function has been assumed (proportional to the energy demand of the fan). Regarding the CO emissions, a polynomial function with a strong increase at a chosen emission limit ($20 \mu\text{L L}^{-1}$ in the present case) was supposed.

The constants A and B of the second order polynomial function ($\gamma = -2$) have been determined in a way to achieve roughly the same contribution of the pressure loss and the CO emission to the weight function at the respective limits of the output variables ($\Delta P = 2500 \text{ Pa}$ – maximum allowable pressure for fan design; CO emissions = $20 \mu\text{L L}^{-1}$ – emission limit). The values for the constants are given in Table 1.

Within the optimisation process the design parameters are varied and evaluated using the weight function. The optimisation cycle for a selected combination of design parameters works as following:

- Parameterisation of the geometry and definition of design points based on design parameters selected (the variation range of the design parameters is shown in Table 2)
- Automatic performance of CFD simulations with ANSYS® FLUENT® for the defined design points within the ANSYS® Workbench™
- Evaluation of the output variables and calculation of the weight function for the design points
- Minimisation of the weight function to find the optimum geometric configuration (input parameters)

Table 1 – Values of the model constants used in the weight function.

Constant	Value	Units
A	10	Consistent unit ($\mu\text{L L}^{-1}$) ⁻²
γ	-2	–
B	1	Consistent unit (Pa^{-1})

Table 2 – Design parameters and their variation range.

Design parameter	Range
Diameter (mm)	10–35
Angle (deg)	1–30

2.4. Case study description

To investigate the efficiency of the method developed, a design optimisation for a pilot-scale moving grate furnace equipped with a hot water fire tube boiler (180 kW_{th}) using Miscanthus as fuel has been carried out. Table 3 provides the most relevant operating conditions of the furnace and the fuel composition.

Fig. 1 illustrates the different sections of the biomass combustion plant considered. The simulation domain comprises the combustion chamber from above the fuel bed up to the exit of the radiative fire tube. While the primary combustion zone is equipped with six flue gas recirculation nozzles, eight secondary air nozzles are located at the entrance of the secondary air combustion chamber.

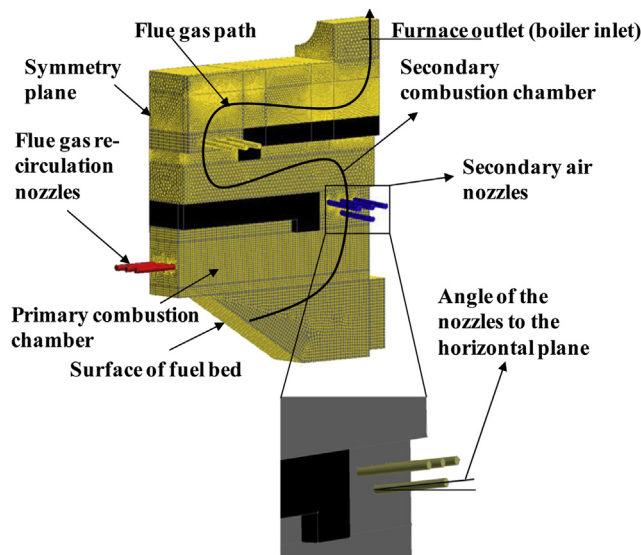


Fig. 1 – Geometry and computational grid of the pilot-scale grate furnace (top) as well as design parameters (nozzles angle to the wall and diameter) (bottom).

3. Results and discussion

To verify the efficiency of the optimisation strategy concerning the reduction of the overall time for the performance of the case study in comparison to conventional manual methods, at first a manual optimisation run was carried out (as a reference). Since this method is very time-consuming, only the diameter of the nozzles has been changed (for 10 design points). A computational grid with 700,000 cells in total was used in the manual optimisation study. In the next step, the automatic optimisation routine was performed for the two selected design parameters for 80 design points. The number of computational cells was about 1 million for the automatic optimisation study using the tetrahedral cell type. Figs. 2 and 3

Table 3 – Operating conditions and fuel characteristics of the pilot-scale grate furnace.

	Unit	Value
<i>Operating conditions</i>		
Boiler load	kW _{th}	180
Adiabatic flame temperature	°C	937
O ₂ content in dry flue gas	Volume fraction	0.084
Flue gas recirculation ratio		0.3
<i>Fuel characteristics</i>		
C	Mass fraction d.b.	0.483
H	Mass fraction d.b.	0.059
O	Mass fraction d.b.	0.43
N	Mass fraction d.b.	0.0034
Moisture content	Mass fraction w.b.	0.154
Ash	Mass fraction d.b.	0.022
NCV	kJ kg ⁻¹ w.b.	14.86
GCV	kJ kg ⁻¹ d.b.	19.31

Explanations: w.b.: wet basis; d.b.: dry basis; GCV: gross calorific value; NCV: net calorific value.

show the calculated results concerning CO emissions and pressure losses for the manual and the automatic optimisation method. The black circles in the diagrams represent the evaluated design points within the automatic CFD simulations for each pair of design parameters (diameter and angle). The red line (in the web version) in the diagrams represents the results obtained with the manual optimisation method. Based on the results of the automatic CFD simulation (black circles), a response surface was created by a second order polynomial fit. The trends for both methods generally are in good agreement for comparable design points.

Next, a sensitivity analysis has been carried out to outline and evaluate the impact of the input design parameters on the output variables (CO emission, pressure loss). According to Ref. [22], the single parameter sensitivities are defined as the

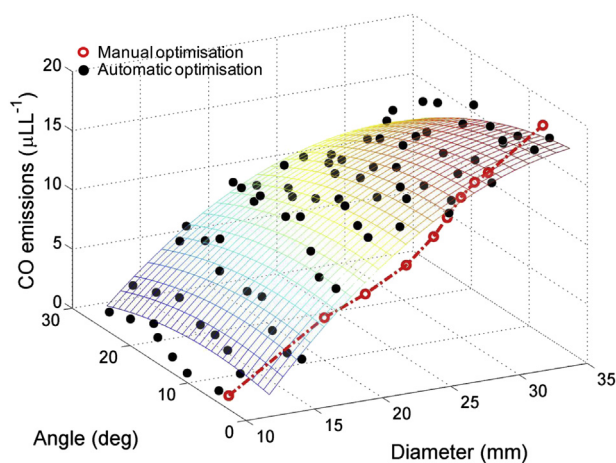


Fig. 2 – Response surface plot of CO emissions calculated with the automatic optimisation method.

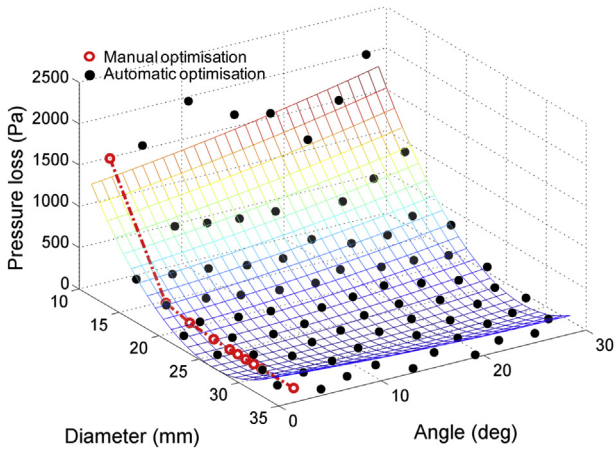


Fig. 3 – Response surface plot of pressure losses calculated with the automatic optimisation method.

difference between the minimum and the maximum of output variable divided by the average value of all the design points. They are obtained by varying one input parameter while holding the other input parameters constant. The larger the sensitivity of the output variables, the more significant the role of the input parameter is.

This analysis provides helpful information especially when there are more than two design parameters. Input design parameters with a low sensitivity can be skipped since they have no strong influence on the output variables. Therefore, within the automatic optimisation study the sensitivity analysis was performed to achieve a better understanding about the impact of the design parameters on the output variables.

Fig. 4 shows the local sensitivity of the pressure loss and CO emission regarding the change of the nozzles diameter and angle. The positive sign in the chart indicates that an increase of the design parameter increases the output variable as well, and vice versa.

It is shown from Fig. 4 that the diameter has a large (negative) impact on the pressure loss and a moderate positive impact on CO emission. This means that by increasing the diameter of the secondary air nozzles the pressure loss

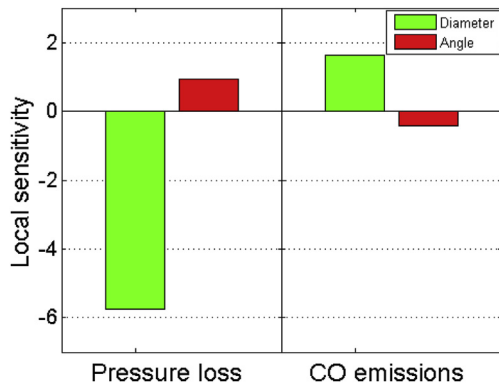


Fig. 4 – Sensitivity diagram of the impact of the design parameters on the output variables.

decreases while the CO emissions increase. The reduction of the diameter of the secondary air nozzles causes a higher gas velocity at nozzle exit. This results in a better mixing of secondary air with the flue gas due to a deeper penetration of the air jets into the flue gas which results in a higher net CO reaction rate. Furthermore, the pressure loss increases due to the higher kinetic energy loss with smaller nozzle diameters. Fig. 5 shows the dependency of CO emissions on the angle of the secondary air nozzles for different diameter ranges. The results show that the CO dependency on the angle is low for smaller diameters and increases for larger diameters. Furthermore, the sensitivity graph shows that the angle of secondary air nozzles has a moderately negative impact on CO emissions while it has a relatively high positive impact on the pressure loss. This implies that with an increasing angle the CO emissions slightly decrease and the pressure loss increases. Generally, the sensitivities of both output variables concerning the diameter and the angle variation have an opposite sign which indicates that theoretically the variation of the two input parameters could compensate the effect of each other when they are varied simultaneously and in the same direction. However, the sensitivities of the CO emissions and the pressure loss on the diameter are considerably larger than on the angle.

Fig. 6 shows the values of the weight function calculated according to equation (1) for different combinations of nozzle angles and diameters. By screening through the weight surface, many local minima can be detected. These local minima represent the smallest values in a certain investigated area, while the global minimum represents the smallest value within the total definition range of the variation parameters. The absolute minimum represents the optimum combination of nozzle diameter and nozzle angle (15 mm diameter and 5° nozzle angle in the present case). While in the automatic optimisation study the whole parameter range is investigated systematically, only a few simulations based on trial-and-error can be performed during a manual optimisation study. Therefore, the automatic optimisation provides considerably higher possibility to find the global optimum.

In Fig. 7 the CO emissions are plotted against the pressure loss for all design points. Here, the Pareto front represents the design points which have the lowest CO emission for a chosen pressure loss and the lowest pressure loss for a chosen CO emission, respectively. Hence, by the Pareto front not only the global optimum can be found but also the best possible design for a certain restriction e.g. concerning the pressure loss.

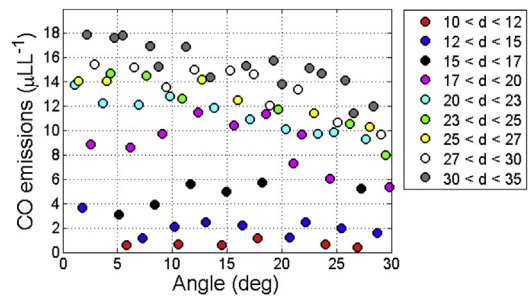


Fig. 5 – Dependence of CO emissions on the angle of secondary air nozzles for different diameter ranges.

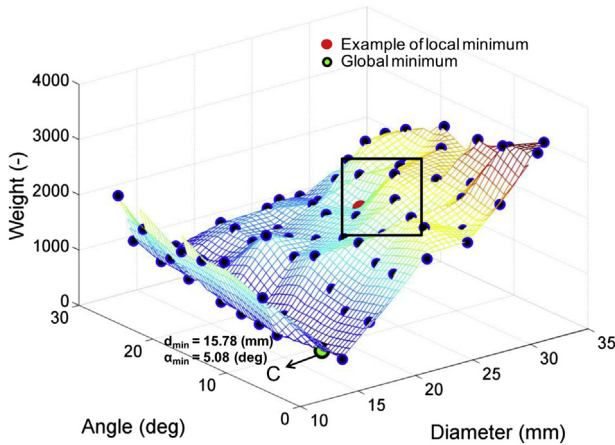


Fig. 6 – Weight surface from automatic optimisation calculated based on 80 design points (tetrahedral mesh type with 1 million grid cells).

Additionally, a further automatic parameter study has been carried out to investigate the influence of the grid type on computation time and accuracy. For this purpose, two sets of grid have been studied: a tetrahedral mesh and a polyhedral mesh. While the first grid type has been used as reference grid with 1 million cells (high resolution), the polyhedral type was generated by a conversion of the tetrahedral mesh type. This method reduces the number of mesh cells to approximately 250,000 cells.

The influence of the different grids on the results is shown in Fig. 8. The CO emission calculated with the polyhedral mesh shows deviations from results which have been achieved with the tetrahedral mesh for diameters larger than 20 mm, since the penetration of the secondary air is underestimated due to large cell sizes in the region of the nozzles. The calculated weight function for the different meshes is shown in Fig. 9. While for a diameter of approximately 15 mm the pressure drop is below 200 Pa, the CO concentration at the outlet of the secondary combustion chamber is still below 8 ($\mu\text{L L}^{-1}$) (see Fig. 8). Although the CO emissions calculated with

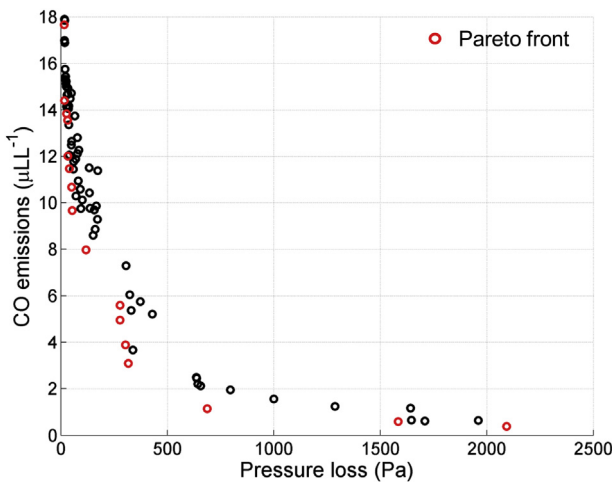


Fig. 7 – Results for design points with Pareto front.

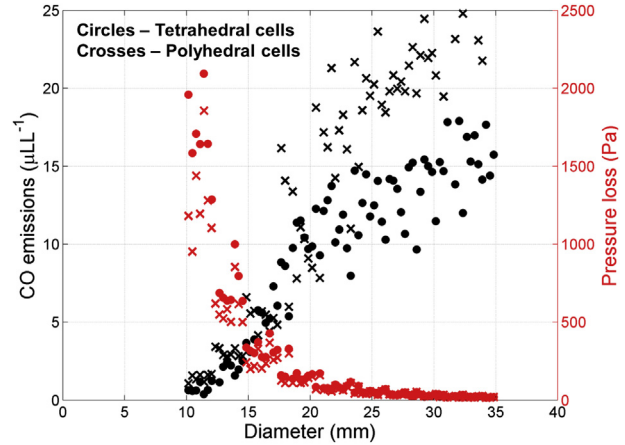


Fig. 8 – Effect of mesh type on the calculated CO emissions and pressure losses for the pilot-scale grate furnace.

the polyhedral mesh show deviations from the values calculated with the tetrahedral mesh, the optimum of the weight function (point H) is located approximately at the same position (point G) (see Fig. 9). The main reason for the difference between the obtained global minimum from the manual optimisation study (point K) in comparison to the automatic optimisation studies (points G and H) is due to the effect of angle variations which has not been considered in the manual study.

In case of the tetrahedral mesh type the overall optimisation time took one month under consideration of two optimisation parameters (diameter and angle for 80 design points). By using the polyhedral mesh, the optimum of the parameter study was found within 6 days. In contradiction, a manual design study would need approximately 8 months due to the comprehensive number of person-hours to create the numerical grid and to set-up the calculations for each design point.

Despite deviations in CO emission predictions from the reference grid, the polyhedral mesh shows a great potential to accelerate the optimisation cycle. A local mesh refinement in

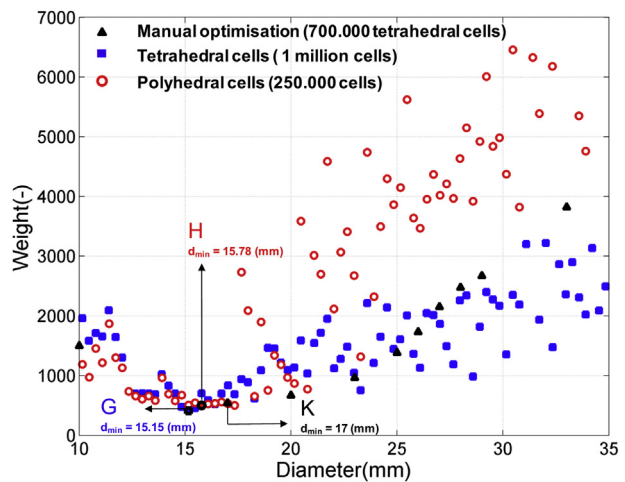


Fig. 9 – Weight function for different mesh types.

the region of secondary air jets is needed for an improved CO prediction and is expected to just slightly increase the mesh size and hence computation time.

4. Summary and conclusions

A new automatic optimisation routine was developed and tested for a biomass pilot-scale grate furnace concerning the minimisation of CO emissions and pressure loss. The sensitivity analysis performed underlines the high impact of the nozzle diameter on the pressure losses and CO emissions in comparison to the nozzle angle. The parameter variation performed automatically is by far more efficient than the manual case study due to the considerably lower simulation time and personnel demand. The overall simulation time for the calculation of 80 design points could be reduced by a factor of 8 in case of the tetrahedral mesh type and by a factor of 32 in case of the polyhedral mesh type. Although the CO emission trends were slightly differing for the two studied grid types, the global minima are located nearly at the same positions. However, the prediction accuracy of the coarser polyhedral mesh can be further improved at an acceptable increase of computational time by a further increased local mesh refinement near the secondary air nozzles. Concluding, the new CFD optimisation routine proved to work efficiently in terms of nozzle design optimisation and time demand. In future it shall be further extended to geometry optimisation issues as well as the automatic simulation of different operating conditions for a defined geometry as a basis for an improved process control.

REFERENCES

- [1] Safikhani H, Hajiloo A, Ranjbar M, Nariman-Zadeh N. Modeling and multi-objective optimisation of cyclone separator using CFD and genetic algorithms. *Comput Chem Eng* 2011;35(6):1064–71.
- [2] Elsayed K, Lacor C. Modeling, analysis and optimisation of aircyclones using artificial neural network, response surface methodology and CFD simulation approaches. *Powder Technol* 2011;212(1):115–33.
- [3] Safikhani H, Akhavan-Behabadi MA, Nariman-Zadeh N, Abadi MJM. Modeling and multi-objective optimisation of square cyclones using CFD and neural networks. *Chem Eng Res Des* 2011;89(3):301–9.
- [4] Elsayed K, Lacor C. Optimisation of the cyclone separator geometry for minimum pressure drop using mathematical models and CFD simulations. *Chem Eng Sci* 2010;65(22):6048–58.
- [5] Sungwook P. Optimisation of combustion chamber geometry and engine operating conditions for compression ignition engines fueled with dimethyl ether. *Fuel* 2012;97:61–71.
- [6] Sungwook P. Optimisation of combustion chamber geometry for stoichiometric diesel combustion using a micro genetic algorithm. *Fuel Process Technol* 2010;91(11):1742–52.
- [7] Derakhshan S, Mohammadi B, Nourbakhsh A. Incomplete sensitivities for 3D radial turbo machinery blade optimisation. *Comput Fluids* 2008;37(10):1354–63.
- [8] Derakhshan S, Mohammadi B, Nourbakhsh A. The comparison of incomplete sensitivities and genetic algorithms application in 3D radial turbo machinery blade optimisation. *Comput Fluids* 2010;39(10):2022–9.
- [9] Kim K, Seo S. Application of numerical optimisation technique to design of forward curved blades centrifugal fan. *JSME Int J Ser B* 2006;49(1):152–8.
- [10] Huai HL, Xu WL, Qu ZY, Li ZG, Zhang FP, Xiang GM, et al. Analysis and optimisation of municipal solid waste combustion in a reciprocating incinerator. *Chem Eng Sci* 2008;63:3100–13.
- [11] Shah KV, Vuthaluru R, Vuthaluru HB. CFD based investigations into optimisation of coal pulveriser performance: effect of classifier vane setting. *Fuel Process Technol* 2009;90:1135–41.
- [12] Scharler R, Benesch C, Schulze K, Obernberger I. CFD simulations as efficient tool for the development and optimisation of small-scale biomass furnace and stoves. In: Faulstich M, editor. 19th European biomass conference & exhibition; June 2011; Berlin; Germany. Florence; Italy: ETA-Renewable Energies; 2011. p. 4–12.
- [13] Scharler R. Entwicklung und Optimierung von Biomasse-Rostfeuerungen durch CFD-Analyse. PhD Thesis. Graz University of Technology; 2001.
- [14] Widmann E. Modellbildung zum Abbrandverhalten von Biomasse unter besonderer Berücksichtigung der N-Freisetzung am Beispiel einer Rostfeuerung. MSc Thesis. Graz University of Technology; 2002.
- [15] Scharler R, Widmann E, Obernberger I. CFD modeling of NO_x formation in biomass grate furnaces with detailed chemistry. In: Bridgwater AV, Boocock DGB, editors. Science in thermal and chemical biomass conversion; Sept 2004. Victoria; Canada. UK: CPL Press; 2006. p. 284–300.
- [16] Scharler R, Benesch C, Neudeck A, Obernberger I. CFD based design and optimisation of wood log fired stoves. In: De Santi GF, editor. 17th European biomass conference & exhibition; June 2009; Hamburg; Germany. Florence; Italy: ETA-Renewable Energies; 2009. p. 1361–7.
- [17] Scharler R, Fleckl T, Obernberger I. Modification of a Magnussen constant of Eddy dissipation model for biomass grate furnaces by means of hot gas in-situ FT-IR absorption spectroscopy. *Prog Comput Fluid Dyn Int J* 2003;3:102–11.
- [18] Scharler R, Forstner M, Braun M, Brunner T, Obernberger I. Advanced CFD analysis of large fixed bed biomass boilers with special focus on the convective section. In: van Swaaij WPM, editor. 2nd World conference and exhibition on biomass for energy, industry and climate protection; May 2004; Rome; Italy. Florence; Italy: ETA-Renewable Energies; 2004. p. 1357–60.
- [19] Scharler R, Obernberger I. CFD analysis of air staging and flue gas recirculation in biomass grate furnaces. In: Kyritsis S, editor. 1st World conference on biomass for energy and industry; June 2000; Sevilla; Spain. London, UK: James&James (Science Publishers) Ltd.; 2001. p. 1935–9.
- [20] Magnussen BF, Hjertager BH. On mathematical modeling of turbulent combustion with special emphasis on soot formation and combustion. In: 16th Symp (Int) combust; August 1976; Massachusetts Institute of Technology; Cambridge; Massachusetts; USA. Pittsburgh, PA; USA: The Combustion Institute; 1977. p. 719–29.
- [21] Brink A. Eddy Break-Up based models for industrial diffusion flames with complex gas phase chemistry. PhD Thesis. Abo Akademi University; 1998.
- [22] ANSYS®. Academic research, release 14.0, help system, design exploration user guide. ANSYS, Inc.

Paper V

AUTOMATIC CFD OPTIMISATION OF BIOMASS COMBUSTION PLANTS

Ali Shiehnejadhesar^{1,2}, Kai Schulze¹, Robert Scharler^{1,2,3}, Ingwald Obernberger^{1,2,3}

¹BIOENERGY 2020+ GmbH, Inffeldgasse 21b, 8010 Graz, Austria

Tel.: +43 (0)316 8739232; Fax: +43 (0)316 8739202; E-mail: ali.shiehnejad@bioenergy2020.eu

²Institute for Process and Particle Engineering, Graz University of Technology, Inffeldgasse 21b, A-8010 Graz, Austria

³BIOS BIOENERGIESYSTEME GmbH, Inffeldgasse 21b, A-8010 Graz, Austria

ABSTRACT:

In this paper, the work on the development and test of a basic design tool for the automatic performance of parameter studies for the optimisation of biomass combustion plants is presented. The model consists of parameterisation and optimisation routines linked with an in-house developed empirical packed bed combustion model as well as gas phase CFD models especially adapted for biomass grate furnaces.

To test and verify the routine developed, it has been applied for the optimisation of a 180 kW pilot-scale grate furnace. The main focus was on the minimisation of CO emissions and the pressure loss by changing the diameter and angle of the secondary air nozzles. The simulation results show that the time of the optimisation process can be reduced considerably by the automatic routine developed and the evaluation of several independent design variables is possible. This new procedure forms an important milestone towards automatic CFD based furnace and boiler optimisations in the future.

Keywords: CFD, optimisation, combustion, biomass

1 INTRODUCTION AND OBJECTIVES

CFD models are being successfully applied for the simulation of biomass combustion plants in order to design and improve the plants with respect to lower CO emissions, the reduction of flue gas temperature peaks as well as increased plant efficiencies. However, even experienced scientific personnel needs a large number of time-consuming simulations during a CFD based design cycle, whereas a “real” optimum typically can not be found due to the complex interactions of the influencing parameters in the plant. While automatic CFD-optimisation methods have been applied for the design of cyclones (see [1], [2], [3] and [4]), the combustion chamber of engines (see [5], [6]) as well as in the field of turbo machinery (see [7], [8], [9] and [10]), only manual optimisation methods have been applied in the field of biomass combustion plants (see [11], [12], [13]) due to the high complexity of the processes in the plant and thus the high number of influencing parameters.

Therefore, at BIOENERGY 2020+ a tool for the automatic CFD-optimisation of biomass grate furnaces has been developed. The model consists of parameterisation and optimisation routines linked with an in-house developed model for biomass grate furnaces (empirical packed bed combustion model and gas phase CFD models especially adapted for biomass combustion). In order to test and verify the efficiency of the routine developed, the procedure has been applied for a pilot-scale grate furnace (180 KW_{th}). The main focus was on the minimisation of carbon monoxide emissions and the energy demand of the secondary air fan by changing the diameter and angle of the secondary air nozzles.

2 METHODOLOGY

As already explained, parameterisation routines and optimisation functions have been linked with an in-house developed model for biomass grate furnaces (empirical packed bed combustion model and gas phase CFD models especially adapted for biomass combustion).

2.1 CFD model for biomass grate furnaces

An empirical model was developed for the

description of solid biomass combustion on the grate (see [14], [15] and [16]). The model describes the mass and energy fluxes on the grate as boundary conditions for the following CFD simulation of the turbulent reactive flow in the combustion chamber. The empirical packed bed combustion model consists of three parts:

- 1D-profiles along the grate, which describe fuel drying and the thermal degradation of the fuel components C, H, O as well as profiles of primary air and re-circulated flue gas supplied below the grate are the basis of the model.
- By the definition of conversion parameters based on literature data and experiments, which describe the conversion of the fuel components C, H, and O to the flue gas components CH₄, CO, CO₂, H₂, H₂O and O₂ in dependence of the local fuel composition and the stoichiometric air ratio on the grate, the local composition of the flue gas released from the packed bed can be described.
- This enables the final calculation of the local mass and energy profiles and hence, the profiles of flue gas velocity, temperature and composition along the grate.

The results of the simulation applications (e.g. [14], [17], [18], [19], [20], [21], [22] and [23]), showed that the empirical packed bed combustion model is sufficiently accurate for the calculation of the boundary conditions for the CFD simulation of flow and gas phase combustion in the furnace. However, it is noted that the processes of solid biomass combustion on the grate can not be described by the empirical packed bed combustion model.

For the simulation of the gas phase usually the Realizable k-ε Model for turbulence, the Discrete Ordinates Model for radiation, as well as the Eddy Dissipation Model (EDM) by Magnussen and Hjertager [24] in combination with a global Methane 3-step mechanism (CH₄, CO, H₂, CO₂, H₂O, O₂) [25] are applied. The sub-models as well as the gas phase models together with the empirical packed bed combustion

model have been experimentally validated ([11] and [16]) and successfully applied for several plants.

2.2 Selection of the design variables

The secondary air nozzles are of special importance when designing and optimising a biomass furnace. They are the key factor for an efficient air staging without backflow in the primary combustion zone (NO_x reduction by primary measures), for a good turbulent mixing and CO burnout, to reduce furnace volume and to lower excess air (increased efficiency). Therefore, the diameter and the angle of the secondary air nozzles were selected as design variables in order to achieve the best geometric configuration concerning low CO emissions and pressure losses over the secondary air nozzles.

2.3 Optimisation routine

A weight function has to be defined to combine the two optimisation parameters (CO emission, pressure loss over the secondary air nozzles) according to their relevance in a common function. While the energy demand of the fan linearly increases with the pressure loss over the secondary air nozzles, the relevance of the CO emissions substantially increases if a certain level of CO emissions is exceeded. Equation (1) shows the weight function.

$$W = A \cdot \left(\frac{1}{Y_{\text{CO}}} \right)^\alpha + B \cdot \Delta P \quad (1)$$

A, B and α are constants, ΔP represents the pressure loss [Pa], Y_{CO} the mole fraction of CO [ppmv] and W the weight function. Here, for the pressure drop a linear correlation has been assumed (proportional to the energy demand of the fan). Regarding the CO emissions a polynomial function with a strong increase at a chosen emission limit (20 ppmv) was supposed.

The design variables and their variation range are shown in Table I. Within the optimisation process the design variables are varied and evaluated using the weight function. The optimisation cycle for a selected combination of design variables works as follows:

- Parameterisation of the geometry and definition of design points based on selected design variables
- Automatic performance of CFD simulations with Fluent for the defined design points within ANSYS Workbench
- Evaluation of the output parameters and calculation of the weight function for the design points
- Minimisation of the weight function to find the optimum geometric configuration (input parameters)

Table I: Design variables and their range of variations

Design variable	Range
Diameter [mm]	10-35
Angle [deg]	1-30

2.4 Case study description

To investigate the efficiency of the method developed, a design optimisation for a pilot-scale moving grate furnace equipped with a hot water fire tube boiler (180 KW_{th}) using Miscanthus as fuel has been carried out. Table II provides the most relevant operational conditions of the furnace and the fuel composition.

Fig. 1 illustrates the different sections of the biomass combustion plant considered. The simulation domain comprises the combustion chamber from above the fuel bed up to the exit of the radiative fire tube. While the primary combustion zone is equipped with six flue gas recirculation nozzles, at the entrance of the secondary air combustion chamber, eight secondary air nozzles are located.

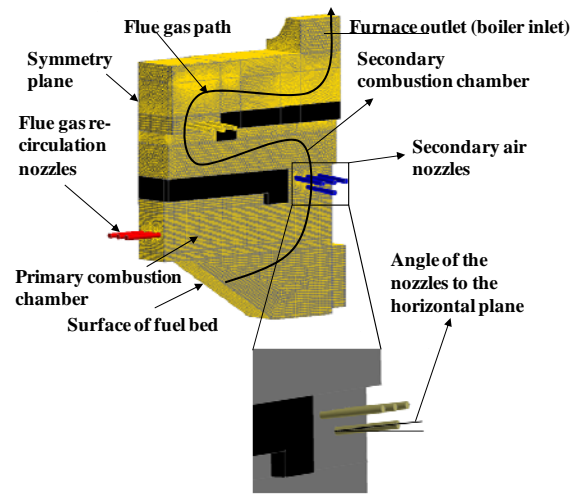


Figure 1: Geometry and computational grid of the pilot-scale grate furnace (top) as well as design variables (angle of the nozzles to the wall and diameter) (bottom)

Table II: Operating conditions and fuel characteristics of the pilot-scale grate furnace

Explanations: w.b.: wet basis; d.b.: dry basis; GCV: gross calorific value; NCV: net calorific value

Operating conditions	Unit	Value
Boiler load	KW_{th}	180
Adiabatic flame	$^{\circ}\text{C}$	937
O_2 content in the dry flue gas	Vol. %	8.4
Flue gas recirculation ratio		0.3
Fuel characteristics	Unit	Value
C	wt. % d.b.	48.3
H	wt. % d.b.	5.9
O	wt. % d.b.	43.0
N	wt. % d.b.	0.3
Moisture content	wt. % w.b.	15.4
Ash	wt. % d.b.	2.5
NCV	kJ/kg w.b.	14.8
GCV	kJ/kg d.b.	19.3

3 RESULTS

To verify the efficiency of the optimisation strategy concerning the reduction of the overall time for the performance of the case study in comparison to conventional manual methods, at first a manual optimisation run was carried out (as a reference). Since this method is very time consuming, only the diameter of the nozzles has been changed (for 10 design points). A computational grid with 700.000 cells in total was used in the manual optimisation study. In a next step, the automatic optimisation routine was performed for the two selected design variables for 80 design points. The number of computational cells was about one million for the automatic optimisation study using the tetrahedral cell type. Figs. 2 and 3 show the calculated results concerning CO emissions and pressure losses for the manual and the automatic optimisation method. The trends for both methods generally are in good agreement for the comparable design points.

The reduction of the diameter of the secondary air nozzles causes a higher velocity at nozzle exit. This results in a better mixing of secondary air with the flue gas due to a deeper penetration of the air jets into the flue gas. Furthermore, the pressure loss increases due to the higher kinetic energy loss with decreasing nozzle diameters.

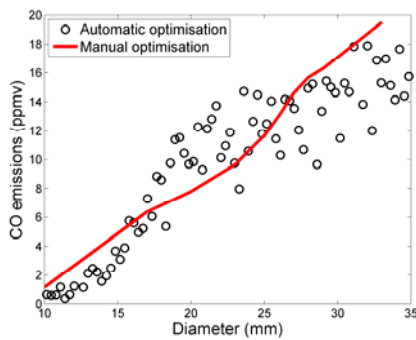


Figure 2: CO emissions calculated with the automatic and the manual optimisation method

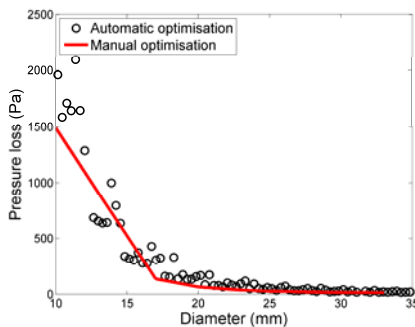


Figure 3: Pressure losses calculated with the automatic and the manual optimisation method

Fig. 4 shows the dependency of CO emissions on the angle of the secondary air nozzles for different diameter ranges. The results show that the CO dependency is low for smaller diameters and increases for larger diameters. On the other hand, for the same diameter range the variation of the angle of the nozzles nearly has no impact on the CO emissions. Generally, it has been found that the output variables are more dependent on diameter rather than on the angle.

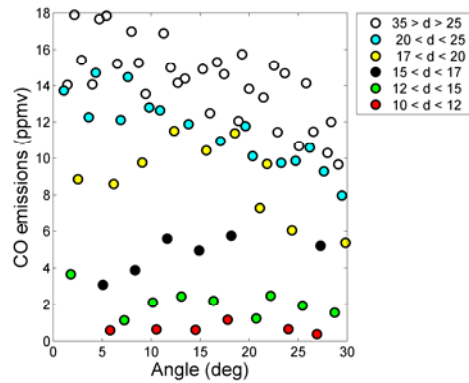


Figure 4: Dependence of CO emissions on the angle of secondary air nozzles for different diameter ranges

Fig. 5 shows the values of the weight function calculated according to Eq. (1) for different combinations of nozzle angles and diameters. By screening through the weight function surface, many local minima (red circles in the chart) can be detected but only one global minimum has been calculated (black circle in the chart). This minimum represents the best combination of the nozzle diameter and the nozzle angle (about 15 mm and 5° to the horizontal direction).

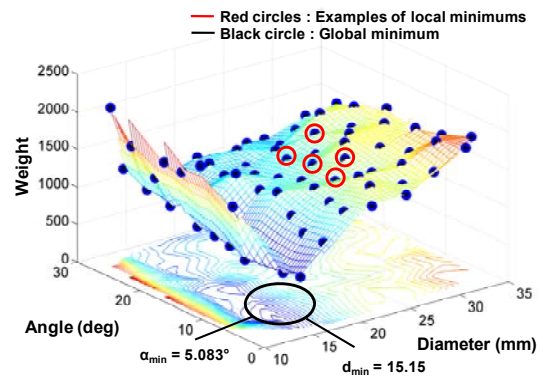


Figure 5: Weight surface from automatic optimisation calculated based on 80 design points (tetrahedral mesh type with 1 million computation cells)

Additionally, a further automatic parameter study has been carried out to investigate the influence of the grid type on the computation time and the accuracy. For this purpose, two sets of grid were studied: a tetrahedral mesh and a polyhedral mesh. While the first grid type has been used as reference grid with 1 million cells (high resolution), the polyhedral type was generated by a conversion of the tetrahedral mesh type. This method reduces the number of mesh cells to approximately 250.000 cells.

The influence of the different grids on the results is shown in Fig. 6. The CO emissions calculated with the polyhedral mesh show slight deviations from the results with the tetrahedral mesh, since the penetration of the secondary air is underestimated due to large cell sizes in the region of the nozzles. The calculated weight function

for the different meshes is shown in Fig. 8. While at a diameter of approximately 15 mm the pressure drop is below 200 Pa, the CO concentration at the outlet of the secondary combustion chamber is still below 8 ppmv (see Fig. 6). Although the CO emissions calculated with the polyhedral mesh show slight deviations from the values calculated with the tetrahedral mesh, the optimum of the weight function is located at the same position (see Fig. 7).

In case of the tetrahedral mesh type the overall optimisation time took one month considering two optimisation variables (diameter and angle for 80 design points). By using the polyhedral mesh, the optimum of the parameter study was found within 6 days. In contradiction, a manual design study would need approximately 8 months due to the comprehensive number of person-hours to create the numerical grid and to set-up the calculations for each design point.

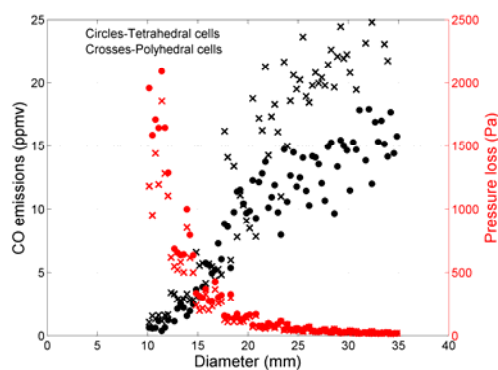


Figure 6: Effect of mesh type on the calculated CO emissions and pressure losses for the pilot-scale grate furnace

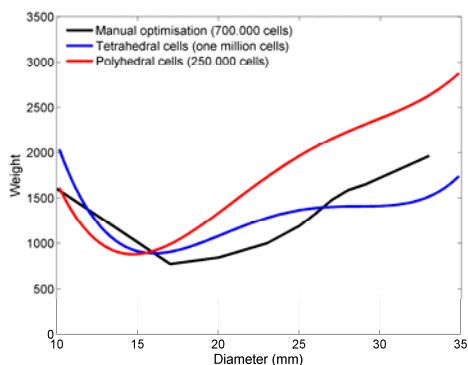


Figure 7: Weight function evaluated for different mesh types

Despite slight deviations in CO emission predictions from the reference grid, the polyhedral mesh shows a great potential to accelerate the optimisation cycle. A local mesh refinement in the region of secondary air jets is needed for an improved CO prediction and is expected to just slightly increase the mesh size and hence computation time.

4 SUMMARY AND CONCLUSIONS

A new automatic optimisation routine was developed and tested for a biomass pilot-scale grate furnace concerning the minimisation of CO emissions and pressure loss. The results showed that the diameter had a considerably higher impact on the pressure losses and CO emissions than the nozzle angle. The parameter variation performed automatically is by far more efficient than the manual case study due to the considerably lower simulation time and personnel demand. The overall simulation time for the calculation of 80 design points could be reduced by a factor of 8 in case of the tetrahedral mesh study and by a factor of 32 in case of the polyhedral mesh study. Although the CO emission trends were slightly differing for the two studied grid types the global minimums are located nearly at the same positions. However, the prediction accuracy of the coarser polyhedral mesh can be further improved at an acceptable increase of computational time by further increased local mesh refinement near the secondary air nozzles. Concluding, the new CFD optimisation routine proved to work efficiently in terms of nozzle design optimisation and time demand. In future it shall be further extended to geometry optimisation issues.

5 REFERENCES

- [1] H. Safikhani, A. Hajiloo, M. Ranjbar, N. Nariman-Zadeh, Modeling and multi-objective optimisation of cyclone separator using CFD and genetic algorithms, *Computer & Chemical Engineering*, (2011), Vol., 35 (6), pp. 1064-1071.
- [2] K. Elsayed, C. Lacor, Modeling, analysis and optimisation of aircyclones using artificial neural network, response surface methodology and CFD simulation approaches, *Powder Technology*, (2011), Vol., 212 (1), pag. 115-133.
- [3] H. Safikhani, M.A. Akhavan-Behabadi, N. Nariman-Zadeh, M.J.M. Abadi, Modeling and multi-objective optimisation of square cyclones using CFD and neural networks, *Chemical Engineering Research and Design*, (2011), Vol. 89 (3), pp. 301-309.
- [4] K. Elsayed, C. Lacor, Optimisation of the cyclone separator geometry for minimum pressure drop using mathematical models and CFD simulations, *Chemical Engineering Science*, (2010), Vol. 65 (22), pp. 6048-6058.
- [5] P. Sungwook, Optimisation of combustion chamber geometry and engine operating conditions for compression ignition engines fueled with dimethyl ether, *Fuel*, (2012), Vol. 97, pp. 61-71.
- [6] P. Sungwook, Optimisation of combustion chamber geometry for stoichiometric diesel combustion using a micro genetic algorithm, *Fuel Processing Technology*, (2010), Vol. 91 (11), pp. 1742-1752.
- [7] S. Derakhshan, B. Mohammadi, A. Nourbakhsh, Incomplete sensitivities for 3D radial turbo machinery blade optimisation, *Computers & Fluids*, (2008), Vol.37 (10), pp. 1354-1363.
- [8] S. Derakhshan, B. Mohammadi, A. Nourbakhsh, The comparison of incomplete sensitivities and genetic algorithms application in 3D radial turbo machinery blade optimisation, *Computers & Fluids*, (2010), Vol.39 (10), pp. 2022-2029.

- [9] K. Kim, S. Seo, Application of numerical optimisation technique to design of forward curved blades centrifugal fan, Japan Society of Mechanical Engineers International Journal Series B, (2006), Vol. 49 (1), pp. 152–158.
- [10] Y. Lü, Q. Lu, J. Wang, J. Zhang, 3D Numerical simulation of centrifugal fan inside flow field and modification investigation, Proceedings of the International Conference on Power Engineering, (2007), pp. 429–433.
- [11] H.L. Huai, W.L. Xu, Z.Y. Qu, Z.G. Li, F.P. Zhang, G.M. Xiang, S.Y. Zhu, G. Chen, Analysis and optimisation of municipal solid waste combustion in a reciprocating incinerator Chemical Engineering Science, (2008), Vol. 63, pp. 3100-3113.
- [12] K.V. Shah, R. Vuthaluru, H.B. Vuthaluru, CFD based investigations into optimisation of coal pulveriser performance: Effect of classifier vane setting, Fuel Processing Technology, (2009), Vol., 90, pp. 1135-1141.
- [13] R. Scharler, C. Benesch, K. Schulze, I. Obernberger: CFD simulations as efficient tool for the development and optimisation of small-scale biomass furnaces and stoves. In: Proc. of the 19th European Biomass Conference & Exhibition, June 2011, Berlin, Germany, ISBN 978-88-89407-55-7, pp. 4-12, ETA-Renewable Energies (Ed.), Italy
- [14] R. Scharler, Entwicklung und Optimierung von Biomasse-Rostfeuerungen durch CFD-Analyse, PhD thesis, Institute for process and particle Engineering, (2001), Graz University of Technology.
- [15] E. Widmann, Modellbildung zum Abbrandverhalten von Biomasse unter besonderer Berücksichtigung der N-Freisetzung am Beispiel einer Rostfeuerung, MSc thesis, Institute for process and particle Engineering, (2002), Graz University of Technology
- [16] R. Scharler, E. Widmann, I. Obernberger, CFD modeling of NOX formation in biomass grate furnaces with detailed chemistry, Proceeding of the International Conference Science in Thermal and Chemical Biomass Conversion, Sept 2004, Victoria, Canada, ISBN 1-872691-97-8, (2006), pp. 284-300, CPL Press (Ed.)
- [17] R. Scharler, I. Obernberger, Numerical optimisation of biomass grate furnaces, In: Proceeding of the 5th European Conference on Industrial furnaces and Boilers, April 2000, Porto, Portugal, ISBN-972-8034-04-0, INFUB (ed), Rio Tinto, Portugal
- [18] R. Scharler, C. Benesch, A. Neudeck, I. Obernberger, CFD based design and optimisation of wood log fired stoves, In: proceeding of the 17th European Biomass Conference, June 2009, Hamburg, Germany, ISBN 978-88-89407-57-3, pp. 1361-1367, ETA-Renewable Energies (Ed.), Florence, Italy
- [19] R. Scharler, T. Fleckl, I. Obernberger, Modification of a magnussen Constant of Eddy Dissipation Model for biomass grate furnaces by means of hot gas in-situ FT-IR absorption spectroscopy, Progress in Computational Fluid dynamics, (2003), Vol. 3, Nos.2-4, pp. 102-111
- [20] R. Scharler, M. Forstner, M. Braun, T. Brunner, I. Obernberger, Advanced CFD analysis of large fixed bed biomass boilers with special focus on the convective section, In: Proceeding of the 2nd World Conference and Exhibition on Biomass for Energy, Industry and Climate Protection, May 2004, Rome, Italy, Volume II, ISBN 88-89407-04-2, pp. 1357-1360, ETA-Florence (Ed.), Italy
- [21] R. Scharler, I. Obernberger, A. Weissinger, W. Schmidt, CFD-gestützte Entwicklung von Pellet- und Hackgutfeuerungen für den kleinen und mittlern Leistungsbereich, In: Brennstoff-Wärme-Kraft (BWK) Bd. 57 (2005) No. 7/8, pp. 55-58
- [22] R. Scharler, C. Benesch, I. Obernberger, CFD-Simulationen als innovatives Werkzeug für die Entwicklung und Optimierung von Biomasse-Kleinfeuerungsanlagen und Kaminöfen, In: Proceeding of the 3rd Mid-European Biomass Conference, Jan 2011, Graz, Austria, Austrian Biomass Association (Ed.), Austria
- [23] R. Scharler, I. Obernberger, CFD analysis of air staging and flue gas recirculation in biomass grate furnaces, In: Proceeding of the 1st World Conference on Biomass for Energy and Industry, June 2000, Sevilla, Spain, ISBN 1-902916-15-8, Volume II, James&James Ltd. (ed), London, UK, PP. 1935-1939
- [24] B. F. Magnussen, B. H. Hjertager, On the mathematical modeling of turbulent combustion with special emphasis on soot formation and combustion, In: Proceeding of the 16th Symp. (Int.) on Combustion, (1976), pp. 719-729, the Combustion Institute (Ed.), Pittsburgh, USA
- [25] A. Brink, Eddy Break-Up based models for industrial diffusion flames with complex gas phase chemistry, Ph.D. thesis, (1998), Abo Akademi University, Finland, ISBN 952-12-0302-1

bioenergy2020+



BIOENERGIESYSTEME GmbH

Research, Development and
Design of Plants for Heat and
Power Production from Biomass



Inffeldgasse 21b
A-8010 Graz
Tel.: +43 (0)316 481300-0
Fax: +43 (0)316 481300-4

Email:
office@bios-bioenergy.at
Homepage:
www.bios-bioenergy.at

